Component-led Integrative Optimisation Methodology for Avionic Thermal Management

by

Andy Jones

A Doctoral Thesis submitted in partial fulfilment of the requirements

for the award of Doctor of Philosophy of

Loughborough University

2017

i. Abstract

The modern military aircraft can be defined as a System of Systems (SoS); several distinct systems operating simultaneously across boundary interfaces. As the on-board subsystems have become more complex and diverse, the development process has become more isolated. When considering thermal management of distributed heat loads, the aircraft has become a collection of individually optimised components and subsystems, rather than the implementation of a single system to perform a given task. Avionic thermal management is quickly becoming a limiting factor of aircraft performance, reliability and effectiveness. The challenge of avionic thermal management is growing with the increasing complexity and power density of avionic packages.

The aircraft relies on a heat rejection growth capacity to accommodate the additional through-life avionic heat loads. Growth capacity is defined as an allowable thermal loading growth designed into the system by the underutilisation of spatial and cooling supply at aircraft introduction; however, this is a limited resource and aircraft subsystem cooling capability is reaching a critical point. The depleted growth capacity coupled with increased avionic power demands has led to component thermal failure. However, due to the poor resolution of existing data acquisition, experimental facilities or thermodynamic modeling, the exact inflight-operating conditions remain relatively unknown.

The knowledge gap identified in this work is the lack of definitive methodology to generate high fidelity data of in-flight thermal conditions of fast-jet subsystems and provide evidence towards effective future thermal management technologies. It is shown that, through the development of a new methodology, the knowledge gap can be reduced and as an output of this approach the unknown system behaviour can be defined. A multidisciplinary approach to the replication, analysis and optimisation of a fast-jet TMS is detailed. The development of a new Ground Test Facility (GTF) allows previously unidentified system thermal behaviour to be evaluated at component, subsystem and system level.

The development of new data to characterise current thermal performance of a fast jet TMS allows recommendations of several new technologies to be implemented through a component led integrative system optimisation. This approach is to consider the TMS as a single system to achieve a single goal of component thermal management. Three technologies are implemented to optimise avionic conditions through the minimisation of bleed air consumption, improve avionic reliability through increased avionic component isothermalisation and increase growth capacity through improved avionic heat exchanger fin utilisation. These component level technologies improved system level performance. A reduction in TMS bleed air consumption from 1225kg to 510kg was found to complete a typical flight profile. A peak predicted aircraft specific fuel consumption saving of 1.23% is seen at a cruise flight condition because of this approach to avionic thermal management.

ii. Acknowledgements

I would like to express my appreciation to my academic supervisor, Professor Rui Chen, for his support throughout undergraduate and postgraduate studies at Loughborough University. He has been extremely generous with his time and counsel throughout the last 9 years. I look forward to working together again on future research endeavours. I would like to thank academic staff outside our department who have provided critique at various reviews; specific thanks go to Peter Hubbard for his advice, friendship and truly impartial guidance.

I would like to extend my thanks to colleagues in the Aeronautical and Automotive Engineering Department. Firstly, my colleague Thomas Childs for his company in the lab and assistance in writing publications for the last few years. Along with all the technical, administrative and support staff, I would like to specifically thank Gren Cunningham for his assistance throughout the project. He always made time to provide me with measured and invaluable advice on all matters technical. Thanks go to Dave Travis and Pradip Karia who were very helpful in the development, build and operation of our new laboratory space.

My industrial supervisor, Angus Murray, has been instrumental to this project. Through the complete project Angus has gone above and beyond to ensure the continuation of research at Loughborough through the procurement of equipment and information. Angus always guaranteed we had the highest possible levels of collaboration from BAE Systems and always had a high calibre audience to receive our research. Thank you. I would also like to thank the staff at BAE Systems Warton, Brough, Gt. Baddow and Rochester for their supervision and review of my work; specifically, Ian Harrington, Mike Wiseman, Richard Seed and Mark Joslin.

Finally, I would like to thank my family and friends for their assistance; Mum for her continued support and care, Dad for his technical guidance and inspiration to follow him in into engineering. I know they lived through this project with me and it's not taken for granted. Finally, I'd like to thank my girlfriend, Daisy, who has shown unbelievable patience and support throughout the project. This would have been a whole lot more difficult without her.

Andy.

iii. Contents

List of Figures

iv. List of Tables

v. List of Abbreviations

ACM	Air Cycle Machine
AFRL	Air force Research Labs
AH	Absolute Humidity
APU	Auxiliary Power Unit
ATC	Advanced Technology Centre
ATR	Air Transport Rack
CAD	Computer Aided Design
CAU	Cold Air Unit
CDI	Concept Development Investigation
CED	Classical Engineering Disciplines
Cnd	Absolute Condensate
CoP	Coefficient of Performances
CTCV	Cabin Temperature Control Valve
ECS	Environmental Control System
EE	(ECS) Equipment Exhaust
EGM	Entropy Generation Minimisation
ETCV	Equipment Temperature Control Valve
FCC	Flight Control Computer
FN	Net Thrust
FPI	Fins Per Inch
FTIT	Fan Turbine Inlet Temperature
G	Gravity
GTF	Ground Test Facility
HPWE	High Pressure Water Extraction
INVENT	Integrated Vehicle Energy Technology
IPR	Intellectual Property Rights
ISA	International Standard Atmosphere
LPWE	Low Pressure Water Extraction
MAI	Military Air and Information
MBB	Messerschmitt-Bolkow-Blohn
MDO	Multidisciplinary Design Optimisation
MRCA	Multi-Role Combat Aircraft
NAMMA	NATO MRCA Management Agency
NAMMO	NATO MRCA Management Organisation
NFF	No Fault Found
OEM	Original Equipment Manufacturer
PID	Proportional Integral Derivative
PRSOV	Pressure Reducing and Shut Off Valve
PRV	Pressure Relief Valve
PTBI	Total Pressure of Interstage Bleed
PWM	Pulse Width Modulation
RAF	Royal Air Force

RH	Relative Humidity
SAM	Surface to Air Missiles
SDSR	Strategic Defence and Security Review
SFC	Specific Fuel Consumption
SHX	Secondary Heat Exchanger
SOS	System of Systems
SOV	Shut Off Valve
STOVL	Short Take Off Vertical Landing
TCPR	Total Pressure Ratio of the Cycle
TCV	Temperature Control Valve
TIM	Thermal Interface Material
TMS	Thermal Management System
To	Turbine Out
TSE	Traditional Systems Engineering
TTBI	Total Temperature of Interstage Bleed
UK	United Kingdom
USA	United States of America
USAF-ASD	United States Air Force Aeronautical Systems Division
VCHS	Vapour Chamber Heat Spreader
VCS	Vapour Cycle System
VPRSOV	Variable Pressure Relief Shut-Off Valve
WBI	Bleed Air Flow Rate
WE	Water Extractor

vi. Nomenclature

AH_C	Condensate Ratio
AH_S	Absolute Humidity at Saturation (g/kg)
A_s	Heat Transfer Surface Area (m^2)
C_d	Discharge Coefficient
CoP_{ECS}	Environmental Control System Coefficient of Performance
C_p	Specific Heat Capacity (kJ/kg.K)
$\Delta T_{ECS\ Branch}$	Temperature Differential across an Avionic Supply Branch Pipe (°C)
ΔT_{Module}	Temperature Differential across an Avionic Module (°C)
ΔT_{Tray}	Temperature Differential across an Avionic Tray (°C)
e_S	Saturation Partial Pressure (Pa)
e_V	Absolute Partial Pressure (Pa)
F	Force (N)
h	Convective Heat Transfer Coefficient (W/m^2K)
K	Material Thermal Conductivity ($Wm^{-1}K^{-1}$)
L	Length (m)
$\dot{m}$	Mass Flow Rate (kg/s)
N_u	Nusselt Number
p	Pressure (Pa)
P_M	Mixture Pressure
P_r	Prandtl Number
P	Power (W)
$\dot{Q}$	Heat Transfer Rate (W)
Q_{AV}	Avionic Heat Load (J)
$Q_{AV.Bay}$	Forward Avionic Bay Heat Load (J)
$Q_{C.AV}$	Cabin Avionic Heat Load (J)
Q_{Cab}	Cabin Heat Load (J)
Q_{ECS}	Environmental Control System Heat Rejection (J)
$Q_{Kinetic}$	Kinetic Heat Load (J)

Q_{met}	Metabolic Heat Load (J)
$\dot{Q}_{out}$	Net Useful Heat Transfer Rate (W)
Q_{pilot}	Pilot Heat Load (J)
$Q_{R.Av}$	Rear Avionic Heat Load (J)
$Q_{R.AV\ Bay}$	Rear Avionic Bay Heat Load (J)
Q_{sl}	Solar Radiation Intensity (J)
Q_{Solar}	Solar Heat Load (J)
$Q_{U.Av}$	Underfloor Avionic Heat Load (J)
$Q_{U.AV\ Bay}$	Underfloor Avionic Bay Heat Load (J)
$\dot{q}_v$	Volumetric Flow Rate (m^3s^{-1})
R	Thermal Resistance (KW^{-1})
R_{const}	Specific Gas Constant ($J\ kg^{-1}K^{-1}$)
R_e	Reynolds Number
R_V	Vapour Gas Constant
T_{Amb}	Ambient Temperature (°C)
T_{ECSE}	Temperature of Environmental Control System Exhaust (°C)
$T_{Mod\ Exhaust}$	Avionic Module Exhaust Temperature (°C)
$T_{Mod.Inlet}$	Module Inlet Temperature (°C)
T_{Rec}	Recovery Temperature (°C)
T_s	Surface Temperature (°C)
T_{stag}	Stagnation temperature (°C)
v	Velocity (ms^{-1})
$\dot{W}_{Bleed\ Air}$	Bleed Air Power (W)
W_c	Compressor Work (J)
$\dot{W}_{EECS}$	Environmental Control System Exhaust Air Power (W)
$\dot{W}_{in}$	Total Inlet Power (W)
$\dot{W}_{Inducer}$	Inducer Power (W)
$\dot{W}_{Ram\ Air}$	Ram Air Flow Path Power (W)
W_{RamHX}	Ram Air Heat Exchanger Heat Rejection (J)

vii. Greek Symbols

ε	Emissivity Coefficient
γ	Polytrophic Coefficient
μ	Fluid Dynamic Viscosity (kg $m^{-1}s^{-1}$)
η_c	Engine Compression Efficiency
η_{cc}	Environmental Control System Compressor Efficiency
η_t	Environmental Control System Turbine Efficiency
σ	Stefan-Boltzmann Constant (W m^{-2} K^{-1})
ρ	Density (kg m^{-3})
ρ_M	Density of Mixture (kg m^{-3})
τ	Panel Transmittance

1. Introduction

1.1. Motivation

The modern military aircraft can be defined as a System of Systems (SoS); a number of distinct systems operating simultaneously across boundary interfaces (Clark 2009). As the on-board subsystems have become more complex and diverse, the development process has become more isolated. When considering the thermal management of distributed aeronautical heat loads, the aircraft has become a collection of individually optimised components and subsystems, rather than the implementation of a single system to perform a given task. In particular, the avionic thermal management is quickly becoming a limiting factor of aircraft performance, reliability and effectiveness (Tybrandt 2012).

The avionic module conditioning airflow is generated by the aircraft Environmental Control System (ECS), which is also responsible for the cabin temperature and pressure regulation, oxygen generation, canopy demist system, wing de-icing, radar cooling, pilot anti-G suit pressurisation, and additional thermal management. The ECS is a cooling cycle that utilises high pressure and high temperature bleed air from the propulsion system as a working fluid, with ambient ram air acting as a heat sink. The bleed air supply is at a cost of fuel

consumption, while the ram air flow rate generates aerodynamic drag. The complete system is defined as the Thermal Management System (TMS). The TMS is a highly integrated system linking the propulsion, external aerodynamics, power generation, cabin, fuel and avionic subsystems.

The TMS is an increasing area of research as the modern military aircraft continues to expand capabilities of inter-operability, communications, navigation and weapons system. The requirement for increased platform capability is met with the requirement for increased range, reduced specific fuel consumption, reduced radar cross section and thermal signature. The drive for increased aircraft efficiency is reducing the availability of fuel energy for the TMS.

The main focus of this project is the TMS of 4th Generation Fighter Aircraft (designed from 1970's to 2000 and currently in service). These aircraft are expected to be in service for up to five decades and maintain mission effectiveness across the complete life cycle. This is achievable by periodic avionic updates; which increase the avionic thermal loading against the aircraft fixed heat rejection capability.

High rates of avionic failure are a feature of fast jet combat aircraft as a consequence of the increasing complexity of aircraft mission systems. However, as a result of the design process, aircraft age, lack of data acquisition and heavy reliance on steady-state one-dimensional numerical and analytical tools, the engineer's knowledge of the thermal system performance is limited. The poor definition of avionic subsystem thermal conditions across the complete flight and atmospheric envelopes leads to the use of high safety factors on heat rejection requirement calculations. For the in-service aircraft, component reliability and mission effectiveness are prioritised above thermodynamic efficiency and the avionics are typically oversupplied with cooling airflow. However, the spare cooling capacity is quickly diminishing against the trend of increasing thermal loads.

The lack of knowledge about the avionic module thermal conditions throughout the flight envelope is defined as unknown system behaviour. The engineers understand that this

behaviour exists, but to date they have been unable to identify the time-dependent thermal conditions due to lack of visibility with traditional analysis techniques. The knowledge gap identified in this work is the lack of a definitive methodology to generate high fidelity data of the in-flight thermal conditions of fast-jet subsystems and provide evidence towards effective future thermal management technologies. It will be shown that through the development of a new methodology the knowledge gap can be reduced and as an output of this approach the unknown system behaviour can be defined.

1.2. Aims and Objectives

The aim of the project is fundamentally to deliver high confidence data to replicate, analyse and optimise the in-flight thermal conditions of fast-jet subsystems. The data must have the capability to replicate the in-flight conditions of the TMS across a complete flight envelope throughout the extremes of the atmospheric envelope of operation. The in-flight conditions will be analysed to identify key system thermodynamic behaviours and relationships. This information will be used to identify and evaluate an optimisation approach. The aim of this work is to answer the three research questions detailed below.

1. How can the in-flight conditions of a fast jet military aircraft thermal management system be accurately replicated using a ground test facility?
2. How can this ground test facility be utilised to characterise the thermal performance of the thermal management system?
3. What are the optimisation strategies when considering real-world restrictions on aircraft solutions?

The objectives of the work are detailed below:

- To develop new Ground Test Facilities (GTF) for the identification of in-flight thermal behaviours of a 4^{th} generation aircraft TMS;
- To identify a methodology for the development of a facility to output data of low uncertainty, high fidelity and high flexibility;

- Assess thermal performance across the range of flight and atmospheric envelopes;
- Evaluate the facility outputs against validation data supplied by BAE Systems;
- Identify key thermodynamic behaviours and relationships at component, subsystem and system level;
- To develop and evaluate an optimisation methodology to provide system level performance improvements;

1.3. Research Contributions

It is considered that a number of key research contributions have been made.

1. A new multidisciplinary approach to the replication, analysis and optimisation of a fast-jet thermal management system will be detailed. The approach takes key concepts from three areas of related literature, applying a conceptual design approach to mature technology. The approach is defined as a component-led integrative optimisation methodology for avionic thermal management.
2. The previously unidentified system thermal behaviour has been evaluated across the complete flight and atmospheric envelopes at system level. Analysis of this data detailed that the TMS is essentially a steady state solution to a dynamic problem. The TMS showed poor thermodynamic efficiency across the flight profile due to the oversupply of avionic mass flow. Aircraft thermal loading is variable with operating conditions; however the TMS configuration is fixed throughout the flight profile and has limited capability to actively regulate the heat rejection capability.
3. Analysis of experimental ECS subsystem data detailed that the industry standard metric of performance is misleading. The Coefficient of Performance is used as a ratio

of the heat absorbed to the total energy consumed. However, this metric can be misleading when used at subsystem level and does not accurately define the subsystem cost to the aircraft level efficiency. It was found that airflow temperature is used as a feedback measure for system control and system interface management. Air temperature is easily measured and easily communicated across subsystem boundary interfaces; however it does not define the cooling capacity. It will be shown that the ECS can operate with a partial failure and achieve the same temperature at a much reduced flow rate. This partial failure is beyond the capability of the control system to identify and it is concluded that future system designs should move away from these metrics.

4. A number of new technologies are implemented to the TMS to provide a component-led integrative system optimisation. The optimisation technologies are based on findings from an experimental investigation into TMS operating conditions. The technologies act to minimise bleed air consumption through the optimisation of the component level thermal operating condition.
5. An aircraft-level response can be measured by the optimisation of the thermal conditions at the component level. The bleed air consumption and subsequent specific fuel consumption reduction is the detailed at the mission-level across a complete flight envelope.

1.4. Thesis outline

Following this introductory chapter, Chapter 2 covers a background to the research area through a literature review of military fast-jet TMS. Initially, the literature review provides the reader with a familiarity of the equipment, terminology, operational demands, heat

loads and requirements of a TMS. The second section of the chapter introduces the concept of the unknown system behaviour, which is the central motivation for this work. The generation of this behaviour can be traced back to a combination of scientific, technological, organisational, political and financial factors. The requirement to understand these factors is critical to the development of a new methodology for system replication, analysis and optimisation.

Chapter 3 details the development of a new methodology for a multidisciplinary approach to system replication, analysis and optimisation. The methodology is developed from a literature review of contemporary approaches to thermal management, systems engineering and the second law of thermodynamics optimisation principles. Core principles of each theory have been combined to provide a new approach.

Chapter 4 details the development of a Ground Test Facility (GTF), which acts as a high fidelity test bed to evaluate the multidisciplinary approach. The GTF requires the decomposition of the TMS, which integrates multiple-subsystems and operates across many interface boundaries. A detailed decomposition process is discussed based on traditional system engineering concepts. The build and development of each section of the GTF is detailed, with information regarding the physical construction of test facility components and the use of thermodynamic modelling. The findings of this chapter will be used to answer the first research question.

Chapter 5 sets out to evaluate the baseline performance of the TMS based on the data generated by each subsystem of the GTF. The chapter acts to evaluate both the performance of the TMS and of the GTF. A number of key thermodynamic behaviours are identified, which could have been missed through a purely modelling based approach. The GTF is asserted against several sources of validation data provided by BAE Systems to assess the accuracy of the data output. A mission-level thermal sensitivity analysis is completed to identify areas of poor thermodynamic performance across the complete flight (and atmospheric) envelope. The output of this sensitivity analysis is used to guide thermal management technology recommendations for the TMS optimisation. This

chapter highlights key findings as an output of this approach which are not identified through traditional approaches to TMS analysis. The findings of this chapter will be used to answer the second research question.

Chapter 6 details the performance of the thermal management technology recommendations of Chapter 5. This chapter primarily focuses on a component-level study. Through the analysis of validation data from BAE Systems, the failure mechanism of an avionic module is traced to an isolated thermal hotspot rather than the original concept of a saturation of total heat rejection capability. A component-level proof-of-concept test rig is detailed and the implementation of new technologies are assessed. Two further technologies at system level are assessed to optimise the component-level thermal conditions. The performance benefit of each technology is assessed at the component, subsystem and system level for a single flight case and atmospheric condition.

Chapter 7 addresses the expansion of the optimisation technologies to the complete flight (and atmospheric) envelope; a mission-level analysis. A mission-level comparative study is completed between the baseline system and a system optimised by the application of all three thermal management technologies simultaneously, to assess the applicability and robustness of the suggested optimisation. The chapter concludes with the calculation of system level performance indicators (specific fuel consumption) based on component level thermodynamic optimisation. The findings of Chapter 6 and Chapter 7 will be used to answer the third research question.

Finally, Chapter 8 comments on the main findings of the project, it gives a summary of these findings, an evaluation of the GTF and explores the applicability of the technologies. The facilities developed in this project will be utilised for further research and ideas for the future direction of the work are suggested.

2. Background

This chapter provides a literature review of the military fast-jet TMS. This chapter is made of two parts. The first part (section 2.1 to section 2.4) provides the reader with a familiarity of the equipment, terminology, operational demands, heat loads and requirements of the TMS. The second part (section 2.5 to section 2.10) details the development of an unknown thermal system behaviour of operational aircraft, which the central motivation for this work.

Initially, the components and subsystems of a TMS are considered in isolation. The integration and operation of these subsystems at platform level can cause unexpected system behaviours to arise. A system failure can be defined as a system which does not operate according to its design specification, therefore any unknown system performance can be considered as a partial system failure. This thesis details the thermodynamic behaviour of avionic thermal management. The contributing factors to this behaviour are vast and multi-disciplinary, covering technical design processes, company organisational structure, political requirements, financial constraints and chronological factors. These constituents are discussed in detail to provide the reader with an understanding of the boundary conditions faced by the aeronautical engineering industry in designing and

operating a TMS. It is important to clarify these boundary conditions to identify the relevance of the contribution of this work.

Unknown avionic thermal system behaviour has developed in 4th generation fast jets. Its development can primarily be associated to the absence of a scientific methodology to accurately replicate the inflight conditions of the TMS, analyse the thermodynamic performance and evaluate new technologies for system optimisation. This is defined as the knowledge gap of this thesis. It is only through the complete appreciation of the factors contributing to the evolution of current TMS that a new methodology can be defined to fill this knowledge gap. Through the analysis of aircraft design constraints and aircraft operations, several key requirements for the development of a solution can be attained. The background to the problem is defined in this chapter and a methodology for the solution is discussed in Chapter 3.

2.1. Aircraft Specification

The current work addresses a specific aircraft type and this thesis regularly references 4th generation and 5th generation fighter aircraft. Many contributing factors to the development of the knowledge gap are specific to the 4th generation fighter aircraft and most the thesis is based on this airframe class. The United Kingdom (UK) currently operates only 4th generation aircraft and the project sponsor, BAE Systems, produces only 4th generation aircraft. Although BAE Systems is a major partner in the 5th generation F35 Lightning II aircraft project, current production capability is based on the 4th generation. A definition of fighter aircraft generations is presented in Figure 2-1. The life span of a 4th generation aircraft is the longest in modern aviation history with many airframes in service for 4 to 5 decades.

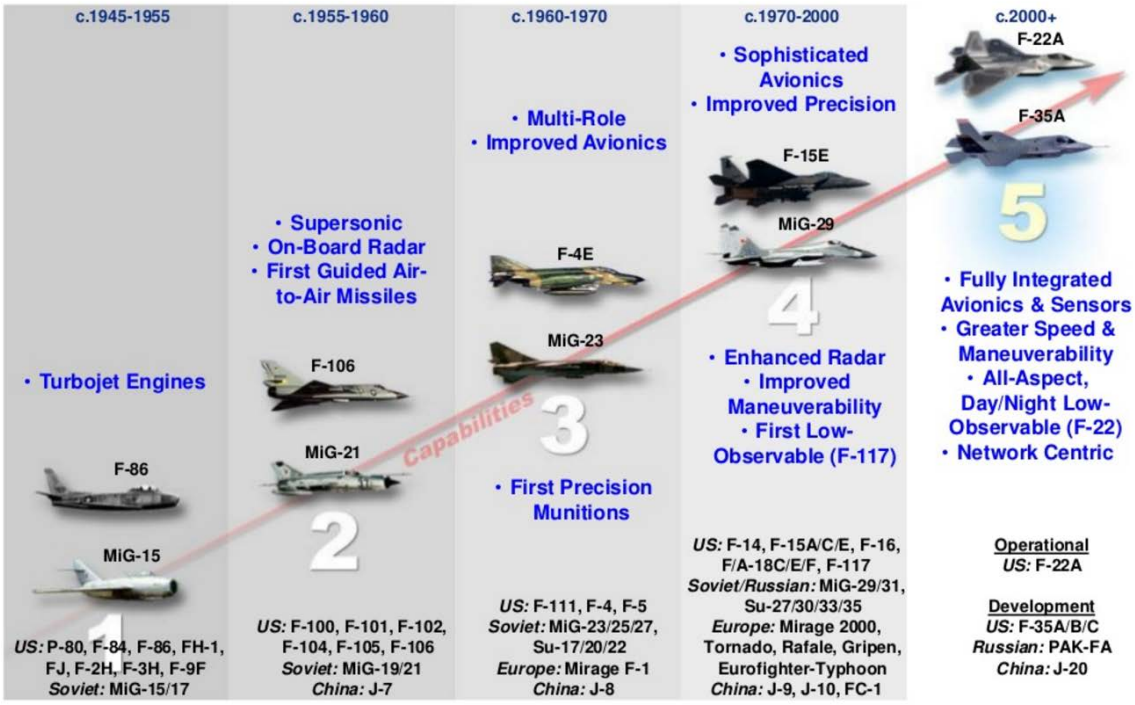

Figure 2-1:Fighter Aircraft Generation Definitions (Lt Gen Hawk 2012)

The 4th generation aircraft is the most advanced military platform currently in service for all countries excluding the United States of America (USA). This comprises of aircraft designed between 1970 to 2000 and built by France, India, Japan, China, Russia, Korea, Sweden, USA and a number of European Consortiums (www.globalsecurity.org 2015). In total, nearly 13,000 4th generation fighter aircraft have been built worldwide.

The majority of UK and USA 4th generation aircraft were designed in the cold war era, when tensions between the 'Western Bloc' and the Soviet Union were high. This led to a military spending race, resulting in the development of a number of aircraft specifically designed for a Soviet Union threat. The Lockheed F-117 Nighthawk (F-117), Lockheed Martin F-22 Raptor (F-22), Eurofighter Typhoon (Typhoon), McDonnell Douglas F/A-18 Hornet (F-18) and Northrop Grumman B-2 Spirit (B-2) were all developed with this reason. Since the Soviet Union was disbanded, the worldwide political landscape stabilised and the budget for research and development of fast-jet military aircraft has reduced. An inflation adjusted US military budget per capita can be seen in Figure 2-2; three peaks are clearly defined around 1968 (Vietnam War), between 1986 and 1990 (Second Cold War) and then 2010 (conflicts in Iraq and Afghanistan) (Office of Management and Budget 2013). The

influx of new airframes in a short timeframe is a key element to the development of the knowledge gap in 4th generation aircraft.

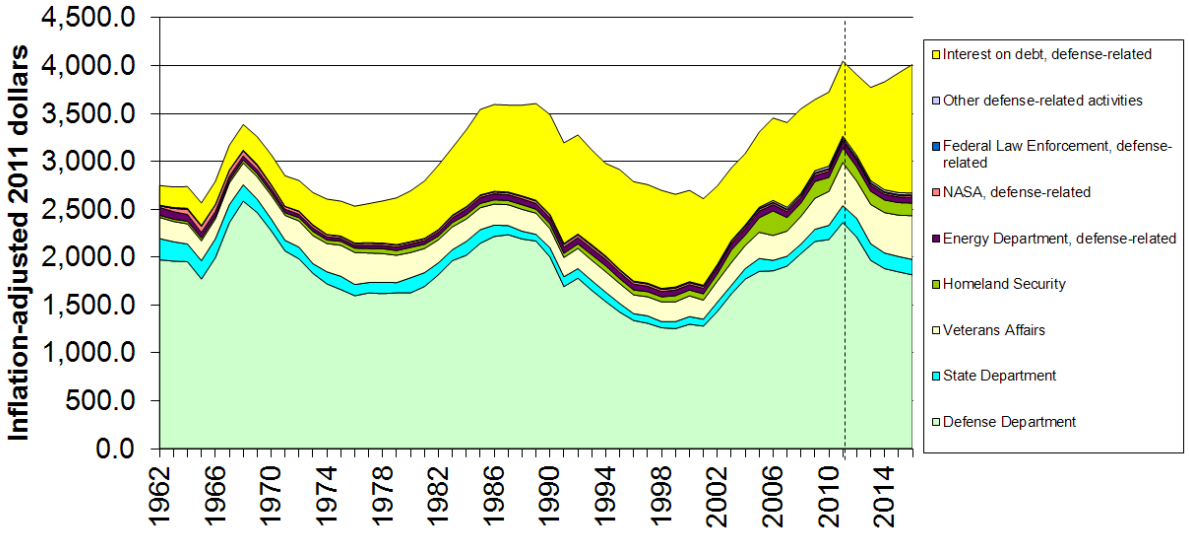

Figure 2-2: USA military budget over the last 50 years(Office of Management and Budget 2013)

2.2. Aircraft Operational Envelopes

The operational envelope is a fundamental specification in the conceptual design of any airframe, driving key decisions throughout the aircraft design process. In terms of thermal management, the operational envelope dictates both the TMS heat loads and the TMS heat rejection capability. It is important to consider this at the top level of system design.

The flight envelope varies with each aircraft and the 4th generation McDonnell Douglas F-15 (F15) flight envelope is seen in Figure 2-3a. The atmospheric condition in which the flight envelope is flown can be seen in Figure 2-3b. The environmental conditions are separated into three categories: Hot (A), Humid (B) and Cold (C). This data expresses the environmental design limits for each category and relates that data to a world-wide map; the geographical destination of the atmospheric temperature zones (A, B, C) can be seen in Figure 2-4.

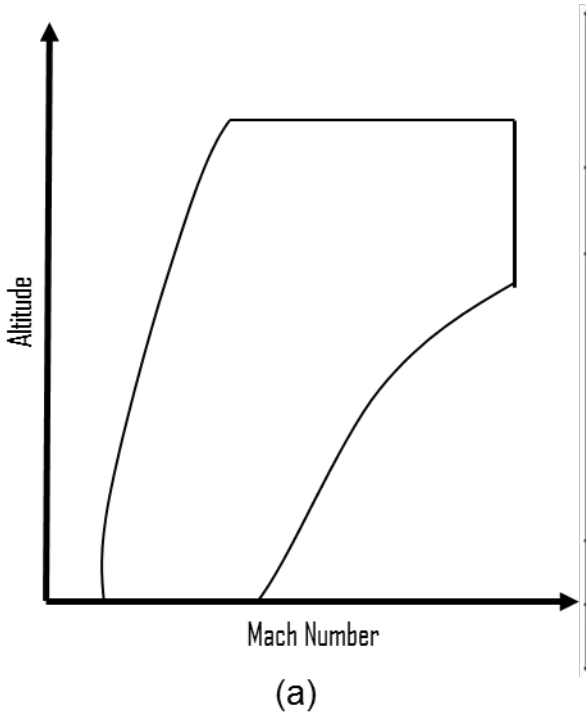

Climatic Design Type	Daily Cycle[1]	Operational Conditions: Ambient Air Temperature[2] °C (°F) Daily Low	Daily High	Solar Radiation W/m² (Bph[3])	Ambient Relative Humidity %RH[4]
Hot	Hot Dry (A1)	32 (90)	49 (120)	0 to 1120 (0 to 355)	8 to 3
	Hot Humid (B3)	31 (88)	41 (105)	0 to 1080 (0 to 343)	88 to 59
Basic	Constant High Humidity (B1)	Nearly Constant 24 (75)		Negligible	95 to 100
	Variable High Humidity (B2)	26 (78)	35 (95)	0 to 970 (0 to 307)	100 to 74
	Basic Hot (A2)	30 (86)	43 (110)	0 to 1120 (0 to 355)	44 to 14
	Intermediate[6] (A3)	28 (82)	39 (102)	0 to 1020 (0 to 323)	78 to 43
	Basic Cold (C1)	-32 (-25)	-21 (-5)	Negligible	Tending toward saturation
Cold	Cold (C2)	-46 (-50)	-37 (-35)	Negligible	Tending toward saturation
Severe Cold	Severe Cold (C3)	-51 (-60)		Negligible	Tending toward saturation

(b)

Figure 2-3: A typical flight envelope and F-15 Flight atmospheric operational conditions (Matullch 1989; Defence 2008)

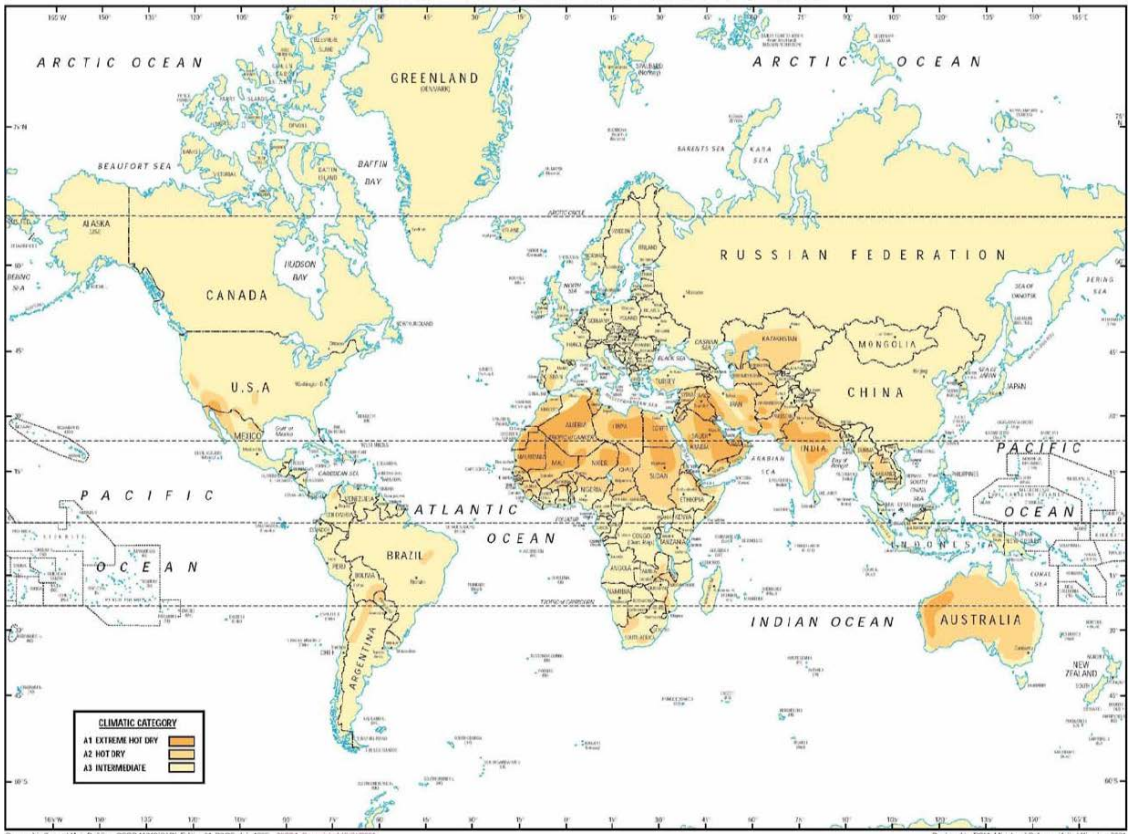

Figure 2-4: Atmospheric Hot conditions categorised by country. Dark orange = Extreme Hot Dry, Pale Orange = Intermediate.

The ability of a TMS to reject heat is based on the coolant and working fluid flow rates which are dependent on vehicle speed and engine load. Heat transfer through the aircraft skin can be positive or negative based on environmental thermal loading due to aerodynamic friction drag, atmospheric temperatures and solar radiation.

2.3. Environmental Thermal Loading

The main source of aircraft heat transfer from environmental conditions is known as kinetic thermal loading and is generated by aerodynamic friction drag. The aerodynamic friction drag of the aircraft is due to the dynamic viscosity of the air it is travelling through. Viscosity is a measure of the fluids resistance to flow caused by intermolecular fiction as a layer of the fluid slides past another (Kestin & Whitelaw, 1964). When a body moves through a gas, the molecules directly adjacent to the body have zero velocity. As a body moves through a fluid, it creates a shear force between layers of the fluid generating a resistance to motion. This shear force produces aerodynamic drag on the moving body and heat as a by-product. The magnitude and direction of environmental thermal loading is based on the difference between the aircraft skin and internal airframe temperatures.

The temperature of the aircraft skin is known as the recovery temperature, T_{Rec}. The recovery temperature is determined the ambient air temperature, T_{Amb}, and the non-dimensional vehicle speed, M, measured as Mach number (Woodfield, A & Haynes, P 1965). The condition at which air comes to a rest is known as a stagnation point and this temperature, T_{stag}, is calculated in a similar manner (Alyanak & Allison 2016). In air,

$$T_{Rec} = T_{Amb}\,(1 + 0.18M^2) \tag{2-1}$$

$$T_{stag} = T_{Amb}\,(1 + 0.2M^2) \tag{2-2}$$

2.3.1. Atmospheric Temperature Variation

The atmospheric component of kinetic thermal loading is the ambient temperature and the flight component is the Mach number. The ambient temperature variation with increasing altitude for a 1% Hot, 1% Cold and International Standard Atmosphere (ISA day) can be seen in Figure 2-5. The '1%' atmospheric condition is based on a 1% minimum and 1% maximum temperature annually recorded. This is defined as a temperature that can be

attained or exceeded for 7.4 hours per month per year. The atmospheric condition stems from data collected at various locations across the world and is not representative of an actual atmosphere, but an amalgamation of the 1% temperatures recorded at various altitudes. As fighter aircraft application is year round, world-wide, long range and the effect of environmental thermal loading is considerable, it is sensible to study harsh atmospheric conditions (Cavcar 2000; SAE 2014).

The thermal lapse rate is the relationship at which temperature varies with altitude. The hot and ISA atmospheric temperature relationship with altitude are mapped according to a linear lapse rate through the troposphere, preceding an isothermal region above that (Cavcar 2000). The lapse rate and height at which the temperature becomes isothermal is dependent on sea level conditions. The cold atmosphere lapse rate is not linear, instead featuring a temperature inversion region (sea level to 5250ft) followed by an isothermal layer (5250 to 9850ft) and a linear lapse rate before the normal high altitude isothermal layer (SAE 2014).

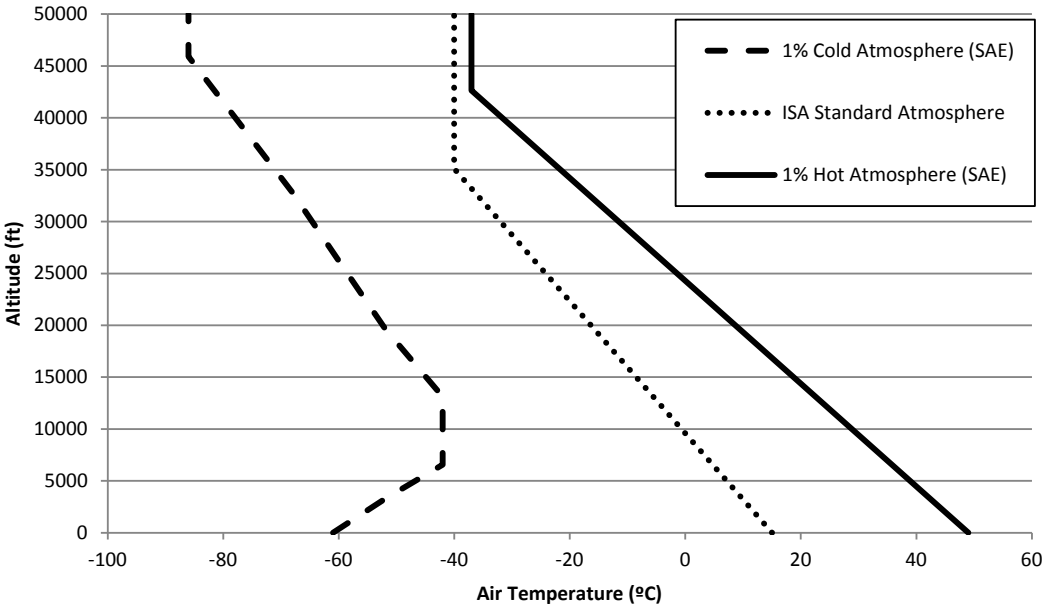

Figure 2-5: Atmospheric temperatures with altitude

2.3.2. Kinetic thermal loading

The dominant heat transfer mechanism of kinetic thermal heating is convection. The heat transfer rate, $\dot{Q}$, is based on the convective heat transfer coefficient, h, convective heat

transfer surface area, A_s, and the temperature difference between the surface temperature and the recovery temperature.

$$\dot{Q} = h\, A_s\, (T_{rec} - T_s) \tag{2-3}$$

The convective heat transfer coefficient can be calculated from an empirical correlation, mapped in Appendix 1. To calculate the convective heat transfer coefficient, the user selects the aircraft Mach number from the left hand x-axis and intersects that with an aircraft angle of incidence. The ordinate of the intersection is then tracked across to the right hand side of the graph to intersect with the aircraft altitude lines. The abscissa of the intersection of these two lines is read as the convective heat transfer coefficient on the x-axis. Finally, a correction factor is applied to the convective heat transfer coefficient based on Mach number and the ratio of recovery temperature against ambient temperature. With this estimate of the convective heat transfer coefficient, the kinetic thermal loading can be calculated from equation 2-3. This map was provided by BAE Systems.

2.3.3. Atmospheric Pressure Variation

The atmospheric pressure decreases with increasing altitude as shown in Figure 2-6. The aircraft engine intakes and compresses ambient air before injecting fuel for combustion to generate propulsion. Between the compression and combustion stages, high temperature high pressure airflow is bled off to power the TMS. This is known as bleed air. The energy consumed in the compression of bleed air is fundamental in the calculation of the TMS energy efficiency.

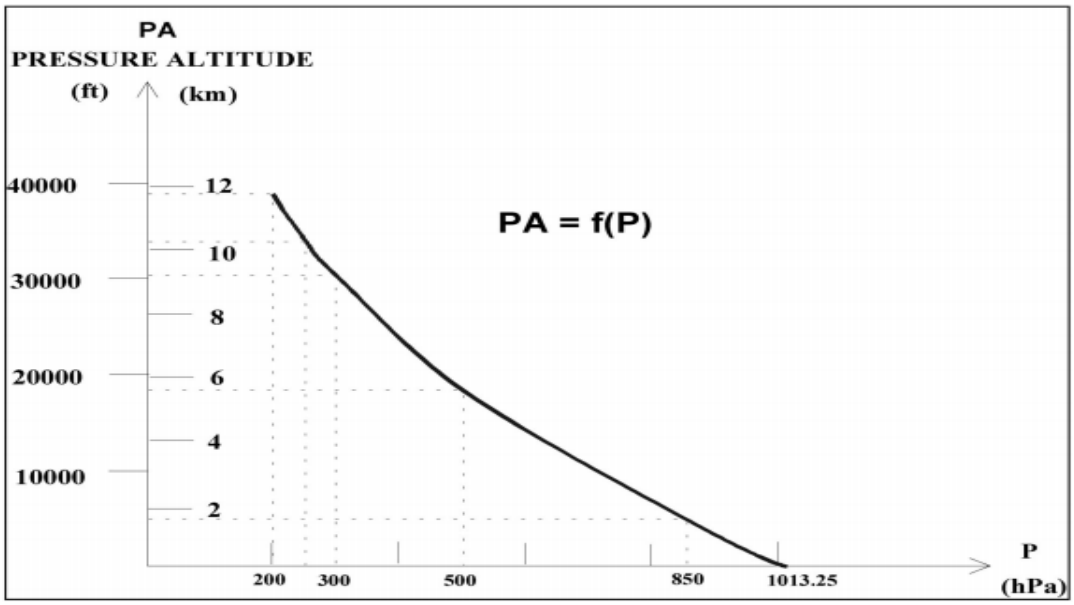

Figure 2-6: Atmospheric pressure variation with altitude

As the ambient pressure reduces, the air density reduces which reduces aerodynamic drag and therefore kinetic thermal loading. In terms of the aerodynamic drag effect on TMS energy efficiency, the aircraft utilises ambient air as a coolant through ram air heat exchangers. The pressure drop across the heat exchanger core (aerodynamic drag) is dependent on the atmospheric pressure. The energy consumed by the heat exchanger aerodynamic drag is based on the force applied to the heat exchanger as a result of the pressure drop across it. From the power, P_{wr}, required to move an item with a force, F, at a velocity, v.

$$P_{wr} = Fv \tag{2-4}$$

The net force on the heat exchanger is calculated given from a pressure difference across the heat exchanger core, ΔP, the mass flow rate, $\dot{m}$ and air density, ρ. The pressure drop data of the heat exchanger is detailed from experimental testing and BAE Systems data.

$$\dot{W}_{Ram\ Air} = \frac{\Delta P\ \dot{m}}{\rho} \tag{2-5}$$

The highest drag conditions are at high speed (high $\dot{m}$), low altitude (high ΔP) flight conditions in a cold atmosphere. At this flight case, the power consumed by heat exchanger aerodynamic drag for a small jet trainer aircraft like the BAE Systems Hawk (heat exchanger size 200x180x140mm) can be as high as 100kW.

2.3.4. Atmospheric Humidity

The final environmental factor to be considered is atmospheric humidity. The TMS working fluid (bleed air) and coolant (ram air) are unfiltered from the ambient environment. The Absolute Humidity (AH) of bleed air is dependent on geographical location and operational condition of the aircraft. The most extreme humidity environment is defined as a 'Hot Humid' atmosphere and is typical of coastal regions of Saudi Arabia, Iran and Kuwait. Atmospheric conditions of up to 88% Relative Humidity (RH) at temperatures of up to 41ºC generate AH as high as 47g of water per kg of air.

Operationally, humidity is only present at low altitudes. RH is a measure of the ability of air to hold moisture and defined as the ratio of the partial pressure of water vapour to the saturation pressure of water at a given temperature. The saturation pressure is dependent on air temperature and because air temperature changes with altitude (Figure 2-5), a direct relationship between altitude and humidity exists. As altitude increases, RH increases to the point at which partial pressure of water vapour is equal to the saturation pressure and water separates from the air (100% RH). This is known as the dew point; above this altitude, absolute humidity can be assumed negligible.

2.4. Thermal Management System

The TMS is fundamentally the system which cools aircraft heat loads. Those heat loads are environmental, human, and airframe related. The TMS in this study takes a feed of compressed air from the engine and therefore is a cost to fuel consumption. TMS is an umbrella term for multiple smaller subsystem, such as the Environmental Control System, cabin, and avionics. The TMS of this investigation is typical of a 4^{th} generation aircraft.

The following section details the bleed and ram airflow streams through a typical 4^{th} generation aircraft TMS. The path follows the compression of ambient conditions, tapping of bleed air, cooling of the Environmental Control System (ECS), thermal conditioning of aircraft subsystems, and rejection overboard back to ambient conditions.

2.4.1. System Level

A generic 4th generation airframe TMS architecture is detailed in Figure 2-7. This configuration shares similarities with 4th generation aircraft such as the Grumman F-14 (Hoffman 1985), the McDonnell Douglas F-15 (Dieckmann et al. 1986), the General Dynamics F-16 (Laster et al. 1990), the Panavia Tornado(Gunston 1980), the BAE Systems Hawk (Jones et al. 2015), the Eurofighter Typhoon (Pearson & McCoy 2011), and the Saab JAS 39 Gripen among others.

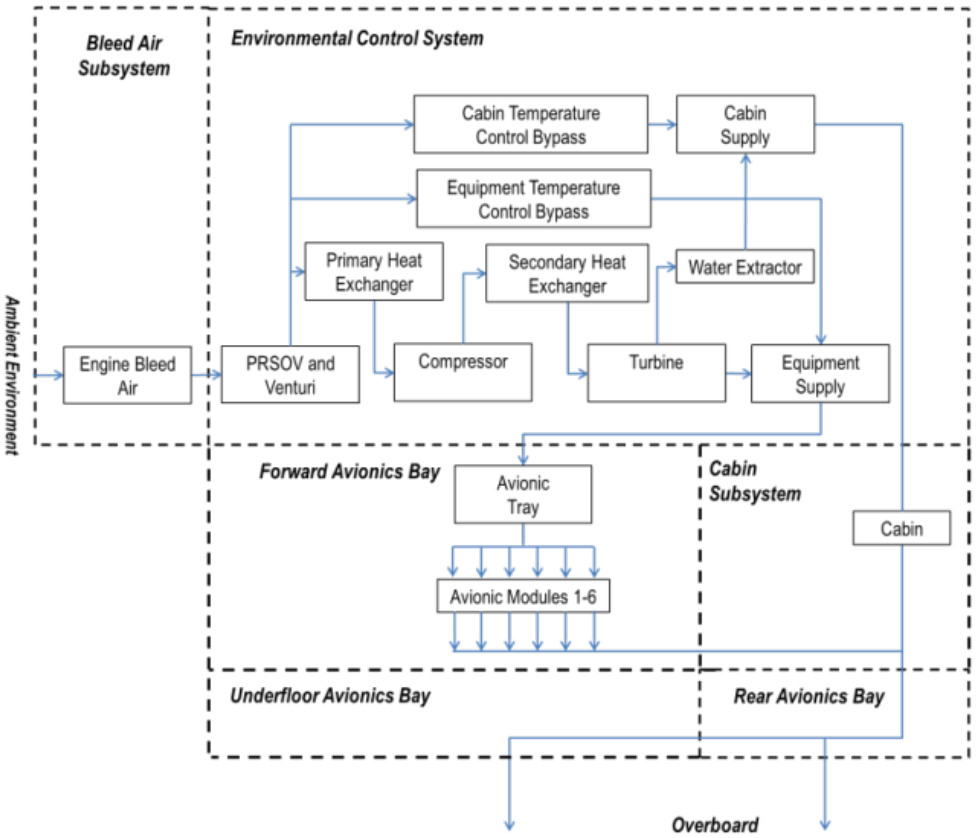

Figure 2-7: System Level Thermal Management System

The fast-jet TMS is single pass in that the airflow passes through the system and is jettisoned overboard with no re-circulation. A single pass system carries less weight and is utilised because the total flowrate is low, the pilot has a separate oxygen supply and the system temperature differential is high. This arrangement differs from that of a commercial airliner, where the TMS flow rate is substantially higher and the temperature differential across the cabin is low, allowing the use a highly re-circulatory system (Mitani

& Saito 2002). The TMS of Figure 2-7 can be split into six distinct subsystems; which are detailed below.

1. **Bleed Air Subsystem** - Compression of ambient air and bleed off before combustion.
2. **Environmental Control System** – An air cycle machine to reduce the temperature and pressure of bleed air before its use as a cooling fluid.
3. **Cabin Subsystem** – A sealed environment which requires conditioning of pilot, avionic, environmental heat loads in addition to pressurisation and canopy sealing.
4. **Forward Avionics Bay** – The primary avionics bay of high power density populated by forced convection cooled avionic modules.
5. **Underfloor Avionics Bay** – A secondary avionic bay which is distributed around the airframe for ease of packaging and to provide redundancy.
6. **Rear Avionics Bay** – Another secondary avionic bay which is distributed around the airframe for ease of packaging and redundancy.

The subsystems are discussed in the following section in the order of the airflow path from the bleed air subsystem to the avionics bays.

2.4.2. Engine Bleed Air (Working Fluid)

The TMS utilises the expansion of high pressure bleed air as a source of power for the cooling cycle. Bleed air is the only TMS energy supply of Figure 2-7; it has no direct mechanical or electrical work input. Bleed air is generated from the compressor stage of the aircraft engine, producing high specific enthalpy airflow (high temperature and pressure). A typical configuration of the bleed air port is detailed for the Pratt and Whitney F100-PW-220 engine used in the F-15 and F-16 aircraft in Figure 2-8, which is typical of 4^{th} generation platforms (Evans 1991).

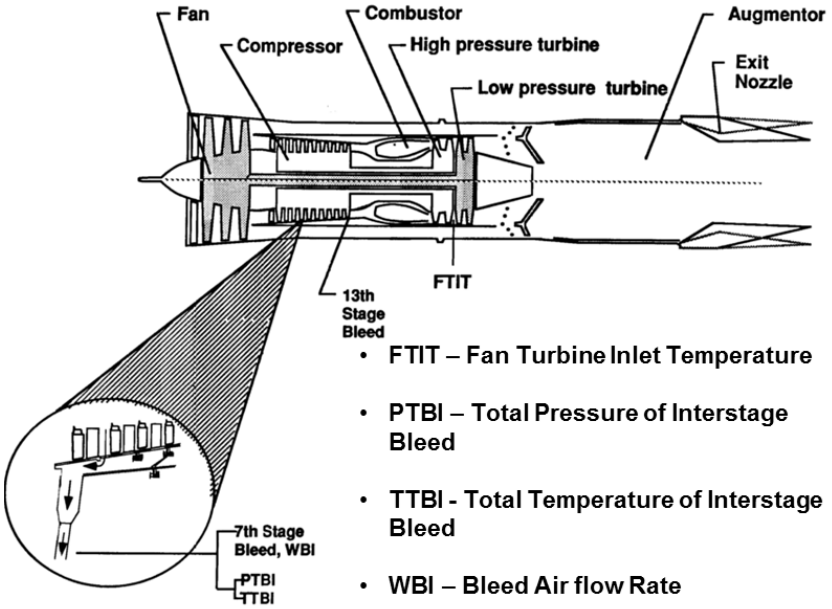

Figure 2-8: A simplified diagram of the F100-PW-22 Afterburning Turbofan Engine (Evans 1991)**.**

The TMS heat rejection capability is based on the pneumatic power supply. At low engine loads, the bleed air enthalpy is low and hence TMS heat rejection capability is low (Matullch 1989). To account for the variation in bleed air pressure across the flight envelope, some engines feature a high and a low pressure bleed port, as sketched in Figure 2-8.

The consumption of bleed air requires work output from the compressor which is not recovered in the combustion process and therefore the generation of bleed air is responsible for a reduction in the engine performance. The relationship between bleed air consumption, net thrust (FN) in pounds and Specific Fuel Consumption (SFC) for the engine sketched is Figure 2-8 are detailed in Figure 2-9 and Figure 2-10.

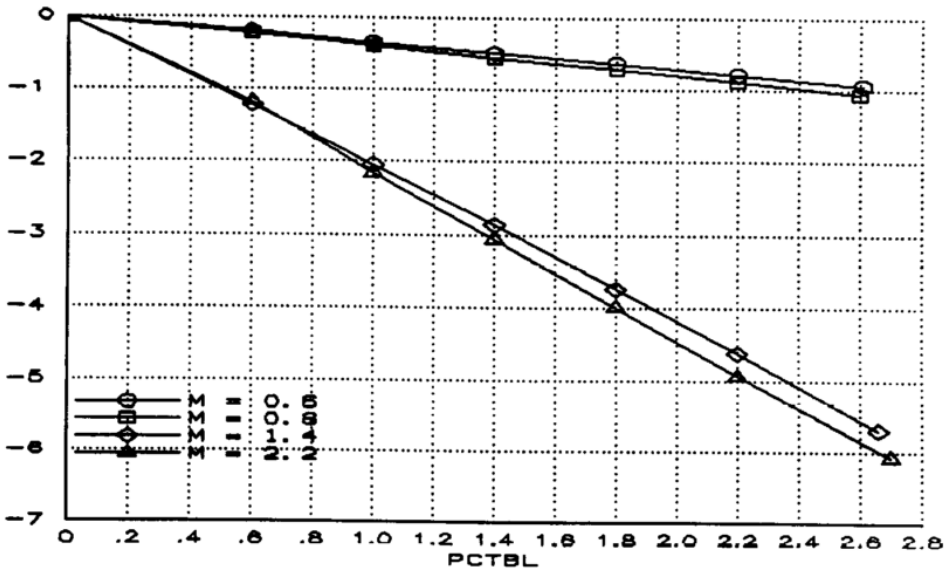

Figure 2-9: Percent change in net thrust per percent of bleed air. Flight case 40,000ft, Power Lever Angle 130º.

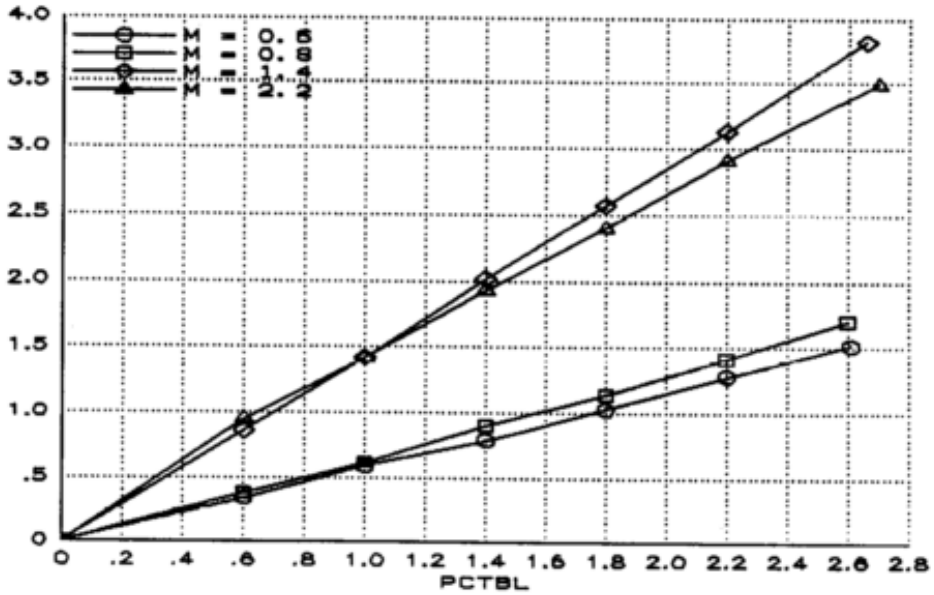

Figure 2-10: Percent change in specific fuel consumption per percent of bleed air. Flight case 40,000ft, Power Lever Angle 130º.

Figure 2-9 and Figure 2-10 show that net thrust decreases linearly with increasing bleed air mass flow rate, while the SFC increases. It is clear that the minimisation of bleed air consumption is desirable for improve speed and range. The path to bleed air minimisation is through the maximisation of the TMS efficiency; that is to achieve the same heat removal at a reduced system inlet enthalpy for energy inputs.

2.4.3. Environmental Control System

The ECS of Figure 2-7 is defined as an open loop Air Cycle Machine (ACM), which is a technology used in the majority of 4th generation fast-jet military airframes. The 5th generation aircraft are moving towards a highly integrated TMS architectures, inclusive of closed loop ACM's, a Vapour Cycle System (VCS), liquid loops and fuel based heat sinks (Sprouse 1996; Baird & Ferentinos 1998; Hitzigrath 1993). The advantage of the traditional 4th generation ACM is the proven reliability of a mature technology. The working fluid is air, which reduces the risk of contaminating the airframe from a system leak. The ECS output is utilised for a number of functions including cooling, oxygen generation, canopy demist, bay pressurisations and anti-G pilot clothing. The low specific heat capacity of air means that a large temperature difference can be achieved with a relatively small heat rejection. In terms of the ACM, a positive temperature difference can be maintained between the bleed and the ram air temperatures regardless of flight or atmospheric condition. As the purpose of the system is to transfer thermal energy out of the airframe, it is fundamental that the temperature delta to atmospheric conditions always remains positive.

The system is relatively simple and comparatively lightweight through the use of a single fluid to complete tasks of cooling, evaporation, pressurisation and oxygen delivery (Moir & Seabridge 2001; RANNENBERG 1969; Rosenbush 1982; Matulich 2011; Hunt et al. 1995; Cronin 2010).

The TMS coolant is ram air through an air-to-air heat exchanger with the bleed air path. The ram air heat exchanger performance (heat rejection and aerodynamic drag) is based on both flight and atmospheric conditions. The heat rejection capability is dependent on ambient temperature, pressure, aerodynamic kinetic heating and aircraft speed. The ram air coolant requires no pumps, pipework or control; however is expensive aerodynamically and in terms of the radar cross section.

The ECS is discussed at a component level in the next section, following the airflow path of Figure 2-7.

2.4.3.1. Bleed Air Pre-Conditioning: Pressure Relief and Shut Off Valve, Venturi and Primary Heat Exchanger

The Pressure Relief and Shut-Off Valve (PRSOV), venturi and primary heat exchanger work to deliver relatively constant downstream airflow characteristics, regardless of the flight condition. The purpose of the three components is to pre-condition the bleed air upstream of the ACM. They effectively act as a thermal and pressurisation plenum, converting a variable input to a constant output. The primary heat exchanger thermally conditions the bleed airflow temperature, with the PRSOV and venturi regulating the pressure and the mass flow.

The BAE Systems Hawk PRSOV performance is detailed in Figure 2-11, regulating an upstream pressure of up to 16.4 Bar.g to a range of 3 to 3.8Bar.g.

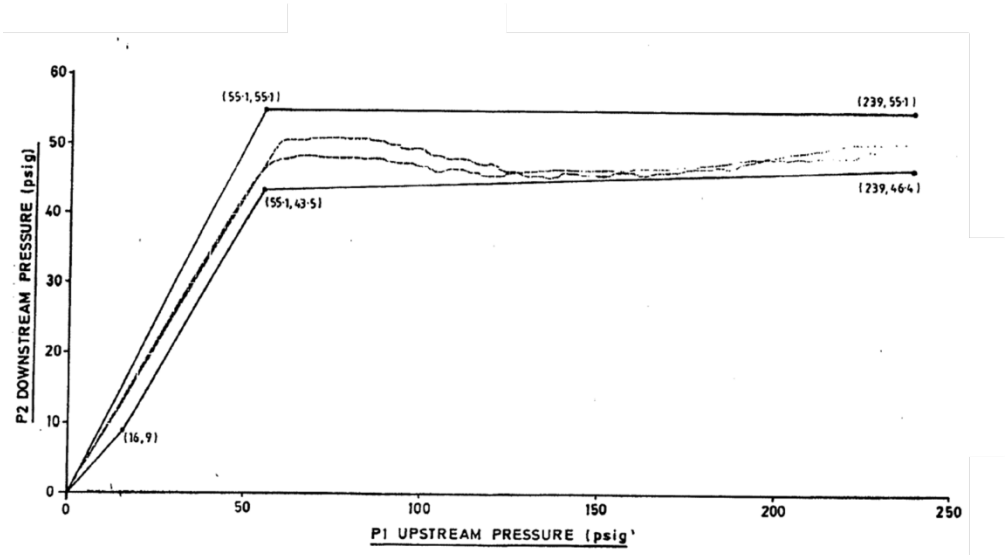

Figure 2-11: BAE Systems Hawk PRSOV performance

The venturi sits downstream of the PRSOV and regulates mass flow rate by controlling the ECS back pressure. The function of PRSOV and venturi is for downstream component protection, to de-couple any dynamic TMS flow conditions from the propulsion system and to shut down the ECS when required. As airflow into the cabin is unfiltered, a typical ECS shutdown would be fume ingress from the propulsion system due to a damaged oil seal.

2.4.3.2. Cold Air Unit

The Cold Air Unit (CAU) is a term for the conditioning pack of the ECS. The simplest CAU is the pre-cooling of bleed air before a single expansion process, known as a turbofan

refrigeration system (referred to as the simple cycle). The work generated by the turbine in the expansion of high pressure air is utilised to produce ram airflow for the pre-cooler heat exchanger, through a fan attached to a common shaft. The conditioning of pack outlet temperature is controlled by the mixing of unconditioned bypass air through a Temperature Control Valve (TCV). The simple cycle can be seen in Figure 2-12.

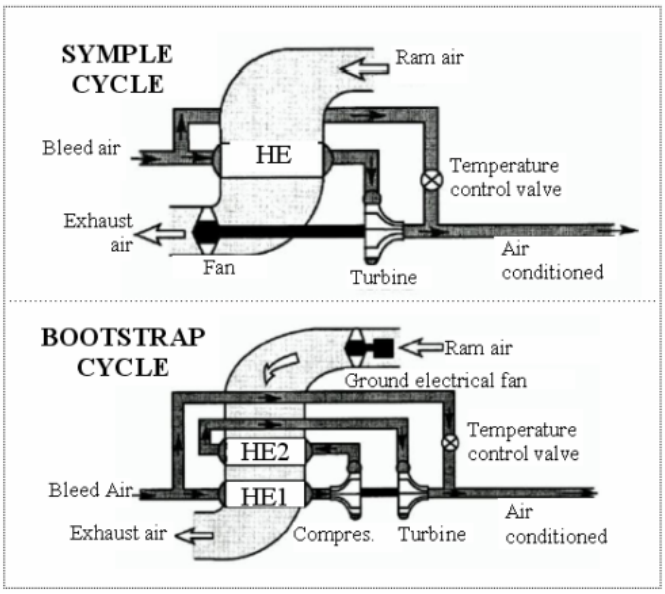

Figure 2-12: Simple Cycle (turbofan cycle) and the bootstrap (Brayton cycle) ACM(Andrade, R & Zaparoli 2004).

The simple cycle exhibits poor thermodynamic efficiency as only a small fraction of the work generated by the turbine is used. Messinger calculated that the shaft power required to condition aircraft loads was only 3.7kW, however 54kW was available at the turbine. It was concluded that a more efficient cycle should be capable of harnessing all available energy transferred from pneumatic expansion (Messinger 1946).

The next generation cold air unit is the bootstrap cycle. The ram air fan is replaced by a compressor to better recover the work produced by the turbine through a secondary compression process. The compression process increases the bleed air temperature and pressure, increasing the temperature difference between the charge air (bleed air) and coolant (ram air) at the heat exchanger and the turbine pressure ratio (Pérez-Grande & Leo 2002; Rogers & Mayhew 1992; Defrancesco 1993).

The commonly used metric of ECS efficiency is the Coefficient of Performance (CoP). CoP is a ratio of the rate of heat extracted against power consumed, as seen in Equation 2-6 (Bejan 1997).

$$CoP = \frac{\dot{Q}_{out}}{\dot{W}_{in}} = \frac{Net\ Useful\ Heat\ Transfer\ Rate}{Total\ Work\ Consumption\ Rate} \quad (2\text{-}6)$$

In this instance, the heat extracted is defined as ECS heat rejection and the total work consumption rate is defined as power consumed in the compression of bleed air. The theoretical efficiency of the turbofan and Brayton cycles can be seen in Figure 2-13. The data shows calculated ECS CoP based engine compressor ratios, for different aircraft types, as stated on the abscissa.

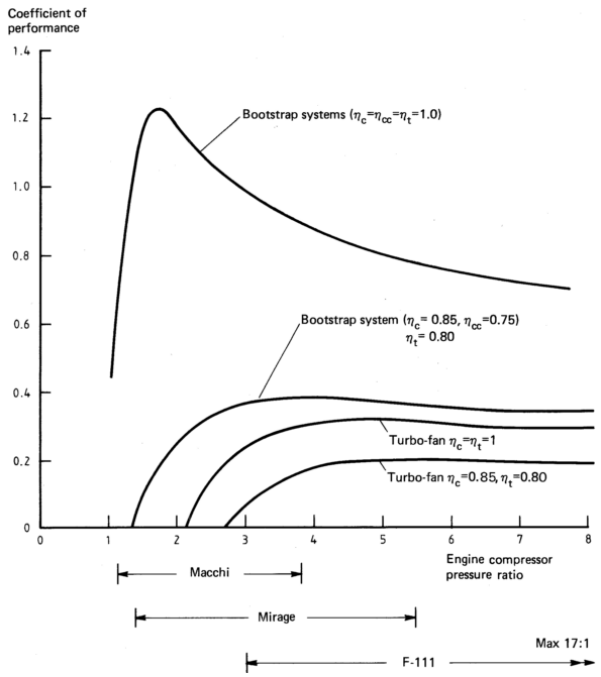

Figure 2-13: CoP of bootstrap and turbofan cycles (Rebbechi 1980).

The CoP of each system should be considered with realistic component efficiencies; an engine compressor efficiency, η_c, of 0.85, a cycle compressor efficiency, η_{cc}, of 0.75 and a turbine efficiency, η_t, of 0.8. The bootstrap cycle operates around twice the CoP of the turbofan cycle based on the compression of dry air. These values of CoP echo other research within this area (Buckingham 1984; Conceição et al. 2007; Matullch 1989). While the bootstrap cycle has a poor CoP, it is still used in the majority of 4th generation fighter jet and commercial aircraft such as the Boeing B747 and B737, Airbus A320, A340 and

A380 and the Embraer EMB120, EMB145 and EMB 170 among others. This popularity is due to the bootstrap cycle being small in size, low in weight, simple in design, low in cost and high in reliability (Conceição et al. 2007).

The general form of the CoP (Equation 2-3) uses the heat absorbed in the numerator. When considering the system in isolation the drag force of the heat exchangers is not considered. Based on literature, to condition a 30kW aircraft heat load, the overall aircraft system penalty is estimated to be around 700kW (300kW bleed air, 400kW ram air drag and system mass)(Rebbechi 1980). The installed system CoP is calculated to be as low as 0.043; therefore 95.7% of the fuel energy consumed in bleed air compression is not recovered. The coupling of this information with the effect of bleed air consumption on net thrust and specific fuel consumption (detailed in Figure 2-9 and Figure 2-10) highlights the criticality of this research area.

2.4.3.3. Water Separation

The control of the condensate in cabin and equipment airflow in a fast jet military aircraft is the remit of the ECS. While there is no specific control over the cabin and equipment air absolute humidity, the requirement is to ensure that any water content remains in gaseous form (Matulich 2011). The ingress of free water in the cabin environment leads to increased risk of component corrosion, micro-organism growth and difficulty in de-mist of the canopy. Free water within the equipment airflow poses a serious risk to the avionic component reliability. While the architecture of each avionic module is dependent on component power density, some modules have a direct contact between the cooling airflow and active circuit cards (Strattan 1983).

A case study of 4th generation bleed air water extraction is the F-15. This aircraft originally featured a Low Pressure Water Extractor (LPWE) and was later fitted with a High Pressure Water Extractor (HPWE) while in service (Dieckmann 1988; Cole 1974). The LPWE is downstream of the turbine and the HPWE is upstream of the turbine, as seen in Figure 2-14.

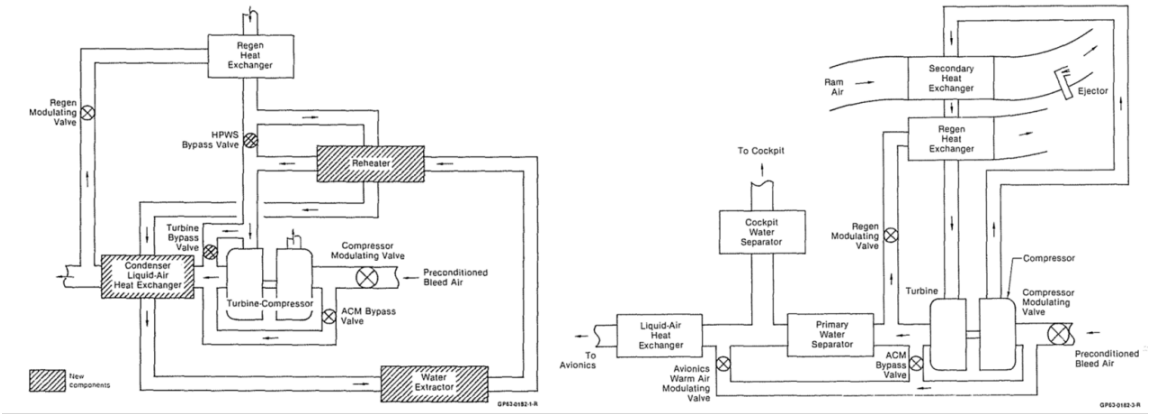

Figure 2-14: HPWS and LPWE of the F-15

The LPWE works by two processes, a water separation and a water extraction process. The water separation is achieved by lowering the airflow temperature below its dew point by expansion through the turbine. The water content is released from its gaseous form as pure condensate (Lawrence 2005). The water extraction process consists of collecting the moisture over a coalescing element to amalgamate the condensate into larger droplets. The large droplets are then simply centrifuged from the airflow and removed by a gravitational drain (Fourquet et al. 2000). However, the LPWE process is inefficient and some water remains within the flow. In order to prevent unwanted condensate from entering the avionic subsystem, the 'avionics warm air modulating valve' opens to heat the airflow and evaporate the remaining condensate. The avionic supply air is controlled to 28ºC from 0ft to 34,200ft, where the control is reduced to 11ºC on account of the low atmospheric humidity at this high altitude. This temperature schedule was found to be conservative and was subsequently updated, as seen in Figure 2-15. The updated temperature schedule generated an additional 7kW of cooling capacity (Ryan 1990).

The requirement to heat avionic supply air due to poor water separation efficiency is thermodynamically wasteful to the system and reduces the avionic heat rejection capability. The solution is to move the water extractor to the high pressure region of the system (pre turbine). Relative humidity is determined by the total and saturation pressure of a mixture. As the total pressure increases, the capability of the air to hold moisture as vapour reduces and condensate is produced more readily. The HPWE utilises an additional regenerative heat exchanger in the high pressure region of the cycle to reduce airflow

temperature and water droplets are formed on the fins of a condenser. The water droplets are then removed by a swirl-type extractor. The HPWE process is up to 95% efficient as drier air can be expanded across the turbine to a much lower temperature than humid air(Dieckmann et al. 1986). The expansion of dried air reduces the risk of ice formation which could potentially damage the turbine blades and negates moisture ingress to the avionic subsystem at low airflow temperatures. The addition of HPWE and updated temperature schedule increased avionic heat rejection capability by 15kW over the baseline ECS.

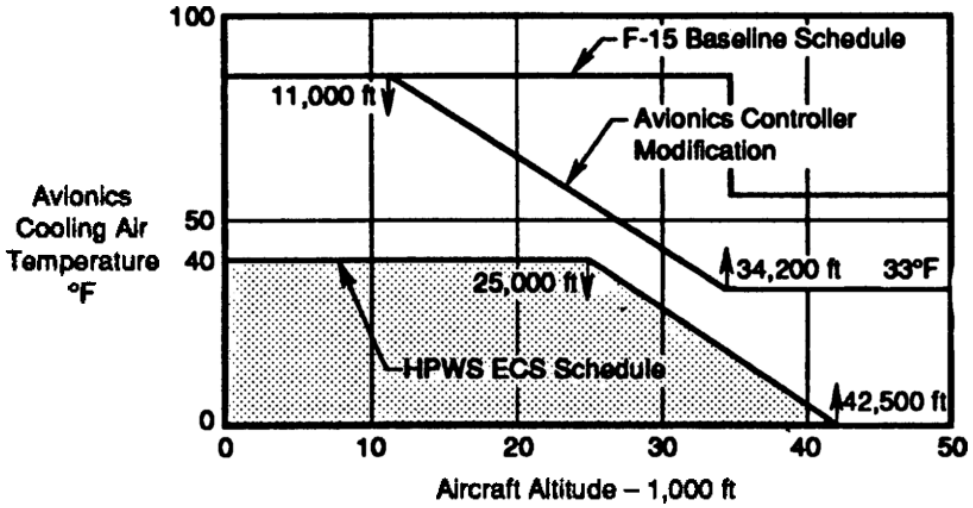

Figure 2-15: F-15 LPWE avionic supply temperature schedule(Ryan 1990).

2.4.3.4. System Temperature Control

The Hawk ECS temperature control of the system is through Temperature Control Valves (TCVs). The TCV allows hot airflow to bypass the Cold Air Unit (CAU) to achieve a demanded temperature downstream. The CAU heat rejection is a function of the bleed air pressure (dependent on the flight condition) and of the heat exchanger heat rejection (dependent on the flight condition). The ACM has no active throttle but uses bypass airflow to control the air temperature downstream. The bypass flow works in two processes. Firstly, by adding heat to the cooled airflow and secondly by reducing the CAU pressure ratio for a given bleed air condition. The two functions work simultaneously to reduce the heat rejection capability of the bootstrap cycle as required.

In the equipment detailed in Figure 2-7, the ECS has two temperature control valves, one for the equipment and one for the cabin feed. The equipment feed is maintained between

0ºC and 4ºC by the Equipment Temperature Control Valve (ETCV) with a temperature feedback at the water extractor exhaust. The temperature control valve has two main purposes, maintain a cooling capacity for aircraft equipment heat loads and maintain favourable airflow characteristics for water extraction. The ETCV position (equipment temperature bypass flow rate) is automatically maintained by the ECS control system with no pilot interface.

The cabin supply temperature is controlled by the Cabin Temperature Control Valve (CTCV) with a temperature feedback in the cabin supply pipe and in the cabin foot well. The bypass controls the fluid temperature by the same process as the ETCV, however the output is pilot controlled. The pilot is able to command a cabin temperature, or manually drive a valve position. The position of the TCVs are not actually measured by the ECS and the control system regulates bypass airflow to achieve a downstream temperature. As both control valves operate on one fluid stream, the ETCV duty cycle is around 10% of the CTCV, which is constantly variable.

2.4.4. Avionic Subsystem

The term avionics is the amalgamation of aviation-electronics and categorises all electronic systems used for navigation, communications, flight control, weapons and data acquisition. Currently, around half of the aerospace industry's turnover is related to avionics and this is expected to continue to rise (Chen 2007). The avionic cooling airflow is provided from the equipment branch of the ECS subsystem.

2.4.4.1. Forced Convection Modules

The computational power of aircraft dramatically increased with the boom of 4th Generation fighter aircraft to facilitate the introduction of new airframe technology (low observability aircraft such as the F117 or B2 bomber) and new airframe capabilities in terms of communications, weapons systems and navigation (Crickmore et al. 2014). The United States Air Force Aeronautical Systems Division (USAF-ASD) launched a project to standardise the avionic housing (Strattan 1983; Franklin & Kramer 1982; Franklin & Charles 1983). A guideline for cooling capacity, allowable junction temperatures, operating air flow temperatures and module pressure drop was developed to provide a standardised operating environment for electronic equipment. The avionic module heat rejection

architecture was also standardised following thermodynamic studies. Three main avionic module architectures were considered; Air Impingement Cooling, Conduction to Cold Wall Cooling and Flow-Through Cooling.

Air Impingement cooling is the simplest design, where cooling airflow is directed across the avionic circuit cards (Strattan 1983). This design is of poor heat removal efficiency as the thermal resistance between the cooling fluid and the active electronics is high. Impingement cooling suffers from the contamination of the cooling fluid with moisture, sand and runway debris which can lead to problems with corrosion and condensation, causing the premature failure of electronic units (Jones & Chen 2015).

The flow through cooling utilises the chassis as air plenums directing airflow through the centre of the circuit card, allowing the minimisation of thermal resistance as the cooling air acts directly underneath the active components. Although this is the most complicated and financially expensive option, it is the most thermodynamically efficient. However, the geometrically small flow paths can become blocked, raising reliability concerns. It features no direct thermal coupling between the active components and avionic chassis heat exchanger; therefore it is very sensitive to a reduction in cooling mass flow rate and demonstrates extremely poor performance in natural convection conditions.

Conduction to cold wall cooling employs heat exchangers in the chassis to generate a cold wall which the circuit cards are thermally coupled to (Franklin & Kramer 1982). The ability of this design to remove heat from the card is based on the thermal conductance of the wall material and the chassis heat exchanger efficiency. A typical conduction to cold wall module architecture is seen in Figure 2-16. This design was adopted for the standardised forced air cooled avionic experiments. It was concluded that air impingement was too inefficient and risked contamination, while flow through cooling determined too complex, expensive and unreliable.

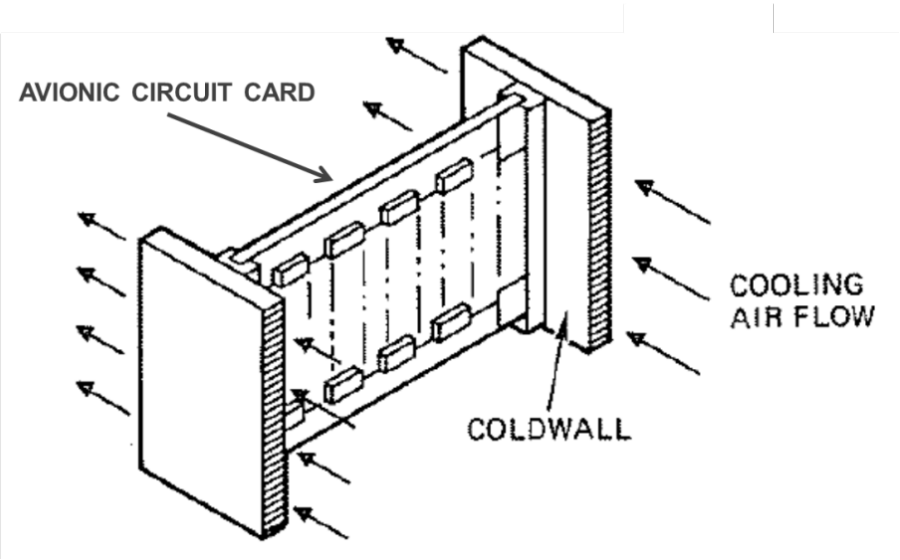

Figure 2-16: Conduction to cold wall avionics module

The conduction to a cold wall chassis remains the aviation industry standard due to the reliability, weight, cost, failsafe performance and simplicity of this heat removal technique. Air is deemed a reliable coolant as the penalty of a system leak within the airframe is minimised and during a TMS failure additional airflow can be supplied from the ambient environment. Conduction to cold wall modules have no direct contact between the coolant and active avionic components, negating contamination. The modules feature a low Fins per Inch (FPI) straight channel heat exchanger, reducing pressure drop and minimising the risk of the fins clogging up. The active components are physically coupled to the heat exchanger wall to provide some heat rejection at natural convection and reduced flow rate conditions. It is an essential criterion that the avionics must operate with a reduced airflow supply; since in the event of an ECS failure, the pilot, cabin environment and flight critical components are prioritised (Strattan 1983; Cirrito 1982; Franklin & Kramer 1982; Zentner & Kramer 2010).

All forced convection avionic modules in this study are assumed to be conduction to cold wall type. A genuine ½ Air Transport Rack (ATR) condition to cold wall chassis mounted to a Typhoon avionics tray is seen in Figure 2-17. The ATR sizing is a standardised avionic module sizing convection. This equipment was donated by BAE Systems and forms part of the experimental facilities discussed in Chapter 4.

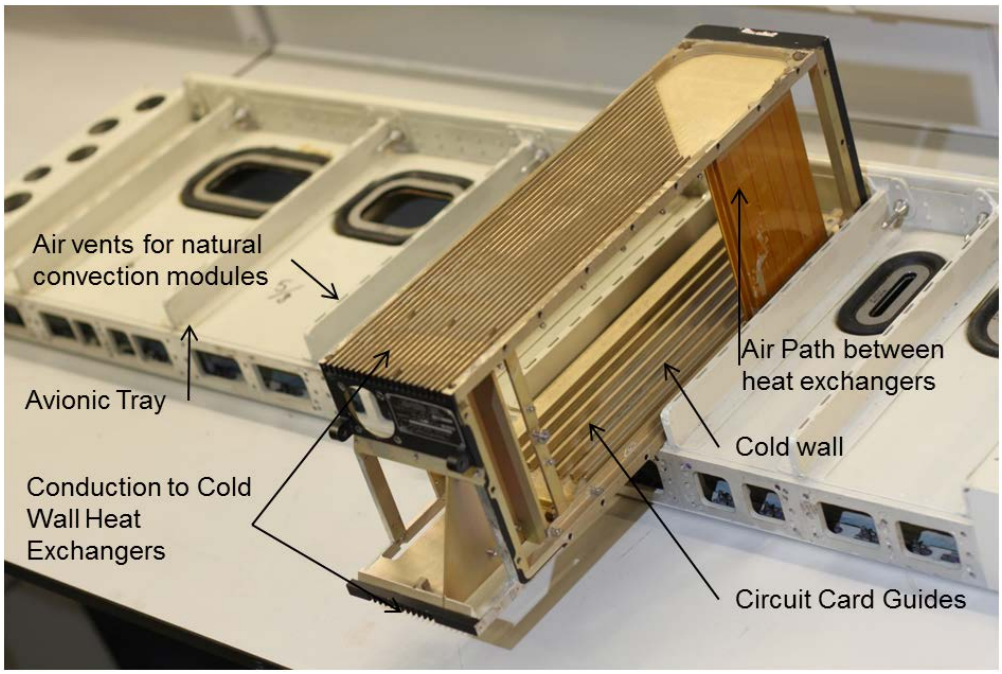

Figure 2-17: Avionic chassis and avionic tray at Loughborough University.

Airflow enters the avionic tray and the flow rate supplied to each avionic module is based on the avionic power output. The avionic module back pressure is calibrated to provide a passive mass flowrate distribution across the tray. The airflow enters the avionic module from the front and is split between a top and a bottom heat exchanger. The circuit cards are coupled to the cold wall by slotting them through the guides seen in Figure 2-17. The avionic tray is located within an avionics bay, which could typically house 40 to 50 modules in total.

2.4.4.2. Natural Convection Modules

Low power density avionic modules are cooled by natural convection. The modules are located within the avionics bay and have no chassis heat exchangers or internal airflow. Circuit cards are coupled to the module wall, which is cooled by the convection air currents inside the avionics bay.

Provisions for natural convection module cooling can be seen in Figure 2-17, through a number of 'piccolo' holes in the spine of the tray between module mounting locations. These allow airflow to condition the external wall of each module. The advantage of this design is a passive cooling technique and high reliability; however it is limited to modules in which the power density is very low.

2.4.4.3. Thermal Design Limits

The thermal design limits are shown in Table 2-1. This presents avionic bay temperatures depending on altitude and operational condition. The data is provided by the BAE Systems Environmental Handbook.

Altitude	In-Flight		Ground Soak			
			Operating		Non-Operating	
	AV Bay Max (ºC)	AV Bay Min (ºC)	AV Bay Max (ºC)	AV Bay Min (ºC)	AV Bay Max (ºC)	AV Bay Min (ºC)
Sea Level	70	-31	70	-31	90	-33
25,000 ft	58	-40				
40,000 ft	40	-40				
55,000 ft	20	-40				

Table 2-1: Avionic thermal design limits with aircraft altitude and operating condition (Pearson & McCoy 2011).

2.4.5. Avionic Bay

The avionics bay has three heat loads applied to it; avionic, Q_{AV} , kinetic, $Q_{Kinetic}$, and solar, Q_{Solar} . The kinetic thermal loading is defined in Section 2.3.2. The avionic heat loads are assumed constant throughout the flight (Pearson & McCoy 2011).

$$Q_{AV.Bay} = Q_{AV} + Q_{Kinetic} + Q_{Solar} \tag{2-7}$$

The solar heat load is dependent on the flight and atmospheric conditions. The relationship of solar radiation intensity against altitude is given in Figure 2-18. Solar loading is calculated as a function of the panel transmittance,τ, heat transfer surface area, A_s, and solar radiation intensity,$\dot{Q_{sl}}$; as follows.

$$Q_{solar} = \dot{Q_{sl}} A_s \tau \tag{2-8}$$

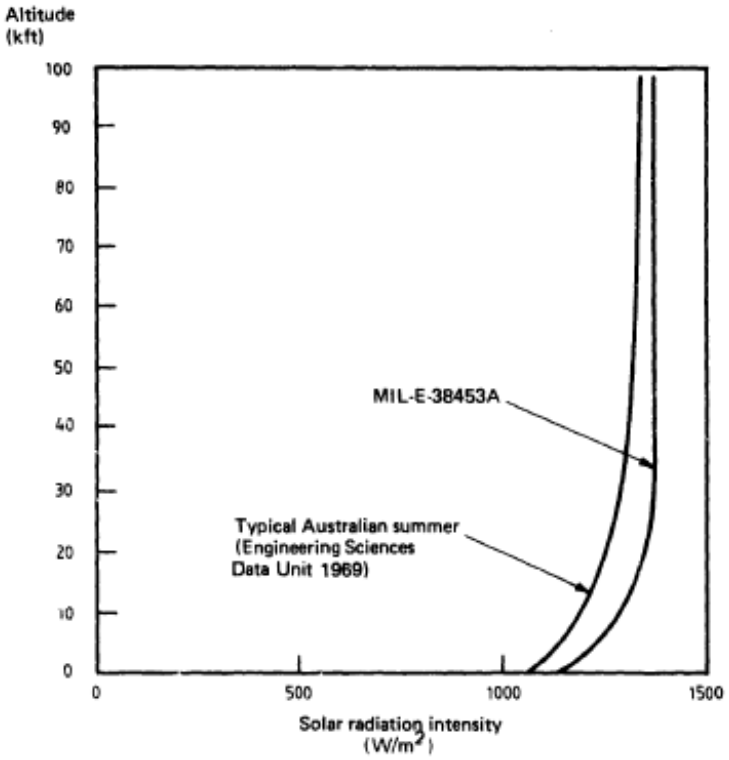

Figure 2-18: Solar radiation against Altitude (Rebbechi 1980).

2.4.5.1. Avionic Module Heat Loads

Avionic thermal loads arise from the waste heat generation as a function of electronic component operation. The power density of each circuit card is matched to the size and heat rejection capability of the module. A thermal image of an avionic circuit card is given in Figure 2-19 (Campo et al. 2014). The modelled circuit card is aluminium in construction and the heat rejection process is by liquid edge cooling. This is a similar heat removal process to the conduction to cold wall, however a liquid coolant is used. It can be seen that the peak temperature is in the centre of the card at 137ºC, with the cold wall maintained at 85ºC.

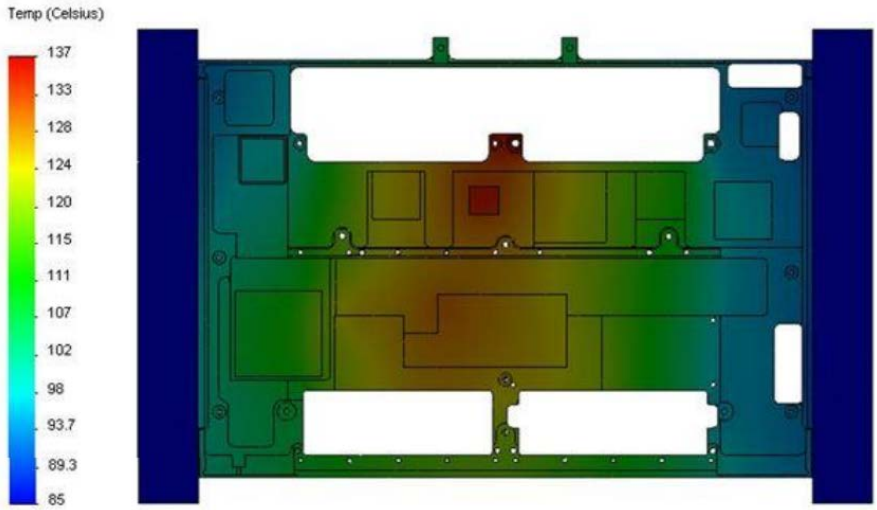

Figure 2-19: Thermal simulation of aluminium conduction card (Campo et al. 2014)**.**

The thermal distribution in Figure 2-19 highlights the difficulty of avionic thermal management. The airframe manufacturer is able to measure coolant and cold wall temperature, with limited visibility of isolated internal conditions.

2.4.5.2. Thermal Failure

The difficulty in avionic thermal management is exacerbated as computational power has continued to increase from the 1980s at the rate predicted by Moore's Law, which states that the number of transistors on an integrated circuit board will double every two years (Schaller 1997). The combination of reduced size and increased power output through the microminiaturisation of electronic components has produced a dramatic increase in power density and in operating temperatures (Arwidson & Arwidson 2013). A concurrent increase in component failures has been reported (Johansson & Leisner 2012; Pearson & McCoy 2011). However, avionic failure is difficult to diagnose, it often presents minimal irreversible damage and it is clouded by the frequency of No Fault Found (NFF) failures.

A NFF failure is categorised as an operational failure that cannot be replicated or isolated in further testing or component analysis. This phenomenon is a serious consideration in the aerospace industry, with 67% of F-16 radar failures being NFF. The aeronautical industry incurs costs of over $10,000,000 each year in exchanging avionic units due to this failure mechanism (Steadman et al. 2002). It has been reported that NFF failures are responsible for contributing to more than 85% of all observed operational failures in aircraft electronics (Söderholm 2007).

'Avionic failures are totally random and can be seen in any flight conditions. The problem is that failure due to overheating is not apparent to the immediate maintenance crew. Overheating damage that may cause a failure will only be visible when the equipment goes back for repair and the covers are off. Of course, in a NFF situation, there may be no visible evidence at all, as the overheat was transient and left no trace.' Angus Murray, Lead Reliability Specialist within Military Air & Information, BAE Systems.

Williams et al. 1998, showed that thermal cycling close to the operational limits of the equipment produced failures which would have been categorised as NFF upon further component analysis. It has also been found that continued operational cycling of avionic components above the thermal design limit leads to an exponential decay in component reliability (MIL-E-85726 1986). It can be concluded that thermal failures of avionic components are a contributing factor to the NFF phenomenon.

2.4.6. Cabin Environment

The cabin environment is featured in this work under the requirement to consider aircraft thermal loading in a more holistic manner and not to directly optimise this subsystem. The main supply of cabin conditioning airflow is split between the canopy demist and the pilot cooling functions. The two flow paths can be seen in Figure 2-20, where the upper flow path features piccolo holes for canopy demist and the lower airflow path provides pilot cooling.

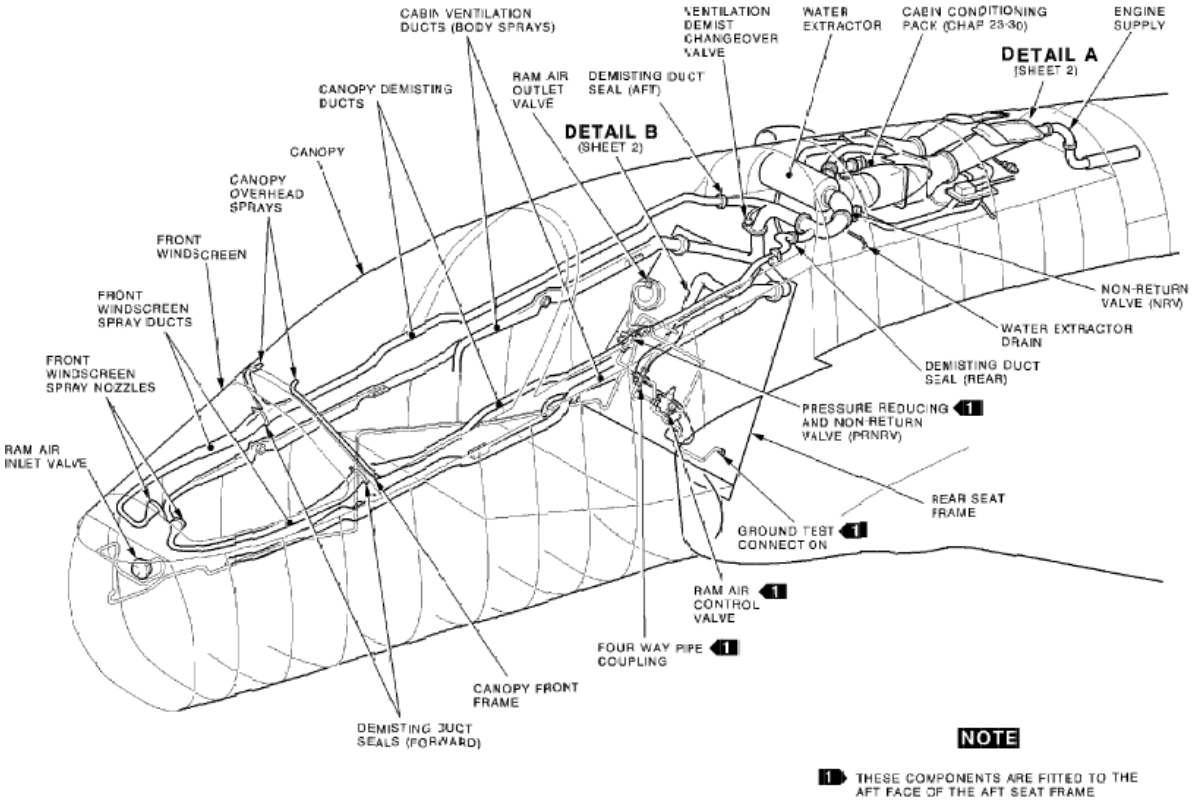

Figure 2-20: BAE Systems Hawk cabin airflow supply (BAE Systems 2007)**.**

The canopy demist is a vital function of the cabin environment, as condensate can accumulate on the aircraft canopy obscuring the pilot's vision. The worst case scenario is a transient 'accelerate and dive' condition. Following a high altitude cruise, the canopy becomes very cold due to the low ambient temperatures. As the aircraft dives into a hot humid atmosphere, the canopy takes longer to warm up due to the thermal inertia of the thick panel. The pilot has a number of controls for rapid de-mist, however these are typically power hungry on ECS air supply or on the electrical power supply (in the case of a heated screen) (Matulich 2011).

The cabin total thermal loads, Q_{Cab}, is the sum of an avionic, kinetic, pilot, Q_{Pilot}, and solar loads.

$$Q_{Cab} = Q_{C.AV} + Q_{Kinetic} + Q_{Solar} + Q_{Pilot} \tag{2-9}$$

The cabin avionic heat load is fixed throughout the flight. Cabin solar loading is the highest of all bays in the aircraft due to the large surface area of the transparencies. The pilot heat load, Q_{pilot}, is a product of metabolic heat flux rates, q_{met}, and of the pilot surface area, A_p.

$$Q_{pilot} = q_{met} A_p \quad (2\text{-}10)$$

It is assumed the average pilot has a surface area of 1.8m² and a typical metabolic heat flux rate of 3.9mL/kg.min throughout the duration of a fast jet military flight (Rossato et al. 2014; Lee et al. 2013). The metabolic heat flux rate is an average of measurements taken across two test flights, where pilot heart rate was found to range between from 100bpm to 165bpm. While a small variation in pilot work rate is expected, the metabolic heat flux rate is assumed constant throughout the flight envelope.

2.4.6.1. Additional Bleed Air Consumption

In addition to thermal conditioning, the pneumatic energy from ECS is utilised for a number of low-flow and non-flow purposes. The cabin pressurisation is achieved by regulation of the cabin exhaust airflow. An example fast-jet cabin pressure control characteristic is provided in Figure 2-21. A commercial airliner pressurises the cabin environment to 6000ft above sea level for the complete flight envelope above this altitude (Hunt et al. 1995). A military aircraft pressurises to around 6000ft below its current altitude, to reduce the pressure differential if the cabin were to be damaged and the pressurisation lost.

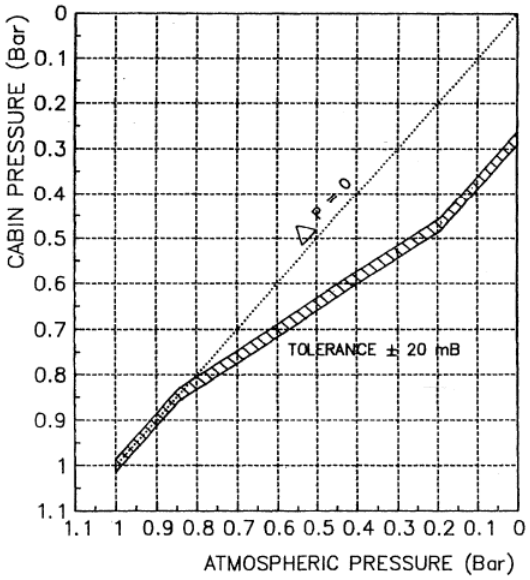

Figure 2-21: Cabin pressurisation control for BAE Systems Hawk (Molyneaux, A et al. 1997)***.***

The canopy seal is pressurised by ECS exhaust airflow as a non-flow process. The pilots anti G suit takes a feed of bleed air to provide compression to the legs and reduce pooling of

the blood in extremities during positive G manoeuvres. The pilots seat is mounted on a spring and coupled to a needle valve for airflow control into the anti g suit. The higher the positive G, the greater the compression through the seat. This increases the valve opening and the suit pressurisation. Bleed air is utilised for the on-board oxygen generation system (OBNOGS), passing flow through a molecular sieve to generate a supply of oxygen.

2.5. Generation of Unknown System Behaviour

The individual subsystems of Figure 2-7 have been discussed in isolation. At the operational level, the TMS operates as a single airflow path. It has been found that, when the individually designed components are coupled into a single airflow path and are operating simultaneously, unforeseen subsystem interactions can generate unexpected thermal behaviours. In this case, this generates unknown thermal conditions of the avionics bay and of the avionic modules.

The following section details the unknown system behaviour of 4th Generation aircraft. This section will discuss how the design, development and operation of the TMS led to the generation of this behaviour. The structure of the analysis will follow the flow chart presented in Figure 2-22; initially detailing the operational contribution and the moving on the design process influence. The flow chart of Figure 2-22 is discussed with the application of relevant aircraft case studies. This behaviour is well defined, but it is not well understood due to the typical industrial constraints (financial, political and time) on implementing a dedicated investigation to better define the thermal relationships. The pragmatic industrial response is to apply additional safety factors to cooling demand, generating a system of high reliability and low thermal efficiency.

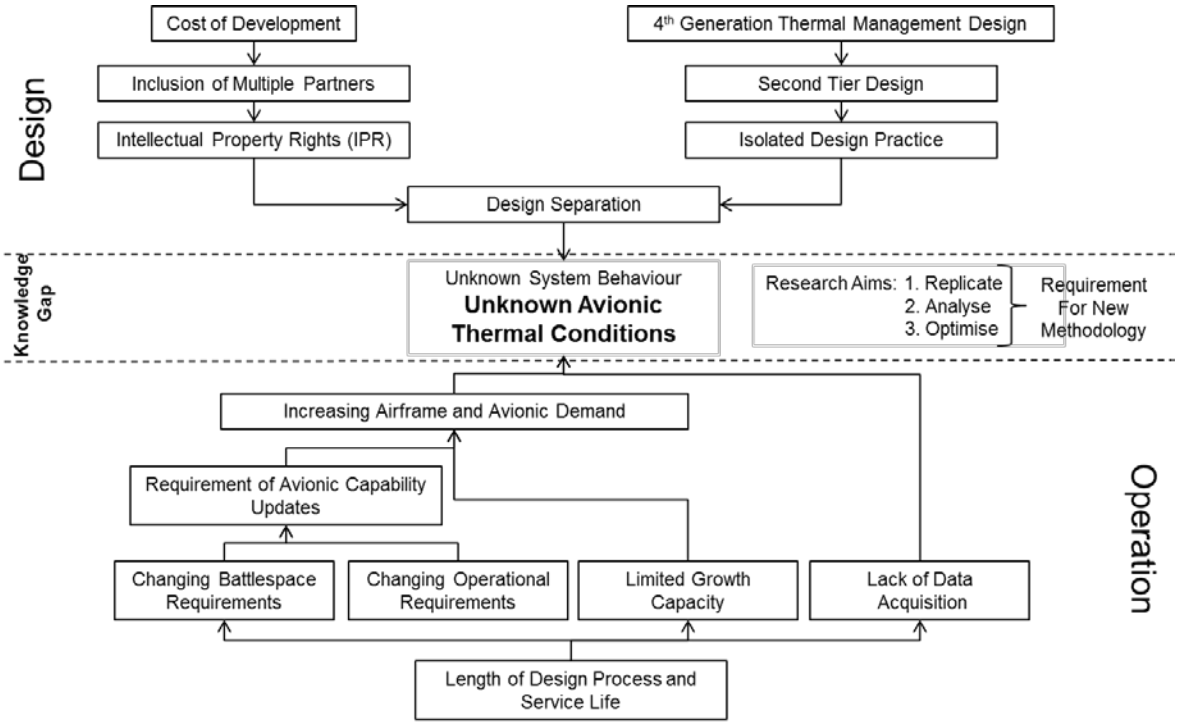

Figure 2-22: A flow chart to describe the generation of unknown system behaviour.

Each flow chart block is analysed in detail in the following sections to provide the reader with an understanding of the constraints of the aeronautical industry. For ease of document navigation, the following section headings match those of Figure 2-22.

The constraints are the combination of scientific, technological, organisational, political, and financial factors. The development of a new methodology to fill the knowledge gap by replication, analysis, and optimisation of in-flight conditions requires an understanding of the existing difficulties. Through the analysis of the current approach, a future direction can be determined.

It is critical to develop an understanding of the industrial constraints on the development of a thermodynamic solution for improving the avionic thermal management. A number of optimisation technologies are suggested later in this thesis (Chapter 6) and these have been determined to work within the constraints of the aeronautical industry. The technologies must be minimally disruptive and operate within the aircraft operational framework discussed in the following sections. Due to the criticality of industrial constraints on both the development of a thermodynamic issue and on its subsequent

resolution, considerable time is spent to illustrate current trade practice through the remainder of this Chapter.

2.6. Operational Contribution

The operational contribution is fundamentally based on the timeframe of the aircraft design and operation.

2.6.1. Length of Design Process and Service Life

The 4TH generation F-15, F-16, F-18, Typhoon and Tornado are all expected to be in service for at least four decades and some in excess of five decades. The Typhoon was introduced in 2003, however the origins can be traced back to a technology demonstrator aircraft, the Experimental Aircraft Programme. The EAP design work started in the late 1970s. The 2015 UK Strategic Defence and Security Review (SDSR) spending review recently extended the Royal Air Force Typhoon service to at least 2040 (HM Government 2015). It is interesting to note that the airframe life cycle is longer than the typical engineer length of service, leading the requirement of having new staff taking over the servicing of aircraft.

The increasing length of the airframe life cycle is primarily a cost reduction exercise, to maximise the use of large upfront investment in design. However, a number of technical challenges develop from the need to maintain the currency of aircraft capabilities and integrate emerging technologies. These challenges need to be met to ensure the aircraft can remain effective against changing battlespace requirements and changing operational requirements across its lifecycle.

2.6.2. Changing Battlespace Operations

The worldwide political structure and subsequent military battlespace requirements will change over the lifecycle of an aircraft. For example, the F-22 (a 5th generation aircraft) and Typhoon were primarily designed for a Soviet Union enemy, which is a capability that is no longer required. In the case of the F-22, the Concept Development Investigation (CDI) phase began in 1970. This process took 13 years to develop the technological capabilities with which to build the next generation aircraft and understand future battlespace requirements. During the CDI phase, it was noted that the aircraft should be able to

operate at a high altitudes (50,000ft to 65,000ft) and supersonic speeds (Mach 1.6 to 2.2) specifically to avoid the primary threat of new-generation Soviet Surface to Air Missiles (SAMs). In 1979 (9 years in to the project), the aircraft requirements were modified in response to two new Soviet Union test aircraft spotted at the Ramenskoye test facility at Zhukovskiy (near Moscow). When the F-22 was launched in 2005, the threat from Soviet Union aircraft was no longer present and the main battlespace had shifted to providing fast-air support to ground troops in the Middle East (Diermen 2015).

2.6.3. Changing Operational Requirements

As the battlespace requirements change over time, the role of an aircraft within an air force changes. To facilitate this, the fast-jet military aircraft is increasingly becoming 'multi-role' or 'swing-role'. Multi-role is a category of airframes that can perform three main sorties; air superiority, bombing and reconnaissance duties. A multi-role aircraft will return to base where operationally specific equipment is fitted. A swing-role aircraft can change its mission profile whilst airborne. The driving force for multi and swing-role aircraft is the ability to perform the three main aerial functions with a single airframe, which represents a further cost reduction exercise.

Considering the RAF Typhoon and Tornado platforms, the Typhoon was originally designed as a pure air superiority aircraft for the purpose of intercepting enemy aircraft and for air-to-air combat. As the aircraft aerial capability was prioritised, a key performance requirement was that the total vehicle weight should be no more than 10 tonnes. Multi-role capabilities were ruled out as the design compromises that would have been required to achieve this would have carried a weight penalty.

The Tornado was designed as a multi-role aircraft and is now used for precision airstrikes (air-to-ground), surveillance and fast-air ground troop support. The Tornado will be retired by 2019 (Kelly 2015). Beyond 2019, the Typhoon will be required to perform the duties of Tornado and the capabilities must be matched to that of the outgoing aircraft. As an aircraft evolves and its primary function changes (as a fighter transitions towards a bomber), the avionic heat loads continue to increase according to the trend of Figure 2-23.

The increased capability is achieved through the introduction of retrospective avionic updates.

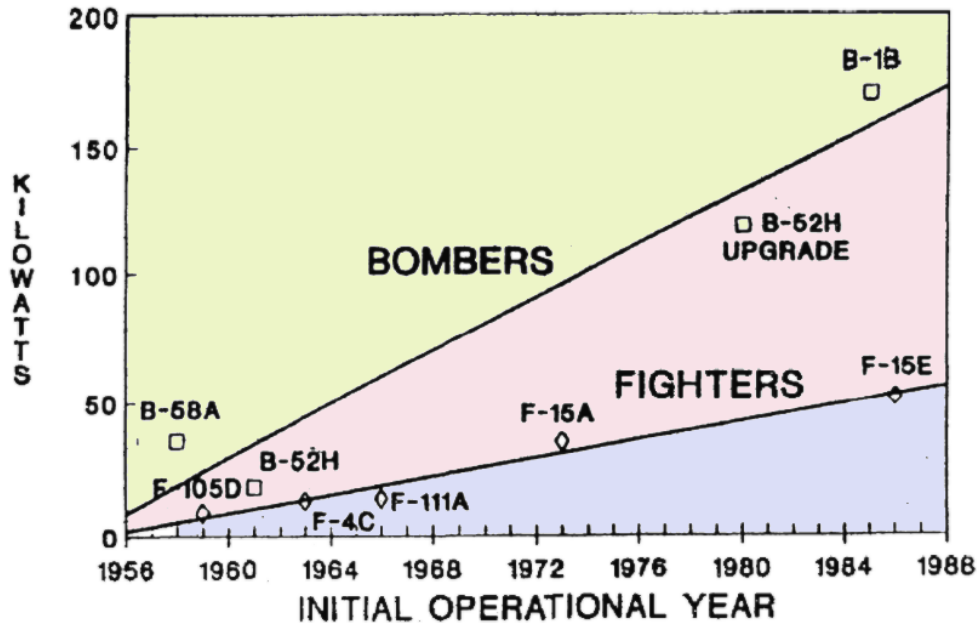

Figure 2-23: Increasing avionic heat loads from chronological and operational demands (Dexter et al. 1990).

2.6.4. Requirement for Avionic Capability Updates

The combination of the changing battlespace environment, changing aircraft operational requirements and unforeseen technological advances forces the airframe manufacturer to offer avionic capability updates. The Typhoon is currently undergoing the Phase Enhancement programme to achieve the required capability upgrades. The BAE Systems Phase Enhancement infographic is seen in Figure 2-24 (BAE Systems 2015).

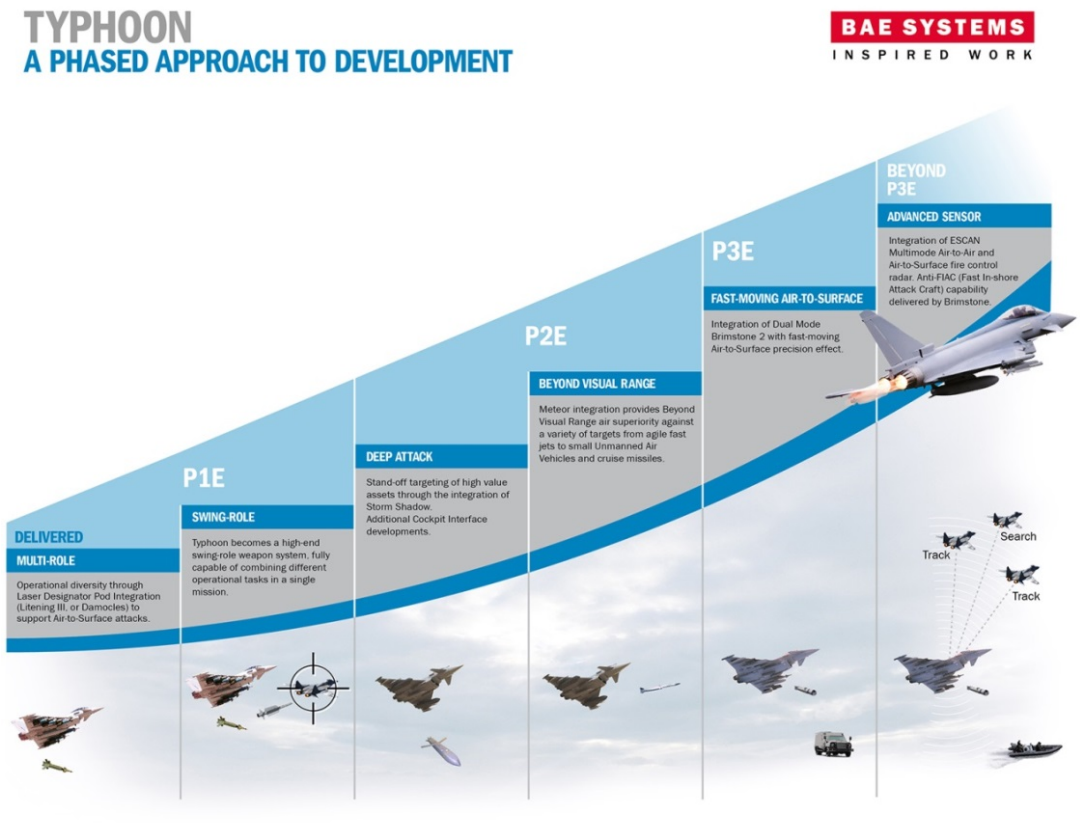

Figure 2-24: Typhoon Phase Enhancement Program (BAE Systems 2015)***.***

At the completion of the Phase Enhancement programme, Typhoon will feature a ESCAN radar (substantial additional cooling requirement), will support the Brimstone 2 missile (additional avionic cooling requirement), will feature the Litening 3 communications pod (additional avionic heat rejection), will support the Storm Shadow missile (additional avionic heat rejection) and Paveway IV missile (additional avionic heat rejection). The aircraft heat loads increase with increasing capabilities, however the TMS remains largely unchanged due cost and time demands. The TMS is a highly integrated system which links the propulsion, fuel, aerodynamic, cabin, avionic, power generation and additional equipment subsystems. An increase in TMS cooling capacity cannot be achieved in isolation, and therefore the aircraft relies on a 'Growth Capacity' to accommodate the additional avionic heat loads. Growth capacity is defined as an allowable thermal loading growth designed into the system by the underutilisation of spatial and cooling supply at the aircraft introduction to active service.

2.6.5. Limited Growth Capacity

The problem of growth capacity is that it is a limited resource. In the case of the Typhoon, additional cooling demands increase aerodynamic drag and aircraft weight. In order to maintain its effectiveness as an air superiority platform, additional weight and aerodynamic drag are minimised on Typhoon. The in-service avionic growth was estimated at 25%, however, the actual requirement is understood to be in the region of 100%. Engineers now understand that the avionics growth was underspecified at the design stage. When considering 4th generation aircraft, the avionic growth capacity problem arose due to the unforeseen increase of computational technology.

2.6.6. Lack of Data Acquisition

An additional difficulty specific of the 4th generation aircraft is their minimal condition-monitoring data acquisition capability. The lack of mission data is a critical component to the generation of unknown system behaviour. Data acquisition capability is not typically retrospectively introduced due to the cost of re-certification. It is considered the lack of data acquisition capability is the primary legacy based difficulty facing 4th generation aircraft over the next 20-30 years of operation. At the time of design, condition-monitoring data acquisition equipment was an immature technology, unreliable, complex and heavy, hence it was not adopted.

The lack of flight data increases the engineer's reliance on partially validated thermal models. The BAE System Hawk ECS performance was primarily analysed using a one-dimensional thermodynamic simulation code, MSC Easy 5. Easy 5 was originally written by Boeing for the simulation of ECS and has since been used for the ECS simulation of the F-14, the Hawk and the Gripen (Jones et al. 2015; Hoffman 1985; Stow et al. 2006). The Hawk Easy 5 ECS model was validated by two processes, firstly at component level by a number of isolated bench tests (Molyneaux, A et al. 1997). This included heat exchanger, turbo-machinery and valve response mapping. The individual components were combined in the simulation and the system modelling results were validated against two ground-test operating conditions; the ground test case was chosen due to the ease of data capture. The model was validated to a typical accuracy of under 5% error in these ground tests (Stow et al. 2006). The flight and atmospheric envelope was split into 46 steady state flight

conditions and fewer than 5% of test cases were validated against full-scale experimental data. The model was not validated against transient behaviours. However, once the model was officially signed off, it became the engineer's main system analysis tool for future studies due to the prohibitive costs of further experimental validation.

The high reliance on steady-state analytical tools reflects the desire to reduce the experimental footprint, however this can limit the engineer's ability to explain and anticipate the dynamic system performance (Letlow & Jenkins 1998). Critical system behaviour can be missed and often only discovered when the aircraft begins flight tests. Lessons learned from the F-22 stated that there is a "critical need for analytical tools and methods to assess the performance of the total integrated system. The complexity and criticality of many sub-system interfaces make it imperative that performance studies and assessments are made at vehicle level rather than subsystem level"(Letlow & Jenkins 1998).

2.6.7. Increasing Airframe and Avionic Demands

The lower section of Figure 2-22 can be read as follows, the combination of changing battlespace operations and operational demands leads to a requirement for retrospective upgrades. The limited growth capability and inability to attain further cooling capacity combined leads to a saturation of the system heat rejection performance. A lack of system performance visibility due to poor resolution of data acquisition equipment and partially validated models removes the engineer's ability to define the thermal relationships of the avionics bay. It should be noted that in this case, the engineers understand the lack of knowledge but are constrained by industrial demands to develop a new approach that improves resolution in time of data. The lack of a definitive methodology is defined as the knowledge gap of this work. A new multidisciplinary methodology to reduce this knowledge gap is detailed in Chapter 3.

2.7. Design Contribution

The following section discusses the contribution of the traditional 4th generation design process to the lack of knowledge about the TMS identified in section 2.6.7. The design

process is split into two streams, a review of the technical design process and a review of the organisational and financial demands of designing a new fast-jet aircraft.

2.7.1. 4th Generation Thermal Management Design

The 4th generation aircraft provided a dramatic rise in the complexity and diversity of on-board systems and the development of these systems became more isolated. The thermal management of airframe heat loads was considered a secondary system (Alyanak & Allison 2016). *"Traditionally, a new concept design is driven by high level performance requirements. The role, size, range, payload, structural needs ('G' capability etc.), required performance, number and size of engines and any restrictions such as weight targets drive the initial design. Systems are not considered until all these factors have been assessed and an outline integrated design is produced. Once the above is settled, only then might someone consider the thermal management requirements."* Angus Murray, Lead Reliability Specialist, BAE Systems, Warton, UK.

2.7.2. Second Tier Design

The design of a TMS is not considered at the top level aircraft design specification stage and traditionally has been the responsibility of segregated subsystem team. The individual subsystem teams manage thermal loads within a given boundary. Inter-system thermal management is achieved through a high dependence on static interface management documentation. Subsequently, the aircraft becomes a collection of individually optimised components and subsystems, rather than the implementation of a single system to perform a given task. A system failure can be defined as a lack of achieving a design goal, or an unexpected behaviour. System failures very rarely occur within a single system but more often at the interface of two systems and therefore the traditional approach promotes system failure (Johnson & Day 2016).

The integration of the avionics within the TMS is a prime case study of segmented design practice through interface management. The majority of avionic modules are developed by equipment suppliers. The equipment supplier specifies the cooling capacity for its module which is not dependant of flight or atmospheric conditions. The airframe manufacturer must ensure that the module receives this cooling capacity; however the architecture of

the module heat exchanger, circuit cards and internal airflow path are the Intellectual Property Rights (IPR) of the equipment supplier. As the equipment supplier will not know the magnitude of the environmental thermal loading, it applies thermal safety factor to the cooling specification they received. As the airframe manufacturer cannot interrogate the internal conditions of the avionic module, they too will include a thermal safety factor to cooling specification. Typically, thermal analysis is completed at steady state conditions. To allow for a highly transient fast-jet flight profile, a further safety factor is applied. Safety factors are multiplied by safety factors as neither party has access to all the information.

2.7.3. Isolated Design Practice

As the thermal management responsibilities are delegated and split among the subsystem designers, the design practice becomes isolated. A main source of traditional TMS inefficiency is poor design specification, safety factor management and interface control. Traditionally, the TMS is designed for a single worst case scenario flight and atmospheric condition with little regard to thermodynamic efficiency at less demanding flight conditions (Bodie et al. 2010). There is minimal incentive for subsystem teams to consider flight-wide thermal optimisation once the system has achieved its specification sign-off. The reliance on a single point specification (essentially a pass/fail) has led to the development of TMS with a limited flexibility to de-rate the cooling capacity at less thermally demanding flight conditions. Inlet energy and system configuration (sizing, flow rate, cooling capacity) is based on the single point specification and, while the system works, no further efficiency studies are conducted. The result is a highly conservative (often over specified) system but a highly reliable system design in terms of thermal management.

The difficulty of implementing a single TMS design team lies in the integrated nature of aircraft systems. Thermal management is required in all subsystem and therefore to consider the complete heath path by a single team requires considering TMS at the highest levels of aircraft design. Organisationally and operationally this is impractical for the company to implement. The application of thermal engineers within separate subsystem teams has served well in the traditional design process and has provided good thermal

reliability. The reliability of this process has led to a reliance on heavily 'legacy' based system design. A 'legacy' based system is to re-use a technology or process from the previous airframe based on its acceptable performance. This concept is based on the old adage 'if it's not broken, don't fix it'. In the case of the TMS, the majority of current military aircraft utilise an open loop bootstrap bleed air cycle machine, originally developed over 60 years ago (RANNENBERG 1969). This approach to thermal management has been proven to give a reliable albeit inefficient TMS.

2.8. Cost of Development

The second stream of the design difficulties which contributes to the development of unknown system behaviour is introduced purely as a function of high development and life-cycle costs. For example, the Lockheed Martin F-22 Raptor (F-22) development cost is quoted as $79Billion for 187 aircraft, equating to approximately $420Million per aircraft (Ferran 2012). The aircraft were produced between 1996 and 2011 and none were sold to an air force outside of the United States (Lockheed_Martin 2015; Piccirillo 1998). These costs are dwarfed by the Lockheed Martin F-35 Lightning II (F-35); the Pentagon's Authoritative Selected Acquisition Report estimates that the total cost of F-35 operation will be $1.58Trillion (Clark 2012). The cost is largely due to the development of technological capabilities, the programme and airframe lifecycle, and the cost of stringent certification processes.

The ability of the Government to award the contract to a single company is dependent on the military budget of that Country. The military expenditure of the United States of America is $581Billion per year ((IISS) 2015), three times that of the UK, France, Italy and Germany combined ($183.1Billion((IISS) 2015)). These European countries cannot currently afford to fund the development of an aircraft in isolation and therefore choose to spread the cost of development, technical expertise and manufacturing capability. This led to the formations of European consortia; such as Panavia Aircraft GmbH (Tornado) or Eurofighter Jagdflugzeug GmbH (Eurofighter Typhoon).

2.8.1. Inclusion of Multiple Partners

The first major European military airframe consortium was Panavia Aircraft GmbH in 1969. This was a conglomerate of three partner nations (UK, West Germany & Italy) brought together to build the Multi-Role Combat Aircraft (MRCA), now known as the Tornado. The three countries combined to form NAMMA (NATO MRCA Management Agency) and NAMMO (NATO MRCA Management Organisation). Panavia is the conglomerate of airframe contractors BAE Systems (UK), Alenia Aeronautica (Italy), Messerschmitt-Bolkow-Blohn (West Germany) and EASAMS Systems Engineering (Italy). The contractual structure of the Tornado programme is detailed in Figure 2-25.

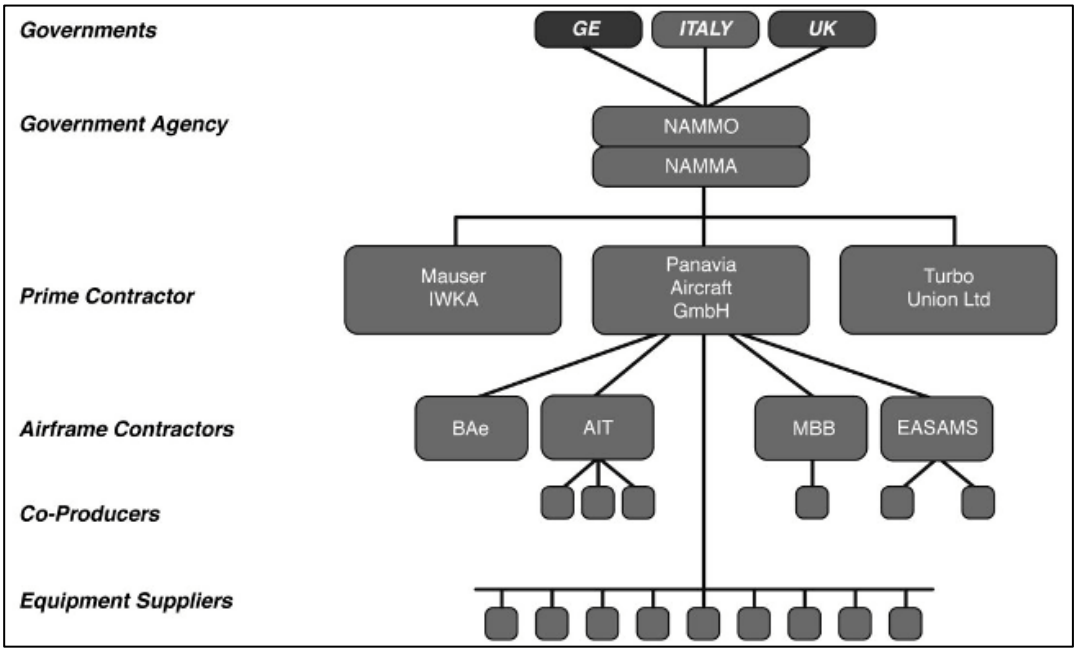

Figure 2-25: Tornado Contractual Structure – Development Phase (Thornber 2002).

The main difficulty of such collaboration is the political difficulties which can stifle technological development. “Some of the difficulties were concerned with the unique demands made of this aeroplane, which had to do everything… More difficult was the basic task of political survival.” (Gunston 1980).

The European political difficulties impacted heavily on the requirements of aircraft subsystems, such as the avionics. Each individual air force had a different requirement for the Tornado and required a different avionic package. This led to the introduction of ‘national fit’ avionic packages. MBB were responsible for the avionic system, however each

country had a secondary responsibility for avionics at a subsystem level. Integrating differing avionic capabilities required the collaborative development from multiple equipment suppliers of three different nations, each of whom was protective of their IPR.

2.8.2. Intellectual Property Rights (IPR)

The presence of multiple Governments, Government Agencies, Prime Contracts, Airframe contractors, co-producers and equipment suppliers brings difficulties of IPR. Each element of the project has a vested interest in disclosing the minimum necessary information regarding property technology. Technological capabilities are protected to safeguard further business interests outside the programme. For the aircraft, it becomes an amalgamation of different protected technologies. This design and information separation means that no single company has the capability to fully understand the complete platform.

2.9. Design Separation

The 4th generation fighter aircraft design process fundamentally encourage a design and knowledge separation. The separation of knowledge produces the generation of unknown behaviour. The lack of system performance visibility is limiting the engineers' capability to accept increasing avionic loads and meet customer driven airframe capability requirements. An absence of definitive flight data or system level experimental data places a high dependence on partially validated thermodynamic models to identify system behaviours. These steady state tools do not have the resolution to accurately identify the thermal conditions within the avionics bay.

2.10. Conclusions

The first objective of this chapter was to provide the reader with critical technical information of the components of a typical 4th generation fighter aircraft thermal management system. The second objective was to define the contributing factors to the development of unknown system behaviour.

The operational contribution to the unknown system behaviour has mainly been driven by the design and operational lifecycle of the aircraft. Across this timeframe, unforeseen

technological advances drove customer demands for increased aircraft capability due to changing battlespace requirements. The aircraft required avionic component updates to improve system capabilities; however the modification to the avionic heat rejection was found to be expensive due to the complexity of the highly integrated TMS. When considering 4th generation fighter aircraft, a very limited data acquisition capability minimised the operational validation window of system models and reduced the visibility of operating conditions. In the interest of reliability, additional safety factors were applied to system cooling capacity ultimately leading to a reliable but thermodynamically inefficient TMS.

The design contribution to the unknown system behaviour are specific to the design process of a 4th generation TMS. The first such contribution is the large development costs of producing a contemporary fast-jet military aircraft. The costs are currently unachievable for a single European country, subsequently requiring the inclusion of partner nations and subsidiary equipment suppliers to the design process. The diversification of the design process reduces the design control of each partner and introduces IPR management issues. As no single company maintains complete control of the entire design process, knowledge is separated. The limitation of engineers to understand and analyse system behaviour is a function of this knowledge separation.

Traditionally, the TMS has been considered as a utility system and designed once the key aircraft operating parameters have been defined. The definition of the TMS as a second tier system often moves the design from a centrally managed responsibility to a requirement of each individual subsystem team. This design methodology generates segregation in design responsibility, isolating the development process and limiting the optimisation process. Ultimately, this leads to each subsystem having a high reliance on interface management documentation and utilisation of safety factors to combat design uncertainty. The segmentation of TMS design process reduces the ability of the engineers to consider the complete system.

A new multi-disciplinary approach to provide increased resolution of avionic thermal management data visibility through a high fidelity GTF is detailed in Chapter 3 and 4.

3. A Multi-Disciplinary Approach

The aim of this chapter is to detail the development of a multi-disciplinary approach to better define thermal system behaviour. The requirement is to provide a methodology to increase the visibility of system performance and deliver high fidelity data, with which informed thermal management decisions can be based on. The knowledge gap in this area of research is the development of a definitive approach which allows the user to replicate the inflight condition, analyse the system from component to system level and finally optimise the system performance. The key differentiator of the method proposed in this work is the application of an interdisciplinary approach, which is heavily grounded in component, subsystem and system validation. The coupling of conceptual design concepts with a mature TMS platform allows the GTF to take advantages from both sides of the design and manufacturing process to deliver high flexibility and high confidence.

A number of key concepts can be drawn from the literature review of Chapter 2 regarding the approach to this new facility. The project must fundamentally provide clarity of the thermodynamic relationships seen across complete TMS airflow path. The analysis must be completed in a single system, to move away from the previously disjointed design approach. To generate data with confidence, the analysis must be grounded in validation

data from genuine aircraft equipment. The data output must be of high certainty, to build system understanding allowing a move away from a reliance on legacy systems and mature technologies. The high fidelity data output will allow the optimisation of the system through the reduction of surplus safety factors around cooling capacity requirements. The facility must allow for a quick turnover of technologies or concepts, allowing engineers to learn from multiple iterations. The organisational structure of the system must allow for multiple partners and encourage data transfer at each level in an attempt to reduce IPR barriers.

The following chapter will discuss how the approach utilises conceptual design concepts with a high fidelity test bed developed from mature technologies to provide a facility in line with the key concepts described above. The methodology (and thesis title) is a 'Component-led Integrative Optimisation Methodology for Avionic Thermal Management' which is developed from areas of literature such as systems engineering, TMS optimisation and the second law of thermodynamic analysis. The following section defines the key areas of this methodology.

3.1. Conceptual Design Approach to Mature Technology

Considerable industrial effort is now being devoted to re-designing traditional design concepts to reduce the length of time and financial cost of building a new aircraft. As part of this work, the aim is to consider thermal management at the highest levels of vehicle performance targets from the beginning of the design process. This represents a progression from the disjointed 4th generation TMS concept. The work is being led by the US Air force Research Laboratory (AFRL) and is focusing on the conceptual design phase (Allison et al. 2016).

The "information and freedom paradox" of a design and manufacturing process is seen in Figure 3-1. The conceptual design phase offers a low cost of change and a high freedom of choice which is an ideal condition for multiple design iterations to achieve an optimised solution. This process is known as Multidisciplinary Design Optimisation (MDO). MDO is defined as "a methodology for the design of complex engineering systems and subsystems

that coherently exploits the synergism of mutually interacting phenomena" (Giesing & Barthelemy 1998). The conceptual design phase is a critical area of the design process as decisions made here can be responsible for up to 80% of the total lifecycle costs (Price et al. 2016). The financial cost of rectifying poor conceptual design decisions gets more expensive as the design process matures (Wang et al. 2002). It was reported by NASA that the retrospective process of weight reduction at a more mature design phase due to conservative structural conceptual design estimates costs $50,000 per pound (Chakraborty & Mavris 2016).

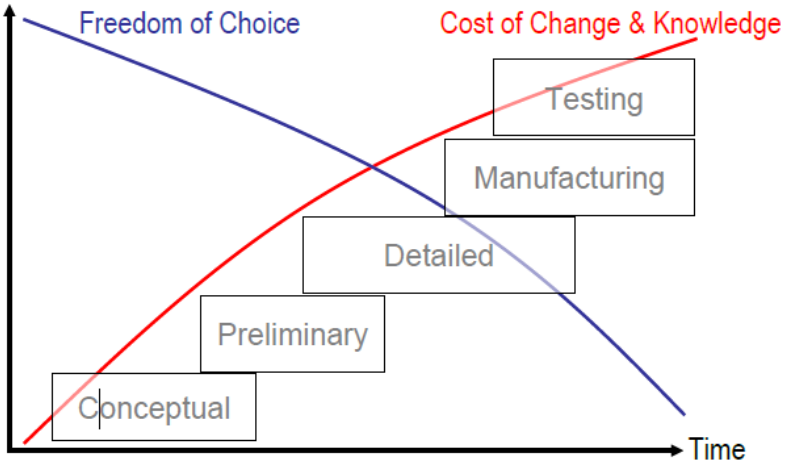

Figure 3-1: The information and freedom paradox in a design and manufacturing process (Safavi 2012).

MDO is considered a promising methodology to holistic system design. However, at the conceptual design phase, system knowledge is low. Detailed information is sparse and often incomplete, requiring the inclusion of 'best estimates' or assumptions within the modelling process. The result is an increase in data uncertainty. The uncertainty of data can be classified in two types: Aleatory and Epistemic. Aleatory uncertainty describes the inherent variation of the system or environment under consideration and this is also referred to as variability. Epistemic uncertainty describes an inaccuracy which is present due to a lack of knowledge and is high at the conceptual design phase (Van Haver, S, F & Vos 2015).

While the inclusion of the MDO approach to TMS is seen as promising, its application has not yet been perfected. The F-35 is the most recent US aircraft and has been plagued with

thermal management difficulties through its development. A high reliance on conceptual design outputs based on poorly quantified data and a lack of dynamic subsystem interface management has led to the development of unexpected thermal behaviour (Letlow & Jenkins 1998). The aircraft presented with higher than expected Short Take Off Vertical Landing (STOVL) fan clutch temperature, generating an increase in system thermal loading. Due to the highly integrated nature of the F-35 TMS, a problem in any subsystem develops into a system-wide saturation of the heat rejection capability. Based on data from the end of September 2011, the F-35 mean flight hours between critical failures was below 2.65 hours for all three variants. The unexpected behaviours of the TMS was defined as a significant contributor to the unexpected failure rates for the F-35A, F-35B and F-35C (Defence 2011). A combination of assumptions made at the conceptual design phase and a lack of early experimental testing to identify transient system behaviours can cause unexpected system behaviours. Many issues were only diagnosed and rectified once ground test work had commenced (Letlow & Jenkins 1998; Sprouse 1996).

The approach presented in this work is to apply conceptual design processes to mature technology. A key part of this methodology is that the investigation aims to operate from the right hand side of the information/freedom paradox and work backwards; reducing epistemic uncertainty. The use of mature technology exploits high system knowledge and the availability of genuine components. The concept is the development of a high fidelity GTF based on the application of 4^{th} generation TMS equipment and information to act as a test bed for the implementation of new methodologies and technologies. The test bed is grounded by validation with operational flight data to reduce data uncertainty. The tool is then used to replicate inflight conditions, identify fundamental system behaviours and optimise the TMS with confidence.

It will be demonstrated that this approach can be used to assess the performance of a new methodology and measure the system response to the implementation of new component-level technologies.

3.2. The Component-led Integrative Optimisation Methodology

The methodology proposed in this thesis is a component-led integrative optimisation approach to avionic thermal management. The approach is to consider the complete airflow path as a single system and optimise the total energy consumption by the modification of component-level performance. In this case, the aim is to reduce the bleed air consumption and subsequently fuel consumption by the optimisation of avionic module thermal operating conditions. The methodology is fundamentally based on the application of key principles of three different areas of literature. The approach takes an input from the US AFRL Integrated Vehicle Energy Technology (INVENT) program, modern systems engineering and 2nd law thermodynamic optimisation theories to output a system wide performance characterisation and optimisation.

This work identifies whether a non-traditional approach to component-level thermal management can deliver global system efficiency gains with its retrospective application to 4th generation aircraft. The future work of the facility will identify if this approach can then be extended as a design methodology to develop future systems. An overview of the three key areas of literature is detailed in the following section.

1. **Integrated Vehicle Energy Technology (INVENT) Programme**
2. **System Engineering Approach**
3. **Integrative Optimisation Technique**

3.3. INVENT Programme

The INVENT programme looks at improving aircraft TMS design processes in anticipation of continued increasing heat loads and airframe efficiency requirements as illustrated in Figure *3-2* (Iden 2012). It is expected that heat rejection demand of the future fast-jet aircraft will continue to rise exponentially. With a traditional bleed air driven TMS, a linear increase in aircraft heat load requires an exponential increase in bleed air system energy

consumption (Allison et al. 2016). Combined with a rising demand for aircraft thermal efficiency (minimisation of fuel consumption), reducing the thermal signature and radar the cross section thermal management is becoming a demanding process (Alyanak & Allison 2016; Roberts & Eastbourn 2014; Dommelen & Vos 2012).

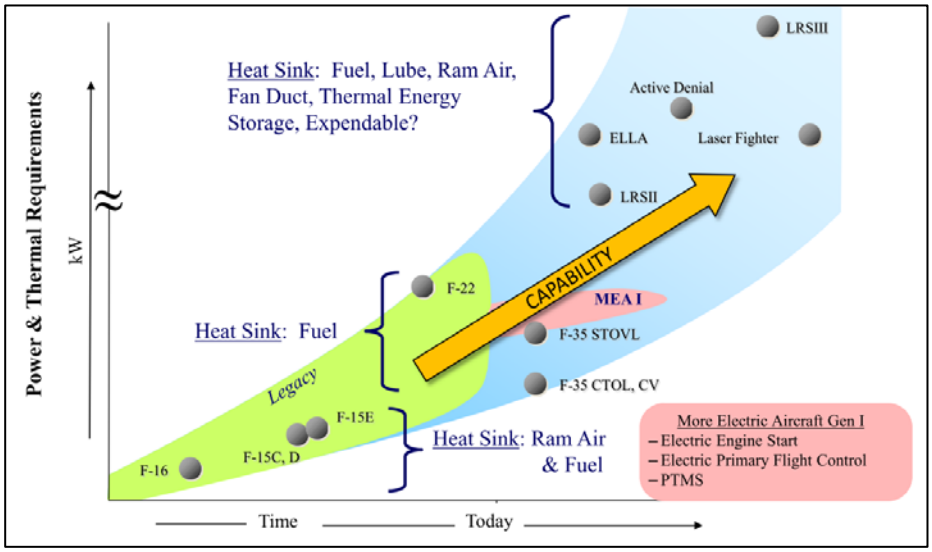

Figure 3-2: Aircraft heat loads against time (Iden 2012)

The AFRL state that *"If designers continue to neglect the increasing power and thermal demands, it is likely that the resulting designs will not close when these demands are included late in the process when it is very expensive and difficult to make any changes to the design. The end result will be a vehicle that costs more than it could have, with diminished capability than what was promised."* This extract well captures the 4th generation design process and 4th generation TMS output.

3.3.1. Organisational Structure

INVENT is a case study on thermal management concepts, design processes and future methodologies. The organisational structure of the INVENT program is to move the research away from the manufacturers through the application of the AFRL and multiple academic partners. The move away from industry allows for the development of a highly flexible working group who is free from the typical industrial constraints presented in Chapter 2.

In order to achieve this, BAE Systems set up the 'ECS/ Electronic Working Group' at Loughborough University. The aim of the Thermal Management group is to interface the industrial research demands with University led research abilities. The Thermal Management programme is led by BAE Systems, Military Air and Information, Warton, with involvement from several other business units and partner Universities and equipment suppliers (ATC Great Baddow, ATC Sowerby, EI&S Rochester, SEIC Loughborough, Loughborough University, Leicester University, and Cranfield University). The following extract is taken from this report.

"The main goal of the Thermal Management research programme is to identify any failures/problems, within the avionics bay, associated with overheating and develop solutions. Therefore, the first aim of this programme is to identify potential 'hot spot' areas within a generic avionics bay environment. This will enable the Electronic Equipment Conditioning engineers to build up an understanding of the in-flight conditions within the confines of an avionics bay.

Once the 'hot spot' areas have been identified it is then possible to begin the process of improving the thermal management inside the avionics bay. At this stage some of the improvements maybe a redesign of how the conditioned air from the ECS enters and exits the bay, providing an improved airflow, or the design of the avionic boxes maybe updated in some way to improve the removal of heat from inside the boxes.

A more innovative solution to the thermal management problem inside the avionics bay maybe to use new thermal materials either for the avionics bay construction or in the box design. These materials may aid in the transfer of heat away from the avionics bay resulting in a reduction, or removal, of the 'hot spot' areas identified during testing."

In the summer 2012, the central hub of the working group was closed down and the facility has since evolved into the "Loughborough University ECS Research Facility". The fundamental concept of a smaller, more flexible research arm with the support of Industry

but without the organisational, political and financial constraints remains a core principle of this project.

3.3.2. INVENT Thermodynamic Methodology

The Integrated Vehicle Energy Technology (INVENT) programme focuses on high fidelity modelling and simulation capabilities at the conceptual design phase (Bodie et al. 2010). However, many of the key principles of are applicable to a more experimental-based approach. The programme highlights a requirement for mission-level high fidelity modelling.

3.3.2.1. Tip-to-Tail Model

The 'tip-to-tail' model is a platform to assess system-level performance at mission-level conditions. The model is used to establish a system behaviour characterisation, before investigating design space trade-offs. The aim of the programme is to better deal with increasing thermal loads and minimise energy consumption through reduced bleed air, reduced subsystem weight and reduced engine power extraction (Iden 2012). The tip-to-tail model has become a test bed for future TMS developments through the application of MDO (Alyanak & Allison 2016; Allison et al. 2016; Reuter et al. 2016; Roberts et al. 2016; Donovan et al. 2015; Nuzum et al. 2016; Nuzum et al. 2015). The transferability of the concepts relates to the requirement of any TMS analysis to consider a holistic approach and minimise the effect of subsystem boundary interfaces by the application of a more dynamic interface management.

3.3.2.2. Mission-Level Analysis

A mission-level analysis is the capability to assess the performance across representative mission conditions. The analysis of the system across the complete flight and atmospheric envelopes is critical to establishing a true system performance. The analysis at a single flight case and/or atmospheric condition can mask critical system behaviours.

3.3.2.3. Methodology Process

The process of INVENT is to complete an extensive evaluation process to understand the thermodynamic behaviour before starting the optimisation phase of the system. The

process sequence is to replicate, analyse and optimise. This thesis originally was tasked with problem identification, which required approximately 18 months of development time to provide an accurate replication of inflight conditions. Only after the GTF had demonstrated the capability to replicate conditions, a system-wide evaluation was completed to understand the complex inter-subsystem thermodynamic relationships. This was achieved through a system characterisation study at mission level. The final step is the optimisation of the system utilising the knowledge built through the characterisation. This process has proved effective in this analysis.

The replication of inflight conditions is detailed in this chapter. The analysis of the system is detailed in Chapter 4, and the optimisation is detailed in Chapters 5 and 6.

3.4. System Engineering Approach

A systems engineering approach to the TMS is considered. A key advantage of the conceptual design phase is that it allows the model to be analysed as a single system, outside the organisational and operational requirements of a commercial operation. The disassociation of TMS design and analysis is well documented in Chapter 2. A concept posed to explain these systems is the Island of Rigor Vs. Continent of Rigor. "Classical Engineering Disciplines (CED) form 'continents of Rigor', which are linked in Traditional Systems Engineering (TSE) by rickety wooden bridges constructed of natural language. Since TSE provides little rigor to the way in which the CEDs are integrated, the inherent ambiguities and miscommunication possibilities of natural language allow all kinds of misunderstandings to exist between CEDs, that could never exist inside CEDs. What we aim to create is a 'Discipline of Systems Engineering' that enables just as much rigor between CEDs as exists inside of them. This will create a "Continent of Rigor" equal in scope to the system itself." (Johnson & Day 2016).

The application of the Continent of Rigor theory is to manage the design process from the onset with the effective use of systems engineering concepts rather than retrospectively apply these concepts to a number of isolated subsystem design teams. By improving the information flow across the subsystem interfaces, system failures can be reduced. There is

clearly a requirement to conduct the analysis within a single facility, or at least to accurately control the data flow across subsystem boundary interfaces.

3.5. Integrative Approach to System Optimisation

The systems engineering and INVENT concepts focus mainly on the replication and analysis of the system. The final part of the methodology is the application of the 2nd law thermodynamics optimisation concepts. The integrative optimisation approach is a concept successfully utilised to thermodynamically optimise the ECS of commercial aircraft.

Considerable work was completed in the early 2000's into the thermodynamic optimisation of civilian aircraft. The work was focused around the second law of thermodynamic ECS analysis to develop an Entropy Generation Minimisation (EGM) optimisations (Vargas & Bejan 2001; Ordonez & Bejan 2003; Vargas et al. 2001; Bejan 1997). Entropy change can be used as a criterion of thermodynamic irreversibility of a process (Rogers & Mayhew 1992). An ideal process can be defined as completely reversible and therefore the process has no losses (typical losses present in the form of friction and heat transfer to ambient conditions) and all energy can be recovered in its original form. In reality, no process is completely reversible and the change in entropy across that process can be calculated as a measure of the process irreversibility. The minimisation of entropy generation is the maximisation of the thermodynamic process quality. While the work presented in this project does not approach the optimisation from a second law of thermodynamics basis, the findings of these techniques are applicable. The applicability of these concepts is due to common ECS architecture between the optimisation study and this thesis. In both cases, the work is based on the optimisation of a bootstrap cycle ECS. Two key ideas are taken from the second law optimisation literature, the integrative optimisation approach and the minimum power requirement approach.

3.5.1. Integrative System Analysis

The integrative optimisation approach is to consider the entire airflow path as a single system designed to optimally achieve certain global objectives, not as an ensemble of already existing components and subsystems (Gambill et al. 1993). There is considerable

agreement with the core principles of the INVENT program and the systems engineering approach. This approach requires the consideration of all subsystems within a single analysis as it is often found that a global optimum is the result of sub-optimal solutions of individual components and subsystems (Vargas & Bejan 2001).

The integrative approach has been previously utilised (Vargas et al. 2001) to optimise the performance of an ECS heat exchanger to drive total ECS thermodynamic gains. Typically the heat exchanger optimisation was completed in isolation and then integrated with the ECS cycle. The concept presented in this work is that the entropy generation of the total system could be minimised by the optimisation of the heat exchanger as installed within the system. The ability to consider the complete airflow path allowed for the optimisation of the heat exchanger in terms of its size and weight contribution alongside its installed thermodynamic performance, this cannot be achieved through an isolated benchtop optimisation process. It was concluded that the thermodynamic optimisation is to modify a components behaviour based on its global system impact. As the thermodynamic interactions link the system through a single airflow path, to optimise any componentry in isolation can negatively affect global system performance (Vargas & Bejan 2001; Vargas et al. 2001). The requirement of the work in this thesis is to take this concept outside of the ECS subsystem and consider the total TMS.

3.5.2. Minimisation of Power Requirement

The minimisation of the power requirement is an approach to thermodynamic optimisation that considers a 'bottom up' systems approach. This analysis determines the minimum required power consumption to achieve a given system goal. The typical TMS approach is to define the system performance target at the subsystem interface, for instance, the goal would be to deliver an airflow temperature at a given mass flow rate. These airflow characteristics (eg, flow rate and temperature) are easily communicated across subsystem boundaries. This typical approach does not consider the performance of the airflow on subsystems down to a component level (eg. communicating a maximum component temperature). It was found that the total power consumption requirement could be optimised by the consideration of localised component level conditions (Ordonez

& Bejan 2003). This concept links the integrative design approach, the INVENT concept, and the systems engineering continent of rigor theories.

3.6. Conclusions

This chapter has discussed a methodology to replicate, analyse and optimise the inflight thermal conditions of a fast-jet TMS. The analysis and optimisation methodology is based on key concepts from the literature. The typical 4th generation design process has been proved to be ineffective when considering thermal management as detailed in Chapter 2. The current system design procedure (constrained heavily at the conceptual design phase) deals with high uncertainty data and can lead to the generation of unexpected system behaviours, as seen with the F-22 and the F-35 TMS. The concept of this approach is to marry the contemporary design philosophies with existing high certainty genuine equipment in a single GTF; a conceptual design approach with mature technology.

The INVENT study provides the direction for the process of TMS development at the conceptual design phase. However, the high levels of uncertainty present at the conceptual design phase can only be minimised by extensive computational time and industrial support. Even with these efforts, the uncertainty cannot be reduced to the levels of experimental testing and small miscalculations at this phase can be critical to the future aircraft effectiveness, as seen with the F-35. Many of these concepts are applicable to a more experimental approach, such as the system-wide analysis and structure of the project.

The systems engineering approach is rooted in the INVENT and integrative optimisation techniques. Both concepts strive to minimise the effect of system interfaces on the characterisation of system performance. The application of the 'continent of rigor' consist in removing the isolation of the design and analysis approach and treating the complete TMS as a single end-to-end system. System failure can be defined as unexpected system behaviour, which is the case with avionic thermal management. System failures very rarely occur within a single subsystem but more often occur at the interface of two subsystems. If the number of interfaces can be reduced, the system reliability can be increased. This

concept is the driving force behind the requirement to assess avionic performance across the complete air path from the initial compression of bleed air through to the avionic exhaust outlet.

The integrative approach carries key concepts of the INVENT and systems engineering approach by the application of a 2nd law of thermodynamics optimisation. The integrative approach aima to reduce the entropy generation of the thermal system to achieve a given task. This concept provides a bottom-up approach or component-led approach to system optimisation.

The key areas of literature have been identified from a multidisciplinary literature review. The application of genuine equipment is a new approach to the development of a test-bed which is beneficial in two ways. Firstly, the results of this work can be used directly for retrospective aircraft thermal management technology recommendations. Secondly, the test-bed can be used to identify future methodologies and technologies which are not airframe specific. It will be shown that studies into bleed air humidity and partial ECS failures can be conducted to generate knowledge that is platform transferrable.

This approach is achievable through the strong industrial links between Loughborough University and BAE Systems. Industry has access to genuine equipment, but limited time for long research activities. Academia is free from some of the industrial time constraints, but has limited access to genuine equipment and data. The ability to operate within the middle of these two areas and take advantage of both sectors is a key strength to this project. A new test facility has been built at Loughborough University based on the supply of genuine fast-jet aircraft equipment from BAE Systems. The advantage to basing this investigation around a 4th generation platform is the avoidance of IPR issues. The genuine aircraft components utilised for this investigation are from 'in-service' 4th Generation aircraft, allowing a much greater flow of data from Industry to Academia. This approach could not be utilised for a 5th generation platform at this time due to IPR restrictions. The development of this facility is detailed in the following chapter.

4. Development of a New Ground Test Facility

4.1. Introduction

This chapter will detail the development of a new GTF to evaluate a Component-led Integrative Optimisation Methodology for Avionic Thermal Management. The GTF is detailed in terms of the hardware experimental rigs, simulation tools, and outputs. This chapter will not provide any data outputs other than for the calibration/validation of the facility and numerical models. An experimental investigation of the facility is detailed in Chapter 5.

The keys aim of this GTF is to provide platform to perform a high fidelity analysis of TMS performance. In order to provide reliable data, the process is to anchor the facility in existing and well understood hardware which can be validated against genuine operational data. However, a contribution to the unknown system behaviour discussed in Chapter 2 is the disjointed and sporadic nature of validation data. To overcome this, the GTF requires the capability of accepting multiple sources of component-level and of subsystem level

validation data from either flight or isolated bench top testing and outputting a single stream of high confidence system-level data. Lesson learnt from the literature review have been used to develop five key requirements the GTF must be developed around.

1. **Output data grounded in system validation:** The main requirement of the facility is to provide high-fidelity output data and therefore validation is critical.
2. **A system level analysis tool, capable of representing component, subsystem and global performance in a single facility:** The facility must replicate the complete airflow path from bleed air compression to avionic exhaust air. The GTF must allow for the interrogation and optimisation of component-level thermal performance and the measurement of this at the subsystem and at the system levels.
3. **Minimisation of subsystem boundary interface effect on data:** The BAE Systems engineering concepts highlight the requirement to minimise the interface boundaries (Johnson & Day 2016). If the complete system is treated as a single airflow path, unexpected system behaviour may be minimised. The analysis in a single facility allows the interaction of subsystems to be studied and its effect on the system performance documented.
4. **Assessment of system at mission level:** A requirement of the system analysis is not just to consider the complete airflow path in terms of hardware, but also to consider the complete atmospheric and operational envelopes.
5. **Flexibility of the system for thermal performance evaluation and optimisation:** The same facility is required to replicate, analyse, and optimise the system performance. Flexibility is required to evaluate new methodologies and technologies.

A schematic of the TMS under analysis is shown in Figure 4-1. The TMS is architecturally similar among aircraft including the Grumman F-14 (Hoffman 1985), McDonnell Douglas F-15 (Dieckmann et al. 1986), General Dynamics F-16 (Laster et al. 1990), Panavia Tornado (Gunston 1980), BAE Systems Hawk (Jones et al. 2015), Eurofighter Typhoon (Pearson & McCoy 2011), and the Saab JAS 39 Gripen.

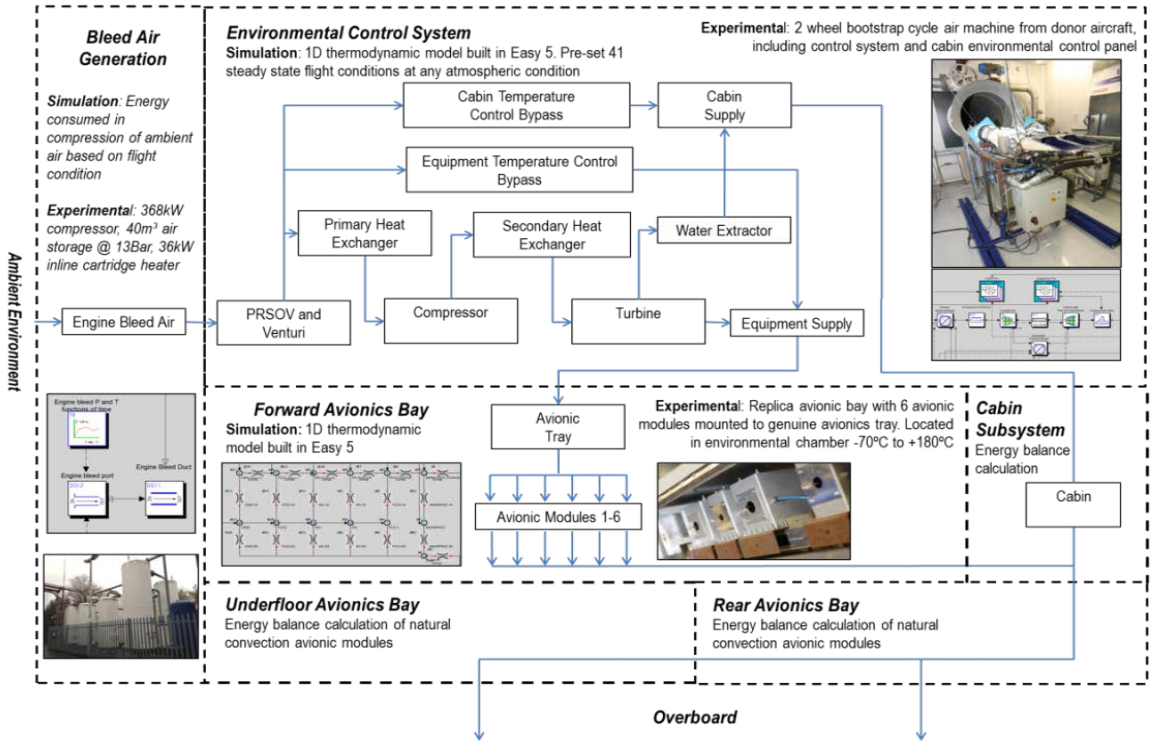

Figure 4-1: TMS Schematic.

4.2. Validation Data

The available validation data provided by BAE Systems is seen in Table 4-1. It should be noted that only two sources of validation data are from full scale flight conditions. The first is presented in its entirety in Table 4-1. This is an email from the Principal Mechanical Analysis Engineer at BAE Systems Rochester regarding the inflight thermal conditions of the Flight Control Computer (FCC) avionic module. The second is sporadic bay temperature measurements from the BAE Systems Hawk. A total of 6 flight conditions and 3 ground conditions is provided with limited accuracy on the atmospheric conditions of the test data. The remaining validation data is component-level and laboratory based provided from a total of 6 further sources. This data also serves to highlight the requirement and importance of a single facility to provide thermal management analysis.

Validation Data	Data Type	Data Source	Notes
FCC Exhaust Airflow Temperature	Flight Data	BAE Systems Rochester	"The FCC records min and max data between power up and engine spool down. The minimum we have recorded is 5°C and the maximum we have recorded is 65°C. We usual see a 20°C increase between the min and max temperatures recorded per FCC. The average temperature is between 15°C and 35°C"
Hawk Avionic Bay and Cabin Mean Bay Temperature	Flight Data	BAE System Brough	Limited flight data measurements of mean bay air temperature for the cabin and avionic environment. The data is limited to 6 flight and 3 ground conditions. Often lacking accurate specification of atmospheric conditions
Avionic Module Characteristic Pressure Drop	Lab Data	BAE Systems Warton	Each avionic module characteristic pressure drop is measured and set to achieve the correct avionic bay mass flow rate distribution. No thermal consideration.
Avionic External Thermal Signature	Lab Data	BAE Systems Warton	Thermal imaging of active avionic in a lab setting. The avionic modules are on electrical and reliability test and are oversupplied with coolant. Magnitude of temperatures is irrelevant however thermal signature is valid.
FCC Thermal Survey	Lab Data	BAE Systems Rochester	Bench top thermal survey of genuine avionic module for thermal pass-off test. Data of airflow, ambient and circuit card temperatures are supplied.
Hawk ECS Pressure Relief and Shut-Off Valve (PRSOV) performance	Lab Data	Normalair Garret Limited (NGL)	Upstream – downstream pressure profile for ECS inlet PRSOV from component testing
Hawk cabin pressurisation characteristic control	Lab Data	BAE Systems Brough	Atmospheric pressure vs cabin pressurisation control characteristic curve.
Hawk ECS Compressor and Turbine Performance Maps	Lab Data	BAE Systems Brough/ NGL	Turbine and compressor efficiency maps. The compressor efficiency shown for a given pressure ratio and inlet flow parameter with shaft speed indication curves. The turbine maps detail pressure ratio against efficiency for a given shaft speed.
Hawk ECS Heat Exchanger performance Map	Lab Data	HS Marston	The performance map details heat exchanger charge air thermal ratio against charge and coolant flow rate.
Hawk ECS Water Extractor Pressure Drop	Lab Data	BAE Systems Brough/Doeley Aviation Ltd.	The water extractor pressure drop against mass flow rate is detailed for the region between absolute humidity's of 0g/kg and 20g/kg

Table 4-1: GTF validation data.

Information is provided by BAE Systems in terms the configuration of components (size, flow rates, power outputs, etc.). For some equipment, validation data is unavailable and genuine aircraft components are supplied to circumvent this requirement. The most notable equipment loan is a complete ECS from the BAE Systems Hawk. The GTF is required to decompose the wider thermal management system, validate performance where required, evaluate genuine equipment and to consolidate the data into a single, trusted data stream.

4.3. Ground Test Facility Specification

The facility requirement is to analyse the large and distributed TMS in a ground-based laboratory setting through the application of system engineering concepts. The methodology is to use an interdisciplinary approach to enable the realisation of a successful system (INCOSE 2016). The application of multiple disciplines allows the flexibility of the GTF to ensure the various level of validation. The grounding of all data in validation of existing equipment reduces the uncertainty of the data and increases confidence in the end product of system optimisation.

The approach to building an interdisciplinary GTF is based on theories of the typical Systems engineering V model. The V model features two key processes; a 'decomposition and redefinition' process and an 'integration and re-composition' process. The wider engineering system is de-composed into quantifiable blocks whose performance can be assessed in isolation through high-fidelity numerical or experimental means. The performance is assessed against available validation or evaluated with genuine aircraft equipment. The individual blocks can then be re-integrated back into a single data stream for system analysis. The combination of both genuine hardware and numerical simulation models generates data across the hardware/software boundary. Both tools are used with an overlap in the test envelope to produce accurate results and extend the test envelope.
Experimental facilities are utilised to validate simulations within the limitations of the rig. Simulations are used to offer insight into system performance throughout the full flight and atmospheric envelopes. Hardware and software operate within separate time domains, with an offline integration process producing a single data stream. The offline

data flow facilitates the overlap between the numerical simulation and the experimental hardware, therefore removing some of the typical subsystem interfaces seen through the design process. The resulting data flow is of higher fidelity and features no boundaries in the airflow path from the initial bleed air compression to the aircraft exhaust. The technique ensures the accuracy of the analysis at component, subsystem and global system performance while minimising the complexity, cost and time of full scale experimental testing. A schematic for the process is seen in Figure 4-2 with a detailed description of each stage shown below.

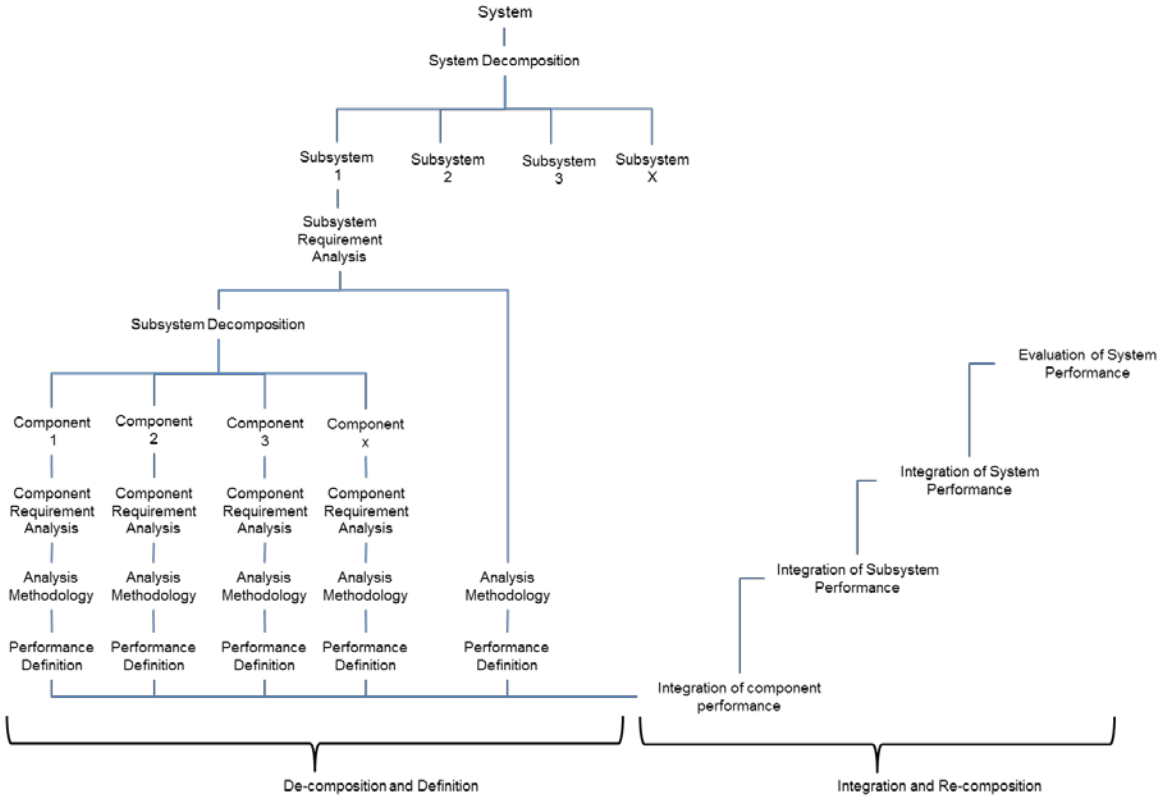

Figure 4-2: V model schematic. Graphic created by Author.

The process is presented as a generic analysis which can be expanded out if additional subsystems are to be included in the analysis. The system can be decomposed into multiple subsystems and the subsystems can be decomposed into multiple components, with limits. The process can be used to integrate any size of system into a single data stream; it is a requirement of the approach to be scalable.

4.4. Decomposition and Redefinition

4.4.1. System Decomposition

The system cannot be analysed with confidence as a single entity, so the first part of the analysis is to decompose it into subsystems. The decomposition of the system into subsystems is fundamentally a logic-based process. The definition of each subsystem is dependent on where component-level performance interactions can be separated. In this instance, the easiest way to define the subsystem boundaries is by the physical location of those subsystems on the aircraft. Any point on the aircraft where the airflow is transported a significant distance through a duct or pipe can be considered a subsystem boundary. At the point of airflow transportation, the pipe (component-level performance) is considered to not directly interact with the performance of other components as the system is suitably sized. The subsystems are defined in Figure 4-1.

4.4.2. Subsystem Requirements Analysis

As each subsystem is defined, a subsystem requirement analysis is performed. This consists in determining what analysis is required in terms of output data and GTF infrastructure. The output data requirement is based around the capability of the test facility to validate and subsequently optimise the subsystem performance. The validation requirement drives the majority of the output data requirement analysis. Typical questions at this point would be; how can the data be validated? What accuracy is required with this analysis? What flexibility (system adaptation) is required? Can the approach be applied for subsystem replication, analysis and optimisation?

Secondly, the operating environment of the subsystem is considered. Typical questions at this point would be; what are the heat loading and heat rejection processes? What are the typical variations in these processes with flight and atmospheric envelopes? What are the airflow requirements (temperature, pressure, mass flow rate)? Is there a dependency on another subsystem to accurately define the operating environment? The answers to these questions drive the direction of the output data requirement analysis.

It is common that the output of the requirements analysis is that the subsystem level data is insufficient. The data may not be used for performance validation, or system replication, analysis and optimisation. At this point, the subsystem requires further decomposition to component-level.

4.4.3. Component Decomposition

The subsystem is decomposed to the smallest component level required for the performance validation. Considering the avionics subsystem, the validation data in Table 4-1 details the performance of the avionic module and therefore the subsystem must be decomposed to the level where the avionic module performance can be considered.

4.4.4. Component Requirement Analysis

The component requirement analysis is a validation-led process analogous to that of the subsystem requirement analysis. The process is completed to determine what data outputs are required and what GTF infrastructure is required to achieve this. The type of analysis is largely driven around the type of validation data available and how the facility can be evaluated against this data. Through the consideration of the same questions presented at the subsystem requirement analysis, the component requirement analysis can be determined. This produces a detailed plan of the required GTF infrastructure to generate high quality output data.

4.4.5. Performance Definition

The performance definition is the output of the output data requirement analysis at either component or subsystem level. As this process is used to replicate and analyse the existing system performance, the output data is purely a performance definition. As the same process is utilised to optimise the system, the output data will be a performance re-definition in response to the implementation of a new technology.

The process of the optimisation is to re-define a component thermal performance and monitor the heat propagation back through the system. The system analysis process detailed in Figure 4-2 allows the user to analyse the system-level response by the isolated redefinition of the component-level performance. The result is the ability to assess isolated

'bench top' component optimisation data within a global system. The system performance is grounded through experimental testing with multiple points of validation to return a high confidence system response to component optimisation.

4.5. Ground Test Facility Build

The multi-disciplinary approach to avionic thermal management proposed in Chapter 3 requires the application of a conceptual approach to mature technology. The system to replicate, analyse and optimise is the inflight thermal conditions of a 4th generation TMS. The replication of such TMS is attempted for the first time in this work, therefore the facility to evaluate this approach must be bespoke. The development of the GTF to replicate bleed air, ECS, avionic and cabin sub-systems is detailed in the following section. The facilities are developed specifically for this project and have been designed and built from scratch as part of this investigation. Extensive time has been allocated to the development of an appropriate laboratory space provided with utilities such as electrical power supply, lighting and partitioning, as well as to the procurement and set-up of genuine aircraft equipment. The test facilities discussed in this chapter did not exist before this investigation.

4.5.1. Bleed Air Subsystem

The bleed air subsystem is responsible for the supply of the ECS inlet energy. As the ECS is replicated in both hardware and software, the air supply also requires both a hardware and software modelling approach. Bleed air data for a given flight and atmospheric condition has been supplied by BAE Systems for the relevant ECS. This data is not considered validation data but a system input.

The ECS configuration is based on the BAE Systems Hawk ECS and the bleed air supply replicates the axial compressor conditions of this aircraft engine. The Hawk utilises a single non-reheat Rolls Royce Turbomeca Adour Mk871 (Fraser-Mitchell 2013). The total engine inlet flow ranges between 8kg/s (landing) to 60kg/s (high speed, low level) with a bleed air flow rate between 0.2% and 1.3% the of total engine mass flow rate (Joslin 2015).

4.5.2. Bleed Air Subsystem Hardware

Experimentally, the bleed air is replicated with a three cylinder 368kW compressor which charges a number of receiver tanks (totalling 40m³ of air storage) to 13.8Bar. The compressor intakes ambient air. The ambient air in water content is removed after compression through the use of a desiccant drier. The flow rate is regulated by a 4" pilot-controlled diaphragm valve, with fine and coarse regulators in the control room. Inside the test cell, inline flow conditioning consists of an electro-pneumatic Shut-Off Valve (SOV), an orifice plate flow measurement device and a 5Bar Pressure Relief Valve (PRV) for component protection. The orifice plate flow measurement device is implemented with upstream and downstream pipes of appropriate length to provide upstream flow stabilisation, downstream flow recovery, and a fixed valve orifice plate discharge coefficient (McClain 1947).

The design specification for maximum humidity is an AH of 27g/kg. The desiccant driers remove moisture upstream of the receiver tanks; therefore a downstream humidification system is required. High pressure water is controlled and injected into the air stream using a bespoke injection system. The injector is from a 3 cylinder direct injection Ford Eco-boost automotive engine. The Original Equipment Manufacturer (OEM) fuel rail is maintained (shortened to accommodate a single injector) to ensure correct sealing and mounting. A high pressure water supply is provided from a 0.75hp pneumatic pump with a 42:1 pressure ratio, capable of supplying 130Bar at 1000cc/min. The injector is controlled by a signal generated from a bespoke driver box which receives a Pulse Width Modulation (PWM) signal from the data acquisition equipment. The injector is calibrated by mapping the injector pressure and pulse width against the total injection flow rate. The data acquisition software uses the inlet air mass flow rate from the orifice plate and the injection flow rate map to command to a user defined absolute humidity inlet. Experimentally, an absolute humidity of up to 34g/kg has been achieved at representative bleed air conditions.

The limitation of the bleed air supply is the capability to re-heat the air flow due to infrastructural limitation of the electrical power available in the test cell. A 415volt three-

phase supply with a 32amp local distribution board is available to provide power bleed air heating and ram air flow rate, the remaining power loads are supplied by mains 240volt. To reduce the total power requirement of the bleed air heating, the ECS primary heat exchanger is bypassed. The ECS inlet conditions are matched to the ECS compressor inlet, reducing the temperature requirement to a maximum of 180ºC. This temperature range is achievable with an inline 36kW cartridge heater, located at the ECS inlet (Osram Sylvania 2012). From the point of heating, all pipe run lengths are minimised and pipework is thermally insulated to minimise losses to the ambient laboratory. The heater temperature is Proportional Integral Derivative (PID) controlled, with a temperature feedback at the heater exhaust. A photograph of the installation is seen Figure 4-3.

Figure 4-3: Bleed air supply emulators subsystem.

4.5.3. Bleed Air Subsystem Simulation

The software model is built in MSC Easy 5, a one-dimensional thermodynamic simulation code (Molyneaux, A et al. 1997). The bleed air subsystem has no compression calculations, instead it uses a look-up table to determine the bleed air temperature, pressure and humidity based on flight and atmospheric condition. The look-up table data is provided by BAE Systems. The model consists of 46 flight conditions, 11 ground conditions and 9 transient conditions covering a Hot, Cold and Humid atmosphere, as detailed in Table 4-2.

Case Number	Day	Description	Altitude [feet]	Mach Number	Humidity [kg/kg]
Flight Cases					
F01	Cold	High speed low level	0	0.84	0
F02	ISA	High speed low level	0	0.83	0.01
F03	Humid	High speed low level	0	0.79	0.027
F04	Hot	High speed low level	0	0.78	0.017
F05	Cold	Cruise	0	0.60	0
F06	ISA	Cruise	0	0.60	0.01
F07	Humid	Cruise	0	0.60	0.027
F08	Hot	Cruise	0	0.60	0.017
F09	Cold	Take off	0	0.20	0
F10	ISA	Take off	0	0.20	0.01
F11	Humid	Take off	0	0.20	0.027
F12	Hot	Take off	0	0.20	0.017
F13	Cold	Landing	0	0.20	0
F14	ISA	Landing	0	0.20	0.01
F15	Humid	Landing	0	0.20	0.027
F16	Hot	Landing	0	0.20	0.017
F17	Cold	High Speed	20k	0.85	0
F18	ISA	High Speed	20k	0.85	0
F19	Hot	High Speed	20k	0.84	0.005
F20	Cold	Maximum range	20k	0.50	0
F21	ISA	Maximum range	20k	0.50	0
F22	Hot	Maximum range	20k	0.50	0.005
F23	Cold	Low speed	20k	0.34	0
F24	ISA	Low speed	20k	0.34	0
F25	Hot	Low speed	20k	0.34	0.005
F26	Cold	High Speed	30k	0.85	0
F27	ISA	High Speed	30k	0.84	0
F28	Hot	High Speed	30k	0.84	0
F29	Cold	Maximum range	30k	0.60	0
F30	ISA	Maximum range	30k	0.60	0
F31	Hot	Maximum range	30k	0.60	0
F32	Cold	Low speed	30k	0.45	0
F33	ISA	Low speed	30k	0.45	0
F34	Hot	Low speed	30k	0.45	0
F35	Cold	High Speed	40k	0.83	0
F35	Cold	High Speed	40k	0.83	0
F36	ISA	High Speed	40k	0.82	0
F37	Hot	High Speed	40k	0.82	0
F38	Cold	Maximum range	40k	0.70	0
F39	ISA	Maximum range	40k	0.70	0
F40	Hot	Maximum range	40k	0.70	0
F41	Cold	Low speed	40k	0.60	0
F42	ISA	Low speed	40k	0.60	0
F43	Hot	Low speed	40k	0.60	0
F44	Cold	Maximum altitude	48k	0.70	0
F45	ISA	Maximum altitude	48k	0.70	0
F46	Hot	Maximum altitude	48k	0.70	0
Ground Cases					
G01	Cold	Engine idle	0	0.00	0
G02	ISA	Engine idle	0	0.00	0.01
G03	Humid	Engine idle	0	0.00	0.027
G04	Hot	Engine idle	0	0.00	0.017
G05	Cold	APU	0	0.00	0
G06	ISA	APU	0	0.00	0.01
G07	Humid	APU	0	0.00	0.027
G08	Hot	APU	0	0.00	0.017
G09	Cold	APU	6K	0.00	0
G10	ISA	APU	6K	0.00	0.005
G11	Hot	APU	6K	0.00	0.015
Transient Cases					
T01	Cold	High Speed Dive	5K	0.9	0
T02	ISA	High Speed Dive	5K	0.9	0.005
T03	Hot	High Speed Dive	5K	0.9	0.01
T04	Cold	High Speed Dive	25K	1.065	0
T05	ISA	High Speed Dive	25K	1.045	0
T06	Hot	High Speed Dive	25K	1.020	0
T07	Cold	High Speed Dive	40K	1.2	0
T08	ISA	High Speed Dive	40K	1.2	0
T09	Hot	High Speed Dive	40K	1.2	0

Table 4-2: Hawk ECS Pre-set Model Flight Conditions.

4.5.4. Environmental Control System

The ECS subsystem forms a majority of this analysis as very little subsystem level validation data is available. The cost and time of full scale flight testing is prohibitively expensive and therefore flight data is not available. However, aircraft components are available for their experimental evaluation. BAE Systems have provided the project with a complete Hawk ECS. With the application of correct bleed air inputs, flight data can be generated within a GTF and therefore validation data is not required to ensure the accurate performance of this subsystem.

The infrastructural limits of the laboratory space (power consumption, air supply) and project funding limited the ability to replicate the full flight envelope. To overcome this, the ECS thermal performance was assessed in both hardware and by simulation. The hardware is used to validate the simulation within the infrastructural limitations of the GTF and the simulation is used to expand the results to the full extent of the flight envelope.

4.5.5. Environmental Control Subsystem Hardware

The ECS experimental rig is an original equipment manufacturer (OEM) fast-jet bleed-air driven two-wheel bootstrap cycle, with a low-pressure water extraction. The cabin and equipment temperature was controlled by two independent bypass branches with PID-controlled servo valves. As previously mentioned, in order to reduce the infrastructural demand of the bleed air subsystem, the primary heat exchanger (pre-cooler) provides no cooling (no ram air mass flow rate). A schematic of the ECS in the experimental setup is shown in Figure 4-4.

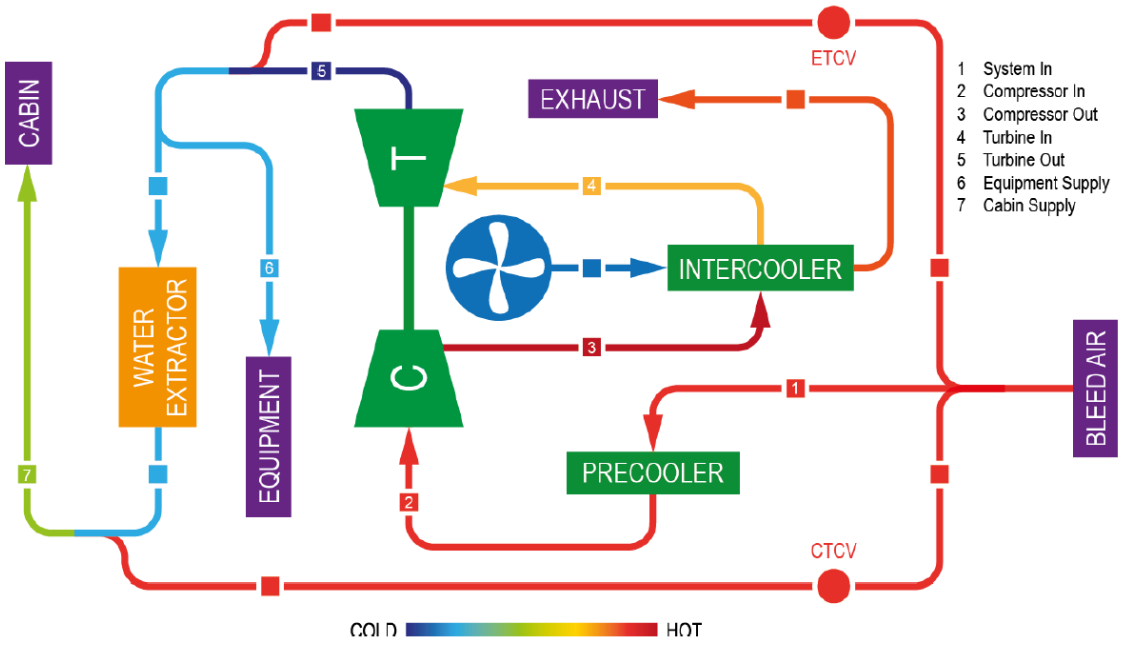

Figure 4-4: ECS Schematic Diagram

4.5.5.1. ECS Temperature Control

The ECS control system is provided from the donor aircraft, complete with wiring loom and valve control. The control system is modified to allow the user to either run in automatic valve position mode or manually demand an ETCV position.

The ECS has no capability to measure the bypass flow rate, however at any point a pressure differential exists within a fluid flow the mass flow of the fluid can be calculated with known geometry (Jones 1995). The bypass flow rate is calculated by the pressure drop across the valve based on its position. The flow rate is calibrated against the bleed air orifice mass flow rate device by sweeping each valve individually. The valve response is

insensitive as the position tends to fully closed or fully open and it is very sensitive in the central part of its operation, giving the typical performance characteristic of a butterfly valve. The bypass mass flow rate against valve position for a given inlet pressure can be seen in Figure 4-5.

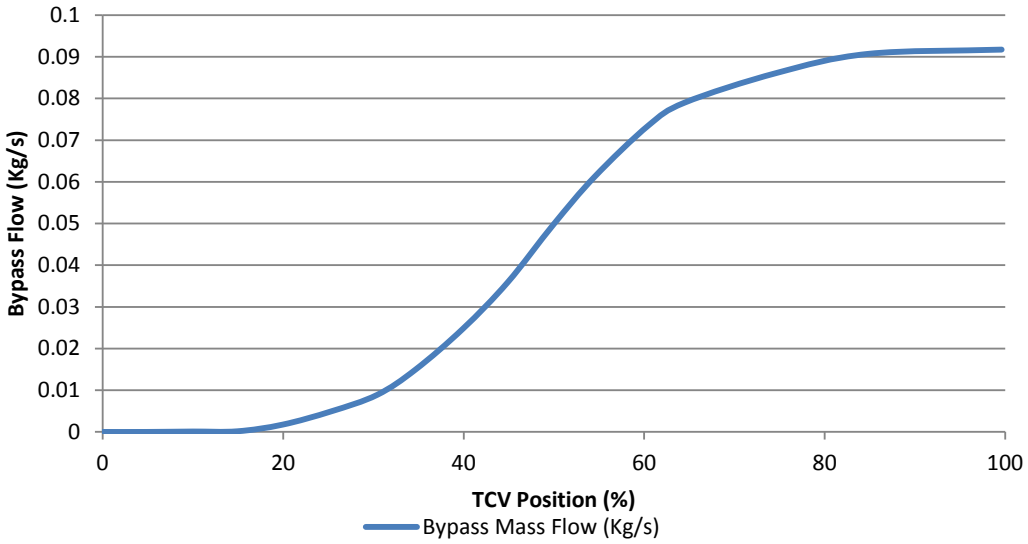

Figure 4-5: TCV flow characterisation.

4.5.5.2. Ram Air

The secondary heat exchanger ram air flow rate is provided by a 5.5kW high flow, low volume centrifugal air fan. The fan mass flow is calibrated as installed with a bespoke bell-mouth, contraction and diffuser section fitted at the fan intake, with the exhaust flowing through the ECS heat exchanger. The bell mouth is assumed to be perfectly smooth and therefore no losses are assumed (Cd = 0). The contraction and diffuser section are no greater than a total angle of a 7º and therefore flow is assumed not to separate. Between the contraction and diffuser section sits a parallel section of known diameter (measured to an accuracy of 0.01mm) with a static pressure tapping mounted flush to the wall. The ambient environment temperature and pressure are measured and the ambient velocity can be assumed as zero. The application of Bernoulli's theory allows the calculation of the airflow velocity in the parallel section, based on the differential pressure and the airflow density, as shown in Equation 4-7. The fan mass flow rate is mapped against a fan motor speed for ease of mass flow rate calculation. The temperature of the ram air is not actively controlled and is a function of the ambient laboratory temperature and of the mass flow

rate (increased temperature from increased heat exchanger pressure drop). The laboratory ambient temperature remained reasonably constant across testing (±3ºC).
The GTF is limited by the ram air mass flow rate and by the air heat supply. The conditions of ram air flow rate cannot realistically aim to complete the full flight envelope due to the vast air speed and temperature variations (within budgetary constraints). The ram air flow rate is assessed by a comparative cooling approach, where the heat rejection of the heat exchanger is matched even if the flow conditions are not exact.

4.5.5.3. Data Acquisition, Facility and Environment Control Subsystem Control

The data acquisition hardware is a National Instruments compact Rio equipped with a temperature module (16 thermocouples), a 24 channel analogue voltage input module and a 4 channel digital output module. The software is a bespoke code written in the National Instruments Labview object-oriented language. Signals are digitally acquired at 200 Hz and each data log is averaged over 20 seconds. The software also allows the user to collect a 'Transient Log', whereby the data is collected at 200Hz to measure dynamic system response. Temperature and pressure data are collected before and after each major thermodynamic component. All temperature and pressure data signals are calibrated as installed (GE Measurement & Control 2016; Martell Calibrators 2016).

Humidity measurements are taken using two Michell PCMini 52 hygroscopic polymer capacitance relative humidity sensors. The humidity sensors are calibrated prior to delivery and therefore the measurement is based on the manufacturer original calibration data (humidity span against measurement span). The LPWE drain is collected in a measuring jug for ease of measurement and measured over a given time span.

The CTCV and ETCV rotary potentiometers are calibrated against a manual sweep between two physically measured locations. The response between these two locations is assumed linear.

The compressor-turbine shaft speed is not directly measured, however the compressor and turbine maps have been provided by BAE Systems. The speed can be calculated from

the empirical relationship between component pressure ratio and component flow parameter. The flow parameter is defined as the product of the compressor, work, W_c, and the square root of compressor inlet temperature, T_c, divided by the inlet pressure, p_{in} .

$$\frac{W_c \sqrt{T_c}}{P_{in}} \tag{4-1}$$

The compressor pressure ratio is defined as the outlet pressure divided by the inlet pressure.

$$\frac{p_{out}}{p_{in}} \tag{4-2}$$

The measurement of these parameters can be used to identify the compressor shaft speed using the flow parameter on the x-axis and the pressure ratio on the y-axis of Figure 4-6. At the point of intersection, the compressor efficiency and shaft speed can be determined. Shaft specific speed is given as the rotational speed, N, divided by the square root of the airflow temperature.

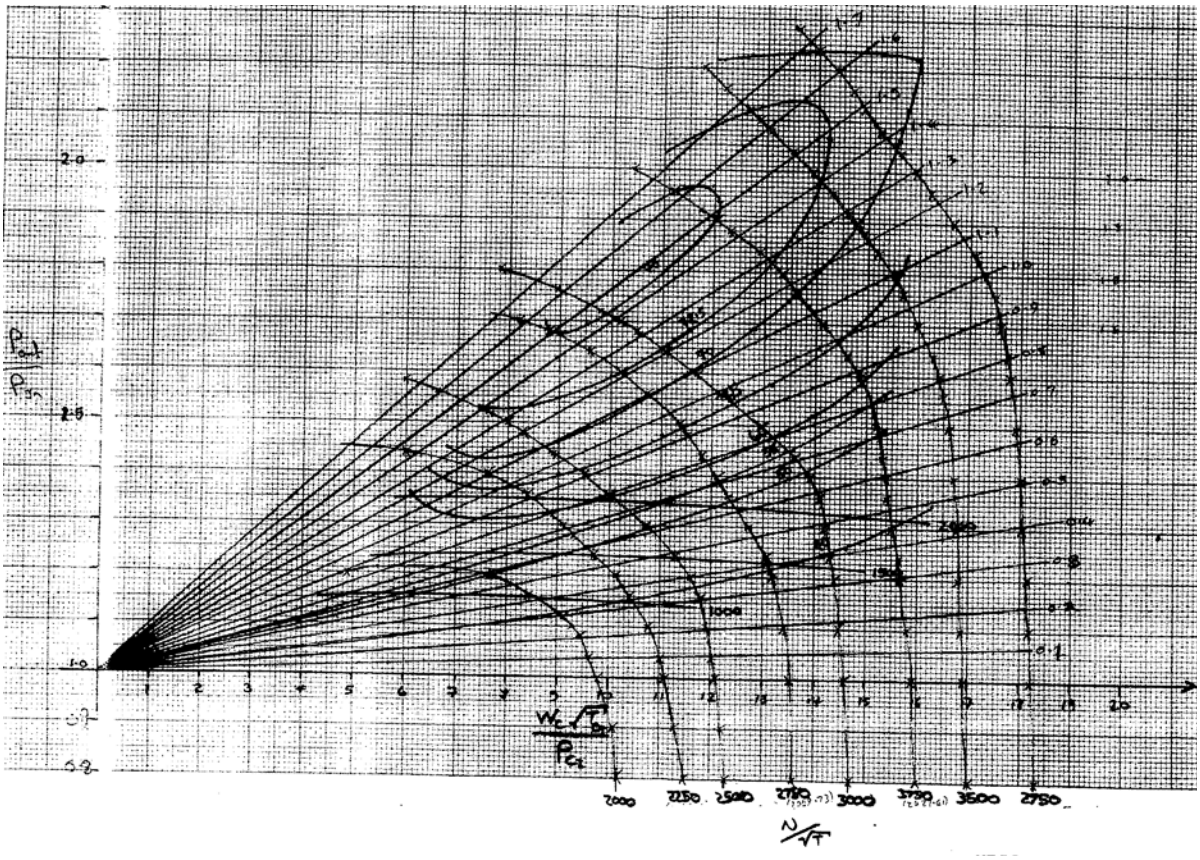

Figure 4-6 – Compressor efficiency map (Molyneaux, A et al. 1997).

The map provided in Figure 4-6 was generated by the compressor supplier during the design of the Hawk ECS. The map has been used to determine shaft speed and compressor efficiency throughout the modelling process.

The equipment and cabin flow rate split is determined by the pressure drop of each supply pipe, which is experimentally controlled by an orifice plate. A mass flow rate split of 15% equipment, 85% cabin was achieved matching the design split of the BAE System Hawk. The equipment and cabin feed orifice is also used to generate a pressure drop for the calculation of the mass flow rate. The orifice plate calculation of both the cabin and the equipment air lives is calibrated against the main bleed air mass flow rate orifice plate.

At any point a pressure differential exists within a fluid flow, the mass flow rate, $\dot{m}$, of the fluid can be calculated with known geometry (Jones 1995). Using Bernoulli's theory of continuity equation, rig geometry and measured pressure and temperature data the theoretical mass flow rate, $\dot{m}_t$, can be estimated. This assumes a reversible process where flow constriction provides no total pressure loss and the post orifice pressure measurement is taken at the point of the fastest fluid flow. In reality, the losses must be accounted for by the application of a discharge coefficient, C_d, where:

$$\dot{m} = \dot{m}_t \times C_d \tag{4-3}$$

The theoretical mass flow is calculated from Bernoulli's theory of conservation of mechanical energy continuity equation, where the total fluid mechanical energy upstream must equal the fluid mechanical energy at the orifice. The static pressure, p, kinetic energy per unit volume (half the product of fluid density, ρ, and velocity squared, v,) and potential energy of the flow must be equal.

$$p_1 + \frac{1}{2}\,\rho\,{v_1}^2 + pgz = p_2 + \frac{1}{2}\,\rho\,{v_2}^2 + pgz \tag{4-4}$$

The volumetric flow rate, $\dot{Q}_v$, can be calculated as a product of the velocity of the flow and the area of the flow path, A.

$$\dot{Q}_v = A_1\,v_1 = A_2\,v_2 \tag{4-5}$$

The mass flowrate is calculated as the product of the theoretical volume flow rate, the air density and the discharge coefficient.

$$\dot{m} = Q_v \, \rho \, C_d \tag{4-6}$$

Rearranging equation 4-4 to give an expression for the mass flow rate from the measurement of the upstream and downstream static pressure, pipe dimensions and the fluid density which is applicable for incompressible flows (Jones 1995):

$$\dot{m} = \left(\frac{A_2}{\sqrt{1-\frac{A_2}{A_1}}} \times \sqrt{\frac{2\,\Delta P}{\rho}} \right) \rho \, C_d \tag{4-7}$$

The user has extensive control of both the ECS inputs and of the ECS cycle. The input temperature, pressure, mass flow (through the cabin and equipment orifice sizes), the humidity of the bleed air and the ram air flow rate are user controllable. The rig TCV's can be run in manual (complete control) or automatic (as installed in the airframe) configurations. Through the control of these valves, the ECS back pressure (therefore mass flow rate), the cabin and equipment temperature, the compressor-turbine shaft speed, the heat exchanger heat rejection, the water extraction efficiency and the ECS efficiency can be controlled.

4.5.6. Environmental Control System Simulation

The ECS simulation is a one-dimensional thermodynamic model built in Easy 5 as shown in Figure 4-7. The model performance is validated against the experimental rig and detailed in the following section. The model presented in this study is built with extensive component data generated from isolated bench-top experimental data. The compressor, turbine, heat exchanger and PRSOV maps are imported from the manufacturer data and the duct sizing and lengths are physically measured from the experimental rig. The use of empirical component data is the first stage of model validation, the second stage is to assess total component performance against the experimental facility.

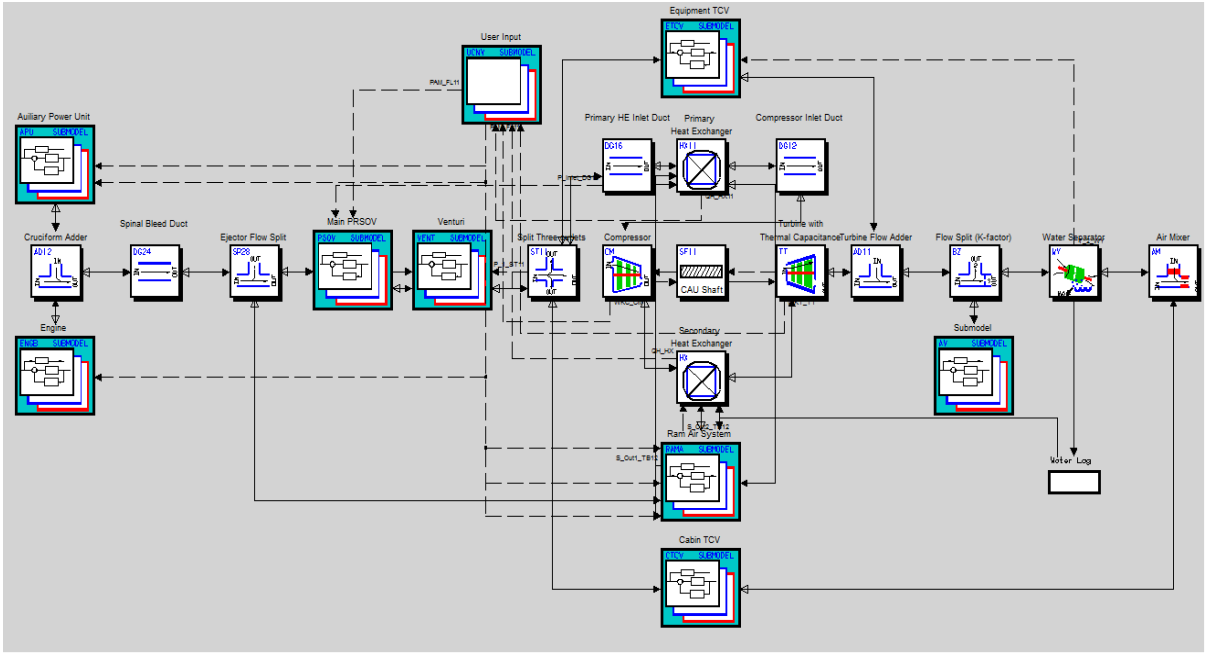

Figure 4-7: ECS Model

4.5.6.1. User Inputs

The user defines a flight condition from Table 4-2 by the application of a model 'modifier'. The modifier overrides component variables within the model, allowing different flight conditions to be tested without having to alter the core model. The flight condition defines the altitude, Mach number, and the atmospheric conditions which drive the bleed air pressure, temperature and cabin temperature settings (for the CTCV control).

4.5.6.2. PRSOV, Turbine, Compressor and Heat Exchangers

These components have been matched to experimental data in the Easy 5 model using the maps shown in Figure 4-8. The top left map shows the secondary heat exchanger charge air thermal ratio against charge and coolant flow rate. The top right shows the PRSOV downstream pressure against upstream pressure. The bottom left shows the compressor map efficiency for a given pressure ratio and inlet flow parameter with shaft speed indication. Finally, the bottom right displays the turbine map pressure ratio against efficiency.

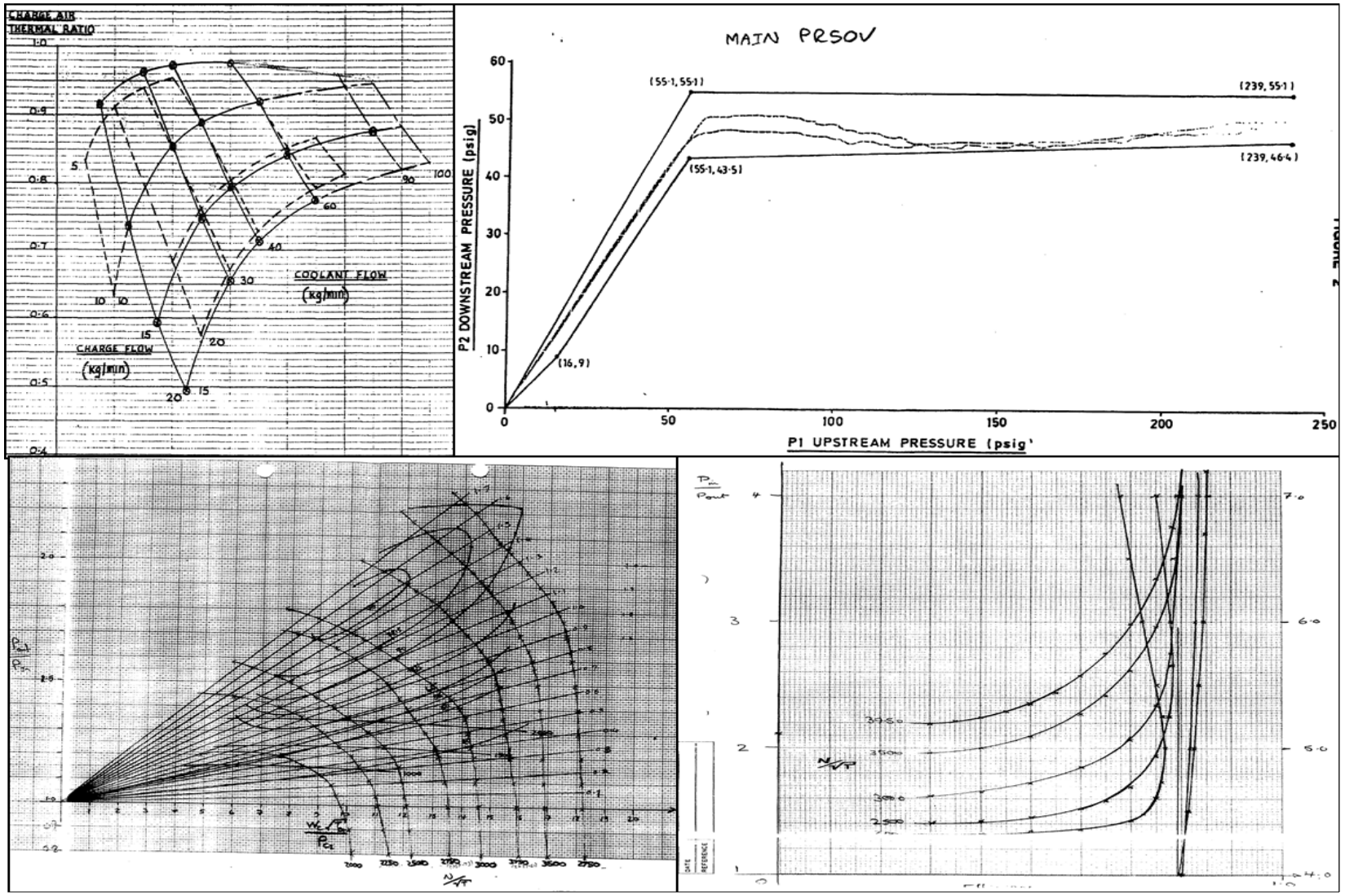

Figure 4-8: Component performance maps for model validation.

4.5.6.3. Water Separation and Humidity Calculation

The water separator is a partially validated component. The pressure drop against mass flow rate is supplied by the equipment supplier, however no water separation efficiency is provided. The water separator efficiency is modelled as a fixed extraction of 70% of free water content at all flow conditions. The water extraction efficiency is defined as the ratio of free water content at component exhaust against the free water content at inlet. The water separator has no effect on the water vapour entrained within the airflow. The real water separation efficiency and the effect of humidity on the ECS is the focus of extensive experimental validation and is detailed in Chapter 5. This is an area of literature commonly misunderstood and therefore miscalculated.

Easy 5 calculates airflow humidity through a non-iterative process. At each component, the outlet data is calculated in two stages. The first stage calculates temperature and pressure using ideal gas assumptions and assuming that values of the specific humidity and of the liquid water content do not change. The second stage performs a humidity compensation, taking these values of temperature, pressure, specific humidity and liquid water content to account how condensation or evaporation affects the thermodynamic properties. The code then updates the final value of the output parameters. The humidity compensation has four conditions depending on the conditions of the humid air inside the component.

The case of no condensation and no liquid water content is the most basic to calculate. The specific humidity at saturation for temperature is calculated and this will be higher than the specific humidity of the airflow at this condition. This means no condensation will occur. As no condensate is present at this component, the properties do not change and no humidity correction is required in the exit temperature.

In the case of condensation, the airflow specific humidity is greater than the specific humidity at saturation. Assuming that condensation is an isenthalpic process (enthalpy is constant) the specific humidity at saturation is determined using a psychometric chart. The condensate is calculated as a difference between the specific humidity and the specific humidity on the saturation line. The condensate affects the thermodynamic properties of the point on the saturation line. The final temperature is calculated by an energy balance.

This approximate procedure avoids an iterative process to determine the final temperature.

In the case of evaporation, the airflow specific humidity is less than the specific humidity at saturation value and therefore no condensation occurs. However, free water condensate is present inside the airflow so a calculation correction is required. The updated specific humidity can be determined assuming that evaporation is an isenthalpic process and all condensate evaporates. The corrected temperature is determined by an energy balance. Using the updated temperature, the specific humidity at saturation is re-calculated. Finally, the computed specific humidity must be verified to rule out condensation due to an excessive amount of condensate in the inflow.

If the evaporation continues to saturation, the same steps as the above case are followed until a second justification of the specific humidity value. Condensation occurs because the airflow specific humidity is greater than the specific humidity at saturation. In this case, the amount of condensate is excessive and the thermodynamic properties obtained represent a relative humidity over 100%. The condensate is calculated as a difference between the specific humidity and the specific humidity on the saturation line of the psychometric chart. The final temperature can be determined by an energy balance.

While the non-iterative process reduces computational time by the simplification of the humidity calculation, it also reduces the accuracy. The airflow between the turbine and LPWE is not thermally insulated and it is extremely sensitive to the heat transfer through the pipe walls. The temperature difference between these two components can be large and the flow field is probably 3D and unsteady. The location of temperature measurement (for calculation of specific humidity) is critical and lacks accuracy due to the airflow temperature fluctuations.

4.5.7. Environmental Control System Simulation Validation

The ECS model is validated against the ECS experimental data. Due to infrastructural limitations, the GTF is primarily limited by the ram air flow rate supply and has no primary

heat exchanger ram air flow. The ram air flow through the secondary heat exchanger generates up to 12kW of heat rejection, this allows to replicate 27 design flight cases from a total of 46 flight conditions. The input temperature and pressure are controlled and matched at the compressor inlet. The temperature and pressure sweep of the experimental and simulated data for a flight case (Mach 0.2, sea level) is reported in Figure 4-9 and for a ground case is reported in Figure 4-10.

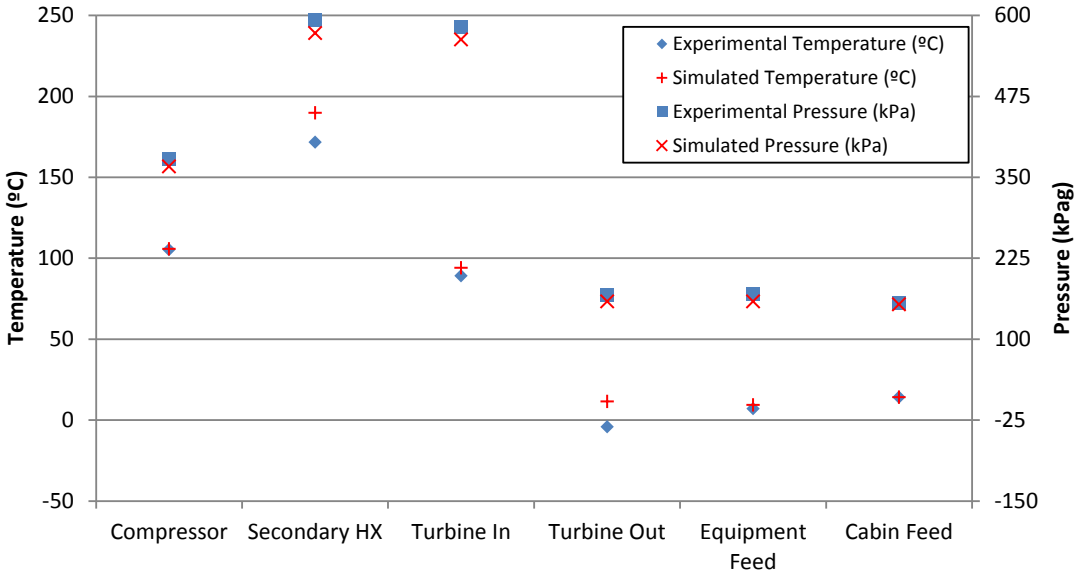

Figure 4-9: Simulated against experimental data of the ECS for a flight test case of sea level 0.2M.

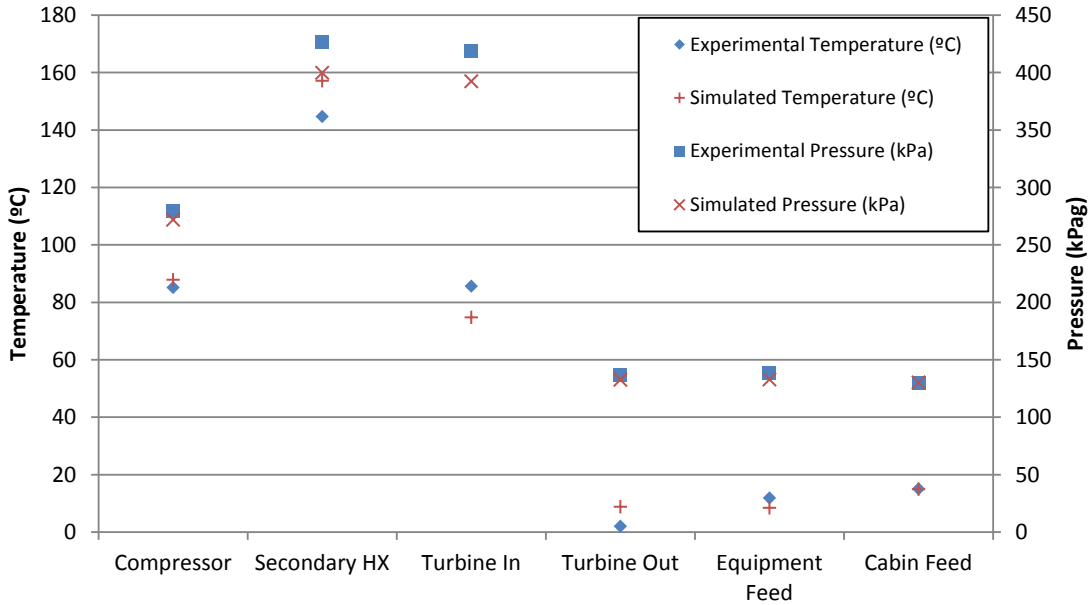

Figure 4-10: Simulated against experimental data of the ECS for a ground test case.

The experimental results presented in Figure 4-9 and Figure 4-10 is averaged data from five test repeats. To ensure test repeatability a strict experimental protocol was developed and followed in regards to the test rig was run and data was collected; explained in Section 5.1.

It was found that to achieve an acceptable temperature and pressure simulation accuracy, the inlet mass flow rate had to be set approximately 8% higher than the experimental data. The resulting increased flow rate across the CAU generates an increase in shaft speed between the simulated and the real data. The simulated data operates with a near identical CAU pressure ratio, but an increased flow parameter driving a marginally lower compressor efficiency and a higher turbine efficiency. The net result is an increased temperature difference across the turbine. When considering cabin and equipment feed temperatures, the resultant temperature difference is accounted for by the system bypass. The discrepancies between simulated and real data are noted above, however the flow path averaged temperature error is 5.1%, the pressure error is 3.4% and the mass flow rate error is 4.8%. The modelled discrepancies are all mid-CAU cycle, as the bypass mass flow rate equalises the ECS exhaust temperature and pressure. The error is deemed acceptable for the purpose of this investigation, as the ECS exhaust conditions are correct and the flight profile will be compared as model data versus model data.

4.5.8. Avionic Subsystem

The avionic heat flow validation is available at both the subsystem and at the component level, therefore it is a requirement to decompose the model down to the component level. This subsystem has the least comprehensive validation data and the worst availability of genuine components due to IPR constraints. While some flight test data is available, the information is of very low resolution, detailing only the highest, lowest and average temperatures recorded from over 11,000 operations. However, the flight and atmospheric conditions are unknown and the inlet airflow temperature can only be assumed based on knowledge of the ECS equipment supply temperature control.

The forward avionic bay is replicated in both the experimental rig and in the numerical modelling. The knowledge gap regarding this project is focused around the current inability

to accurately determine the inflight thermal conditions of the forced cooled avionic modules. The experimental facility has the capability of covering part of the flight and atmospheric envelopes. The simulation extend this coverage to the full flight and atmospheric envelopes. The simulation is then used to implement new technologies without the requirement for expensive and time consuming rig modifications. This facility forms one of the few thermal avionic test rig used for BAE Systems research.

4.5.9. Avionic Subsystem Hardware

The facility consists of six forced convection cooled replica avionics modules mounted to a genuine BAE Systems Typhoon avionics tray, as shown on the bottom right of Figure 4-11. The tray is housed within a replica avionics bay environment (top right of Figure 4-11), which is tested within an environmental chamber. The thermodynamic performance is of the avionic modules calibrated to the corresponding aircraft components in terms of power output, pressure drop, flow rate, airflow temperature difference, external thermal profile and geometric dimensions. The aircraft avionics bay installation and location in the airframe is shown on the left of Figure 4-11.

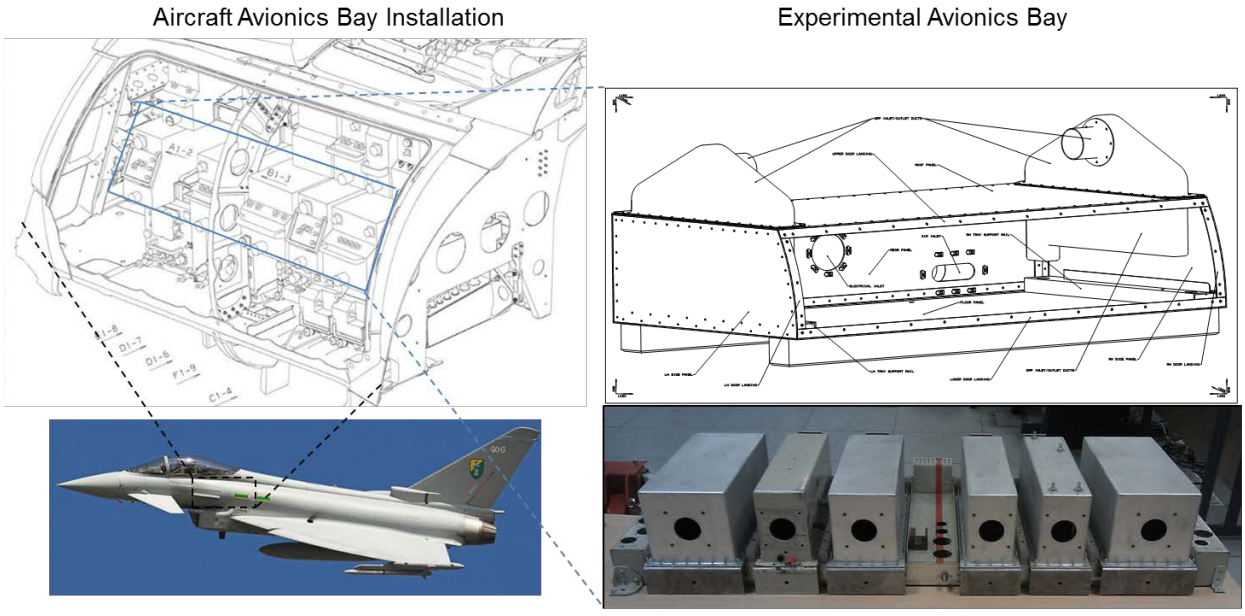

Figure 4-11: Experimental rig and aircraft avionic bay.

The total avionic module thermal loading is the combination of component and environmental thermal loading. The avionic bay temperature is dependent on the avionic

cooling air mass flow rate, the kinetic thermal loading and the solar loading through the aircraft skin.

4.5.9.1. Avionic Module Calibration

Information on the avionic thermal loads, physical size and location within both the airframe and the avionic tray are provided by BAE Systems. The physical size of the avionic module is dependent on the power output; the larger the module, the more circuit cards, the bigger the heat rejection requirement and therefore the larger the conduction to cold wall heat exchanger installed.

The replica modules are based on equipment used by BAE Systems to balance the mass flow distribution across the avionic system which is a 'cold' avionic test facility at BAE Systems Warton. The modules in this investigation are modified by the addition of a thermal load. The thermal loading is providing by 5 resistive heaters and finned "heat sinks" mounted within the module. A Computer Aided Design (CAD) image detailing the internal heat source geometry of the modules is shown in Figure 4-12.

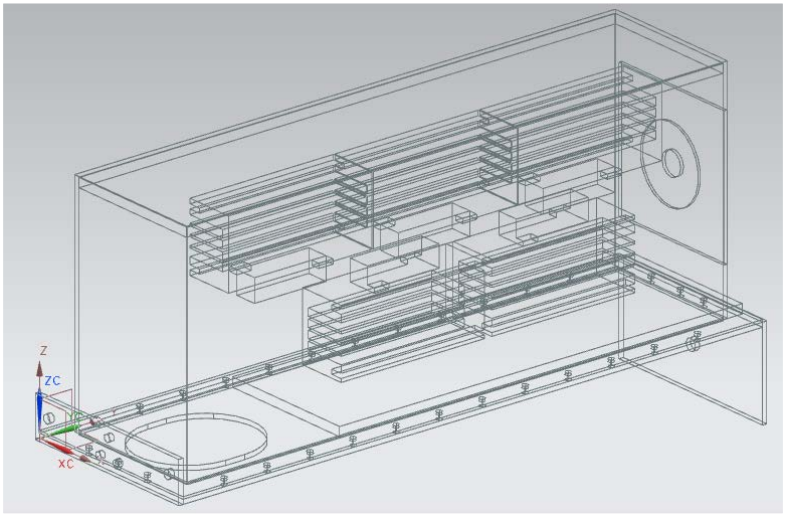

Figure 4-12: CAD of a typical avionic module with heater elements.

The mass flow rate distribution across the 6 avionic modules on a single tray is controlled by the module characteristic pressure drop, which is a parameter that is defined by BAE Systems. The characteristic pressure drop is obtained y squaring the orifice plate Equation 4-7, differentiating it by the mass flow rate squared. Using the equation for the state of air and assuming the flow density is constant. The replica module characteristic pressure drop

is controlled by an exhaust orifice plate. The size of the orifice plates is varied to control the characteristic pressure drop of each module and therefore calibrate the mass flow rate distribution across the tray.

The pressure drop across the orifice plate is utilised to calculate the flow velocity and the air mass flow rate. When measuring a mass flow rate based on the pressure drop across an orifice plate, a correction factor is applied to account for vena contractor effect; known as the discharge coefficient. The mass flow calculation is based on an ideal gas and assumes that a pressure measurement can be taken at the point of peak airflow velocity. In reality, this is not possible so a discharge coefficient is applied to account for these inaccuracies. The discharge coefficient is determined through the orifice plate calibration of each module. On board the aircraft, the module is supplied a known mass flow rate from a manufacturer calibrated mass flow rate controller. The mass flow rate controller is calibrated to within 0.2% full scale deflection. The discrepancy between the calculated and the measured mass flow rates are accounted for by the discharge coefficient. The calibration process is an off-rig 'bench top' process, where the mass flow rate controller is used to generate the characteristic pressure drop data and the orifice plates discharge coefficient for mass flow rate calculations.

The thermal interaction between avionic modules in flight is an area of interest and the exterior thermal signature of the avionic module is critical to establishing the correct thermal footprint inside the avionics bay. A thermal image of a genuine avionic module was acquired at BAE Systems Military Air and Information (MAI), Warton. This is shown in Figure 4-13.

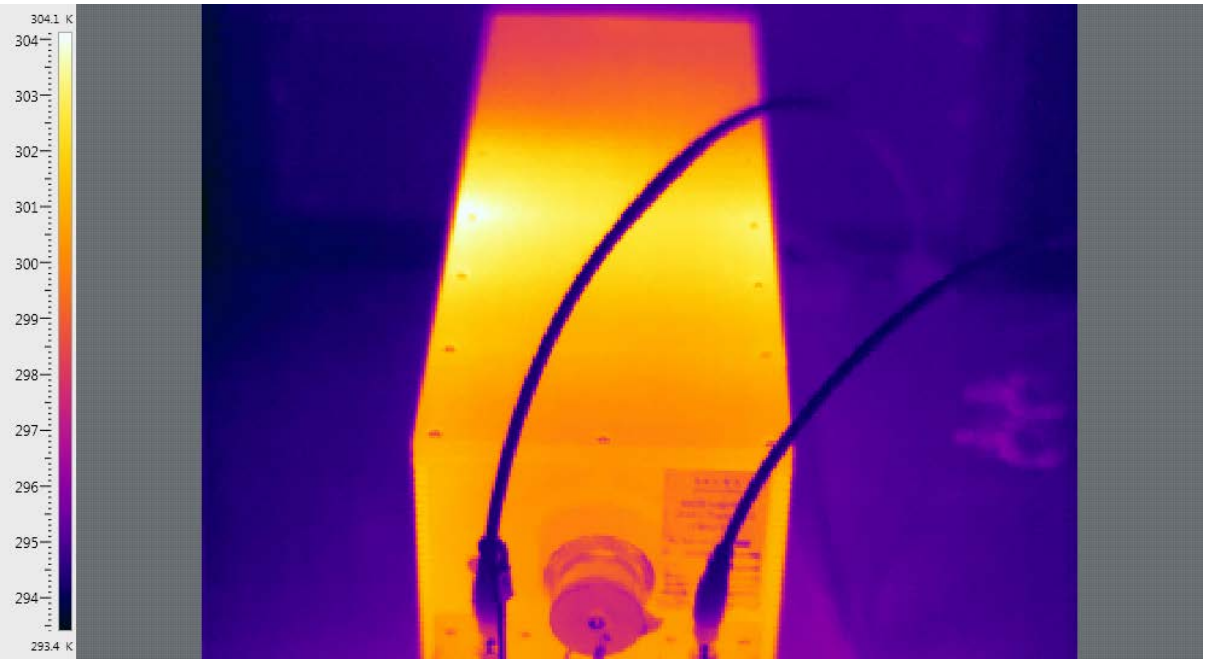

Figure 4-13: A thermal image of an avionic module on test at BAE Systems Warton.

Operational avionic modules were found to have a nearly isothermal surface temperature distribution. This is an expected result, due to the high thermal resistance from the circuit cards to the outside wall.

The final component for the calibration of the model avionic modules was to achieve the correct airflow temperature differential across the module with the pre-determined fixed heat load, pressure drop, mass flow rate distribution and external thermal signature. The replica module heat loads were mounted on a very low thermal conductivity internal floor/ceiling, which was adjusted in the vertical plane to achieve a given internal aspect ratio. This allowed the tuning of the air flow path to heat sink area ratio, of the internal airflow velocity and of the internal turbulence. This allowed to adjust the overall heat transfer rate of each avionic module without varying other parameters. As the floor/ceiling was made of a very low thermal conductivity material, all heat loads were conditioned by forced convection cooling and the replica modules also replicated the isothermal external surface signature of the ones on board the aircraft. The thermal calibration data was provided from pass-off certification testing of a FCC (Maxwell et al. 2010)

4.5.9.2. Avionic Bay Thermal Conditions

The avionic module performance is sensitive to the environmental thermal loading due to the location of the avionics bay, shown in Figure 4-11. A Typhoon avionics bay door has been supplied by BAE Systems. Using the genuine composite bay door in the GTF ensures the door thermal conductivity will replicate those seen in flight. The avionic bay is mounted within an environmental chamber temperature with a temperate range of -70ºC to +180ºC, which is wider than the range of recovery temperatures seen in flight. However, the inflight convective heat transfer coefficient on the avionic bay door exterior is beyond the range that is obtainable with an environmental chamber. In order to generate comparative recovery temperature conditions, the temperature difference between the door surface and the environmental chamber must be adjusted to obtain the correct rate of heat transfer.

The convective heat transfer coefficient governs rate at which energy is passed from a fluid to a solid. The Nusselt number is the non-dimensional ratio between the convective heat transfer coefficient and the conductive heat transfer coefficient of the fluid, and is commonly utilised to compute heat transfer rates at a fluid/solid boundary. Many studies have concluded that a direct correlation exists between air flow condition (Reynolds number) and heat transfer rates (Nusselt number) (Igarashi et al. 2004; Jubran et al. 1996; Sparrow et al. 1982). The Reynolds number is a non-dimensional measure of the flow state (turbulence). A direct correlation between the Reynolds number and convective heat transfer coefficient can be provided by dimensional analysis and the Reynolds numbers inside an environmental chamber do not match those seen in flight.

In order to replicate the flight conditions using a ground test rig, the heat transfer rates through the door must be equal. The local energy transfer through the bay door is governed by using Newton's law of cooling (Sanitjai & Goldstein 2004). The avionic bay has been subjected to a number of differential temperatures ranging from +20ºC to +140ºC. The thermal response inside the avionic bay has been measured to determine the relationship between the recovery temperature and bay the temperature. Experimental data from this test have been used to develop a number of time based polynomial

functions which describe the response of the bay air temperature to kinematic bay door thermal loading at any given time. These functions can be used to assess the response of bay temperatures across wide changes of recovery temperature. The changes in flight condition are assumed to be instantaneous. The above functions can be used to calculate the thermal response of avionic bay air to a change in recovery temperature, as shown in Figure 4-14.

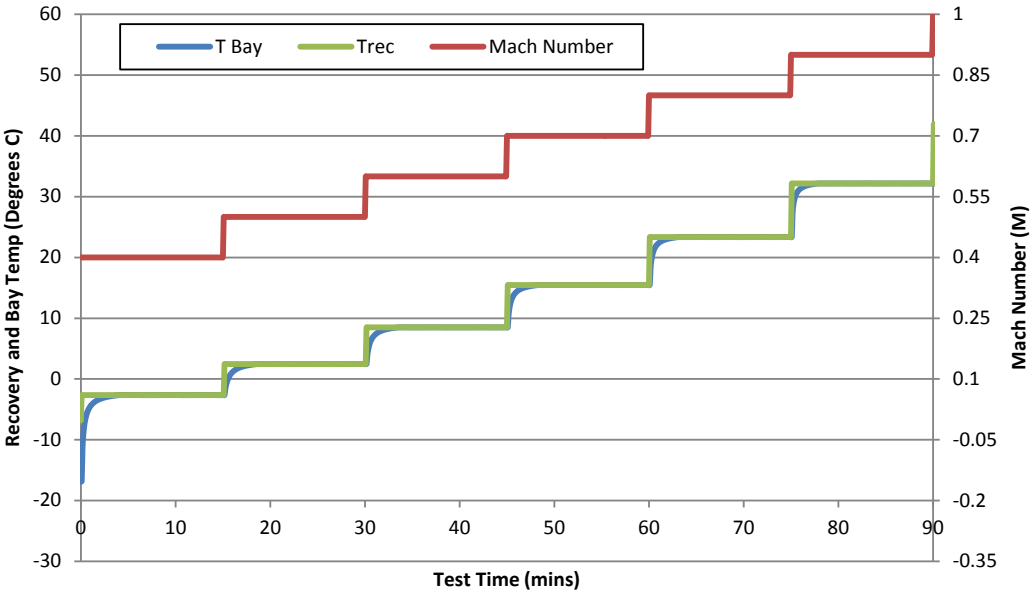

Figure 4-14: **The response of avionic bay air temperature to changes in flight condition**

It can be seen that, following a small stabilisation period, the recovery and the bay temperatures are equal. The larger the temperature differential across the bay door, the smaller the stabilisation period. Across a typical flight profile, the magnitude of variations in Mach number and altitude are such that the stabilisation period can be assumed as negligible. Therefore, the avionic bay temperature can be assumed as equal to the recovery temperature.

4.5.10. Avionic Subsystem Simulation

Numerical simulation is used to apply new technologies. MSC Easy 5 is utilised to provide compatibility with the ECS model. The IPR restrict some avionic information flow to the wider academic community, making 3D simulations impractical. Forced cooled avionic modules are modelled as two orifices (inlet and exhaust) and a node (a volume). Natural

convection modules are modelled as a single orifice with no heat transfer, as just pressure drop and flow rate data is required for calculating the ECS supplied airflow. The airflow is modelled as a constant property ideal gas. The flow through an orifice is calculated with the assumption that the upstream fluid and the fluid in the orifice throat have equal energies. Easy 5 solves for pressure and temperature using the equations of continuity and energy balance across a node.

The tray is modelled with an orifice and a node per avionic module. The ECS branch is modelled as two orifices and a node. The avionic modules are modelled with an energy transfer from the volume wall to the gas (avionic power output) and an energy transfer from the environment to the node (bay temperature). The model requires two user inputs, a system inlet pressure (supplied from the experimental data for tray validation by BAE Systems) and a flight condition. The relationship between component temperature difference and recovery temperature is validated against experimental data from the avionic tray.

The MSC Easy 5 model predictions were found to be accurate to within ±4% in mass flow rate prediction, ±5% in avionic module exhaust temperature and ±8% in module pressure drop. The validation against experimental data is displayed in Figure 4-15. Two validation cases are displayed for a single avionic module experimental data against simulation data. The temperature difference across the module is compared for a mass flow rate sweep and a recovery temperature sweep.

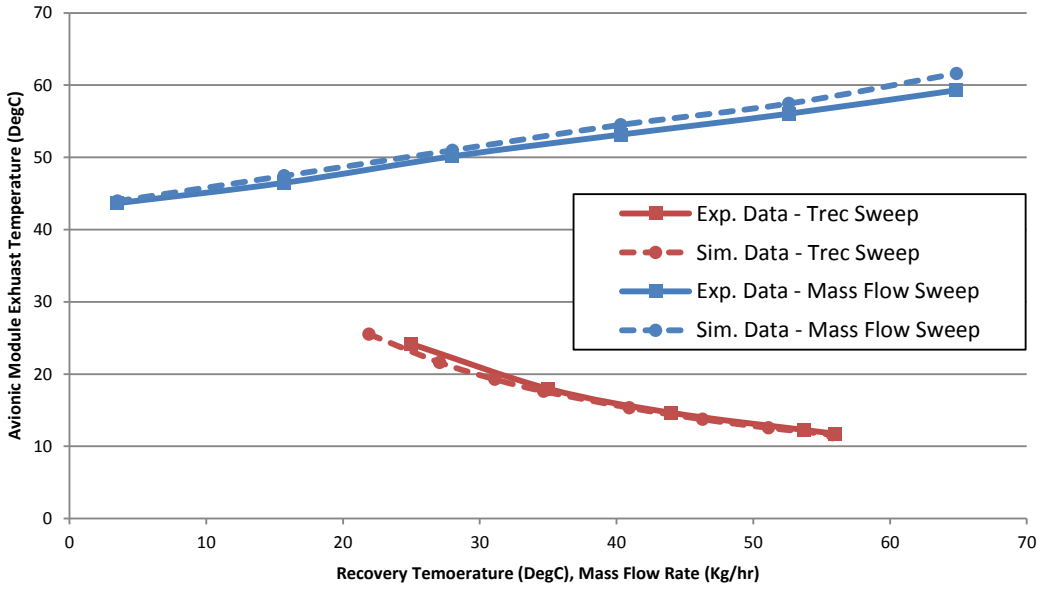

Figure 4-15: Avionic bay model validation.

4.5.11. Cabin Environment and Natural Convection Avionic Bay Simulation

The cabin and secondary avionics bays are considered as pressurised volumes which are thermally conditioned by the ECS airflow and thermally loaded by avionic, kinetic, solar and (for the cabin) pilot metabolic loads. The analysis did not include performing any physical experiment and does not consider the component temperatures in these bays. The analysis is included for the requirement to consider the complete avionic airflow path when optimising the avionic thermal management. The cabin environment is modelled only by software and it is based on measurements taken from the BAE Systems Hawk at Loughborough University.

The rear and underfloor avionic bays consist of natural convection cooled modules and the bays are considered a thermally conditioned volume. No method for calculating the electronic component temperature has been included in this study. The avionic module health is assessed from the calculation of the avionic bay temperature, which must adhere to the thermal design limits detailed in Chapter 2. The avionic heat load in each bay is fixed throughout the flight profile. The heat balances for the underfloor avionics bay ($Q_{U.AV\ Bay}$) and rear avionics bay ($Q_{R.AV\ Bay}$) are respectively:

$$Q_{U.AV\ Bay} = Q_{U.Av} + Q_{Kinetic} + Q_{Solar} \quad (4\text{-}9)$$

$$Q_{R.AV\ Bay} = Q_{R.Av} + Q_{Kinetic} + Q_{Solar} \quad (4\text{-}10)$$

4.5.12. Bay Temperature Validation

Flight data was provided by BAE Systems for validating for bay temperature predictions from the Easy 5 model. The temperature scale resolution and the atmospheric and operational coverage of the flight data is limited. Temperature measurements are taken at bay inlet and bay exhaust and the mean bay temperature is assumed as the average of the two measurements. A total of 6 flight conditions and 3 ground conditions are available, with an assumed ISA atmosphere. The data in Figure 4-16 is displayed for flight condition F21 (20,000ft, Mach 0.5 maximum range) and F30 (30,000ft, Mach 0.6 maximum range); the full list of flight case definitions is shown in Table 4-2. The highest discrepancy is an over-prediction of the cabin mean temperature by 2.7ºC.

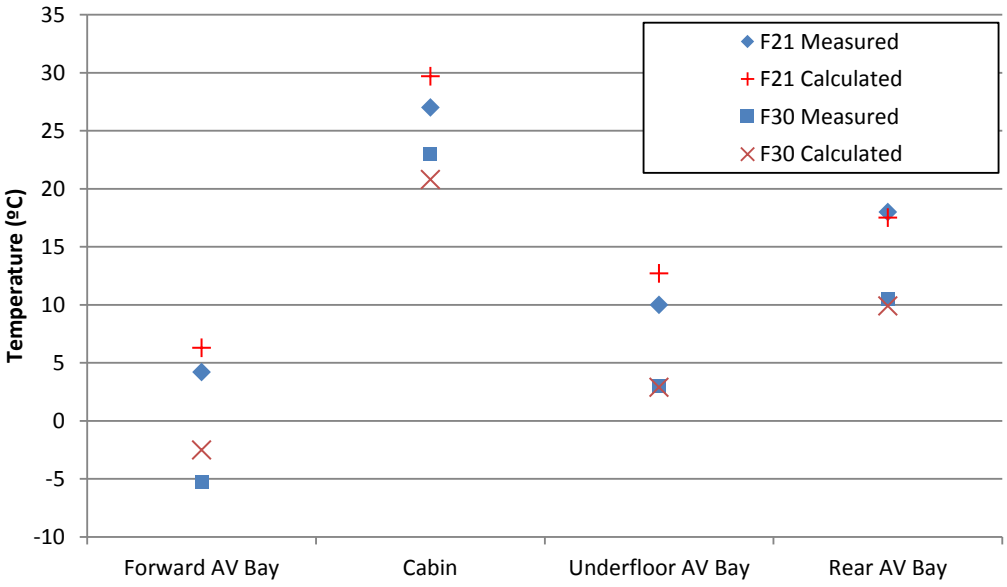

Figure 4-16: Bay Temperature data comparison of calculated and flight data.

4.6. Conclusion

A multi-disciplinary approach has been adopted for the design and operation of the GTF. The system performance analysis is obtained with the combined use of hardware,

software, and of thermodynamic calculations. This chapter has detailed the development of the GTF and has provided an experimental validation of all modelled tools. Through the validation of the avionic and of the ECS subsystems, a number of key thermodynamic relationships have been established. An example of this is the exterior thermal profile of an avionic module, or the relationship between the avionic bay door recovery temperature and the avionic bay temperature. The development of these relationships is a key step towards the replication of inflight thermal conditions. Once the conditions can be accurately replicated, the system performance can be analysed and subsequently optimised.

A new GTF has been developed to act as a test bed for the application of a new methodology for avionic thermal management optimisation. The design, development, and build of this new test facility has been completed, and the GTF has become operational in 2016. The GTF has been proved to be reliable and able to generate highly repeatable test data through the careful installation and calibration of all components and instrumentation. The facility allows the experimental replication of the bleed air, ECS and avionic subsystem thermal conditions over a subset of the flight envelope. The ECS test rig has been subsequently utilised for an experimental investigation as part of a joint project between BAE Systems, Cranfield University, Boeing and Loughborough University, outside of this research. The avionic subsystem GTF is one of the few thermal avionic test rigs that BAE Systems utilise for research. A 1D thermodynamic model was developed and calibrated for the bleed air, ECS, avionic and cabin subsystems, to expand data beyond the infrastructural limitations of the GTF.

Extensive time has been allocated obtain to a robust and high-fidelity test facility. The procurement, development and build of this facility is the direct result of this project. This included obtaining new laboratory space, completing infrastructural and utility updates (power supply, single and three phase), and commissioning the new test rigs. Prior to this project, very little of the equipment was available such as the Hawk ECS and the avionic test plates. This key equipment and was gained through the extensive strengthening of the

industrial contacts. It should be noted the time, resources and effort allocated to the development of a new test facility represent a significant portion of this project.

The key requirements of the GTF have been identified based on the review of previous literature. The GTF has been specifically designed to form a test bed for the evaluation of the methodology discussed in Chapter 3. The total TMS has been decomposed to the level at which each subsystem or component can be validated against data supplied by BAE Systems. The decomposition of the full system into subsystems with clear interfaces allows the flexibility of the facility to use validation data from various sources at component, subsystem or system level. The integration of these components and subsystems into a single data flow provides a single analysis tool with the capabilities listed in the introduction of this chapter.

The following chapter evaluates the performance of the GTF to provide information to fill the knowledge gap. After this, a thermal management optimisation strategy is defined in Chapter 6.

5. Experimental Investigation of a Multidisciplinary Approach

The aim of this chapter is to evaluate the equipment detailed in Chapter 2 through the application of the methodology detailed in Chapter 3 with the GTF detailed in Chapter 4.

The focus of this work is centred on the ECS and on the forced cooled avionic subsystems. These subsystems represent the biggest knowledge gap of the TMS and therefore required the most extensive experimental evaluation. The requirement for a high-fidelity, mission-level analysis in a single facility will be evaluated. A number of key system, ECS and avionic subsystem findings are identified which have not been reported by past single-component analysis. It is shown that traditional system performance metrics and control feedbacks are misleading. This finding is an output of this whole-system time-resolved approach as the resolution of the data is beyond that of a traditional steady-state approach. It is suggested that by continuing to use the traditional 1D modelling approach as detailed in Chapter 2, this information could not be identified and unexpected system behaviour will continue to be built into future systems.

When considering the ECS, the subsystem cannot be effectively controlled using temperature as a feedback metric. It will be shown that the CoP is a weak ECS subsystem performance metric when it is used improperly, furthermore it does not convey the TMS cost to the aircraft. It will also be shown that bleed air humidity is misunderstood and fundamentally drives performance degrading system level design decisions. By considering mission-level data, the avionic modules were proved to be both undercooled and overcooled, depending on the flight and the atmospheric conditions. The issues listed above have not been previously identified either in the literature or by BAE Systems through the traditional approaches to system replication and analysis.

Initially, results are given to define the constituents of a system performance calculation and then a mission-level system characterisation is performed. The characterisation provides a thermal sensitivity analysis of the system that outlines an optimisation approach. It will be shown that the avionic modules have two main areas of operation; they remain substantially overcooled throughout the flight envelope in all atmospheric conditions and marginally undercooled at ground case in a hot atmosphere. The conclusion of this chapter is an optimisation strategy of the system based on a component-led integrative approach to improve the thermodynamic efficiency of the TMS from the baseline configuration.

5.1. Experimental Test Protocol

Previous to discussing the results of experimental testing, it is a requirement to explain the strict experimental test protocol that was developed throughout this investigation and then adhered to for all testing. This was implemented to ensure a high repeatability of test procedure and deliver scientifically valid results.

It was discovered that the performance of the ECS was experimentally sensitive to the operational process (as detailed later in Figure 5-32). This defined the requirement for a test protocol to cover considerations such as the order in which inputs should be changed, a requirement to ‘baseline’ measurements before each test point, test limits (temperature,

pressure, flow rate), sensor calibrations, safety critical processes and component protection procedure.

5.1.1. Test Procedure

All experimental data presented in the following chapter is presented as an average of test repeats for each point with the exception of Figure 5-2, Figure 5-3, Figure 5-4, Figure 5-5 (these show each test point) and Figure 5-16 (a transient test completed once and presented against time). Typically, all tests points are averaged from 3-5 test repeats (depending on investigation). The experimental elements can be split into the ECS and avionic rigs. The ECS rig is the most complex and required the heaviest control on test procedure.

5.1.1.1. ECS Rig

A 3-cylinder compressor provided a high pressure air feed to the collector tanks in the air farm. As the ECS consumed more air than the compressor could produce, the tanks are slowly depleted over time. As the head pressure of the rig changes, the control valves move to provide a constant pressure at ECS inlet. It was noted that at lower tank pressure (under 5Bar) a mass flow rate reduction was seen with the control valves in automatic operation. Tank pressure was strictly controlled between 13 and 7BarA. A test was aborted if the tank pressure dropped below this value. The air farm is maintained by technical staff at Loughborough University, completing regular filer and desiccant drier checks to provide regular feedback on system health.

With a constant airflow rate supply, inlet temperature is controlled through the heater with a PID controller. The controller gains are tuned to match the condition of the airflow rate if a number of tests are to be completed at similar flow rates. These measured ensured rig inlet conditions are highly repeatable; measured at ±0.5°C and ±0.005kg/s.

As detailed in Figure 5-32, the ECS performance was sensitive to how the rig was controlled. To improve system repeatability, each new test point would be approached through the same procedure. The rig would return to a baseline operating system (both

TCV's open), before being driven to the operating condition of interest. With the application of this procedure, the rig was very repeatable. The exception to this rule was when the test required a control procedure to be followed to simulate flight condition changes following a designated flight profile.

A temperature stabilisation criterion of $\Delta<0.2°C\ min^{-1}$ was established and strictly adhered to. The data acquisition system was coded to include a rate of change graphic for each variable to improve the ease of monitoring and achieving the stabilisation requirement.

5.1.1.2. Avionic Rig

The most challenging control of the avionic rig conditions was the inlet air temperature, as the fan pulled from ambient lab temperature. Throughout the year, this was found to vary between 16° and 25°C. To avoid error in avionic component readings, the initial thermodynamic configuration work of the avionic modules was completed in terms of temperature difference. This allowed the components to be normalised to a single input temperature, the results of this are presented in Figure 5-28. The normalisation for avionic component thermal performance allowed easy integration with the simulation work discussed in the following chapter.

5.1.2. Sensor Calibration

To produce repeatable data, frequent calibration checks on measurement equipment is required. The main sensors are used in both rigs are pressure sensors, thermocouples and potentiometers. The calibration procedure of these components is described in Chapter 4. Due to the nature of the test work, these sensors were not calibrated on a regular time based schedule, but re-calibrated before and after every round of testing.

5.1.3. Safety Specific Procedure

When working with high pressure (13BarA storage vessels), high velocity and high temperature equipment, the test procedure required safety elements. Each rig was covered under its own risk assessment, which was completed as part of this project. Training was undertaken for the use of the air farm, system welding was completed by certified high pressure welding facilities and all wiring was completed by or signed off by

the Loughborough University electrical technicians. Additional safety critical processes included safety interlocks on laboratory doors, wearing of appropriate PPE and rig cool down procedures to avoid contact with high temperature components.

5.1.4. Component Protection

In aircraft operation, the ECS has a Pressure Relief Valve (PRV) at the inlet to the compressor for component protection. This component was not provided to Loughborough University with the loan of the ECS as the tapping was utilised for additional instrumentation. It was therefore possible to damage ECS components by an overpressure and subsequent over temperature incident. To avoid damaging the ECS at all costs, the test procedure involved instructions for rig start up and cool down; as follows.

- Open ECS TCVs and close main air control valve (G4 Valve)
- Close cell doors and release electro-mechanical SOV
- Slowly open G4 Valve until mass flow rate reached 0.08kg/s and allow ECS to stabilise
- Switch on inlet heater and set to desired temperature. If required, switch on humidity injector and set to desired injection rate
- Close TCVs to desired position and commence testing if tank pressure is adequate

When shutting down the rig, the process would be repeated in reverse. Open the TCVs, switch off heater and switch off water injection to flush the rig with ambient air and allow all components to cool. Reduce airflow rate with the G4 valve to 0kg/s and then shut the electromechanical SOV. Following this procedure allowed the protection of the ECS and test equipment such as the heater elements and water injector.

In conclusion, in terms of test repeatability a temperature tolerance of ±1.5°C was measured at a given operating point across all rig temperature sensors. As this is within the thermal tolerance of the measurement equipment (k-type thermocouples), it was agreed this level of accuracy is acceptable.

5.2. Energy Study

The system effectiveness is given by the CoP. When considering a system-level analysis, it can be considered that the total work consumption rate is the work rate input required for generating the coolant stream. The useful heat transfer rate is the removal of the pilot, the avionic and the environmental thermal loads of the cabin and subsystems. In this analysis, the ECS is considered to provide no useful heat transfer by itself, but it generates a cooling capacity to enable the transfer of heat in subsequent sub-systems. The following section defines the measurement or calculation of the total work consumption rate and the net useful heat transfer rate terms of the CoP Equation 2-6.

5.2.1. Total Work Consumption rate

The system power consumption, $\dot{W}_{inlet}$, is the calculation of power required to deliver a stream of ram and bleed air to the ECS. This is the summation of the power consumed in the compression of bleed air stream,$\dot{W}_{Bleed\ Air}$, the power to overcome the aerodynamic drag of the heat exchangers at the aircraft flight speed, $\dot{W}_{RamHX}$, and the power to generate any additional inducer flow rate. An inducer flow is unconditioned bleed air which is injected in the ram air exhaust duct and rapidly expanded to generate a low pressure region behind the heat exchanger. The low pressure region then induces an airflow through the heat exchanger to provide a coolant flow at zero vehicle speed. The inducer flow is shut down in flight when the landing gear retracts into the airframe.

In order to provide at accurate estimate of the system performance, the total input power calculation must account for the rate at which energy is jettisoned overboard which could have otherwise been used for further useful work. The power in the airflow at the system exhaust, $\dot{W}_{Exhaust}$, allows the future addition of further subsystems, without compromising the accuracy of this analysis. Therefore,

$$\dot{W}_{inlet} = \dot{W}_{Bleed\ Air} + 2\,\dot{W}_{RamHX} + \dot{W}_{Inducer} - \dot{W}_{Exhaust} \quad (5\text{-}1)$$

The compression of bleed air, inducer flow and expansion of exhaust airflow is calculated as an irreversible constant property ideal gas process, based on the axial compressor isentropic efficiency, η_{cc}, of the engine by;

$$\dot{W}_{Bleed\ Air}, \dot{W}_{Inducer,} \dot{W}_{Exhaust,} = \frac{C_p \ T_{amb}\, \dot{m}}{\eta_{cc}} \left[\left(\frac{P_2}{P_1} \right)^{\frac{\gamma-1}{\gamma}} - 1 \right] \quad (5\text{-}2)$$

The temperature and pressure ranges seen throughout the cycle allow for air to be approximated as a perfect gas (Rogers & Mayhew 1992). The equation assumes the standard form of the steady flow energy equation, neglecting changes in gravitational potential energy and in the fluid velocity. The power consumed by the generation of ram air is detailed in Chapter 2.

5.2.2. Net Useful Heat Transfer Rate

The net useful heat transfer rate from the avionic bay is defined as the total heat rejection rate which is the summation of the avionic thermal load, $\dot{Q}_{F.AV}$, kinetic loading, $\dot{Q}_{Kinetic}$, and solar thermal loading, $\dot{Q}_{Solar}$ according to equation 5-3. The kinetic and solar loading across the flight and atmospheric envelopes are detailed in Chapter 2 and summarised by equations 5-4 and 5-5.

$$\dot{Q}_{F.AV.Bay} = \dot{Q}_{F.AV} + \dot{Q}_{Kinetic} + \dot{Q}_{Solar} \quad (5\text{-}3)$$

$$\dot{Q}_{Kinetic} = h\, A \left(T_{Rec} - T_{Bay} \right) \quad (5\text{-}4)$$

$$\dot{Q}_{Solar} = A\, \tau\, \dot{Q_{sl}} \quad (5\text{-}5)$$

The met useful rate of heat transfer from of the cabin ($\dot{Q}_{Cab}$) is the summation of avionic, kinetic, pilot and solar heat load;

$$\dot{Q}_{Cab} = \dot{Q}_{C.AV} + \dot{Q}_{Kinetic} + \dot{Q}_{Solar} + \dot{Q}_{Pilot} \quad (5\text{-}6)$$

The cabin avionic heat load ($Q_{C.AV}$) is fixed throughout all flight conditions and it is provided by BAE Systems. The kinetic and solar heat loads are calculated by equations 5-4 and 5-5, although the transmittance of the panel (τ) is considerably larger for the transparent cabin canopy. The physical dimensions of the cabin heat transfer surfaces are based on the measurements of the BAE Systems Hawk 200, located in the Department of Aeronautical and Automotive Engineering at Loughborough University. The transmittance of the panel material is provided from literature (Rebbechi 1980).

The rear and underfloor avionic bays are fitted with natural convection cooled modules and the bays are considered a thermally conditioned volume. As these modules have no forced convection heat exchangers, an exhaust temperature cannot be calculated. The avionic heat loads in each bay is fixed throughout the flight profile with the bay exhaust and the mean bay temperature calculated as per the forward avionics bay. The heat balance is shown in equations 5-7 and 5-8:

$$\dot{Q}_{U.AV\ Bay} = \dot{Q}_{U.Av} + \dot{Q}_{Kinetic} + \dot{Q}_{Solar} \tag{5-7}$$

$$\dot{Q}_{R.AV\ Bay} = \dot{Q}_{R.Av} + \dot{Q}_{Kinetic} + \dot{Q}_{Solar} \tag{5-8}$$

The avionic loads are assumed constant throughout all flight conditions and are provided by BAE Systems. The kinetic and solar thermal loadings are calculated with equation 5-4 and 5-5. The physical dimensions of the bay are also measured from the BAE Systems Hawk 200 at Loughborough University.

The following section discusses the measurement and calculation of these heat loads at different operating conditions. The work will characterise the thermal management system performance at a subsystem level, before providing a mission level-thermal sensitivity study.

5.2.3. Input power

The calculation of bleed air characteristics (power consumption, temperature, pressure) does not include the effects of engine performance in any further detail than through empirical relationships from literature. While it is understood that the consideration of engine and TMS performance should be simultaneous, the complexity of the propulsion system cannot be included in the scope of this work. The generation of bleed air is defined as an irreversible compression of a fluid; accounting for inefficiencies in the process by the engine compressor isentropic efficiency, η_{cc}. This assumption is valid as the calculation of energy in the exhaust flow is an isentropic expansion, therefore the bleed air power is a differential across the system. In terms of defining TMS efficiency, this approach is

accurate. In terms of defining an accurate cost to the aircraft, the approach would need to fully consider the effect of the bleed air minimisation on the propulsion system.

The bleed and ram air input power consumption is detailed in Figure 5-1 for a flight profile of ten flight conditions. The flight conditions operating in an ISA standard day atmosphere are detailed in Table 5-1. Each case is considered to be a to the steady state condition.

Flight Case	Ground Ops	Take Off	Climb 1	Cruise 1	Accelerate and Dive	Combat	Climb 2	Cruise 2	Land	Ground Ops
Mach Number	0	0.2	0.5	0.6	0.83	0.85	0.5	0.7	0.2	0
Altitude (Ft)	0	0	20000	30000	1000	20000	20000	40000	0	0
Ambient Pressure (kPa)	101.3	101.3	46.6	30.2	101.3	46.6	46.6	18.8	101.3	101.3
Ambient Temperature (ºC)	15.2	15.2	-24.8	-44.3	15.2	-24.8	-24.8	-56.5	15.2	15.2
Duration (mins)	15	10	5	20	3	15	5	35	7	10

Table 5-1: Flight profile cases operating in ISA atmospheric conditions.

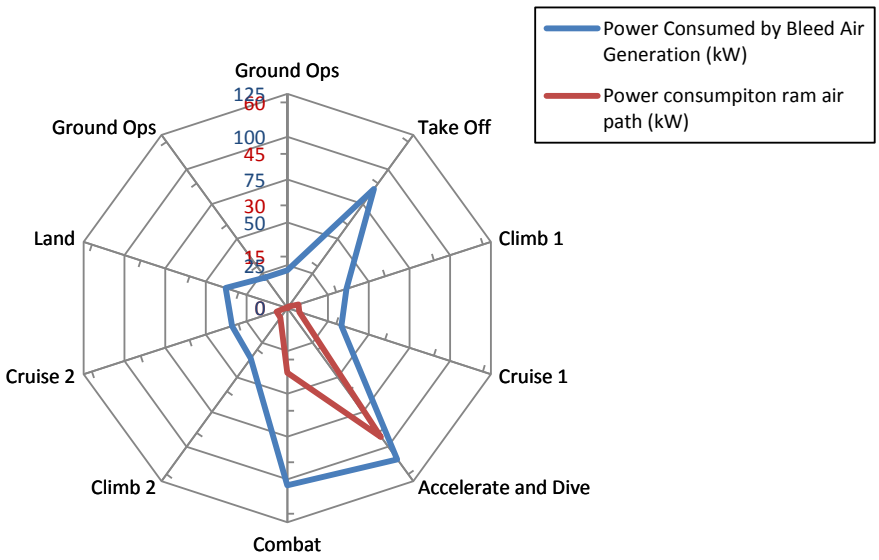

Figure 5-1: Bleed and ram air power consumption across a flight profile. Simulated Data.

The bleed air input power is highest at high engine load flight conditions; take off, accelerate and dive and combat. The bleed air system has a single tapping and therefore the input power is purely a function of the engine load. The ram air input power is also highest at low altitude and high speed flight conditions, due to the high mass flow rate and high density of low altitude air.

The 'Ground Ops' condition displays a negative ram air input power due to the inducer flow. The pressure drop across the heat exchanger is negative in this condition, therefore the ram air heat exchanger input power is also calculated as negative. The cost of inducer flow to system efficiency is measured by the power consumed in the compression of additional bleed air, which completes no useful heat removal. The inducer flow is switched off when the landing gear is retracted into the airframe.

5.3. Environmental Control Subsystem

The ECS is considered to be an adiabatic subsystem in this analysis and its purpose is to generate a low temperature airflow which can allow heat transfer to take place. The ECS is analysed in the following section to define its thermodynamic efficiency across a number of operating conditions and provide a full performance map. The ECS is the main input power consumer and the output of this subsystem defines the quantity of useful heat transfer rate the system can deliver.

The work is to also identify key operational areas of the ECS which are not well covered by literature. Only through the development of a thorough system understanding can future optimisation strategies be defined.

5.3.1. System Performance Characteristics

In order to generate a fundamental understanding of the ECS behaviour, the rig was run through independent sweeps of one control variable. This was performed under manual valve position control. CoP is commonly used as a performance metric for ECS (Buckingham 1984; Conceição et al. 2007; Defrancesco 1993; DeFrancesco 1989; Dieckmann et al. 1986; Hitzigrath 1993; Mitani & Saito 2002). However, the use of CoP can

be misleading for the assessment of ECS subsystem performance, as the CoP does not measure the total rate of heat removed by the TMS. The delivery of cooled bleed air is not a measure of the net heat transfer rate in itself; as the cool fluid is then used to remove quantifiable heat loads elsewhere. Meanwhile, the ECS input power is hard to define as no direct mechanical power is supplied to the ECS. In some cases, the measurement the input power includes the ram air stream and in some case only bleed air is considered. All of the fluid streams of interest form thermodynamic open cycles, whereas usually a coolant working fluid would operate in a closed cycle. It is important to clearly define the term CoP in an ECS for use in this sub-specific system.

The CoP within the ECS subsystem is defined as the heat rejection rate of the bleed air, $\dot{Q}_{ECS}$, divided by the work rate to compress and heat the bleed air, $\dot{W}_{Bleed\ Air}$, the power required to drive air through the ram air heat exchangers, $\dot{W}_{RamHX}$, less the power in the flow at the ECS exhaust, $\dot{W}_{EECS}$.

$$CoP_{ECS} = \frac{\dot{Q}_{ECS}}{\dot{W}_{Bleed\ Air} + \dot{W}_{RamHX} - \dot{W}_{EECS}} \tag{5-9}$$

The CoP equation includes the exhaust pressure recovery ($\dot{W}_{EECS}$) term, so that the work potential remaining in the flow at ECS exhaust is accounted for. This is necessary as the pressure of the ECS exhaust flow is not exclusively dependent on the inlet flow pressure or the CAU exhaust temperatures.

A sample result from a bleed air temperature sweep can be seen in Figure 5-2. In this test, all other input conditions remain constant. It is seen that an increasing bleed air inlet temperature increases the ECS CoP. The increased temperature difference between the charge air (bleed air) and the coolant (ram air) across both heat exchangers increases the cycle heat rejection rate.

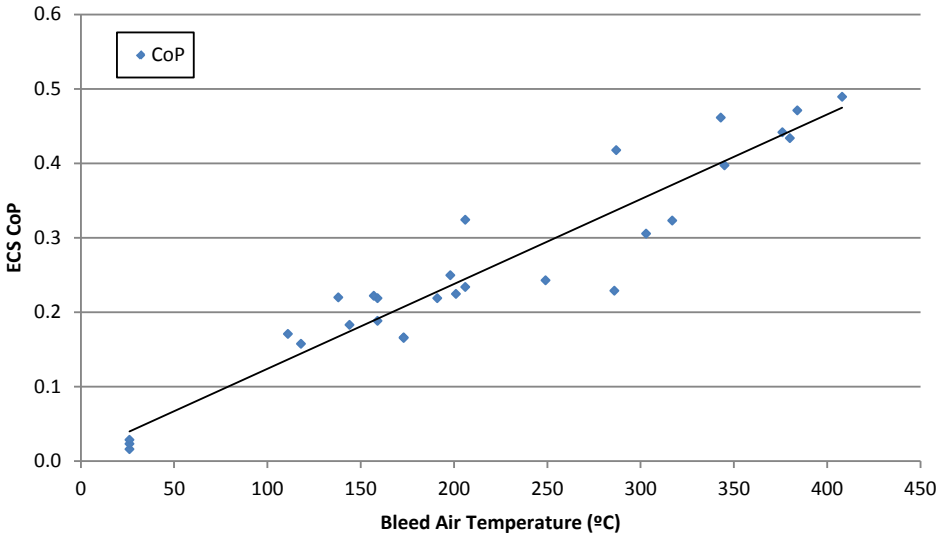

Figure 5-2: ECS CoP response to bleed air temperature change.

A bleed air pressure sweep is shown in Figure 5-3. Increasing the inlet pressure increases the ECS CoP. The performance of the cold air unit is governed by its pressure ratio. The total cycle pressure ratio is the ratio between the compressor out and the turbine out pressure. It is a measure of the pressure energy converted into work by the turbine. Rather than considering turbine pressure ratio in isolation, the efficiency of the compressor and the pressure drop across the secondary heat exchanger affect the pressure through the cycle. A higher inlet pressure yields a greater pressure ratio which generates a higher turbine/compressor shaft power. The cycle inlet pressure is broadly independent of the exhaust (cabin) pressure; therefore higher inlet pressures yield higher refrigeration cycle efficiencies.

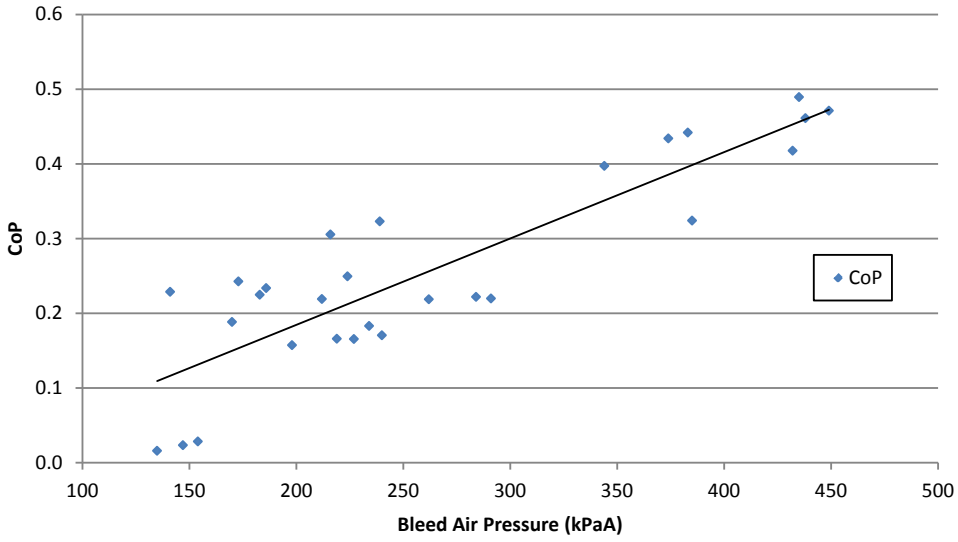

Figure 5-3: ECS CoP response to bleed air pressure change.

A bypass TCV sweep is seen in Figure 5-4. Bypass flow affects the system performance in two ways. By increasing the bypass mass flow rate, the path of least resistance is for the airflow to bypass the cycle. The reduction of the flow rate through the cycle reduces the total pressure ratio and therefore the work which can be produced by the turbine. The reduction in the shaft power reduces shaft speed and ultimately reduces the ECS CoP. The second process of bypass air addition degrades the cycle performance due to the wasteful nature by which the energy of the flow is discharged. The process of adding heat to a heat rejection cycle by definition degrades the heat rejection cycle system efficiency.

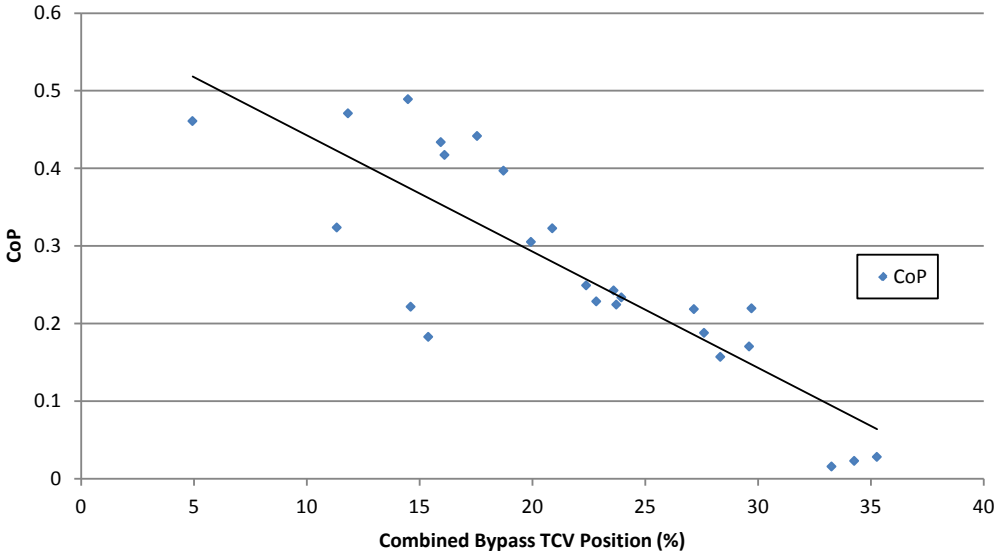

Figure 5-4: ECS CoP response to TCV position.

A secondary heat exchanger heat rejection sweep is detailed in Figure 5-5. It can be seen that the performance of the ECS is driven by the heat rejection through this component. The performance of this component is intrinsically linked to Figure 5-2, Figure 5-3 and Figure 5-4. The process is defined in the following bullet points.

- The increase in bleed air temperature increases the coolant and charge air temperature difference across the secondary heat exchanger, implying that the specific heat rejected (J/kg) through the heat exchanger is higher.
- The increased bleed air pressure increases the total pressure ratio of the system, increasing the work produced by the turbine.
- The increased shaft power increases the compressor pressure ratio and therefore the heat added by the compressor. This acts to increase the coolant and charge air temperature difference across the secondary heat exchanger and therefore increases the amount of specific heat rejected.
- The reduction of the bypass flow rate increases the mass flow rate going through the cold air unit. This has the effect of increasing the system bleed air pressure at the inlet of the CAU and therefore this increases the ECS CoP accordingly.

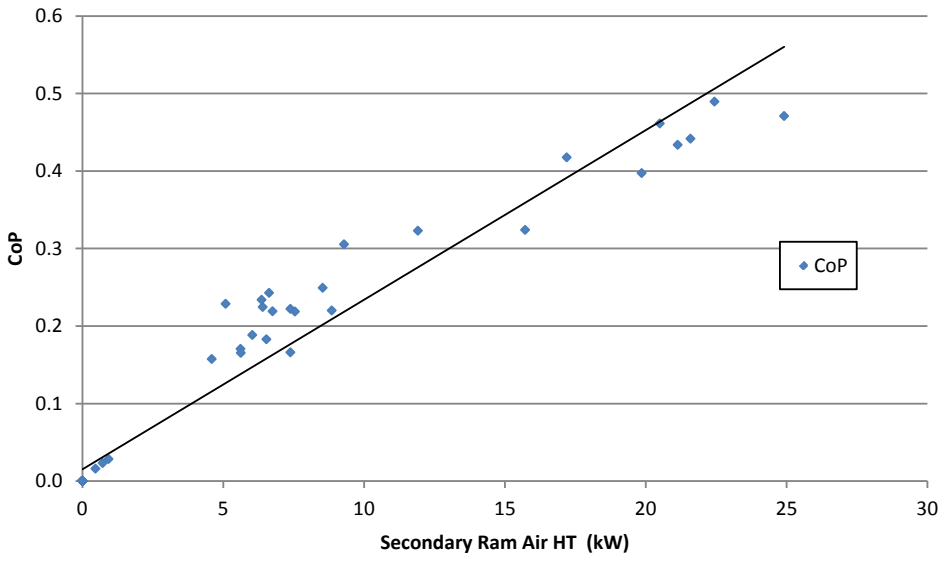

Figure 5-5: ECS CoP response to secondary heat exchanger heat transfer rate.

5.3.2. Environmental Control System - Valve Control System

The previous ECS relationships are achieved by manually positioning the TCVs. The data of Figure 5-6, Figure 5-7 and Figure 5-8 show the response to an inlet pressure sweep, where the cabin and the equipment supply temperature are held constant by the control system of the TCVs. These three figures are collected from the same test and split for clarity of data presentation.

As the system inlet pressure increases, the relationships of Figure 5-3 and Figure 5-5 indicate that total pressure ratio rises, increasing the secondary heat exchanger specific heat rejection. With a fixed TCV position, the ECS outlet temperature would reduce due to the increased cycle heat rejection. However, the test of Figure 5-6 maintains a fixed cabin and equipment temperature, requiring a fixed turbine exhaust temperature. To achieve this, the TCVs open with increasing inlet pressure and the subsequent bypass mass flow rate reduces the system efficiency, as seen in Figure 5-4. The regulation of the system heat rejection rate allows the ECS outlet to remain constant despite a decreasing turbine outlet temperature, as shown in Figure 5-7.

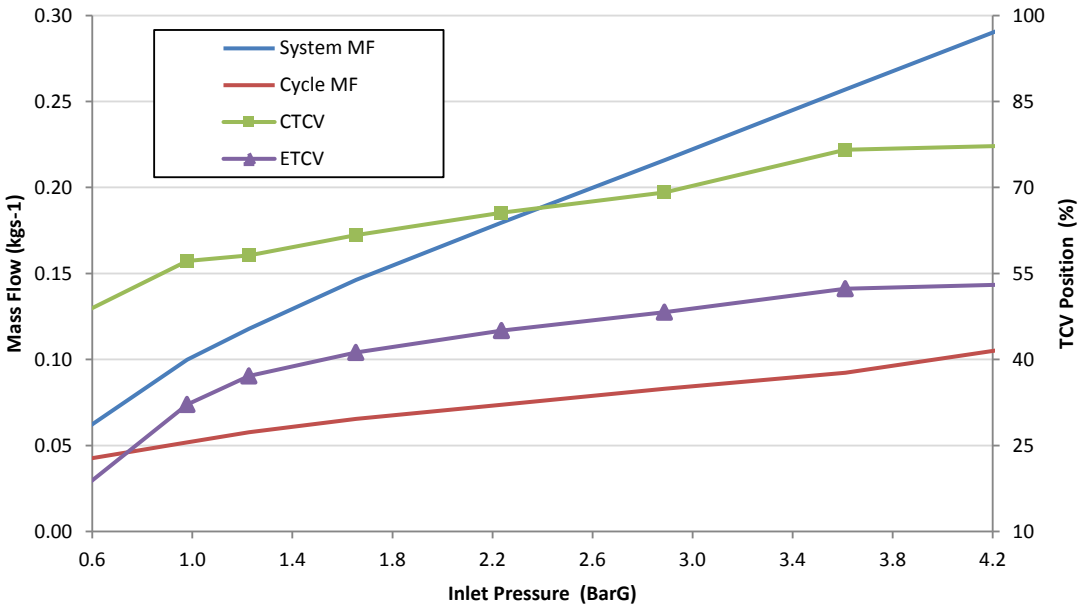

Figure 5-6: ECS response to inlet pressure sweep with controlled equipment and cabin feed temperatures.

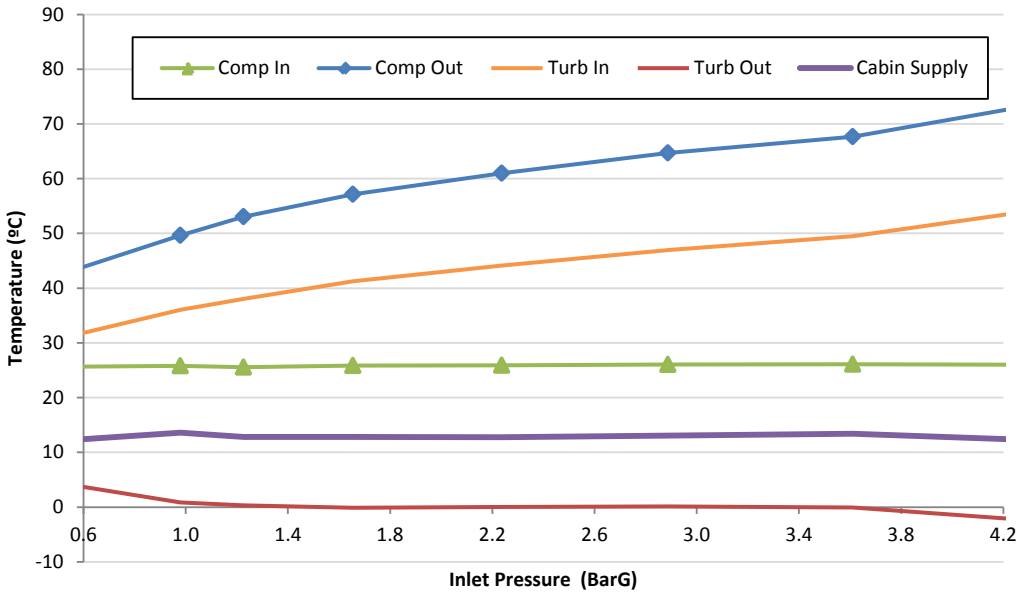

Figure 5-7: ECS response to inlet pressure sweep with controlled equipment and cabin feed temperatures kept constant by the TCVs.

Figure 5-8 shows the system heat rejection rate and ECS CoP against the bleed air mass flow rate. Whilst system power (and hence cooling ability) increases with the bleed air consumption, the system CoP falls. In this instance, the ECS CoP indicates the loss of thrust that the aircraft must overcome per unit of cooling performance. The benefits of minimising bleed air consumption are twofold: the reduced demand of compressed air from the engine is accompanied by more efficient operation of the ECS. A system-level analysis of the minimisation of bleed air is detailed in Chapter 5 and 6, where an in-depth analysis of the system relationship to mass flow rate is detailed.

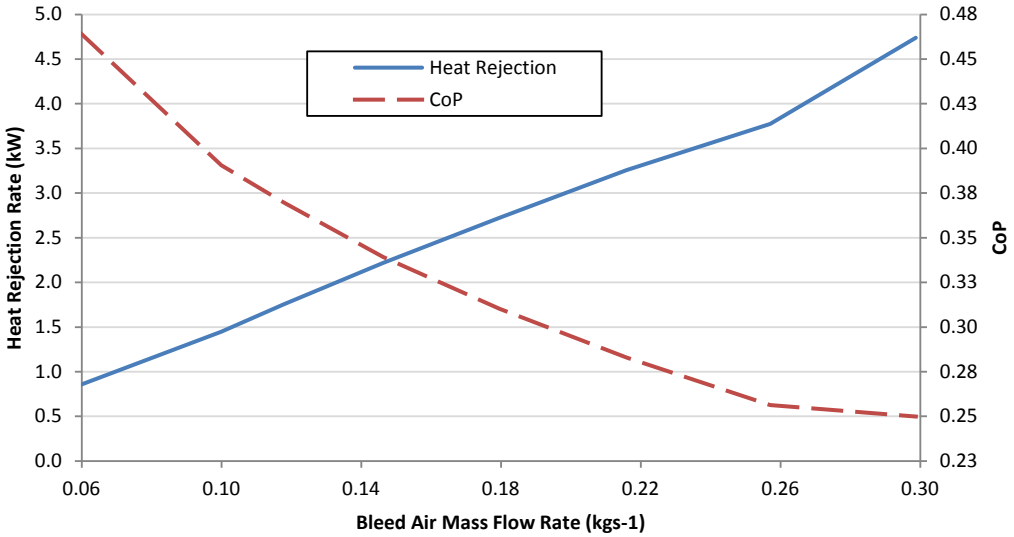

Figure 5-8: ECS CoP and heat rejection rate changes the bleed air mass flow rate with controlled equipment and cabin feed temperatures.

The data of Figure 5-6, Figure 5-7 and Figure 5-8 show how as the system would perform in flight, where the cooling load is constant but the inlet conditions vary. The purely thermodynamic cycle performance and the cycle performance when using a control system have opposite trends. With a fixed TCV position, an increased inlet pressure improves bootstrap cycle performance, as shown in Figure 5-3. With the control system active, performing as installed in the aircraft, the TCVs increase the bypass mass flow rate with rising inlet pressure to deliver a fixed cabin and equipment supply temperature. The response is the degradation of the system CoP with increasing inlet pressure, reported in Figure 5-8.

Figure 5-9 illustrates one of the benefits of testing the real system rather than relying entirely on simulated data. The two lines represent the bleed air temperature change throughout the refrigeration cycle, for two different conditions with constant bleed and ram air inlet conditions. Operationally, this could be the result of diving to an altitude as opposed to climbing. The two operating points are achieved with different TCV positions but with a similar overall level of cycle bypass. State 2 is both working the cycle harder and using more bypass, to achieve the same cabin temperature output as State 1. This means that whilst the system is delivering more performance in State 2 (higher ECS CoP, cycle

efficiency and specific heat rejection), it is at the expense of increased bypass flow. This indicates that the control system is not optimised for peak efficiency.

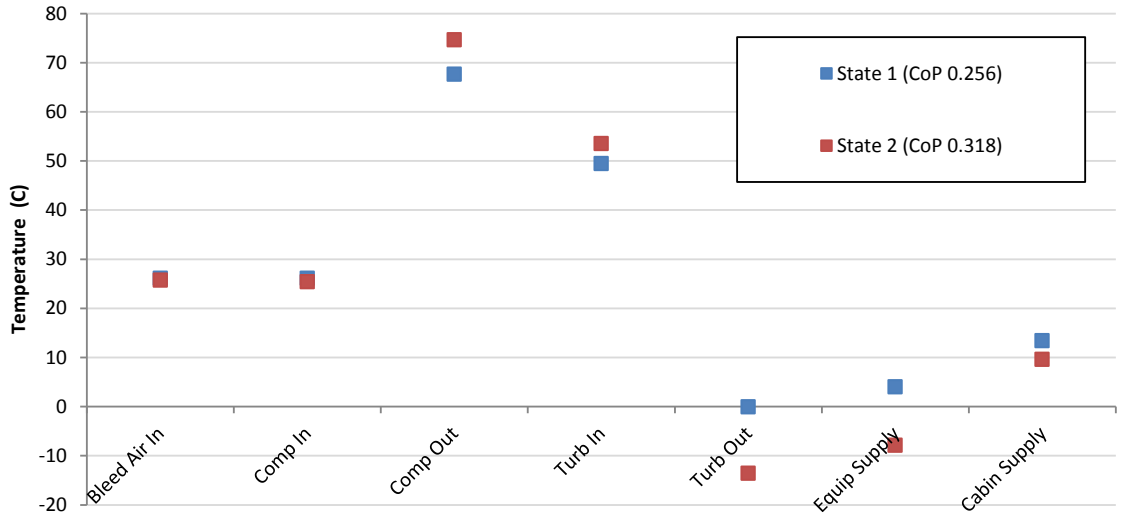

Figure 5-9: ECS airflow temperatures for two similar flight conditions.

This section has documented the governing ECS system response as both a stand-alone system and a system that would operate within the aircraft. The following section looks at specific operational conditions of the ECS. The requirement is to develop a wider understanding of ECS performance to improve the accuracy of the mission-level analysis and to identify potential optimisation approaches.

5.4. Environmental Control System Response to Humidity

An area of ECS performance not well documented is the system performance in relation to bleed air humidity. As a result, the ECS response to humidity is an area in which validation data is limited, both in terms of the cycle response and of the water separation efficiency.

Uncontrolled condensate ingress to the cabin environment has been reported with bleed air driven LPWE ECS architectures (Fourquet et al. 2000; Stow et al. 2006; Brown et al. 2012). Typically, on operational aircraft, these cabin condensation ingress events are experienced in combination with high ECS exhaust temperatures, leading to difficulties in the thermal management of the distributed aircraft heat loads. A hot and humid environment would be typical of equatorial locations. This issue is often compounded by high solar and kinetic loading from the ambient environment and low ECS working fluid

and coolant flow rates. This phenomenon appears to be associated to humidity atmospheric conditions and therefore can be assumed to be a function of ECS working fluid.

The process of water extraction is well documented in fast-jet ECS literature; however only a few studies present an accurate analysis of cabin condensate ingress from a LPWE ECS is limited. (Defrancesco 1993; Ryan 1990; Zhao et al. 2009; Matullch 1989; Fourquet et al. 2000). As a result of the simple relationship between Relative Humidity (RH) and airflow temperature, a one-dimensional modelling approach to compute the condensation in each component of the ECS is normally used for analysis (Conceição et al. 2007). This approach has been previously discussed and it is highlighted that the simplifications and assumptions required for the non-iterative flow calculation reduce the accuracy of the predictions. Modelling is often inaccurate, as the true process of condensation is a two-phase, three dimensional and transient flow process. The transient interactions of the water extraction process bring additional complexity in the system dynamics and reduce the accuracy of one-dimensional saturation calculations.

The calculation of Absolute Humidity (AH) at system inlet is a function of the bleed air mass flow rate measurement and of the water injection rate. An important challenge in performing the humidity analysis is the measurement of the water content at the ECS exhaust, as well as to predict the state of the water content throughout the cycle. (Spencer-Gregory & Rourke 1957; Lawrence 2005; Cramer 1993). The volumetric flow rate of the condensate, from the water extractor drain and supply branches, is measured cumulatively over the duration of a test, while the RH of the air at system exhaust is measured in real-time.

RH is a ratio of the absolute vapour partial pressure in the air, e_V, against the saturation vapour pressure, e_S:

$$RH = \frac{e_V}{e_S} \tag{5-10}$$

An empirical relationship for the saturation vapour pressure is calculated by Equation 5-11, based on the air temperature, T, and empirical constants A, B and C of 17.625, 243.04 and 610.94 respectively (Lawrence 2005).

$$e_S = Ce^{\left[\frac{AT}{B+T}\right]} \tag{5-11}$$

AH is the ratio of the total moisture content mass (kg) to the total dry air mass (kg). The absolute humidity is calculated from the density of the mixture, ρ_M, absolute vapour partial pressure, the vapour ideal gas constant, R_V and the dry air temperature, T (Spencer-Gregory & Rourke 1957):

$$AH = \frac{\rho_M e_V}{R_V T}\left[\frac{kg\ water}{kg\ dry\ air}\right] \tag{5-12}$$

The fluid properties for a mixture of air and water vapour are given by Equations 5-13 and 5-14, which are adapted from the Gibbs-Dalton Law (Rogers & Mayhew 1992). The mixture pressure is denoted by P_M.

$$\rho_M = \frac{P_M}{R_M T} = \frac{P_M(1+AH)}{R_A T}\left[1+\frac{AHR_V}{R_A}\right]^{-1} \quad \rightarrow \quad R_M = \frac{R_A + AHR_V}{1+AH} \tag{5-13}$$

$$h_M = h_A + AHh_V = C_{P_M}\Delta T \quad \rightarrow \quad C_{P_M} = C_{P_A} + AHC_{P_V} \tag{5-14}$$

When the RH is greater than 1, the condensate level is given by the difference between the actual AH and the AH that would be required to saturate the flow, AH_S, known as the condensate ratio, AH_C:

$$AH_C = AH - AH_S \tag{5-15}$$

The absolute humidity at saturation is the same calculation as the absolute humidity, where the absolute vapour partial pressure in the air is substituted by the saturation vapour pressure:

$$AH_S = \frac{\rho_M e_S}{R_V T} \tag{5-16}$$

For a bleed air inlet AH sweep at constant temperature and pressure, Figure 5-10 shows the turbine-out temperature and the ECS CoP for both the entire system and the cycle in

isolation. In the following analysis, the 'cycle' is defined as the CAU and the system is defined as the complete ECS as diagrammatically represented in Figure 4-4. Figure 5-10 shows a typical ECS response to variations in bleed air AH, with all other controls kept constant. The variations in CoP and in turbine outlet temperature shown in Figure 5-10 is purely as a result of the moisture content present in the working fluid.

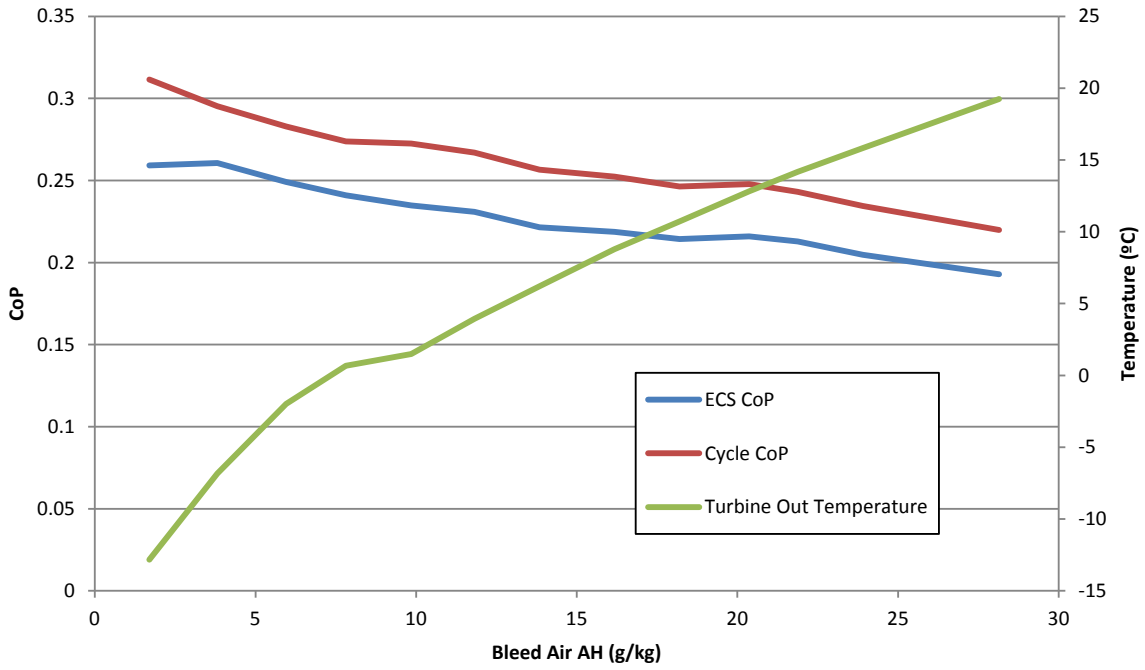

Figure 5-10. CoP and Turbine-Out Temperature against Bleed Air AH.

As the air inlet humidity increases, the CoP decreases for both the CAU cycle and the ECS. At low inlet humidity values, the ECS, CoP and the CAU CoP are further apart due to low turbine out temperatures driving heat flow from ambient through the walls of the pipe run between the turbine outlet and water extractor (WE) inlet. This causes an increase in temperature between the turbine outlet and pack exhaust that degrades ECS CoP. The turbine outlet temperature increases significantly with increasing inlet humidity. A plateau witnessed at 0ºC separates two linear regions of operation. At low humidity values the flow in the turbine can be assumed single phase, whilst the flow is two-phase at high humidity (this is detailed in the following section). The plateau is not reflected in ECS or cycle CoP, highlighting a lack of visibility of this feature when using just CoP for monitoring the system performance.

The relative magnitudes of reduction witnessed in the ECS CoP and CAU CoP are dissimilar: across the range of inlet humidity tested, CoP degrades by 27% whilst turbine out temperature degrades by over 800%. The equipment delivery temperature is regulated by design between 0ºC to 4ºC; this variation in turbine outlet temperature represents around nine times the design specification limit for equipment delivery temperature. Whilst a fall in CoP of 27% is significant, the system sees similar magnitudes of CoP degradation for operational variations in bleed air supply temperature and pressure. These variations however, do not degrade the ability of the system to deliver low turbine outlet and pack exhaust temperatures to the same degree as with increasing absolute humidity.

5.4.1. Analysis of Coefficient of Performance

The cold air unit cycle CoP is greater than the system CoP for two reasons: Firstly, the bleed air specific heat rejection is greater due to the increase in temperature between the turbine outlet and ECS exhaust. Secondly, less power is required due to pressure loss in primary heat exchanger, bypass branches and LPWE unit. Figure 5-11 shows how the constituents of the CoP calculation vary to explain ECS performance. The inlet bleed air power input and the secondary heat exchanger (SHX) heat rejection rate remain constant while the total bleed air heat rejection rate and CAU shaft power fall linearly with increasing AH; following the same trend of the CoP.

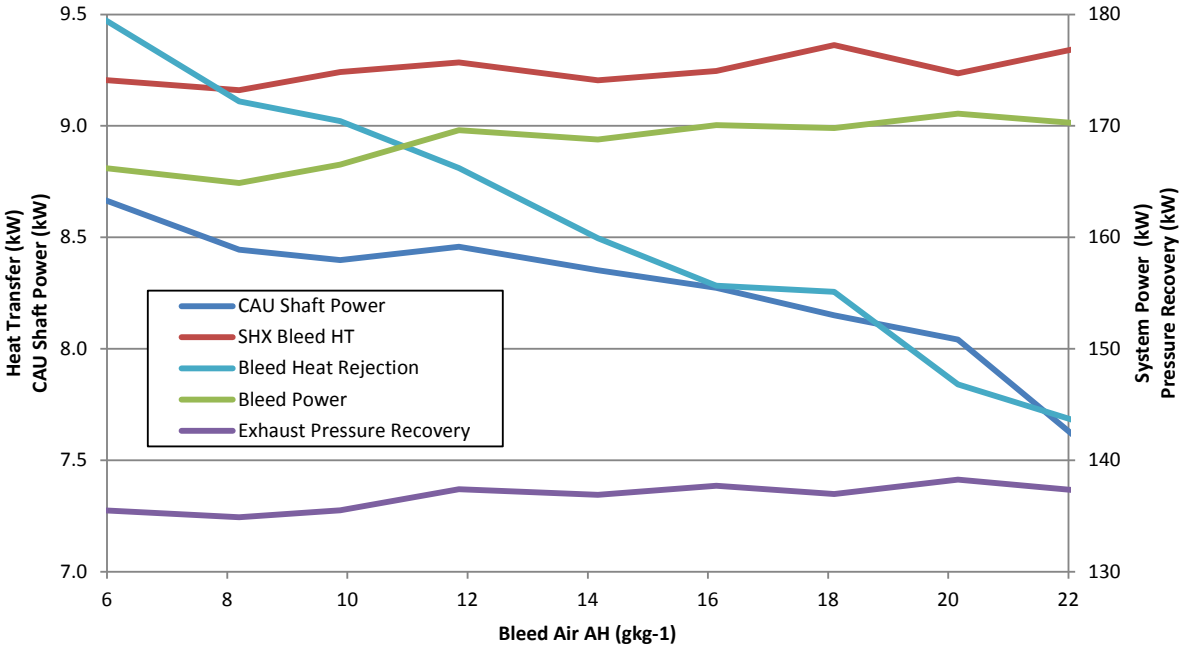

Figure 5-11. Components of System CoP against Bleed Air AH.

The CoP denominator terms of the bleed air power and the exhaust pressure recovery both remain approximately constant, irrespective of the bleed air AH. The reduction in the bleed air heat rejection rate causes the observed reduction in CoP, which manifests through reduction in the CAU shaft power. Across the range of inlet humidity tested, the CAU shaft speed falls from 67krpm to 60krpm, along with a drop of 3.5% in both compressor and turbine isentropic efficiencies. The ability of the CAU to extract energy (shaft power) from the bleed air is reduced as humidity increases because of the lowering of the working fluid density due to the phase change of the water content in the turbine.

Secondary heat exchanger heat rejection rate remains constant throughout. During a constant AH operation, this property is found to exhibit a strong linear relationship with the ECS CoP as seen in Figure 5-5 (Jones et al. 2015; Conceição et al. 2007). As increasing the bleed air humidity does degrade the heat transfer rate at the secondary heat exchanger, the degradation of the system CoP can be traced almost entirely to CAU and specifically to the turbine. The performance of the entire system is driven by the amount of bleed air energy successfully extracted by the turbine which is a function of the working fluid properties.

5.4.2. Analysis of Working Fluid Thermodynamic Properties

The energy balance calculations performed on the system are heavily influenced by the density and by the specific heat capacity at constant pressure of the working fluid. The thermal conductivity of the fluid is influenced by both of these properties, driving changes in the convective heat transfer performance. The constant pressure specific heat capacity describes the change in temperature for a given specific heat change, where a higher constant pressure specific heat capacity enables a higher heat flow rate for a given temperature difference. An increase in the relative humidity for a given absolute humidity reduces the mixture density, due to an increase in the vapour pressure (increasing the tendency of the water content to condense in the turbine).

Figure 5-12 shows how these parameters vary with changes in the bleed air inlet absolute humidity. All parameters are normalised for their standard 'dry' values.

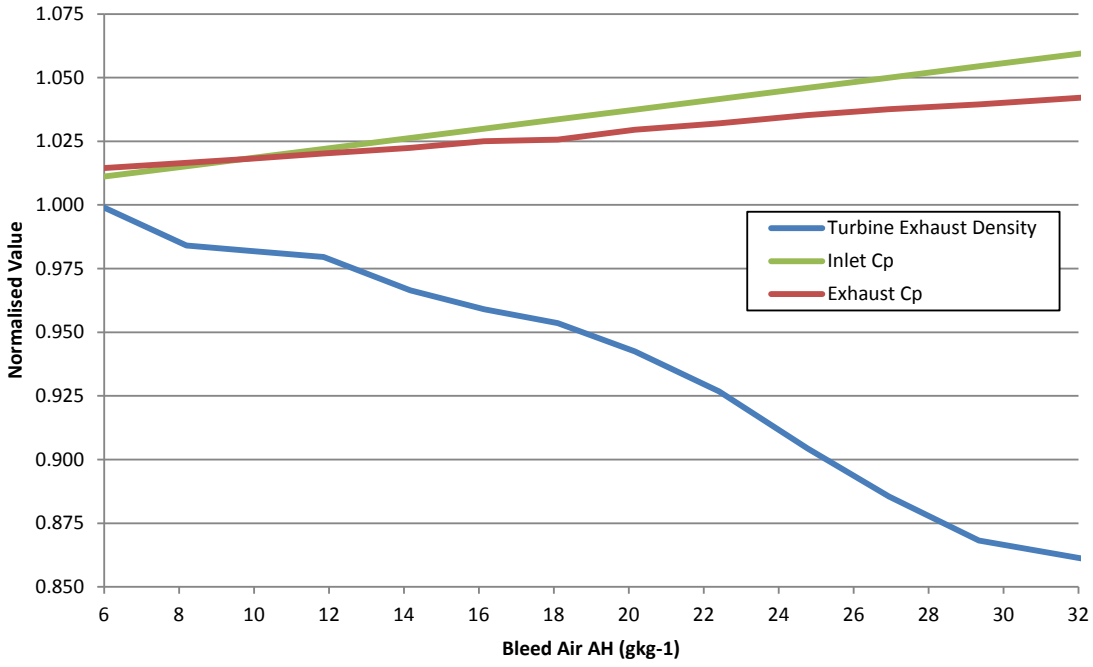

Figure 5-12. Normalised Specific Heat Capacity and Density against Bleed Air AH.

A small increase is found in the constant pressure specific heat capacity with increasing humidity. This serves to increase the amount of specific heat transfer that is possible to obtain in the working fluid for a constant temperature difference. This factor would tend to increase the ECS CoP. However, a significant decrease is found in working fluid density with increasing absolute humidity. This is due to the difference in molar mass between

water vapour (H2O) and the common constituents of air that it displaces (N2, O2). It should be noted that the shape of the density curve closely mirrors that of the CAU cycle CoP (Figure 5-10), indicating a close relationship between the performance of the ECS expressed as CoP and state of the working fluid.

5.4.3. Analysis of Turbine Phase Change Conditions

The second finding of Figure 5-10 was a plateau in the turbine outlet temperatures caused by the water vapour phase change in this component. Figure 5-13 shows how RH varies throughout the system for constant bleed air inlet AH and varying inlet pressure. The calculation of RH accounts for both temperature and pressure effects, where values greater than 1 indicate that the working fluid is saturated and condensate is present. Each curve represents a different inlet bleed air pressure (2.1-3.2 BarA), all other parameters being kept constant.

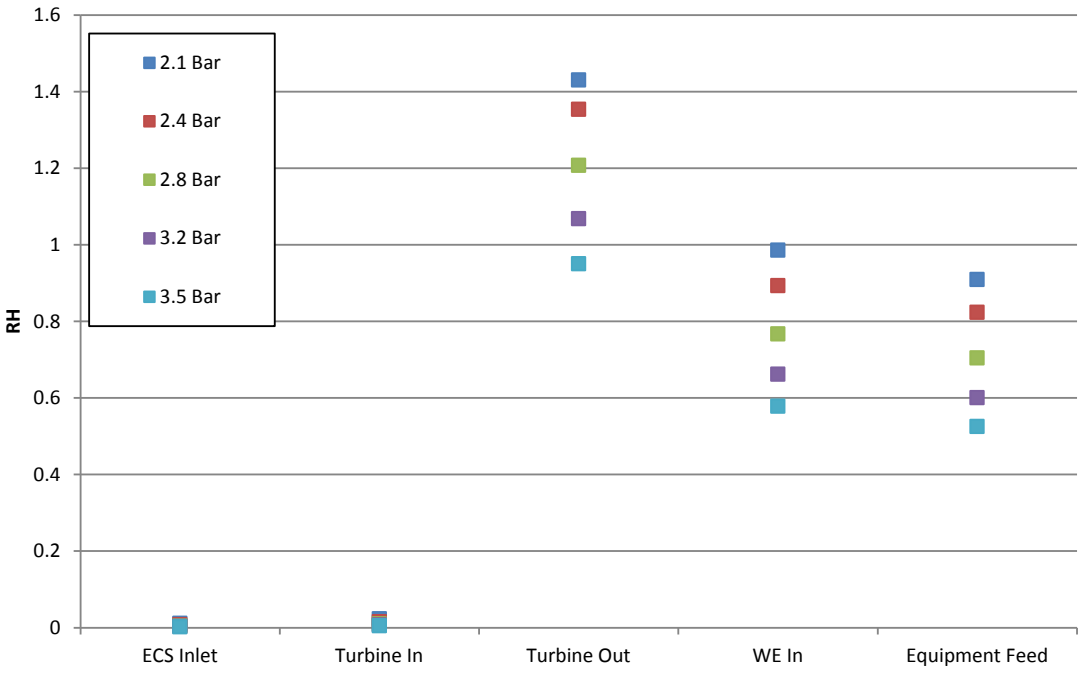

Figure 5-13. RH Variation through ECS.

An increase in bleed air pressure drives greater bleed air mass flow through the CAU, inducing higher levels of irreversibility in the air cycle through turbulence and energy dissipation, as the compressor and turbine are driven at off-design conditions. This increases both the temperature and the pressure at the turbine outlet. Increasing temperature and pressure, when AH is fixed, reduces RH.

As operating conditions drive the relative humidity value at the turbine outlet above 1, the vapour pressure exceeds the saturation pressure which causes condensate to form. At the lowest inlet pressure state tested (blue curve, Figure 5-13), the condensate formed at the turbine exhaust is calculated to be approximately 4.2g per kg bleed air.

This analysis indicates how the effect of the working fluid moisture content on the performance of the system is not limited to the quantity of moisture present. The operating condition of the ECS affects the rate of condensate generation for a fixed absolute moisture content. The formation of condensate is a requirement for water extraction, as gaseous water cannot be separated from air by using a coalescing element and a centrifuge. In order for this method of water extraction to work, condensation must occur in the turbine; which as shown, degrades the performance of the entire cycle. The system has no mechanism in place to recover the latent heat released during the formation of the condensate, which simply remains in the working fluid.

The low pressure water extraction process is based on the turbine generating condensate, which is carried within the flow to the LPWE unit. The purpose of the equipment bypass airflow is to maintain the temperature at the LPWE inlet between 0ºC to 4ºC to maintain water content as condensate. If the flow is too cold, the condensate freezes. If the flow is too hot, the condensate re-vaporises and cannot be separated.

5.4.4. Low-Pressure Water Extraction Investigation

The LPWE process has not been validated by BAE Systems and therefore the ECS model makes is based on psychometric theory alone. Figure 5-14 shows the predicted RH and absolute condensate (Cnd) for the airflow at the turbine outlet (To), at the WE inlet and at the equipment feed (EE), these are the most important locations for water extraction process analysis. The ECS inlet conditions are of low temperature and pressure and correspond to condition in Table 4-2, to provide a low turbine out temperature driving a high relative humidity and condensate content for a given absolute humidity.

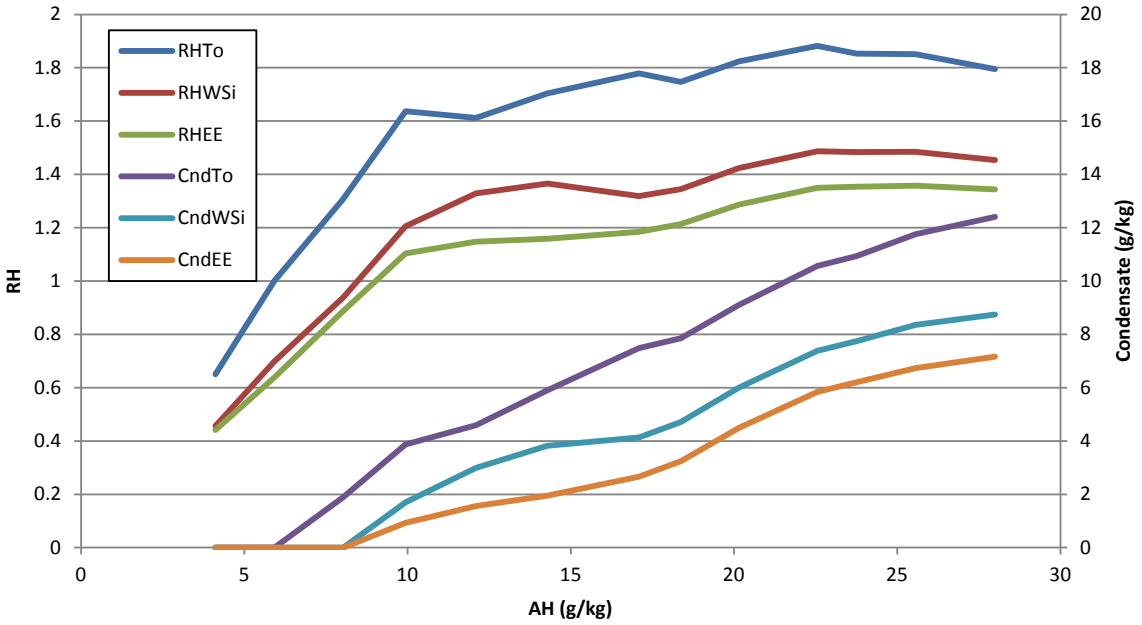

Figure 5-14. RH and Condensate against Bleed Air AH.

The difference between the amount of condensate present at the turbine outlet and at the WE inlet is due to the re-vapourisation of the condensate. The latent heat required for vapourisation is supplied by heat transfer through the pipe walls due to the temperature difference between turbine-outlet and the laboratory ambient. As a result, the location of the water extractor is critical. The equipment feed take-off is upstream of the WE inlet, and therefore it is highly likely that saturated air and condensate is delivered to the avionics at the design temperatures.

In order for the water extractor to perform well at this location, significant amounts of condensate must be generated in the turbine and carried through to the coalescing element. Phase change in the turbine reduces its capacity to generate low turbine-outlet temperatures. The system design goals of bleed air water extraction and low turbine-outlet temperatures are conflicting; phase change across the turbine is required for water separation however phase change across the turbine reduces the cooling capacity of the airflow.

Physical measurements of the condensate collected at the water extractor drain and cabin supply branch against bleed air inlet humidity are shown in Figure 5-15. Also plotted is the calculated condensate at the turbine outlet and the equipment bypass mass flow. The test

was conducted over a period of approximately one hour with automatic ETCV position control. The TCV control system shuts the ETCV at approximately 7g kg-1 AH, while the condensate extracted from the WE does not exceed a peak found at approximately 15g kg-1 AH.

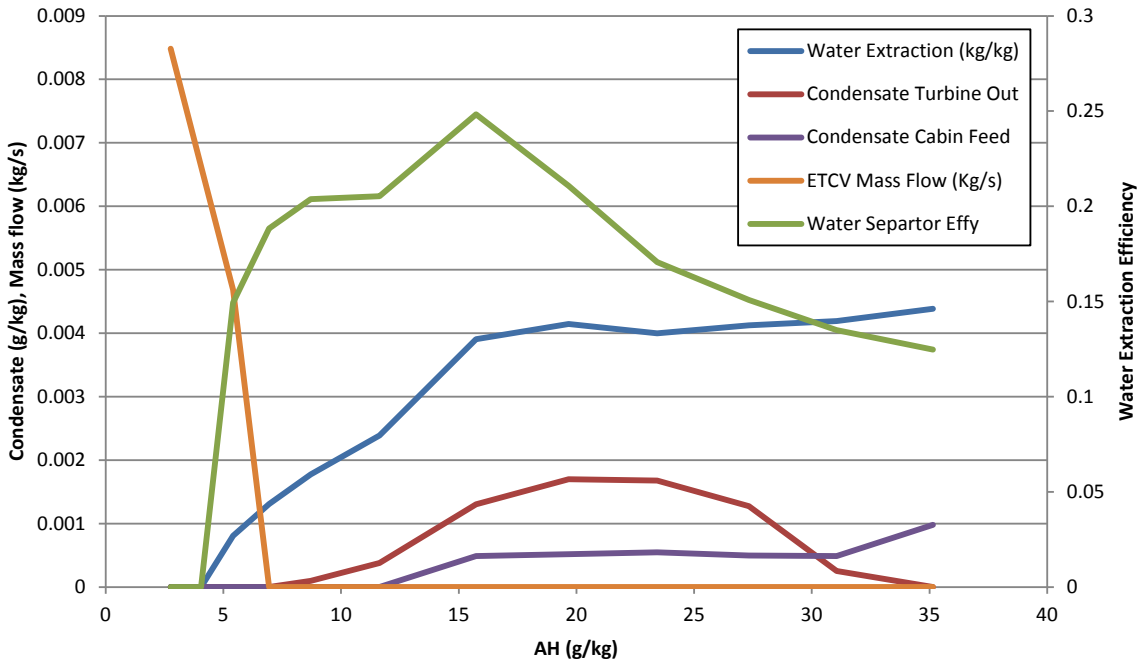

Figure 5-15. Various System and Water Extractor Parameters against Bleed Air AH.

The bypass mass flow is reduced with increasing inlet humidity due to the reduced capacity of the air cycle to generate low turbine-outlet temperatures. The ETCV shuts at approximately 7g kg-1 absolute inlet humidity, which coincides with the point at which condensate starts to form at the turbine outlet.

Condensate is present in the cabin feed at moderate-to-high levels of inlet absolute humidity. This is due to the (relatively) low temperature of the CAU outlet and its correspondingly low saturation vapour pressure, as well as poor water extraction efficiency. The presence of condensate at this location confirms that the cabin delivery air is saturated under certain circumstances (i.e. high inlet humidity, low cabin temperature demand, low turbine-outlet temperature). A key point in the evaluation of the facility is the successful replication of reported inflight conditions.

Turbine-outlet condensate forms at high levels of inlet humidity. This produces a higher turbine-outlet temperature, which is the resultant of the phase change in the turbine flow, which is in turn the resultant of the high inlet humidity. This serves as a reminder of the ability of a bootstrap air cycle machine to self-regulate.

When considering the total water content in the bleed air (at any state or phase), water extraction efficiency of the system peaks at around 25%, at 15g kg-1 absolute inlet humidity for this test. After this point, the condensate extraction is approximately constant for increasing inlet humidity and the water extraction efficiency falls as a consequence of it.

A key reason for poor water extraction efficiency is the addition of bypass airflow prior to the WE inlet. The addition of hot air at this location is primarily for the purpose of component protection, controlling the WE inlet (and equipment feed) temperature between 0ºC-4ºC to avoid blockage of the coalescer sock through icing. However, as a result of increasing the temperature of this flow, the bypass air also acts to re-vaporise condensate before the WE inlet. This behaviour is seen because condensate is only generated at the turbine outlet when the ETCV shuts (below an AH of 7g kg-1). The net result is a reduction in the WE inlet condensate, reducing the efficiency of water extraction purely by this design of the ECS pipework.

At an AH greater than 31g/kg, the water extractor appeared to generate rather than remove condensate. In reality this is incorrect and a consequence of the process by which absolute condensate is measured or calculated. The temperature gradient between the centre of the wheel of the turbine (where phase change takes place) and WE inlet is steep, therefore the measurement location has a strong influence on the calculated levels of humidity present at the turbine outlet. This explains why the calculated level of condensate present at the turbine-outlet is less than the amount of condensate collected from the water extractor drain. This also highlights the requirement of measuring experimentally the bleed air humidity. Even with the increased data acquisition resolution and flexibility in the measurement location, the 1D calculation of humidity has been

proved to be unreliable in certain areas of the operating flight envelope. The air cycle 1D simulation tends to model the flow as single phase at the WE inlet during high AH conditions as a high turbine-outlet temperature allows an increase in the absolute moisture content before saturation conditions are reached. However, as the flow velocity at the turbine-outlet is high (approximately 45 m s-1) and the pipe run between the turbine and the WE is relatively short (approximately 0.3m) there is insufficient time for the water content to completely re-vapourise prior to the WE. It was found in other testing at lower bleed air mass flow levels (lower flow velocity) the measured water extraction was much closer to the calculated levels. This indicates that complex 3-D fluid flow structures are integral to both water extraction efficiency and calculation accuracy.

The fall-off in the water extraction efficiency witnessed in Figure 5-15 is also partially attributed to the duration of the test and to the resultant saturation of the fabric coalescing element in the WE. As the WE system fabric saturates, the back pressure on the air cycle increases. This reduces the Total Pressure Ratio of the CAU cycle (TCPR), reducing its ability to expand air to allow temperature and pressure. Both the ECS CoP and the turbine-outlet temperature are highly dependent on the TCPR, therefore reducing the TCPR due to the back pressure generated by the WE fabric saturation can be attributed as the main cause of the aforementioned poorer working conditions of the ECS.

Once the fabric element in WE is saturated with water, the dynamics of the system are too complex to confidently apply a simple steady-state analysis methods. The WE has a pressure relief valve (PRV) which allows air to bypass the water extraction process. The PRV opens once the pressure at the WE inlet increases past a threshold value, the PRV is allowed to vent over a period of up to 30mins. With the PRV open, the TCPR increases and the performance of the CAU cycle improves. This results in different dynamics of the water content at turbine-outlet, and drives a change in the flow structure in the WE. The PRV has many complex dynamics of its own, primarily due to its limited damping, which influences the rate at which this cycle repeats.

The performance of the system is highly dependent on the previous operating condition when reasonable levels of inlet humidity exist. The system never truly reaches a stable equilibrium. Modelling this behaviour accurately would require extensive knowledge of both the flow structure in the system and of the operating conditions of the system for a significant amount of time prior to the modelled state. This is not the case when operating with dry air, and highlights how system design without consideration of transient effects or a good understanding of humidity behaviour can lead to unexpected results. The difference between calculated and measured data in these tests supports the requirement for the further experimental assessment of the working fluid on the ECS performance and an explanation to the inaccuracies of modelling these transient processes through saturation calculations.

5.4.5. Transient Operational Effects

One significant example of WE transient effects can be witnessed when operating with high bleed air inlet humidity and at a sub-zero WE-inlet temperature. This reproduces an operational fault, in which pilots have reported snow and ice coming out from the cabin cooling vents. Condensate forms as a fog in the turbine and coalesces in WE as usual. However, due to the low temperature, the condensate freezes and therefore cannot drain. This leads to a significant blockage in WE until the PRV opens and ice is discharged from the system. Figure 5-16 below depicts a test where these conditions were sustained for 20 minutes.

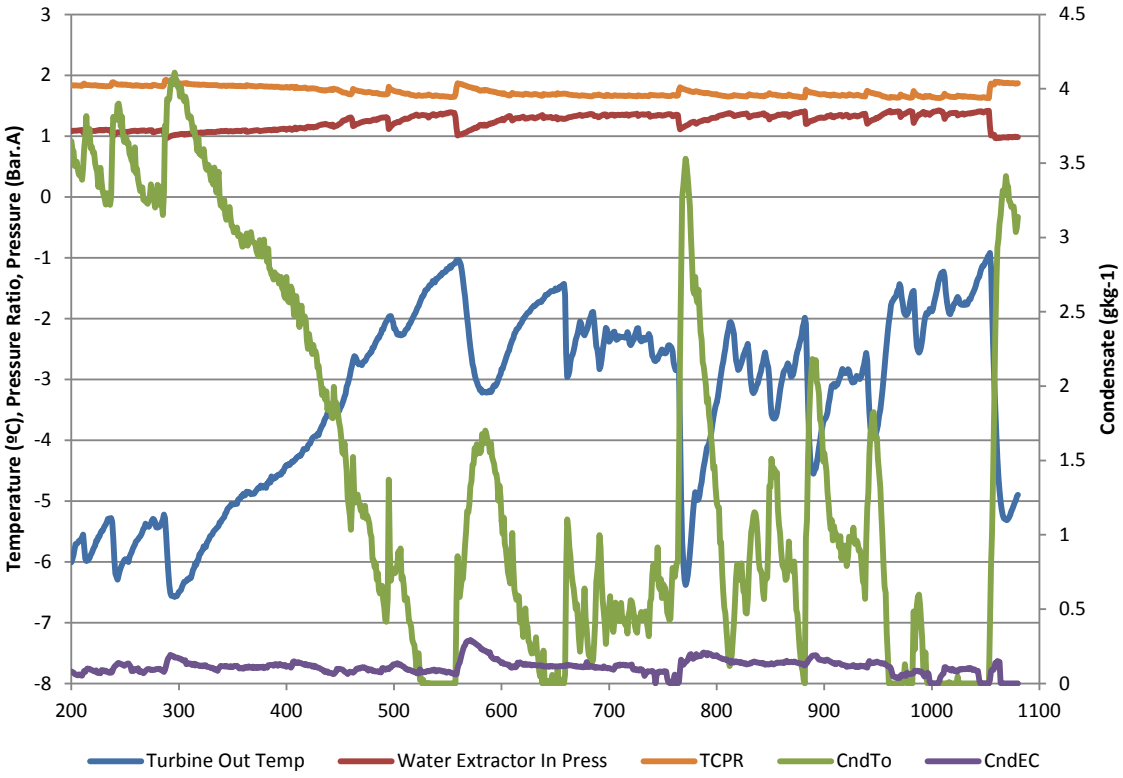

Figure 5-16. System Behaviour during Transient Icing Conditions.

The turbine-out temperature is maintained below 0°C for the duration of the test, while the relative humidity at this location is kept above 1. This allows condensate to freeze and build up in the WE. The WE blockage increases consistently from 200s to 560s. The total cycle pressure ratio of the CAU decreases, while the WE inlet pressure and turbine out temperature increase. The PRV can be seen to open 2-3 times throughout this period.

The WE blockage is relatively constant from 560-1050s. The system finds a near equilibrium state for this period, although this is characteristically large excursions in turbine outlet pressure and temperature. System performance degradation causes elevated turbine outlet temperature and reduced condensate formation. During this period, the PRV opens several times. This allows small amounts of ice and snow to be discharged into the cabin feed. The performance of the system increases when the PRV opens, the turbine out temperature falls, and more frozen condensate is formed to replace that which was previously discharged.

At 1050s, the volume of ice between the fabric membrane and the exhaust of the water extractor blocks completely the WE and the PRV opens fully. This allows the majority of the frozen condensate (of significant mass) stored in WE to rapidly discharge into the cabin feed. The test is aborted at this point in order to inspect the interior of the WE.

Figure 5-17 below shows the interior of the WE and the fabric coalescing membrane directly after the test was aborted. Significant amounts of frozen condensate remain in the component even after the majority is discharged from the system. It is thought that the entire volume between the downstream side of the fabric element and the swirl vanes at the exhaust of the water extractor fills with snow and ice at the test conditions.

Figure 5-17. Water Extractor after Transient Icing Test. (a) shows the interior of WE, (b) shows the outside of the coalescing fabric element.

5.4.6. Humidity Conclusions

The performance of a typical bootstrap air cycle machine degrades with increasing working fluid absolute humidity. This is fundamentally for two reasons:

1. Reduction of the working fluid density leads to a reduced bleed air heat rejection rate capability of the system. The effect of this outweigh that of the increased constant pressure specific heat capacity at that is obtained by increasing the air moisture content.
2. Under certain conditions, the exothermic process of phase change of the water vapour in the turbine limits the temperature change the gas phase can produce by expansion to the turbine outlet pressure. The net result is reduced shaft power,

increased turbine outlet temperature, and a degradation of the system performance.

The working fluid properties are the main driver of the ECS CoP for a given architecture, irrespective of phase change. However, an inability to reject the latent heat released by the phase change in the turbine degrades the cooling capacity of the cycle by increasing ECS exhaust temperature. As energy is conserved, the calculated first-law heat balance is independent of the phase change. During operation, thermal management systems are concerned with air delivery temperature and mass flow rate over the CoP of the thermodynamic cycle.

A system that utilises a LPWE requires a phase change event in the turbine in order to extract any water from the working fluid. This introduces the concept of a trade-off between delivering the cooling capacity and reducing the exhaust condensate content. Cooling capacity degradation is a function of the water condensation at the turbine, rather than a consequence of the water extractor inlet conditions.

At high AH levels, a flow-dependent transient behaviour related to water extraction effectiveness and flow blockage by ice are witnessed. Although the behaviour is localised to the component level (as it is due to the water saturation of the LPWS coalescing membrane), a variation in the system level thermodynamic performance is measured. This is difficult to predict or calculate as it is the function of complex 3D flows and of the time-dependent saturation of the water extractor fabric membrane. These transient behaviours highlight the difficultly and potential inaccuracies of a modelling approach that is purely based on ECS response to changes in the absolute inlet humidity.

In real world LPWE implementation, bleed air bypass is used to maintain WE inlet conditions above 0°C. Whilst the intent of this control is component protection (from frozen condensate), ultimately it masks the true effect of moisture content in the air cycle. Total water extraction efficiency is found to be no more than 25%. Poor water condensate control of the LPWE ECS is as a result of the decoupling of the condensation and extraction

processes. The physical distance between these two processes facilitates secondary uncontrolled phase change events. The re-vapourisation of condensate is due to both the addition of bypass air and heat transfer from ambient. The net result is a reduced condensate level at WE inlet for the same AH and a higher cost to the CAU cycle of forming the condensate.

High levels of bleed air inlet humidity are only found at low altitude in high temperature environments, reducing the cooling capacity of the system through performance degradation. The requirement of low turbine exhaust temperatures is most prevalent at these conditions. Typically, the heat rejection rate required from the ECS is high, due to additional kinetic thermal loading from the ambient environment. Additionally, ram air flow rates and available power are often low, for instance during ground operations and idle descent. The compounding of these factors creates a worst case scenario for the ECS.

It is found that the control system constantly regulates the turbine outlet temperature for a beneficial LPWE airflow condition at all altitudes. This is seen on the Hawk, Typhoon, F-15 and F-16. However, at high altitudes the bleed air contains very little moisture and therefore no water separation is in practice required as the danger of avionic component damage due to ice formation is mitigated. As the effect of humidity is not particularly well understood and the control system has no capability of measuring neither inlet humidity nor altitude, the system provides unnecessary heat addition across the complete flight envelope, degrading the system performance. This behaviour has not been identified previously due to the reliance on steady-state 1-D modelling tools and the knowledge gap surrounding the air cycle machine response to inlet humidity.

The implementation of a HPWS would provide an ability to achieve low turbine outlet temperatures from high bleed air moisture content. The control of the phase change events in the high pressure region allows the conditioning of the working fluid at the turbine inlet to obtain an improved turbine expansion efficiency.

5.5. Environmental Control System Response to Faults

An area of ECS performance which is often misunderstood is the response to partial failures. The ECS service schedule replaces items at set intervals, however it is assumed these components continue to operate within their design specifications prior to their replacement. A study is completed to understand the system thermodynamic response to partial failures, commonly reported from the maintenance staff to try and identify the effect on TMS level effectiveness. The motivation of this work is that typical air cycle ECS maintenance and repair regime can account for downtime of the order 1-5k hrs. per 10k flight hrs (Dieckmann 1988). In addition to the cost of this downtime, the frequency of NFF caused by overheating in avionic modules costs the industry over $10m per year in exchanging avionic units (Jones & Chen 2015). It is important that any ECS degradation or failure are tracked, so that maintenance can be limited as much as possible to planned workshop visits rather than unscheduled grounding due to unexpected failures.

The strength of the methodology of this investigation is to utilise genuine equipment which enables the accurate analysis of replicated ECS failures to be completed. An investigation performed with a 1D thermodynamic simulation would provide results as a function of the way the failures were implemented. A 1-D model is unlikely to capture any effects introduced by sensing or control system anomalies, unless these effects are measured, quantified, and deliberately coded into the model. The 1D model is also unable to fully evaluate the effect of the heat transfer rate to the ambient air where the ECS is located and any irreversibility introduced to the cycle solely as a result of the failure. The higher the quality of the data input for the ECS in all flight conditions and under all operations, the higher the quality of the system level analysis.

The failures reproduced during the ground test have been experienced during flight, without significant risk to pilot or aircraft. The costs associated with instrumenting an existing aircraft (due to certification) and performing extended flight tests are prohibitive. The building of a mature technology test bed allows the evaluation of ECS partial failures

with minimal risk and cost. High-fidelity, high-confidence, repeatable data generated by genuine aircraft equipment operating under faithfully recreated conditions is valuable.

Three main faults are injected into the ECS at the GTR; ram air path blockage, bleed air path blockage and partial TCV failure. Blockages are inserted into the bleed air path by means of an orifice plate sandwiched in the joint between two components. Whilst this method of replicating a blockage does not specifically degrade the performance of the affected component, it does replicate the change in pressure drop of a degraded component. The pressure drop through the system governs the mass flow distribution and consequently the heat transfer rate through the secondary heat exchanger, and the bypass flow mixing. The size of the orifice is easy to quantify. The pressure directly up and down stream of the orifice is easy to measure. The failure can be repeated without risk of damage to the 'blocked' components.

The TCVs are butterfly type, driven by a geared motor. No positional feedback is given to the control software. Temperature control is achieved by applying a forward or reverse voltage to the motor dependent on the control temperature set point. The TCVs operate across a wide range of temperatures and tend to fail (get stuck) at their current position rather than defaulting to one extreme of travel. In order to describe the effect on cycle and system operation of a failed valve, the control system has been modified to allow manual position control on each or both valves simultaneously.

The findings allow a deeper level of ECS analysis and highlight a number of fundamental issues with ECS design approach. This is the misleading nature of temperature and the misleading nature of ECS CoP for control strategies and performance metrics respectively. It will be shown that the ECS can achieve the same exhaust temperature when operating with a considerable fault. However, as the mass flow rate of the system reduces, the cooling capacity is reduced. This is not measured by the ECS control system and cannot be clearly identified in the CoP calculations as a reduction in mass flow rate also reduces inlet air power. The reduced cooling capacity can only be identified by the subsystem performance, when considering the subsequent rise in avionic exhaust temperature.

However, with limited system visibility, it is difficult to understand the origin of this over-temperature condition.

5.5.1. Blockage Testing

Figure 5-18 and Figure 5-19 show how pressure and temperature and distributed through the ECS system under normal operations and with a blockage at mid-cycle and at the ECS outlet. The blockage is 90% by area in both cases, which is enough to severely decrease the performance of the system and to bring out the relative differences in the operation of the cycle across the three different scenarios.

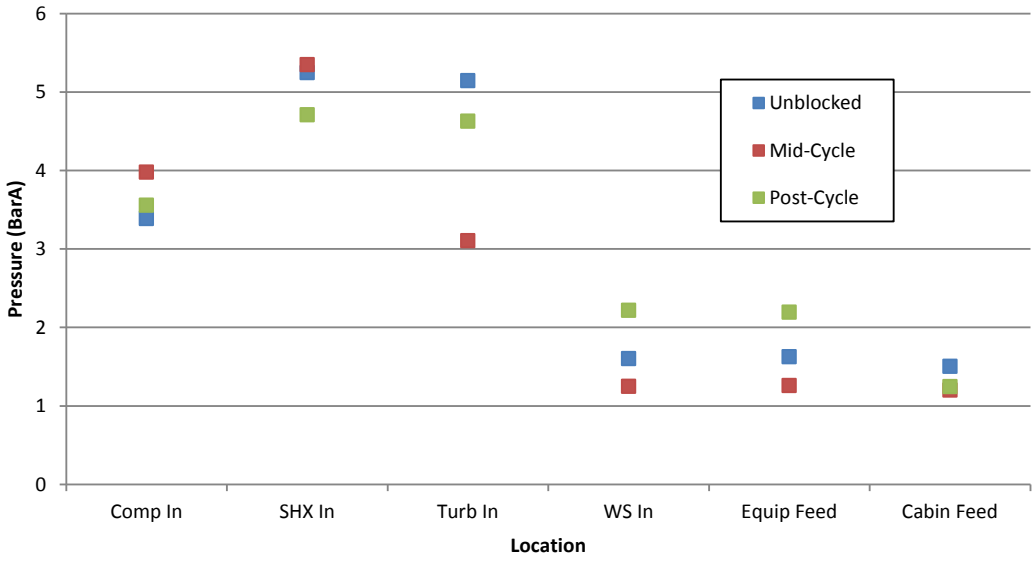

Figure 5-18: Cycle Blockage Comparison of component pressures.

The key features to examine are: the turbine outlet temperature, the ECS exhaust temperature, the total cycle pressure ratio, and the ECS exhaust pressure, which is a measure of the $\dot{W}_E$ term in the ECS CoP equation. Table 5-2 gives key system parameters for the three operating states.

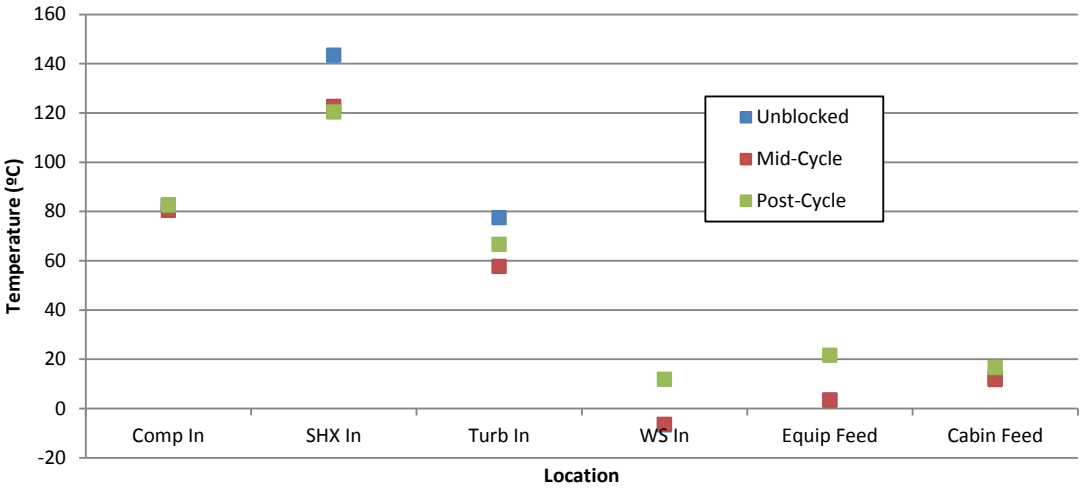

Figure 5-19. Cycle Blockage Comparison of component temperatures.

Parameter	Unit	Unblocked	Mid-Cycle	Post-Cycle
CTCV Posn	%	34	27	0
ETCV Posn	%	19	0	0
T9 - Turb Out	°C	-6.7	-6.5	11.8
T12 - Equip Feed	°C	3.3	3.3	21.5
T15 - Cabin Feed	°C	12.3	11.8	16.6
TCPR		2.11	3.19	1.60
Bleed Air Mass Flow	kgs-1	0.177	0.103	0.136
Cycle Mass Flow	kgs-1	0.165	0.101	0.136
Bypass Mass Flow	kgs-1	0.012	0.002	0
CAU Shaft Power	kW	12.4	5.7	6.7
HXS Bleed HT	kW	11.3	6.8	7.5
HXS Bleed ΔT	°C	67.3	66.0	54.9
Cycle Heat Rejection Rate	kW	15.2	9.1	9.9
Bleed Heat Rejection Rate	kW	13.3	7.6	9.1
Bleed Power	kW	229	138	174
Cycle CoP		0.28	0.19	0.33
System CoP		0.21	0.15	0.18

Table 5-2: Cycle Blockage Key Parameters Comparison.

It is seen in Figure 5-18 that a blockage in the system reduces the CAU exhaust pressure, which in turn drives lower bleed air mass flow. In some different heat pump installations, lowering mass flow has the effect of increasing the CoP of the system, due to the difference in magnitude between input energy and useful heat transfer; however the presence of a blockage negates this. A significant blockage in the low pressure part of the cycle leads to an increased turbine outlet temperature. This is due to the reduced total pressure ratio of the cycle and the corresponding drop in heat exchanger heat transfer and CAU shaft power. The reduced cycle performance when a post-cycle blockage is present means that the ECS can no longer control its exhaust temperature to within 0-4°C (with both TCVs closed). Also, the demanded cabin temperature of 15ºC cannot be achieved in this case.

A blockage in the high-pressure part of the cycle does not by itself increase the turbine outlet temperature. A reduced performance in the compressor and in the heat exchanger is partly accounted for by the increased total pressure ratio of the cycle. The expansion of the bleed air across the post-cycle blockage does not yield a significant drop in temperature, as it does when performed in the turbine. This is because the kinetic energy is dissipated by friction, rather than being recovered into work output and recycled back into the flow by the compressor.

The cycle mass flow rate is significantly less with a mid-cycle blockage than with a post cycle blockage. Despite this, both the heat exchanger and cycle heat transfer rates are of similar magnitude to the post cycle case. This can be explained by the high total pressure ratio.

In the case of a blockage, the ECS CoP is reduced. The complete elimination of bypass flow in the case of a post-cycle blockage means that the ECS CoP is relatively high, as all of the bleed air is directed through the CAU cycle. In the case of a mid-cycle blockage, the ability of the CAU to retain a low turbine outlet temperature means that bypass flow must be used to obtain aggregate exhaust temperature within the target range. The ECS CoP is lowest for this case, due to the presence of the bypass flow around the blocked cycle. This is shown in the difference between the CAU cycle and the bleed air heat rejection rates.

The CAU cycle CoP is high in the case of the post-cycle blockage, due to the high turbine outlet pressure which is directly caused by the blockage. This is due to the amount of internal energy remaining in the flow, which, in this case, it is mainly dissipated across the blockage, hence the reduction in CoP between the CAU cycle and the ECS.

All of the analysis above ignores the fact that a lower conditioning air mass flow is delivered to the cabin when a blockage is present in the system. Whilst certain elements of the system or cycle may appear to perform better in the case of a blocked flow path, this can almost always be attributed to the fact that the mass flow of the system is reduced. A smaller mass flow means less power draw from the bleed air supply.

The following analysis concerns the operation of the system under much smaller relative blockages. The trends discovered above are still present according to the location of the blockage, but in many cases their effects are much more difficult to witness due to the small magnitudes of the resulting changes in the monitored flow state. The blockages only start to make a significant effect when the CAU cycle mass flow rate falls below approximately 75% of the unblocked state.

5.5.2. Post-Cycle Blockage Analysis

Figure 5-20 and Figure 5-21 show plots of increasing CAU cycle blockage, for the total pressure ratio against the aggregate exhaust temperature. The aggregate exhaust temperature is the mass-averaged cabin and equipment feed temperatures by mass.

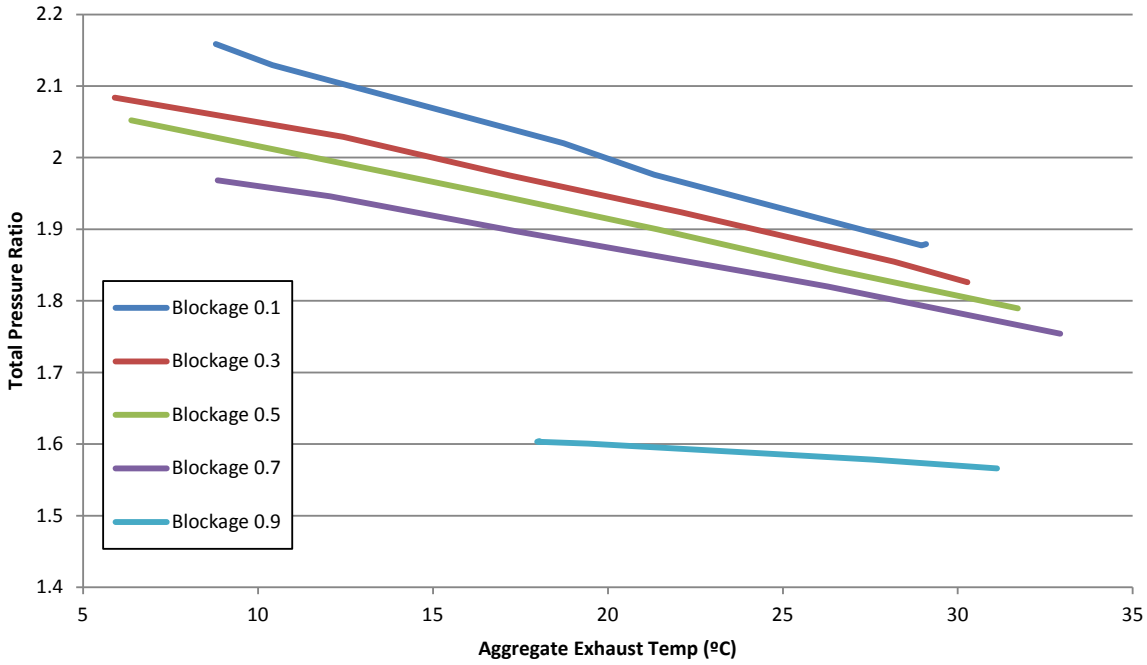

Figure 5-20: Total pressure ratio response to a post cycle blockage.

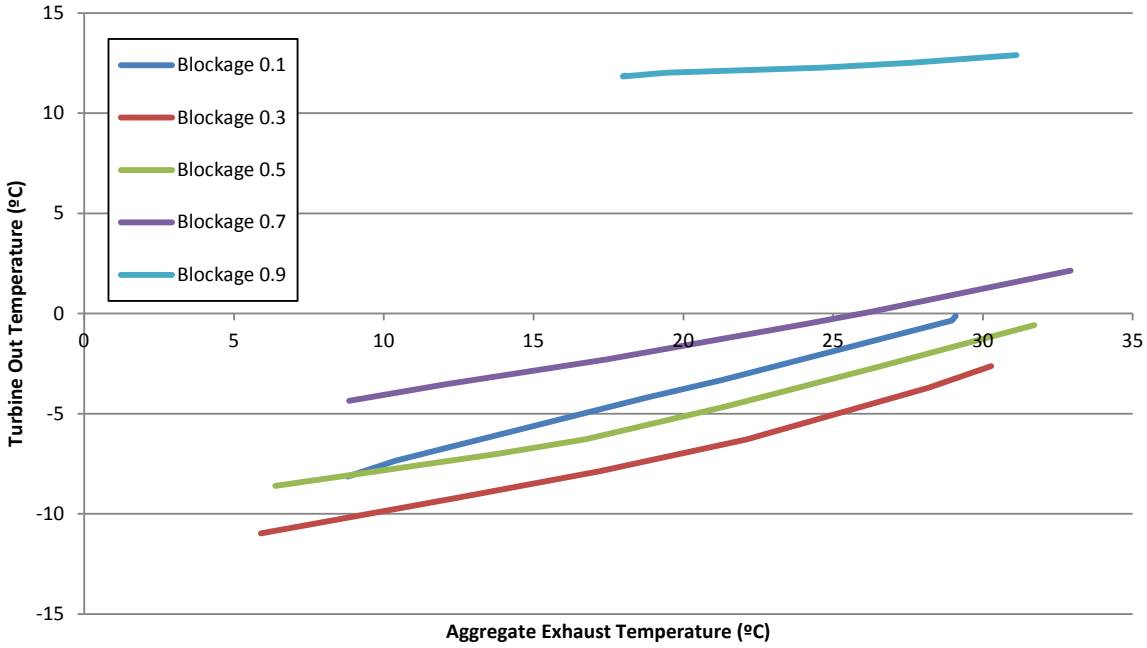

Figure 5-21: Turbine out temperature response to a post cycle blockage.

The range of aggregate exhaust temperatures achievable is limited with the inclusion of a low pressure blockage. The turbine outlet, and hence the equipment feed temperature is severely affected with any blockage greater than approximately 70% by area. The turbine outlet temperature exhibits a local minimum when a blockage of approximately 30% by area is applied. This behaviour is caused by the effect of the back pressure induced by the

blockage on the CAU cycle, which in turn affects the CAU efficiency. The total pressure ratio falls consistently with increasing blockage, for a given ECS exhaust temperature. This leads to reduced conditioning air mass flow and indicates a poor system operation.

A significant blockage experienced post-cycle at low pressure is likely to have a noticeable effect on the performance of the ECS, mainly because of the inability of the system to generate a low ECS exhaust temperature. The system can still operate satisfactorily with a moderate (up to approximately 50% by area) blockage in this location. The degradation in the turbine outlet temperature causes the TCVs to close in order to maintain the demanded ECS exhaust temperature, in turn reducing the overall mass flow of the ECS.

5.5.3. Mid-Cycle Blockage Analysis

Figure 5-22 shows the turbine outlet temperature against the aggregate ECS exhaust temperature, for a range of blockages located mid-cycle in the high-pressure segment of the CAU cycle. Figure 5-23 shows the heat transfer rate and the ECS CoP against blockage per cent by area, at a constant cabin temperature demand of 15ºC.

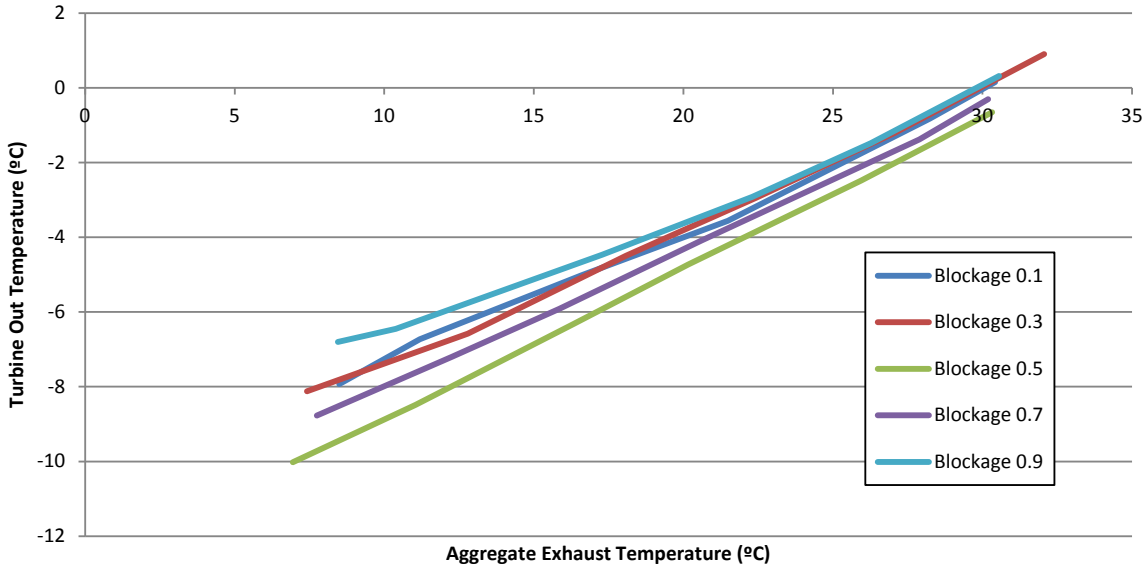

Figure 5-22: Turbine out temperature response to a mid-cycle blockage.

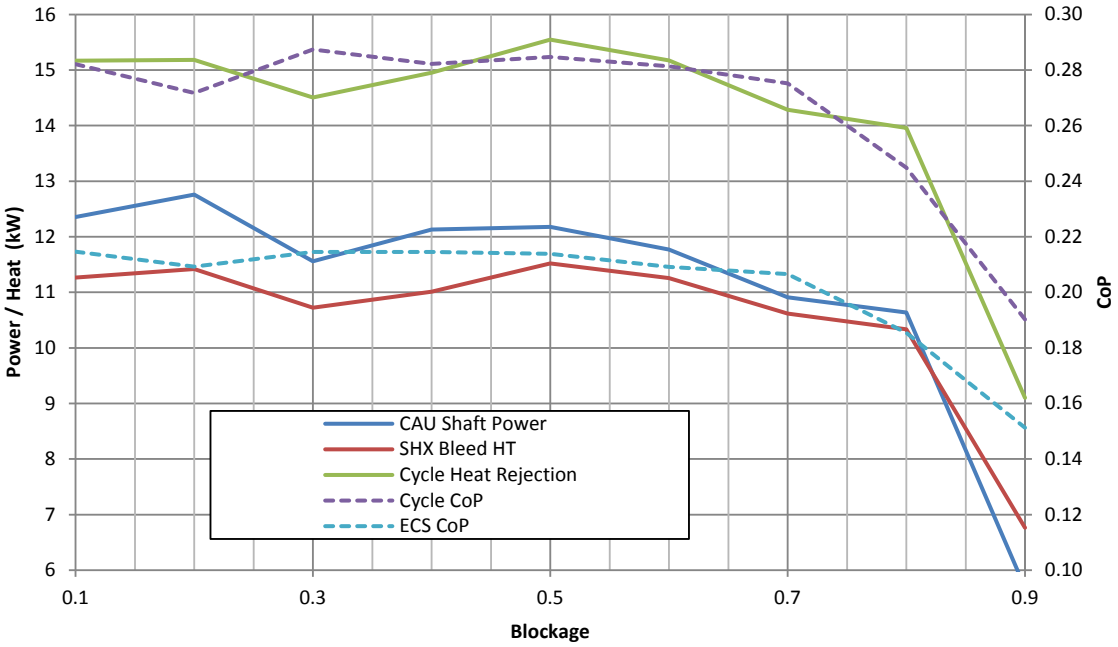

Figure 5-23: System response to a mid-cycle blockage.

The range of aggregate CAU exhaust temperatures achievable is not limited by the inclusion of a high pressure blockage. The turbine outlet temperature for a given aggregate ECS exhaust temperature reduces at lower ECS exhaust temperatures and high blockages ratios. This reduction is not large enough to affect either the equipment or the cabin supply temperature ranges that the ECS is designed to cover. Turbine outlet temperatures in all test cases are almost within the bounds of the test repeatability.

The operation of the cycle, when measured according to the CAU performance indicators and the ECS CoP, remains essentially unaffected below approximately 75% blockage by area. The total cycle pressure ratio follows this same trend. The drop in performance experienced when more than 75% blockage is applied is attributed to the severely reduced bleed air mass flow rate. The net result is a system which is broadly insensitive to a blockage at mid-cycle at high pressure.

5.5.4. Cold Air Unit Efficiency Comparison

Figure 5-24 below shows how the compressor and the turbine efficiency varies with the blockage fraction and location. This serves as both a comparison between the location of

the blockage, and an explanation to why the system reacts to the blockage in the way shown in Section 5.4.3.

Neither compressor nor turbine efficiency are affected by a mid-cycle blockage until this is approximately 70% by area. The compressor efficiency falls steeply after this point, due to increasing compressor-in and -out pressures but decreasing pressure ratio. This helps to explain why the CAU cycle performance is retained until approximately a 75% blockage. With a blockage located at the ECS outlet, the compressor efficiency falls. This is due to decreasing flow through the machine rather than due to a decreasing pressure ratio. Increasing the back pressure on the turbine increases its efficiency, up to a point. This is because of the inherent higher frictional forces associated to the faster flow through the turbine. Applying a back pressure to the machine means that the flow and wall friction through the turbine is reduced and the expansion is closer to a reversible thermodynamic process. The empirical isentropic efficiency detailed in Figure 5-24 is calculated from compressor and turbine maps detailed in Figure 4-8. using process discussed in that section.

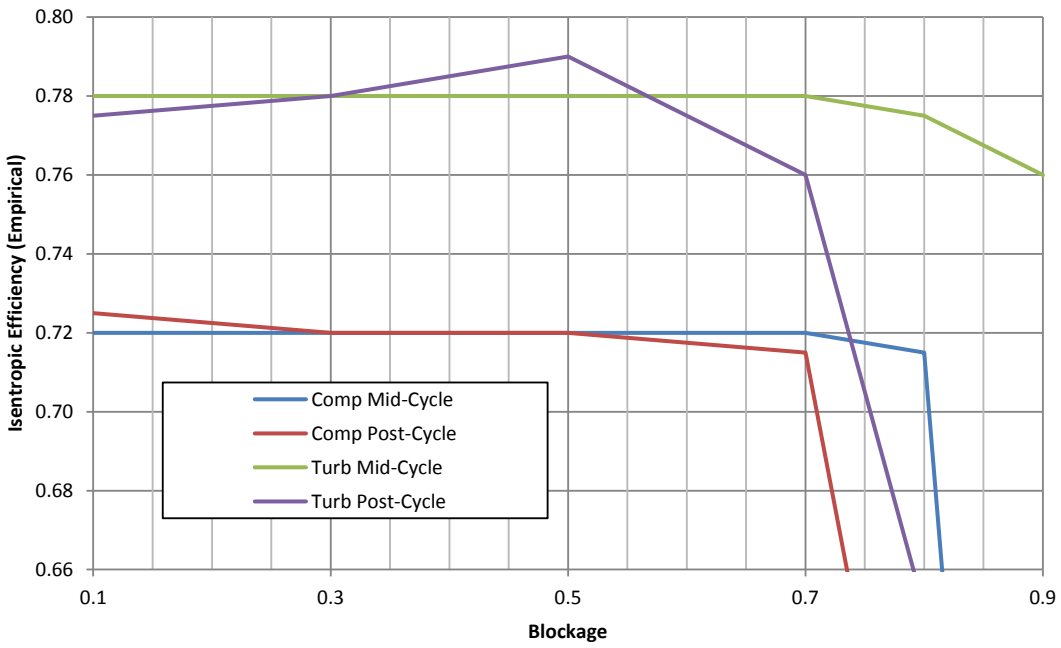

Figure 5-24: CAU Efficiency against Cycle Blockage.

The discovery that the turbine isentropic efficiency increases with a moderate application of back-pressure explains why the turbine outlet temperature reduces when a small blockage is applied downstream of the exhaust of the turbine. Figure 5-24 explains how the CAU cycle CoP increases with a post-cycle blockage as reported in Table 5-2, but also how this gain in efficiency is wasted by the flow expansion through the blockage.

The current system could in theory be improved by adding a second expander device in the same location as the simulated blockage, downstream of the turbine exhaust. The improvement would be twofold: first, this would improve the expansion efficiency in the existing turbine and, second, it would increase the power supplied to the compressor. This finding agrees with the theoretical work conducted by Conceição, et al. (Conceição et al. 2007) that models a bootstrap ECS with two expansion stages to be 5% more efficient at a cruise condition and 90% more efficient during a ground case than a system with a single expansion stage. Even though the efficiency gain found in the turbine is only 2%, the net result is a reduction in turbine outlet temperature by up to 5ºC.

5.5.5. Blockage Testing Conclusion

A blockage in the bleed air path of the bootstrap system will not drastically affect its performance until CAU cycle mass flow rate falls below approximately 75% of its unblocked state. This occurs at a blockage of approximately 60% by area for a low pressure blockage and at a blockage of approximately 75% by area for a high pressure blockage. The capability of the cycle to overcome a blockage, in terms of turbine outlet temperature, is related to the total pressure ratio of the cycle. Therefore, a low pressure blockage downstream of the turbine has a more detrimental effect on the system performance than a mid-cycle blockage in the high pressure segment of the CAU cycle.

5.5.6. Temperature Control Valve Position Testing

Figures 5-25 and 5-26 describe the control system and the thermodynamic responses to varying the TCV positions, respectively. Figure 5-25 shows multiple curves for constant values of cabin delivery temperatures against TCV positions, which indicates the ability off the system to apportion the cooling flow while meeting the design specification on outlet

temperatures. Figure 5-26 shows multiple curves for varying ETCV positions against ECS exhaust temperatures over the control limits of the ETCV, which shows how the control software drives the ECS.

Figure 5-25 shows the possible combinations of valve position that could be used to generate a set cabin temperature, ignoring the variation in the equipment temperature. Figure 5-26 then shows which portion of the total possible range the control system actually uses, by restricting the equipment temperature to the limits on the x-axis. For example, a cabin temperature demand of 20ºC would require an ETCV position over the range 5-20% in order to maintain the equipment temperature below 7.5°C. This would limit the attainable portion of the 20ºC curve in Figure 5-25 to these limits on the x-axis.

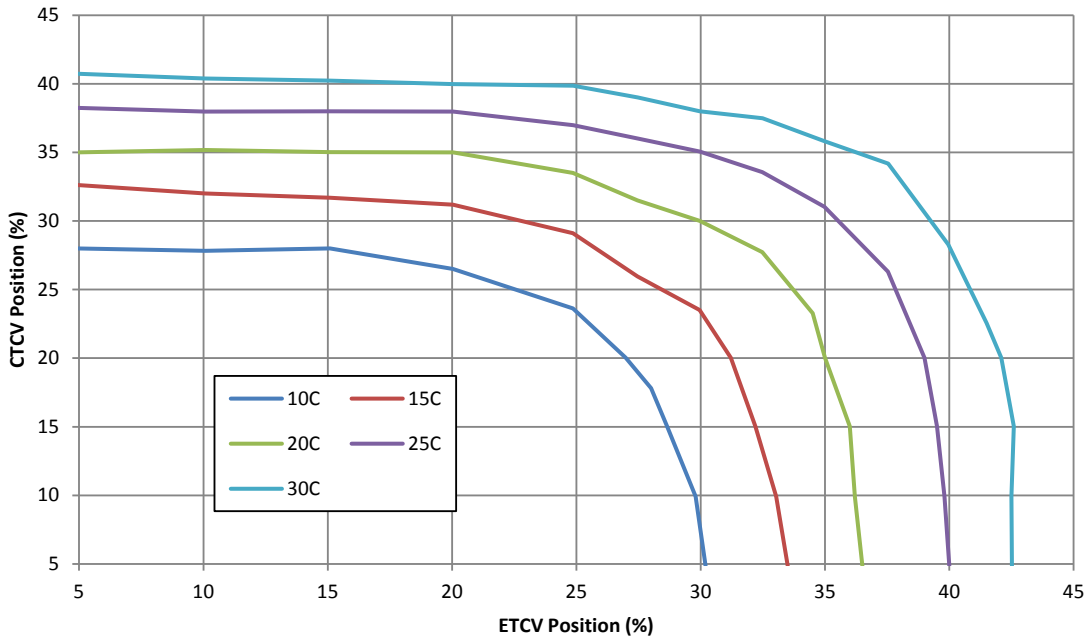

Figure 5-25: ETCV and CTCV positions to achieve a given cabin temperature.

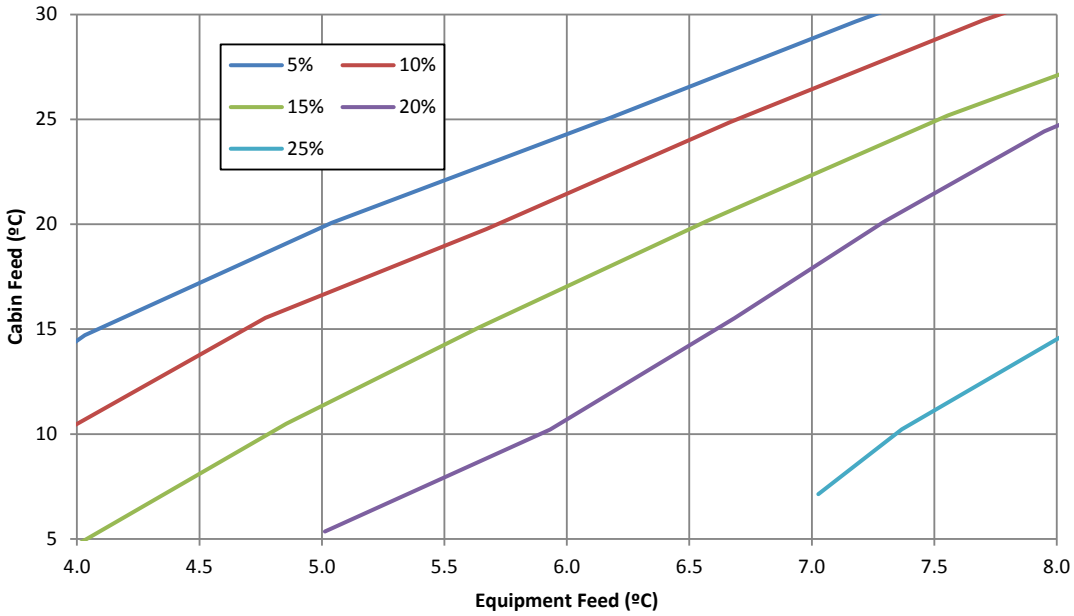

Figure 5-26: Equipment and cabin feed temperature for differing ETCV positions.

It can be seen that a given cabin delivery temperature is achievable with any combination of TCV positions along a constant temperature curve in Figure 5-25. There is little difference in the position required of each TCV in isolation to attain the same pack exhaust temperature. The difference arises through the pressure drop across WE. In the event of a valve failure, consider the constant temperature curves that are tangent to the line drawn perpendicular to the axis of the failed valve at the point of failure. These cabin temperatures are theoretically still attainable.

The control system regulates to the lowest possible ETCV position for the demanded cabin temperature, in order to fulfil the equipment delivery temperature requirements. The ETCV will only move if the equipment temperature falls out of the specifications, which is defined by the x-axis limits in Figure 5-26. It should be noted that Figure 5-26 represents an Equipment feed temperature of 4-8°C, while the design specification is 0-4°C. This figure is for illustration of valve failure, rather than operationally representative temperatures. In the event of a CTCV failure, the ETCV position is not influenced by the cabin delivery temperature. Therefore, the system loses the ability to control the cabin delivery temperature, and delivers the minimum temperature available for that valve position based on the equipment delivery temperature. It is shown that if the ETCV fails at any

point in its usual operating range (below approximately 30%), it is unlikely that the failure would be identifiable, as cabin temperature control is retained. If the ETCV fails at around 25%, the equipment temperature is only in spec at low cabin temperatures. If the ETCV fails much above this point, the curve lies outside of the x-axis limits, and therefore the equipment temperature becomes out-of-specification irrespective of the cabin temperature.

The TCVs theoretically allow for redundancy in the ECS exhaust temperature control. In reality however, an ETCV failure will not be compensated for and a CTCV failure will instantly cause the system to lose its ability to air condition the cabin environment. Equally, this behaviour means that an ETCV failure is likely remain unnoticed unless an indicator is provided to the aircrew that the avionic temperature is out of specifications, whereas the aircrew themselves will readily identify a failure of the cabin TCV to control the cabin air temperature.

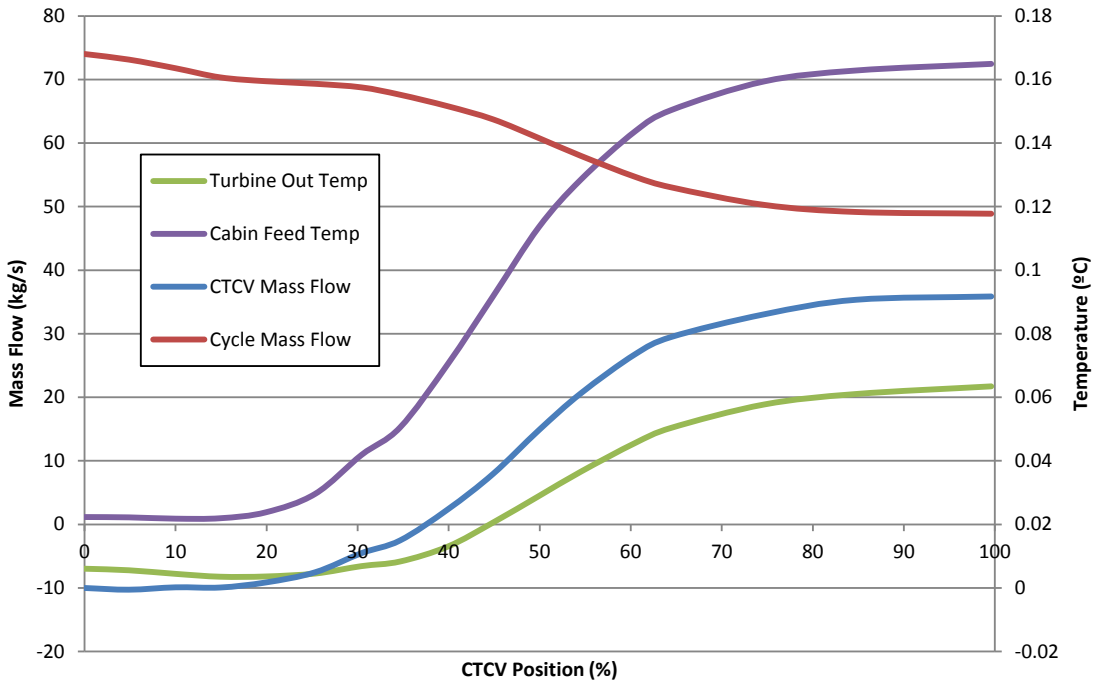

Figure 5-27: System Response to TCV Sweep

The ECS is highly sensitive to the TCV position, as a change of 10% full travel yields a 20C difference in the ECS exhaust temperature. It is vital that ECS exhaust temperature control

is retained, due to the large and varying heat loads placed on the cabin. The sensitivity of the TCVs is explained by their geometry; Figure 5-27 shows how the mass flow through the TCV varies with position.

Another interesting trend from Figure 5-27 is how the turbine outlet temperature finds a local minimum with about 20% of the CTV open. Other data from the same test shows that the CoP and the system entropy generation follow similar trends. It is thought that this is due to the effect of changing the back pressure on the cycle, in much the same way that a small post-cycle blockage does. The net effect is an improvement in CAU CoP.

5.5.7. Temperature Control Valve Testing Conclusion

The thermodynamic performance of the system is directly related to the percentage of CAU cycle bypass air flow. The hardware architecture of this particular ECS allows either of two TCVs to almost equally regulate the turbine outlet and ECU exhaust temperatures, with little influence on system performance / efficiency, dependent on which valve is used. Figure 5-4 displays the relationship between CoP and combined valve opening. The points on this graph are generated with several valve combinations, with a clear line of best fit to substantiate the previous statement. Depending on the position of the valve at the point of failure however, the pack exhaust temperature will be limited in range.

The control architecture of this particular system means that it is comfortably able to mask the failure of the ETCV but not of the CTCV value to the flying view. This is due to the sensor positioning and the path of the signals within the control system. It is likely the control architecture was designed to prioritise the control of the inlet conditions to the WE and therefore the ETCV has no capability to compensate for a CTCV failure. If the software was redesigned to account for the aggregate pack exhaust temperature in the positioning of both TCVs, the robustness of the system would be significantly improved, possibly at the expense of the WE efficiency.

5.6. Environmental Control System Conclusions

Considerable time was dedicated to gain a thorough understanding of the ECS subsystem performance at a number of operating conditions. New knowledge has been developed in the areas of the ECS thermodynamic system relationships, its response to inlet working fluid and its degraded operating conditions. These relationships are established with confidence, as the equipment and operating conditions are matched to in-flight conditions and use was made of a genuine ECS control system in the tests. The data is incorporated into a mission-level analysis later in this chapter.

It is clear that there is a requirement for the development of a robust system performance metric when considering the ECS in isolation. The ECS CoP is not by itself expressive of the system impact on the aircraft cost (bleed air rate and thus fuel consumption). It has been found that, in response to a partial failure, the ECS CoP can remain constant while the cooling capacity is reduced. The use of the CoP as a CAU performance parameter is perfectly adequate when considering a system level analysis, however within the ECS subsystem, this parameter considered in isolation can be misleading.

Through the consideration of partial failures, it has been found that temperature can also be a misleading metric. This concerns the use of temperature in interface management and ECS control strategies. The ECS is controlled with bypass air to deliver a stream of air at 0ºC to 4ºC to the equipment and between 8ºC to 35ºC to the cabin. It was shown in Figure 5-22 that a constant temperature could be delivered at the turbine exhaust within an increasing system failure. The control system has no ability to identify this failure, however, due to the reduction in mass flow rate, this would cause the downstream subsystems to overheat. The reliance on temperature alone as a control strategy metric allows the development of a situation where by the ECS is still providing bypass air to heat the airflow, when the cooling capacity is already insufficient due to a partial system failure.

The control strategy to protect the LPWE is a prime example of serving one sub-system at the detriment of the system perfomance. The system provides a temperature of 0ºC to 4ºC

at the water extractor inlet for optimal water separation. The Hawk ECS, like other aircraft, utilises a specific bypass branch to generate optimal water separation conditions at some point in the cycle. However, as the system has no instrumentation for measuring either humidity or altitude, it continues to heat the turbine exhaust air for water separation at altitudes where the bleed air has a negligible absolute humidity. This is due to the combination of a lack of understanding about the ECS humidity response, a segregated design process, a simplistic interface management (as it is easy to convey a set temperature to downstream equipment subsystem as opposed to a flow characterised by both temperature and humidity) and a poor interpretation of system performance metrics.

The overriding conclusion of the ECS performance evaluation is that the bleed air cycle is fundamentally good for providing conditioned air supply. However, its application within the airframe needs detailed consideration. The bleed air cycle is compact, lightweight, robust, reliable and easily integrated. Future work needs to review the application and interface management information in the design of the system.

5.7. Avionic Module Thermal Performance

The knowledge gap presented in Chapter 2 is unknown system behaviour of the thermal avionic module conditions. Currently, the only University-led thermal avionic experimental facilities for BAE Systems Typhoon platform are those built in this project. The development of the facility was covered in Chapter 4, with the performance evaluation considered in the following section. The validation data of this subsystem is incomplete, due to the IPR barrier to sharing of information on the thermal behaviour of the avionic modules. Two key data sets are provided by BAE Systems Rochester, who supplied the Typhoon FCC.

5.7.1. Pre-Defined Avionic Thermal Relationships

Several logic-based thermal relationships within the avionics bay can be established prior to the experimental testing. The avionic module exhaust temperature ($T_{\text{Mod Exhaust}}$) can be simply defined as the sum of the module inlet temperature ($T_{\text{Mod Inlet}}$) and the temperature differential across the avionic module (ΔT_{Module}), that is

$$T_{Mod\ Exhaust} = T_{Mod\ Inlet} + \Delta T_{Module} \quad (5\text{-}17)$$

5.7.2. Temperature of the Module Inlet

The temperature of the module inlet ($T_{Module\ Inlet}$) is defined as the sum of the ECS outlet temperature (T_{ECSE}) plus any temperature change due to ambient heat transfer before the avionic module, defined as the temperature difference across the avionic tray (ΔT_{Tray}) and the temperature difference across the main ECS branch ($\Delta T_{ECS\ Branch}$). This gives

$$T_{Module\ Inlet} = T_{ECSE} + \Delta T_{Tray} + \Delta T_{ECS\ Branch} \quad (5\text{-}18)$$

The ECS outlet temperature is a function of the bleed air flow (temperature, pressure, and mass flow rate), the ram air flow (temperature, pressure, and mass flow rate) and of the ECS coefficient of performance so that;

$$T_{Bay\ Inlet} = f(Bleed\ Air, Ram\ Air, ECS\ CoP) \quad (5\text{-}19)$$

The ECS typically supplies a fixed mass flow for avionic cooling, conditioned to a temperature between 0 and 4ºC (for Hawk, however original specification F-15 provide equipment cooling up to 30°C to avoid condensate). For this investigation, the ECS outlet conditions are fixed.

The temperature differences across the avionic tray and across main ECS branch are purely a function of the avionic bay temperature (T_{Bay}) as these components are subjected to environmental thermal loading. The temperature differences across the avionic tray and main ECS branch are also a function of the recovery temperature.

5.7.3. Temperature Difference across Avionic Module

It was shown in Chapter 2 that the bay temperature and the recovery temperature can be considered equal. The temperature difference across the avionic modules is a function of the avionic bay temperature (T_{Bay}), the cooling mass flow rate, $\dot{m}$, and the avionic power output.

$$\Delta T_{mod} = f(T_{bay}, \dot{m}, \dot{Q}_{Av}) \tag{5-20}$$

The mass flow rate is determined from the ECS evaluation previously. As the flight engine load changes through the flight conditions, the mass flow rate is variable while the mass flow rate distribution and characteristic pressure drop is fixed. Having established that the bay temperature is also dependant on the flight condition, the system is subjected to a variable thermal loading, but not by design. At high aircraft speed conditions, the mass flow rate is increased as the bay temperature increases due to the higher recovery temperatures. However, the magnitudes of the heat addition and of the heat rejection are not necessarily variable by design, highlighting an opportunity for system optimisation.

5.7.4. Response to Environmental Loading

The following section experimentally derives the correlation between the three components to form an expression for the avionic module exhaust temperature at a given flight case. The FCC response to a variation in the recovery temperature is seen in Figure 5-28. A 60-minute stabilisation period was used following each change of bay temperature to ensure steady-state conditions are measured.

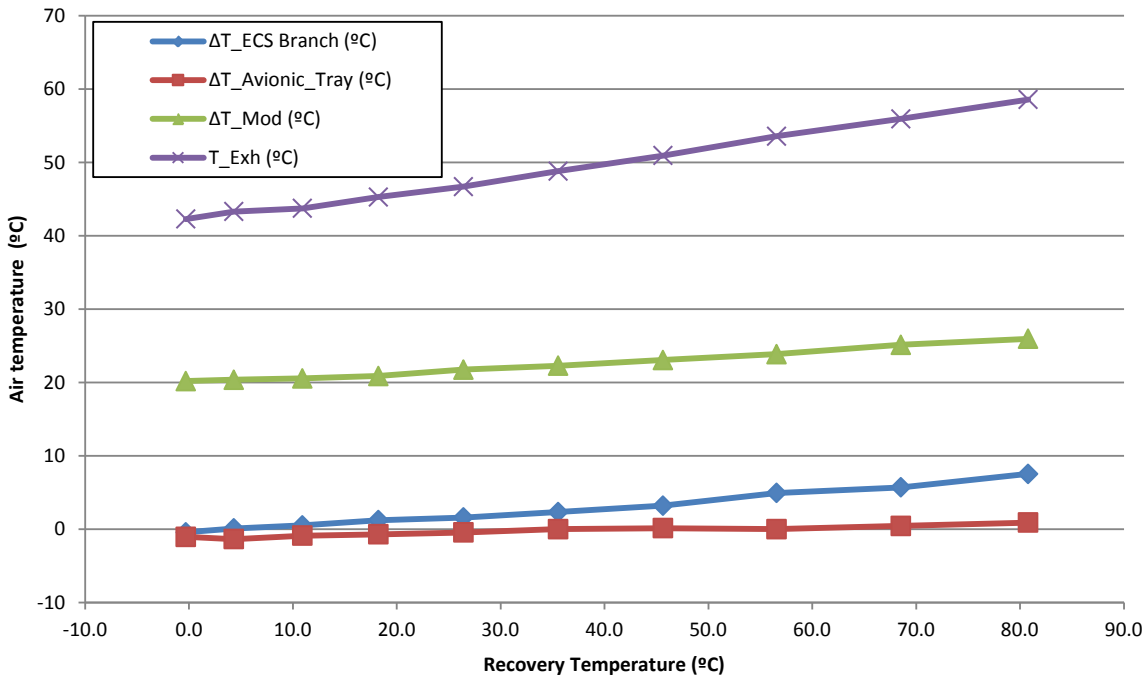

Figure 5-28: **Thermal response of FCC to changes in recovery temperature.**

A positive linear correlation between the FCC temperature and the recovery temperature is shown in Figure 5-29. As the environmental thermal loading has a direct effect on the avionic module exhaust temperatures, the heat rejection CoP of the bay is based on the flight condition. As the heat load of the avionic module is assumed fixed, therefore any heat rejection through negative environmental thermal loading reduces the requirement of bleed air heat rejection.

5.7.5. Response to Flow Rate

For design purposes, the avionic bag flow rate is defined as power-specific, that is, the flow rate is specified per module power output. The baseline figure for this investigation is 3.5kg min^{-1} kW^{-1}. However, as the bleed air conditions vary through the flight envelope, this value also varies. The distribution of mass flow rate is fixed by the characteristic pressure drop of the modules. It is seen in Figure 5-29 that increasing airflow from the baseline figure of 3.5kg min^{-1} kW^{-1} generates a reduction in the heat rejection CoP as heat rejection rate and the component temperature tend to level off. The avionic heat exchanger efficiency is based on the convective heat transfer coefficient at a given airflow condition. The non-dimensional airflow condition is defined by Reynolds number and the non-dimensional relationship between the channel convective and conductive heat transfer is defined by the Nusselt number.

The avionic mass flow rate, the channel velocity and the Reynolds number increase linearly with one another. An increase in the Reynolds number is characterised by a higher airflow turbulence level. The increased unsteadiness in the flow generates an increase in flow mixing, increasing the convective heat transfer coefficient linearly. In response to increasing the convective heat transfer coefficient, the module airflow temperature difference reduces. The resulting heat rejection rate increases with increasing flow rate, as seen from experimental data presented in Figure 5-29. The component temperature is the heat source temperature and the exhaust temperature is measured in the exhaust airflow from the avionics box.

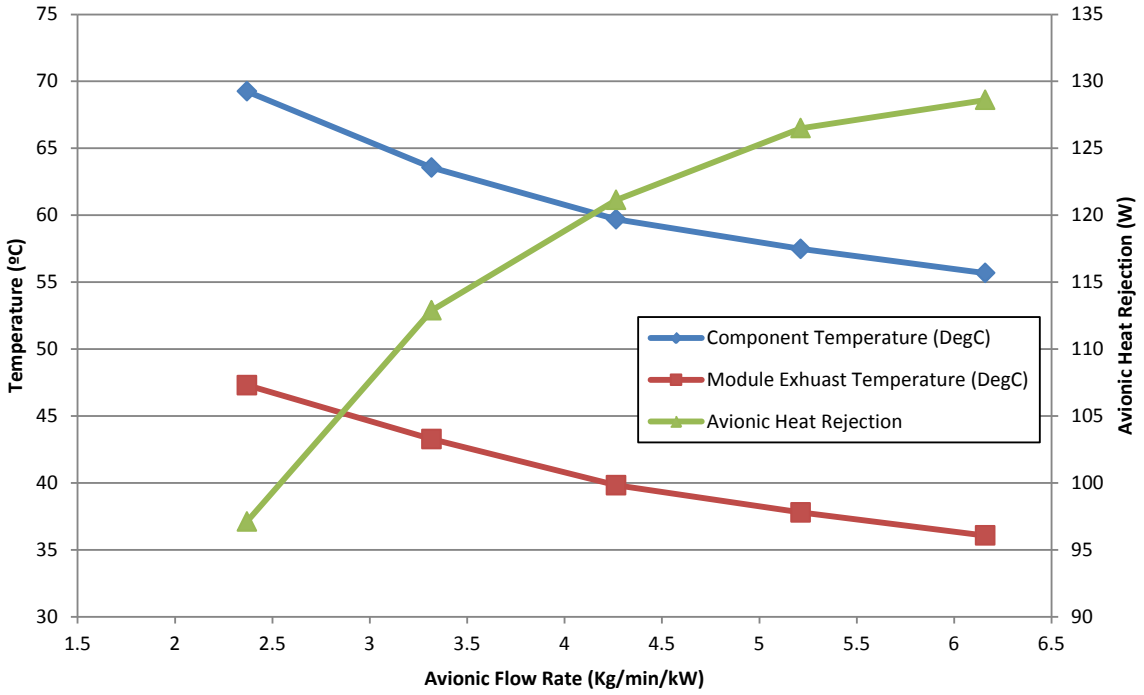

Figure 5-29: Avionic module thermal response to increasing mass flow rate.

As the flow rate increases, the CoP of the avionic heat rejection can be seen to diminish because the cost of generating the cold air (input power) increases and the module heat rejection rate is constant. A similar trend was found with the ECS CoP, where an increasing inlet pressure required an increased bypass mass flow rate to achieve a fixed exhaust temperature. The two findings suggest that to deal with thermal management with the continued increase in the bleed air supply flow rate is thermodynamically wasteful; in agreement with the previous literature reviews in Chapter 2 (Allison et al. 2016).

5.7.6. Response to Power Output

The power output of the avionic modules are assumed constant for the complete flight profile in this analysis, however, to provide data for system optimisation, a variable power output is considered here. Tests were conducted at the same conditions as in Section 5.6.1, but with a constant mass flow rate and a constant bay temperature. The avionic module temperature difference is found to be linear with increasing avionic power output, as shown in Figure 5-30.

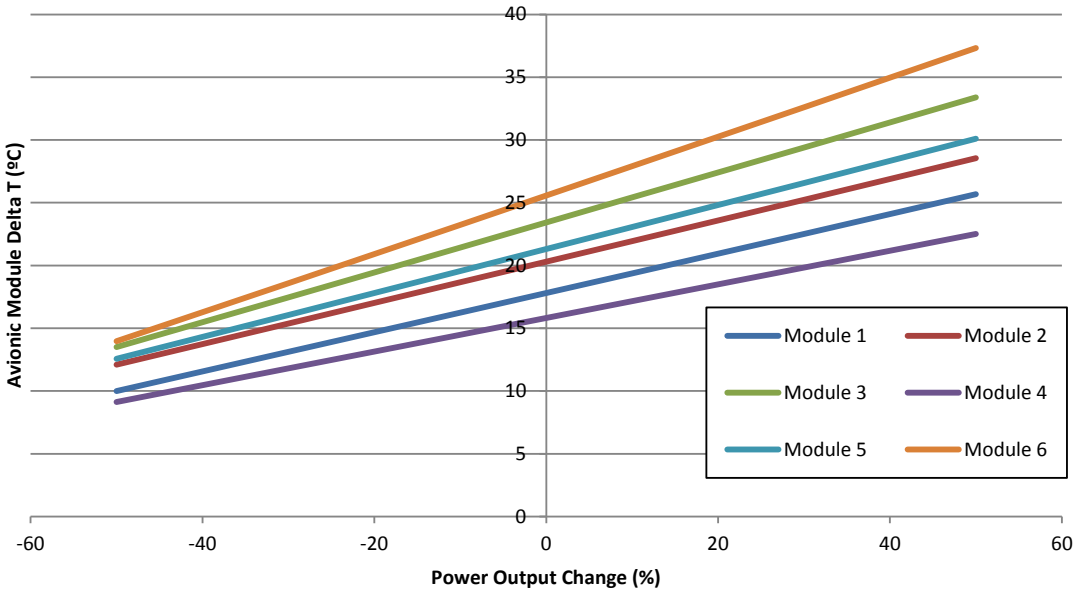

Figure 5-30: Variation in module temperature differential with power output

The avionic modules detailed in Figure 5-30 are measured from the avionic tray experimental rig. The tray supports a total of 1kW (as a baseline) across six avionic modules ranging from 79W to 305W each. The baseline (0%) temperature difference is an output of the calibration process. It was found that the larger modules (therefore more powerful) had a slightly higher temperature difference at a given mass flow rate.

5.8. Avionic Bay and Cabin Thermal Performance

The forward avionic bay, underfloor avionic bay, and the cabin environment are analysed purely in the modelling the software environment as detailed in Chapter 3. These parts of the system are assessed in the following section where the complete system is assembled on the software modelling platform to provide mission-level data analysis.

5.9. Mission Level Analysis

The individual subsystem performance has been evaluated, however the requirement of this analysis is to provide a mission-level analysis. A mission- level analysis is the point at which the system is pulled together into a single data stream to provide an accurate inflight replication. A flight profile is compiled through the input of ten user-defined flight conditions. The flight conditions operating in an ISA standard day atmosphere are detailed

in Figure 5-31. Each flight condition is considered a steady state condition. Three atmospheric conditions are detailed in this analysis, the 1% hot, 1% cold and ISA.

The system CoP response to the flight profile is seen in Figure 5-31. It is shown that the highest CoP is seen at low load cases such as 'Ground Ops' and 'Cruise' conditions, with the lowest CoP being seen at high load cases such as 'Accelerate and Dive' and 'Combat' conditions. The peak CoP is 0.39, meaning that at most efficient operation, the input power only generates a heat rejection rate smaller than it; where ground based heat pumps typically generate three times the heat transfer rate of their input. Bleed air flow is typically up to 3% of the total engine airflow rate, with the compression process powered by fuel consumption. Inefficiencies in the TMS therefore result in additional fuel burn.

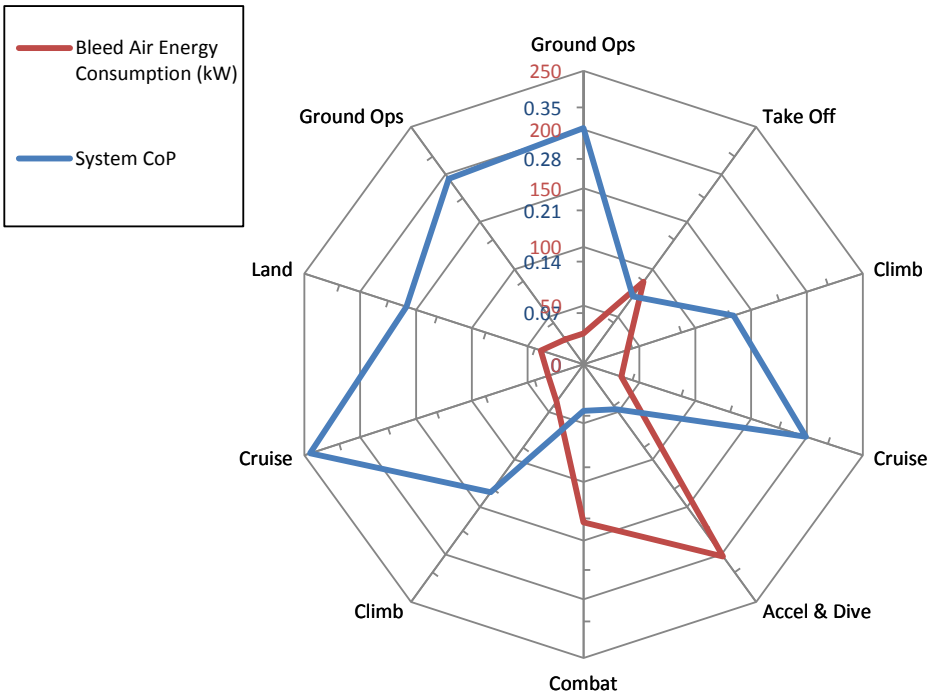

Figure 5-31: CoP and Bleed air consumption across a flight profile. ISA Standard Atmosphere.

An inverse relationship between the bleed air energy consumption rate and the CoP is found in Figure 5-31. The variation across the flight cases in the heat rejection rate is relatively small (8kW to 15kW) in comparison to the variation in the bleed air consumption rate (24kW to 202kW). The bleed air energy consumption rate of an 'accelerate and dive' case is 6.4 times greater than that of a cruise condition, however the heat rejection rate from this flow is only 1.2 times greater, as shown in Table 5-3.

5.10. Flight Case Comparison

When considering the energy consumption rate and the thermal loading at each subsystem, two flight cases are compared (highest and lowest CoP). The data is shown in Table 5-3 for a high load case (accelerate and dive) and a low load case (cruise 2). The following section draws analysis between the two extremes of the performance window. The analysis works through each subsystem of interest, discussing performance and efficiency response to each flight condition.

5.10.1. Energy Consumption rate

The ECS inlet pressure and therefore the mass flow rate is dependent on engine compressor pressure at the bleed air off take. The inlet pressure for the high load case is 1698 kPa.abs in comparison to 256 kPa.abs for the low load case, resulting in twice the ECS inlet mass flow rate. While ambient pressure is lower for the low load case due to the increased altitude, the energy consumption in compressing the bleed air is 33.95kW, which is a total of 75kW less than at the high load condition.

The high load case is a low altitude (1000ft) and high vehicle speed (0.83M) flight condition, resulting in a substantial pressure drop across the ram air heat exchanger. The airflow density at the heat exchanger inlet is 4.2 times greater and the mass flow rate is 7.4 times greater than at the high altitude, low load condition. The resulting power consumed to overcome the heat exchanger pressure drop is seen in Table 5-3. Additionally, as the high load case is operating with the exhaust pressure and the exhaust temperature close to atmospheric conditions, the theoretical energy recovery ($Q_{Overboard}$) from the airflow path is low. At the high altitude cruise condition, the cabin and the avionic bays are assumed to be pressurised to around 6000ft above the local atmospheric pressure and have an exhaust temperature substantially higher than local atmospheric temperature. The energy recovery from an isentropic expansion of the outflow to atmospheric conditions is 9kW, further reducing the TMS energy consumption rate.

		Accelerate & Dive- High Load	Cruise 2 – Low Load
Mach Number	M	0.83	0.7
Altitude	Ft	1000	40000
Recovery Temp	ºC	50.52	-37.60
Bleed Air Compression	kW	109.18	33.95
Inducer Flow Compression	kW	0	0
Q overboard	kW	0.21	8.99
Power consumption ram air path	kW	93.04	6.65
Total Energy Consumption	kW	202.01	31.61
ECS Heat Rejection	kW	111.79	21.12
Total Avionic Heat Load	kW	3.3	3.3
Total Pilot heat load	kW	0.79	0.79
Total Solar Loading	kW	2.5	2.5
Total Kinetic Loading	kW	6.2	-8.3
Total loading	kW	15.26	12.38
CoP		0.08	0.39

Table 5-3: System energy flow for a 'Accelerate & Dive' flight case in comparison to 'Cruise'.

5.10.2. Environmental Control System Performance

A number of similar relationships between the ECS and the TMS performance are identified, mainly due to the ECS being responsible for the largest contribution to the energy budget of the TMS. The performance difference between the high and low load cases can be appreciated by when considering the ECS cycle CoP, shown in Table 5-4. While both flight cases represent extreme high and low ECS flow rates and operate on opposing sides of the compressor efficiency map, the compressor efficiency values is very similar.

The difference between the ECS and the CAU cycle CoP is due to the addition of the bypass air. As detailed in the humidity investigation in Section 5.3, the bypass controls the airflow

temperature to the WE inlet, to ensure that water separation can take place. However, the cruise condition is at an altitude where the ambient air has a negligible water content. The heating of turbine exhaust airflow to provide adequate conditions for water separation of dry air is of no obvious benefit and it degrades system CoP.

		Accelerate & Dive – High Load	Cruise 2 – Low Load
Bleed Air Mass Flow rate	kgs-1	0.305	0.141
Ram Air Mass Flow rate	kgs-1	1.393	0.180
Total Bypass Mass Flow rate	kgs-1	0.028	0.043
SHX Q Bleed	kW	40.4	9.0
SHX Q Ram	kW	30.1	8.3
SHX Effectiveness		0.74	0.92
Compressor Efficiency	%	57	56
Turbine Efficiency	%	82	74
Bleed Air Heat Rejection rate	kW	116	29.9
Cycle Heat Rejection rate	kW	119	31.9
Bypass Heat Addition rate	kW	3.50	1.93
Cycle CoP		0.51	0.88
ECS CoP		0.42	0.46

Table 5-4: ECS Performance for two flight case. ISA Standard Atmosphere.

The reduced mass flow rate of the low load condition through a fixed geometry heat exchanger reduces the channel velocity and increases heat exchanger effectiveness. The high load case has higher turbine efficiency, however this does not compensate for the poor heat exchanger performance when considering the cycle heat rejection rate. The result is a substantially more efficient cycle performance at a low load case with a cycle CoP of 0.88 against 0.51.

The ECS controls to a constant cabin temperature and to a constant equipment supply temperature, with both conditions requiring the inclusion of bypass airflow to add heat. While the absolute value of bypass heat addition rate is comparable in both cases, its

(negative) contribution to the total heat rejection rate is substantially larger in magnitude when considering the low load condition. The control of the ECS exhaust air temperature essentially regulates the ECS CoP to within 0.04. While the total CoP of a bootstrap air cycle machine on an absolute scale is low, the ability to regulate its efficiency within a very small operational range is a major contributing factor to the widespread use of the cycle. This is echoed by an ECS fault injection study, which found the system to be robust across a range of operating conditions, including cycle path blockages and control valve failures (Jones et al. 2016).

5.10.3. Cabin Performance

Cabin solar loading is particularly intense due to the large surface area of the transparencies. However, the variation between sea level and 30,000ft is relatively small, with the solar loading increasing from 1080W/m² to 1250W/m², hence the difference between the two flight conditions from cabin solar loading is around 290watts. Kinetic loading presents a variation of 1.6kW into the cabin and 2.6kW out of the cabin between the two conditions. At a low altitude and high speed, the air density, ambient temperature, and vehicle speed is much greater, generating a larger recovery temperature. At a high altitude cruise condition, the recovery temperature is much closer to the ambient temperature and therefore substantially lower than the mean cabin temperature. When considering a total cabin loading, the low altitude case requires 4.7kW of heat rejection in comparison to the 0.7kW of the high altitude case. While the high load case has a greater utilisation of ECS energy, the absolute values are very small compared to the total input energy.

5.10.4. Forward Avionic Bay Performance

The key parameter of this analysis is the avionic module exhaust temperature variation with flight condition. The avionic module exhaust temperature was found to be very stable, calculated as 27ºC ± 4ºC. The high load case avionic exhaust temperature is 26.6ºC, and the low load is 33.7ºC. The avionic module exhaust temperatures for all cases in found in Figure 5-33.

The flow split between the cabin and the forward avionic bay is based on a fixed static pressure drop, therefore the avionic flow rate reduces proportional to ECS inlet mass flow rate. It is previously detailed in Figure 5-29 that the avionic module temperature difference is more sensitive to a reducing avionic flow rate. The avionic chassis heat exchangers are very basic straight channel, low Fins Per Inch (FPI) high aspect ratio design to mitigate the danger of clogging. The efficiency of heat exchanger is seen to reduce with increasing mass flow rate, as a result of the increased channel airflow velocity. The resulting performance is a non-linear reduction in the module temperature difference and a decreasing heat rejection efficiency with increasing mass flow rate.

While the low load case has a negative kinetic loading of over 2kW, the module exhaust temperatures are the highest due to the reduced avionic flow rate. This highlights that avionic modules are more sensitive to a change in flow rate than to a change in the aircraft exterior ambient temperature.

The analysis suggests that the avionic modules are overcooled throughout the entire flight envelope based on the thermal design limit of 71ºC for the avionic module exhaust temperature. The high avionic flow rate is directly responsible for unnecessary consumption of fuel energy through surplus bleed air compression. Equally, with an increasing avionic flow rate, the heat rejection efficiency of the module heat exchanger reduces and the CoP of the ECS reduces. Therefore, across the complete flight path, excess fuel energy is consumed to operate both subsystems sub-optimally.

5.11. Atmospheric Condition Comparison

The same flight profile is completed on a Cold, ISA and Hot atmosphere and the CoP operating range is detailed in Table 5-5. It can be seen from Table 5-5 that the hot environment offers the greatest efficiency, with the ISA environment generating the worst performance. It is also seen that the ISA flight profile operates closer to its average and the operating range increases with more extreme atmospheric conditions.

Atmospheric Condition	TMS CoP Operating Range
Hot	0.36 ± 0.22
ISA	0.22 ± 0.16
Cold	0.24 ± 0.18

Table 5-5: System CoP operating range for a fixed flight profile in different atmospheric conditions.

An airflow temperature profile from system inlet to system exhaust is displayed in Figure 5-32. The following section makes a comparison between the atmospheric conditions which drive the highest (hot) and lowest (ISA) system efficiency.

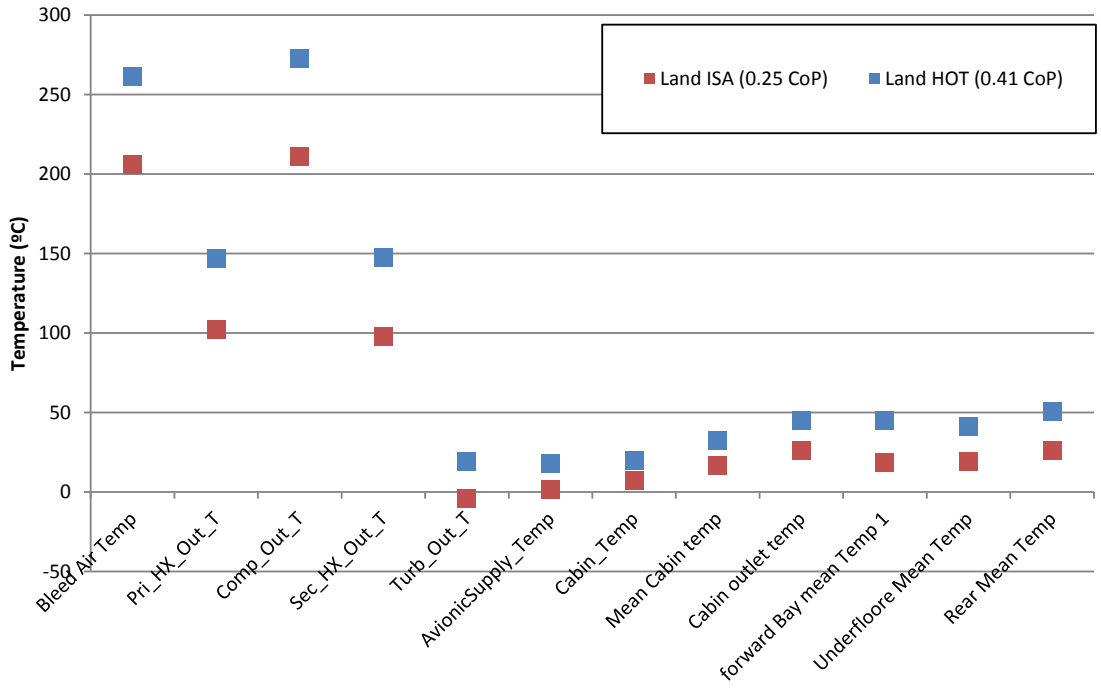

Figure 5-32: Temperature variation through the flow path for a fixed flight condition in three different atmospheres

5.11.1. System Performance

The total energy consumption between the two flight cases remains reasonably constant, with the hot atmosphere consuming 1% more energy as an average across the flight profile. As energy consumption is constant, the system efficiency is purely based on the subsystem heat rejection rate. Assuming all avionic loads are equal, the difference in the cabin and the avionic heat rejection rate is due to kinetic loading. The recovery

temperature of the hot atmosphere is 34ºC hotter, generating a total increase in kinetic loading, and heat rejection rate of 6kW.

5.11.2. Environmental Control System Performance

The energy consumed in the isentropic compression of bleed air is equal in both conditions. The difference between the two flow paths through the ECS subsystem is as a result of ECS bypass mass flow rate. To explain the ECS performance difference, the fundamental performance characteristics of the ECS must be considered to differentiate between these two atmospheric conditions.

If the inlet pressure of a bootstrap ECS increases at a constant temperature, the pressure ratio across the CAU increases, allowing the ECS to reject more heat. The resulting self-regulating system performance is insensitive to inlet pressure, which is a further consideration as to the widespread use of the bootstrap cycle ECS.

When considering an increasing inlet temperature at a fixed pressure, the CAU pressure ratio remains constant, however the air inlet power and heat rejection rate requirement increase. In order to achieve a fixed cabin temperature, the cycle must work harder and the ECS bypass airflow is minimised, which boost the cycle heat rejection rate. The ECS CoF is inversely correlated to the bypass air flow rate. The ECS bypass has two main system effects. Firstly it is a tool to control the CAU shaft speed and the resulting compression and expansion isentropic efficiencies. The second effect is a direct heat addition to a heat rejection cycle, with both processes degrading the thermodynamic cycle performance. The hot atmosphere essentially has a higher utilisation of ECS heat rejection capability and therefore the cycle is not adversely affected by the application of bypass air flow. The increased cycle efficiency results in a lower cabin and equipment supply temperature for a fixed inlet air power input.

The combination of an increased ECS CoP and an increased cabin and avionic heat rejection rate for a fixed air power input result in the increase of this CoP in a hot environment. While the hot atmosphere in general increases the system CoP, this is

achieved by dynamically reducing the system thermal safety factor. The thermal safety factor through a flight profile is variable and can be effectively considered as a measure of the ECS bypass air mass flow rate, as to achieve a complete ECS performance utilisation is to operate the ECS with no bypass flow.

5.11.3. Forward Avionic Bay Performance

The avionic module exhaust temperature safety factor can be measured as the module exhaust temperature difference with the thermal design limit of 71ºC. The closer the avionic module operates to this design limit, the higher the subsystem thermal efficiency is. In this case, the hot environment avionic exhaust temperature is 53ºC in comparison to 30ºC with flight in an ISA atmosphere.

The avionic exhaust temperature for all flight cases in all three atmospheric conditions is detailed in Figure 5-33. While this data is considered at a component level, the data is really a measure of the system-wide performance.

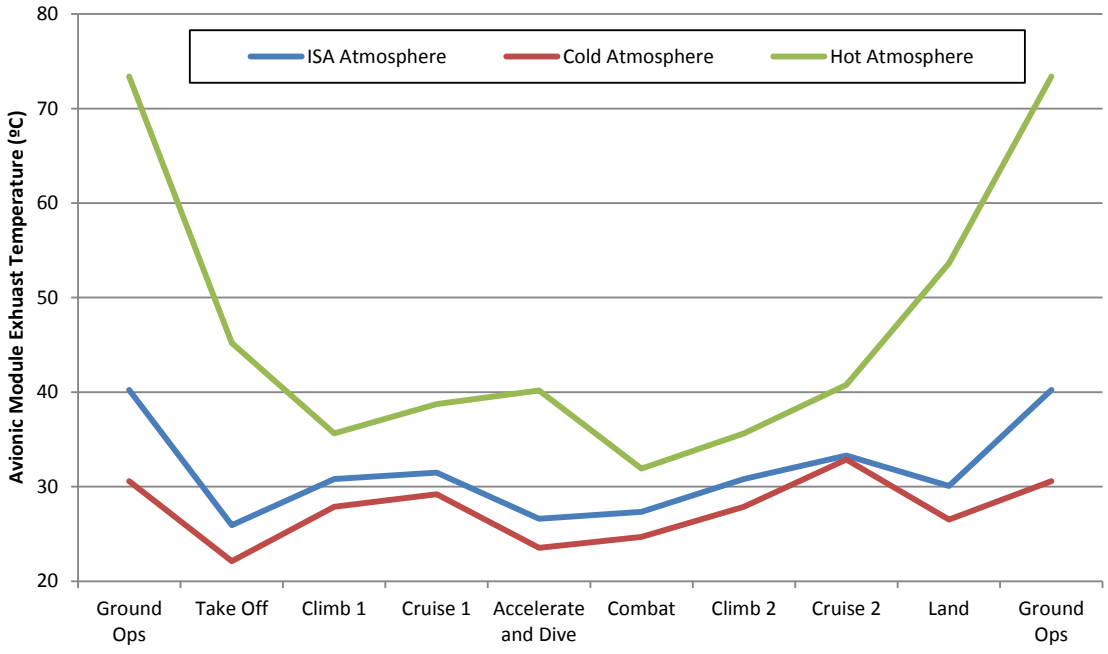

Figure 5-33: Avionic module exhaust temperatures for three atmospheric conditions.

A number of key findings can be taken from Figure 5-33, primarily that the thermal design limit for the avionic module exhaust temperature is calculated to be exceeded by 2ºC

during ground operations in a hot atmosphere. This condition is the worst case scenario for the avionic thermal management system; this is echoed by the cabin temperatures which are also highest at this case.

At ground operations the bleed air and ram air mass flow rates are low due to the low air density resulting from high ambient temperatures, low throttle setting, low ground speed and by the use of the inducers to draw in a cooling flow rate through the heat exchangers. To draw a comparison, the bleed air inlet mass flow rate is under half of an 'accelerate and dive' flight case and the total heat exchanger heat rejection rate is only 18% of the one on the 'accelerate and dive' condition. With both TCUs closed, the ECS cannot reject enough heat energy to meet the equipment supply temperature specification. The equipment supply temperature at ground case is 17ºC, where a temperature of no greater than 4ºC is supplied during the 'accelerate and dive' case.

As discussed previously, the avionic module temperature difference is very sensitive to a reduction in the bleed air flow rate. The combination of the above specification supply temperature, increased module temperature difference and high ambient temperature within the bay lead to an avionic exhaust temperature operating marginally above the design limit. It is understood that some aircraft do utilise additional ground cooling from an independently powered fan using ambient air. However, ground soak in a hot atmosphere remains a difficult condition for the avionic thermal management system as the fan exhaust conditions can be upwards of 50ºC.

It is seen that, as soon as the aircraft gains vehicle speed, the avionic module temperatures fall easily within their design limits. The system features no active control of the airflow distribution and the static design set point is a ground case, hot atmosphere. At all other flight conditions, the heat rejection capability is increased which reduces the avionic exhaust temperature, increasing the thermal safety factor. The resulting performance is a reduction in the ECS CoP and in the system CoP.

5.12. Avionic Temperature Validation

The following avionic module exhaust temperature validation data was provided by BAE Electronic Systems, Rochester who produce the FCC: “The FCC records min and max data between power up and engine spool down. The minimum we have recorded is 5°C and the maximum we have recorded is 65°C. We usually see a 20°C increase between the min and max temperatures recorded per FCC. The average temperature is between 15°C and 35°C”. This information was generated across 11,000 data points; however no information regarding the operational conditions of the aircraft are related to the temperature data. The data shown in Figure 5-33 compares very favourably with the validation statement from BAE Systems. This confirms a number of key performance characteristics and the design process methodologies detailed in Chapter 2, for example the high safety factor that is used on avionic module thermal conditioning.

5.13. Mission-Level Conclusions

The system CoP is primarily based on inlet air input power to the CAU and the heat rejection rate, which remains reasonably constant across the flight profile. As the bleed air inlet power and the ram air pressure drop across the heat exchanger are highest at high load flight cases, the CoP of the system is found to be inversely proportion to the engine load conditions.

The system is most effective when the thermal safety factor is lowest. This is in hot atmospheric and/or low load conditions when the ECS bypass flow rate is low and the avionic module exhaust temperatures are high. While this condition produces the highest CoP, the system has minimal reserve for providing for any additional thermal loading.
The ground operations condition in a hot atmosphere is the worst case scenario, resulting in high avionic and cabin temperatures. While it is understood that the airframe could utilise a ground cart for avionic power and coolant supply, typically this equipment has no cooling function and the inlet air temperature to the avionic units remains above ambient. This condition remains the most difficult one to design the TMS for.

The Hawk ECS system was designed to work on the ground in a hot atmosphere. This limited its ability to operate efficiently across the remainder of the atmospheric and flight envelope. Considerable system gains could be made by introducing an element of active control to reduce the inlet power consumption. This could be achieved through reducing the bleed and ram air consumption when the avionic temperatures are low and ECS bypass flow rate is high.

5.14. Chapter Conclusions

For each section, the publications of the findings have been commented on in the relevant sections. The conclusions of this chapter are related to the evaluation of the analysis and the definition of an optimisation approach based on the information collected.

5.14.1. Multi-Disciplinary Approach

The methodology behind the test facility is to develop high fidelity data which can improve the engineers' visibility of the system performance characteristics with confidence in the output data. A mission-level system analysis has been performed which allowed the understanding of the avionic temperature trends across the complete flight and atmospheric envelope which was a key unknown system behaviour sighted at the start of this project. At the subsystem level, a number of key findings have been identified which validate the approach of this test facility.

Initially, when considering ECS thermodynamic performance with and without the control system, an interesting relationship is identified. It was seen that, if the ECS is treated as a thermodynamic cycle, the increased bleed air pressure leads to an increase in the heat rejection rate. However, when controlling to a fixed cabin and equipment temperature, the same inlet bleed air pressure sweep reduces the system CoP. The control system is robust in terms of its ability to achieve a given exhaust temperature range in a number of cases. A particular performance of this system was highlighted, whereby two similar operating conditions can be achieved through a different control approach. This finding is a key example of an unknown system behaviour that would be introduced operationally which could not be detected by a traditional 1D simulation.

The effect of humidity on a bleed air cycle has been detailed and a number of interesting thermodynamic trade-offs have been identified. The water extraction process is neither well modelled nor well validated in the data supplied by BAE Systems and this investigation has been able to help fill this knowledge gap. The key findings of the humidity investigation have been highlighted previously. However, it should be repeated that these findings could not have been achieved without a high fidelity ground bases test facility.

The FDI analysis detailed two fundamental ECS findings. Firstly, the traditional performance metric and control feedback characteristics can be misleading, which represents a key knowledge development for future ECS design. The reliance on misleading metrics such as the ECS exhaust temperature (regardless of mass flow rate) can generate a situation where a partial ECS failure is only detected if it occurs in downstream subsystems such as in the avionics bay. A partial failure of the ECS can substantially reduce the mass flow rate while the exhaust temperature remains healthy (but this produces a reduction in the cooling capacity). The avionic subsystem can measure a healthy supply temperature but provide an insufficient avionic cooling capacity.

The second finding is that, in this case, the main bleed air cycle weakness is in its control system. The control systems lack of flexibility due to its limited range of input variables causes the systematic degradation of the system performance through the majority of its operating envelope.

5.14.2. Baseline System Performance

The mission-level system analysis provided evidence that the avionic modules either both overcooled or undercooled at different operating points across the flight and atmospheric envelope. The baseline TMS approach can be defined as a static solution to a dynamic problem. The atmospheric conditions provide a constantly moving target for a TMS designed for steady state operations. The static TMS configuration is designed to ensure its reliability at the worst case scenario, with little effort to thermodynamically optimise the TMS for the remaining flight conditions. This is a key driver of the poor thermodynamic

efficiency measured in this investigation. As a result, there is little margin in the system for optimising it at high load cases (hot atmosphere or accelerate and dive) due to the system controls reaching their end stop at these conditions.

The aim of the optimisation is to operate the avionic components closer to their thermal design limit through bleed air minimisation and measure the system level response. The gains from minimising the bleed air mass flow rate are twofold: a reduced net load on the engine is accompanied by a more efficient operation of the ECS and avionic subsystems. The process of bleed air minimisation through a component-led approach is guided by the application of the second law thermodynamics, specifically it involves the minimisation of the entropy generation. By minimising the bleed air mass flow rate to achieve the same heat rejection rate for less input power, the system CoP is increased. This is achieved through the reduction of component-level thermal safety factors based on a high system knowledge developed by the analysis in this chapter. The removal of the knowledge gap allows the system to be configured to operate more optimally as a single airflow path.

While it may seem counter-intuitive to pursue the reduction of the bleed air mass flow rate based on the literature review which indicates increasing heat loads for existing and future aircraft, an optimisation approach based on the 2nd law of thermodynamics is the application of the system. The single airflow path optimisation procedure can be applied to any situation the airframe manufacturer requires. Either the inlet power input can be minimised for a given heat rejection rate (bleed air minimisation), or the heat rejection rate can be maximised for a given inlet power input (thermal load growth capability). The system optimisation path detailed in the following two chapters is based on the minimisation of the bleed air mass flow rate, but the end result could be utilised for either application.

The area of avionic overcooling will be approached by the application of a new temperature control strategy and Variable Pressure Relief and Shut Off Valve (VPRSOV). The control strategy will be used to eliminate all bypass airflow at flight conditions with a low AH. The VPRSOV will be used to limit ECS inlet mass flow based on the thermal

conditions of the avionic module, cabin and avionic bay temperatures. The process is to minimise the bleed air mass flow rate to complete the task of avionic and cabin thermal management.

The use of large bleed air mass flow rate supply settings for thermal management has been proved to be thermodynamically wasteful, therefore the area of avionic undercooling is confronted by the implementation of new thermal management technologies. Utilising the knowledge from system evaluation and the detailed component level analysis from Chapter 5, new technologies are assessed in Chapter 6. The system mission level response to these technologies is detailed in Chapter 7.

6. Component Level Optimisation

The aim of this work is performing a component-led integrative optimisation approach based on the 2nd law of thermodynamics. It has been discussed that the process to system optimisation is a bottom-up approach from the component level conditions. The complete airflow path is considered as a single entity, and it is optimised around delivering component-level thermal conditions. The aim of this chapter is to provide a detailed component level-thermal investigation of new thermal management technologies. These technologies must both satisfy the thermodynamic methodology of the integrative approach, but also fit within the industrial framework discussed in Chapter 2. Each of the three thermal management technologies discussed in this chapter are compact and lightweight and have the potential to remedy some of the shortcomings identified in the TMS in Chapter 5. Considerable time was spent in collaboration with BAE Systems to define suitable technologies to act as a baseline for the application of this new methodology.

This chapter is split into two main sections. The first section covers the definition of component-level thermal management technologies in isolation. The second section covers the application of these technologies at a single flight condition. The optimised

system will be assessed at full mission level in Chapter 7. The system performance characterisation data presented in Chapter 5 detail avionic module exhaust airflow temperatures across a flight profile at three specific atmospheric conditions. It was concluded in Chapter 5 that the present system has room for improvement with respect to reducing avionic under-cooling and avionic over-cooling.

6.1. High Avionic Exhaust Temperature at Ground Cases (Undercooling)

The miniaturisation of electronic components and of the instrumentation in modern military aircraft have generated a substantial increase in the avionic power density. This trend is characterised by a high heat production rate per unit of component area (Jubran et al. 1996). Customer requirements often demand the inclusion of emerging avionic capabilities during an airframe life (Moir & Seabridge 2001). The retrospective fitment of increased power density electronic components generates an increase in the operating temperatures. Continued operational cycling of avionic components above their thermal design limit leads to an exponential decay in the component reliability (Defence 2008).

Figure 5-33 showed that ground operations in a hot atmosphere is the worst case scenario in terms of avionic component temperatures being above their thermal design limits. This design case is the most thermally challenging as the coolant and the working fluid flow rates are low and ambient temperatures are high. As a result, the avionic operating temperatures are found to be 2.8% above the thermal design limit.

6.1.1. Thermal Failure

Operational avionic component failures have been reported by BAE Systems (Pearson & McCoy 2011). Without the ability to measure the avionic component internal temperature distribution, the airframe manufacturer can only assume that any avionic thermal failure is a consequence of insufficient total heat rejection rate. This is often resolved by increasing the coolant mass flow rate at an increased fuel cost for operating the TMS. However, avionic thermal failures can also be attributed to the generation of isolated thermal hotspots within the module. Thermal failures are notoriously difficult to diagnose, often

displaying minimal irreversible damage and hidden by a multitude of NFF failures in avionic equipment.

Figure 6-1 reports measurements from six circuit cards mounted within a ½ Air Transport Rack (ATR) conduction to cold wall module. Specifically, Figure 6-1 shows the minimum, maximum and average component temperature of each circuit card expressed as a percentage of the avionic heat exchanger exhaust air temperature (Maxwell et al. 2010).

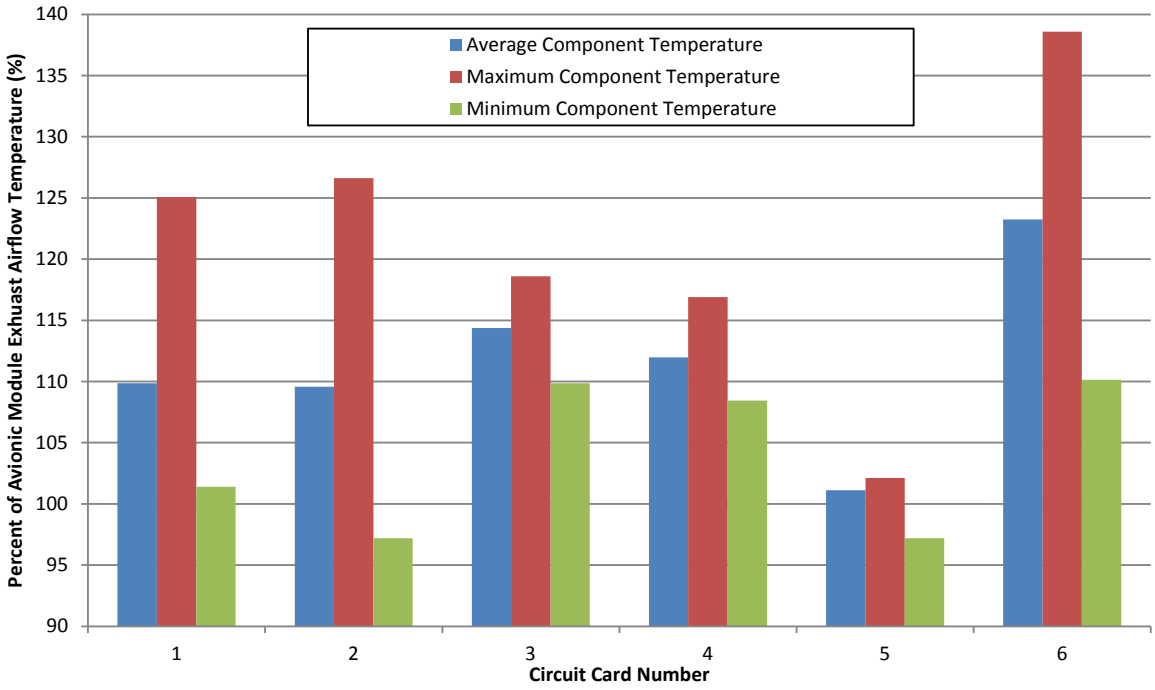

Figure 6-1: Thermal analysis of 6 circuit cards operating within a ½ ATR conduction to cold wall avionic module.

It can be seen that, while circuit cards 3, 4 and 5 display a less than 10% difference between the minimum and the maximum component temperatures, circuit card 6 is reported to be operating up to 38.6% hotter than the avionic exhaust airflow temperature. The generation of a thermal hotspot is the result of a high heat path thermal resistance of the conduction to cold wall architecture and this leads to irregular heat exchanger thermal loading. Even the relatively good thermal conductivity of an aluminium heat exchanger is unable to always ensure an adequate rate of heat transfer by conduction to the cooling air flow. Based on the operational data of Figure 6-1, to provide an adequate cooling capacity for circuit card 6 with a fixed heat exchanger geometry, circuit cards 1-5 would have to be

over-cooled. This is a prime example of the lack of flexibility of the current avionic chassis and heat exchanger design.

The influence from the discussion of Figure 6-1 is that the reliability of an avionic module is probably based on its ability to handle isolated thermal hotspots as opposed to the saturation of its total heat rejection capacity.

6.2. Low Avionic Exhaust Temperature at Flight Cases (Overcooling)

The second area for optimisation for the TMS is its working regime over the remainder of the flight envelope, where the avionic modules are substantially overcooled in all atmospheric conditions. When in-flight, the vehicle air speed provides increased coolant flow and the increased engine load provides a higher working fluid power of the ECS inlet, increasing TMS heat rejection rate capability. As the configuration of the TMS is fixed, the additional heat rejection rate capability tends to over-cool the avionic thermal loads. Over-cooling heat loads generates a reliable TMS of poor thermal efficiency that is typical of 4^{th} generation aircraft. The poor thermal efficiency leads to an increased demand for engine bleed air, which increases the engine fuel consumption rate (Alyanak & Allison 2016). The pneumatic power supplied to the TMS is the dominant consumer of aircraft fuel (after the fuel required for propulsion) and therefore its minimisation is highly desirable (Chakraborty & Mavris 2016).

6.3. Avionic Under-Cooling

The requirement of this section is to provide a solution to the undercooling of avionic modules and reduce the occurrence of isolated thermal hotspots. The avionic module architecture will remain conduction to cold wall and the heat rejection process will remain forced convection. The requirement of a new technology is to efficiently spread thermal energy and increase the effective heat transfer area and the heat exchanger fin utilisation.

6.3.1. Vapour Chamber Heat Spreaders

An alternative approach is the implementation of structurally embedded Vapour Chamber Heat Spreaders (VCHS) within the avionic chassis to act as a baseplate for the integral chassis heat exchanger. A VCHS is effectively a flat plate heat pipe, designed to utilise the efficient heat transportation of a two phase cycle to generate a flat plate of high thermal conductivity. The VCHS is implemented to provide a more uniform temperature distribution across the width of the heat exchanger baseplate. A VCHS schematic diagram is shown in Figure 6-2 (Tsai et al. 2013).

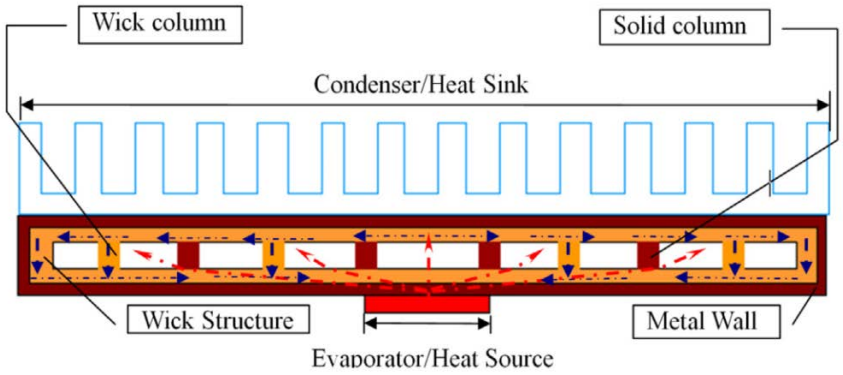

Figure 6-2: Vapour Chamber Heat Spreader schematic diagram

As with heat pipes, a heat source is used to evaporate the working fluid to a vapour, which is transported to a heat sink by an internal pressure gradient. The VCHS internal cavity is lined with a copper duct wick structure to act as high thermal conductivity metallic foam. The heat sink condenses the vapour back to a fluid, which is returned to the heat source through capillary pumping forces of the wick structure to repeat the cycle. The primary function of a VCHS is the efficient transportation of heat energy from a single isolated heat source to a large heat sink. This passive two-phase cooling cycle creates a plate that is ideal for avionic applications.

The capillary pumping forces through the wick allows the cooling cycle operation at negative G conclusions, within limits. This is a critical behaviour for use in fast-jet aircraft and it ensures a constant heat transportation mechanism regardless of transient flight manoeuvres. The sealed unit has no risk of performance degradation through a supply or failure. Most importantly, the implementation of an embedded VCHS within an avionic

chassis offers minimal disruption to the current conduction to cold wall configuration (Reyes et al. 2012; Jaworski 2012; Naphon & Wiriyasart 2012). Numerous VCHS studies have been completed on their thermal performance and optimisation with parameters such as size, shape, fill ratio, material, wick structure, wick material and working fluid medium (Naphon & Wiriyasart 2012; Oshman et al. 2012). The aim of this investigation is to look at the application of this technology into a real world situation rather than the optimisation of the fundamental technology.

6.3.2. Implementation of Vapour Chamber Heat Spreaders

The performance of VCHS for avionic heat rejection is assessed both experimentally (with a bespoke test rig) and numerically (with the use of a thermal resistance network). The experimental rig heat exchanger is based on a genuine avionic module. To facilitate a back-to-back material comparison, interchangeable VCHS and Aluminium plates are inserted in the same test rig. This design requirement forced the design and fabrication of a number of additional material interfaces which are not present with a genuine avionic module and act to further increase the total heat flow path thermal resistance. To combat this, the experimental data will be used to validate a thermal resistance network, which can predict the performance of an aluminium and VCHS avionic chassis with the correct geometry and thermal resistance. Both approaches are used to determine the applicability of VCHS for the conduction to cold wall cooling of an avionic module and assess the potential performance improvement in avionic heat exchanger efficiency.

6.3.3. Experimental Test Setup

A sample VCHS (H,W,D: 122mm,87mm,3mm) has been supplied by Channing Tsai at the Taiwan Nuclear Research Facility for this investigation and an equally sized aluminium plate has been machined, allowing the materials to be directly interchangeable. The VCHS plates are a pressed copper housing with a sintered copper dust wick structure. The fill ratio is one third and the working fluid is distilled water.

A bespoke test plate has been designed for the purpose of quantifying the heat transfer efficiency of the two materials; a schematic can be seen in Figure 6-3. The geometry and

fin design of the test plate has been matched exactly to a FCC avionic module heat exchanger, with the exception of an increased thickness of 3mm to the top plate to allow the implementation of the two test plates.

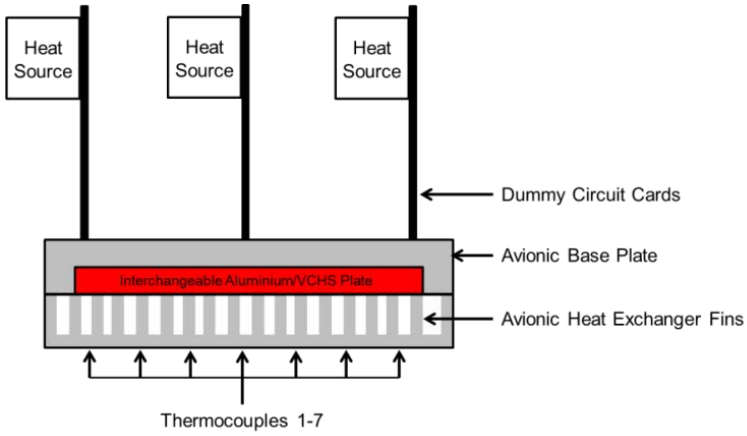

Figure 6-3: Experimental rig schematic diagram

Typically, a chassis of this size would exhibit a power output of 60W to 140W depending on application, with a corresponding cooling air flow mass flow rate of 15kg/hr to 35kg/hr at a heat exchange inlet temperature of 15ºC to 20ºC.

A cooling air mass flow rate is supplied at ambient laboratory temperature from an air fan with integrated smooth bell mouth inlet and venturi. The bell mouth inlet and venturi are used to ensure a measured and calibrated mass flow is supplied to the avionic chassis. The mass flow rate is calculated by measuring the pressure difference between the fan inlet throat and the ambient air, assuming no losses across the smooth bell mouth intake.

In order to replicate the conduction to cold wall cooling process, heating elements are thermally coupled to the circuit card which is mounted against the chassis cold wall. The rig allows a number of circuit cards to be used, with a comparison being made across three cards in this investigation. The heater power output is controlled by a variable desktop power supply. All data acquisition channels are calibrated previous to testing. Temperature readings are taken with both individual thermocouples and a manufacturer calibrated thermal camera (Anon 2016). Thermocouples are used to measure the inlet airflow temperature, the component temperature, and exhaust airflow temperature at seven locations equally spaced across the width of the heat exchanger.

6.3.4. Thermal Resistance Network

A thermal resistance network is used to predict the avionic module chassis thermal performance of a geometrically correct aluminium and VCHS chassis. The first requirement is to establish the thermal conductivity of both materials; this data is collected experimentally with a thermal camera. Both materials are subjected to a heat source of variable power, with an area of 0.00075m² and the plates are suspended within the ambient laboratory environment. The stabilised temperature of each plate is measured to determine the thermal conductivity. A back-to-back comparison of a 30W thermal load is shown in Figure 6-4.

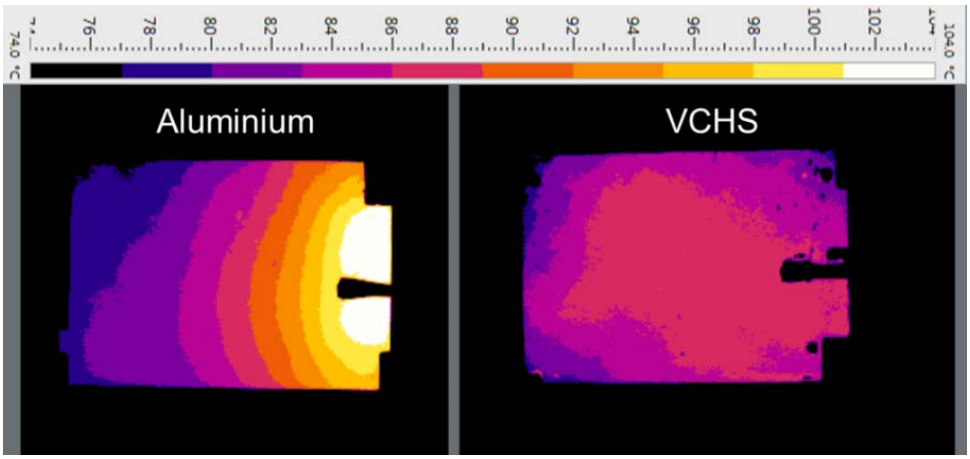

Figure 6-4: Thermal image of a VCHS and Aluminium plates. The measured thermal conductivity from this test shows the VCHS plate at 1481W/mK and the Aluminium plate at 206W/mK.

The temperature distribution shown in Figure 6-4 (left) indicates that the aluminium plate has a lower thermal conductivity, since a clearly defined localised hotspot is present around the heat source. The material temperature reduces monotonically away from this point, along the length of the plate. The VCHS presents a more uniform temperature distribution, characterised by a lower maximum temperature and a higher minimum temperature than the aluminium plate. The measured thermal conductivity of both plates across a range thermal loading is detailed in Figure 6-5. It is seen that, as the power output increases, the thermal conductivity of the aluminium plate remains constant while the thermal conductivity of the VCHS plate increases progressively to a maximum of 7876W/mK.

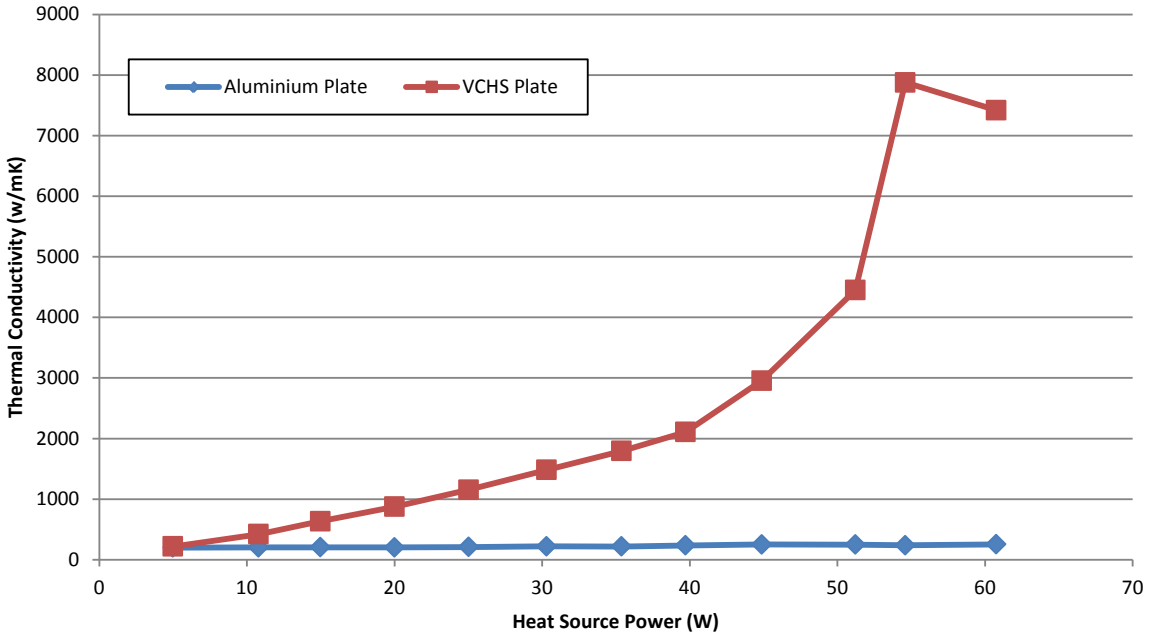

Figure 6-5: Measured thermal conductivity of Aluminium and VCHS plates

The thermal conductivity of a VCHS is dependent on the power applied to it; the greater is the power, the higher is the evaporator temperature. This increases the rate of the working fluid phase change and the internal pressure gradient. The resulting increase of vapour flow rate within the VCHS increases the rate of thermal transportation and therefore the thermal conductivity. As the power continues to increase, the thermal conductivity increases until the VCHS reaches a physical limitation such as the sonic, boiling, entrainment or capillary limit. The test in Figure 6-5 details a plate which is believed to have reached its capillary limit at 63Watts, corresponding to an evaporator temperature of 115ºC. At this point, the input heat flux limit is surpassed and vaporisation at the evaporator exceeds the rate at which fluid can return from the condenser. The working fluid is not available at the evaporator to absorb further thermal energy and the evaporator dries out. It is seen from this data that this VCHS plate will safely operate with a thermal conductivity of 5000W/mK which is over 24 times that of aluminium. The measured thermal conductivity of the VCHS in response to a given heat flux is utilised in the model based on the temperature difference between the evaporator and condenser.

The thermal resistance network schematic for a single circuit card can be seen in Figure 6-7. The following section details the governing equations. The temperature difference, ΔT,

across a heat transfer process is defined as the product of the rate of heat transfer,$\dot{Q}$, and thermal resistance, R, of that process.

$$\Delta T = \dot{Q}R \tag{6-1}$$

The thermal resistance is dependent on the type of heat transfer; conduction, convection or radiation. The thermal resistance of a radiative heat transfer process, R_{Rad}, is based on the radiative heat transfer coefficient, h_{rad}, and the surface area of heat transfer, A_s.

$$R_{rad} = \frac{1}{h_{rad}\ A_s} \tag{6-2}$$

Where the radiative heat transfer coefficient is the product of the emissivity coefficient, ε, the Stefan-Boltzmann constant, σ, the heat transfer area, A_s, and a function of the temperature differenc between the heat transfer surface, T_s, and the surroundings, T_{surr}.

$$h_{rad} = \varepsilon\,\sigma\,A\left({T_s}^2 + {T_{surr}}^2\right)(T_s + T_{surr}) \tag{6-3}$$

A conductive resistance, R_{cond}, is defined as the length of the heat conduction, L, divided by the product of the material thermal conductivity, K, and the area across which the heat is travelling through, A.

$$R_{Cond} = \frac{L}{K\,A} \tag{6-4}$$

The avionic chassis heat flow path features a number of material interfaces which obstruct the heat transfer, such as the circuit card to avionic chassis. The contact interface of two materials can be modelled as the summation of the contact and gap conductance. The total joint conductance is a function of the surface roughness, the material hardness, the clamping pressure and of the thermal conductivities of materials and of the material voids (air). A thermal paste is used as a Thermal Interface Material (TIM) to increase total joint thermal conductance and to improve the estimation of the contact thermal resistance. Assuming the paste behaves like a liquid and fills all air gaps between the two materials, the thermal conductivity of the paste can be substituted in the gap conductance relationship. The distance between the two materials is assumed to be the surface finish for a milled section of aluminium (Teertstra et al. 1997).

A convective thermal resistance, R_{Conv}, is based on the convective heat transfer coefficient, h_{conv}, and the convection surface area.

$$R_{Conv} = \frac{1}{h_{conv}\, A_s} \tag{6-5}$$

Where the convective heat transfer coefficient, h_{conv}, is defined as the product of the Nusselt number, N_u, and material thermal conductivity divided by the length of heat exchange area (fin, channel), L.

$$h_{conv} = \frac{N_u\, k}{L} \tag{6-6}$$

The Nusselt number is a non-dimensional ratio of the convective heat transfer to conductive heat transfer across a boundary. The Nusselt number can be approximated by the Dittus-Boelter equation for turbulent airflows. The approximation for heating of a fluid is defined as a function of Reynolds number, R_e, and of the Prandtl number, P_r:

$$N_u = 0.0023 {R_e}^{4/5} {P_r}^{0.4} \tag{6-7}$$

where the Reynolds number is a non-dimensional characterisation of flow behaviour and can be defined as the product of the fluid density, ρ, velocity, u, and channel length divided by the fluid dynamic viscosity, μ. The Prandtl number is a non-dimensional ratio of the momentum diffusivity of a fluid to its thermal diffusivity and can be defined as the is the product of the fluid viscosity and specific heat capacity, C_p, divided by the thermal conductivity, k.

$$R_e = \frac{\rho\, u\, L}{\mu} \tag{6-8}$$

$$P_r = \frac{\mu\, C_p}{K} \tag{6-9}$$

As the mass flow rate throughout the test is variable, from 15kg/hr to 35kg/hr, and assuming an even distribution of air flow across the 17 heat exchanger fins, channel airflow velocity ranges from 8m/s to 23m/s. The channel flow condition ranges from the upper transitional to the fully developed turbulent flow and therefore some inaccuracy is expected from the Dittus-Boelter approximation of Nusselt number; leading to an over-estimated convective heat transfer coefficient. The initial network is set to replicate the

experimental conditions and a measured convective heat transfer coefficient is determined as the plate heat rejection rate, $\dot{Q}$, divided by the product of the channel area, A, and temperature difference between the surface temperature, T_s, and airflow free stream temperature, T_∞. The measured convective heat transfer coefficient is used to generate a correction factor which is applied to the calculated convective heat transfer coefficient.

$$h_{exp} = \frac{\dot{Q}}{A\,(T_s - T_\infty)} \tag{6-10}$$

The module exhaust temperature is averaged from the seven localised temperature readings and the plate heat rejection rate is calculated as the product of the channel mass flow rate, $\dot{m}$, the specific heat capacity of the fluid, C_p, and the temperature difference of airflow at inlet, T_{in}, and the exhaust, T_{ex}.

$$\dot{Q} = \dot{m}\ C_p(T_{ex} - T_{in}) \tag{6-11}$$

The avionic module heat flow path is essentially an amalgamation of the thermal resistances detailed above. Depending on the configuration, some heat transfer is considered to be simultaneous (in which case thermal resistances are in parallel) and some heat transfer is considered to be consecutive (in which case thermal resistances are in series). When calculating the rate of heat transfer through thermal resistances in series, as with electrical resistances, the total resistance, R_{total}, is the sum of the individual resistances, i.e. R_x. When calculating the rate of heat transfer through thermal resistances in parallel, the total resistance is computed as

$$\frac{1}{R_{Total}} = \sum_{i=1}^{n} \frac{1}{Ri} \tag{6-12}$$

The thermal network calculates seven exhaust air temperatures which correspond to the location of the seven thermocouples of the experimental set up. This allows the interrogation of localised and averaged plate heat transfer conditions to define the state of plate isothermalisation. Once the network is validated against experimental data, the calculations are adapted to predict the system energy flow for a geometrically correct module. The network is then adapted for multiple heat sources to more accurately replicate the conditions of the genuine component. Additional heat sources are replicated

by the duplication of T1 through T6 for each heat source location. The ability to simulate unequal thermal loading across the avionic base plate allows the replication of the real life conditions displayed in Figure 6-7.

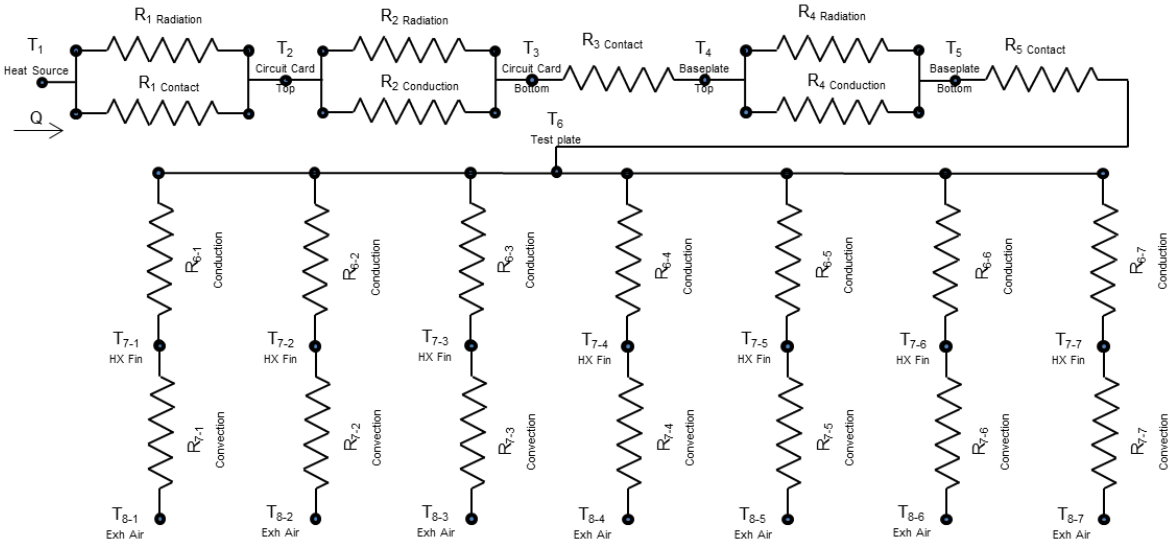

Figure 6-6: Single heat source thermal resistance network of schematic diagram shown in Figure 6-3

6.3.5. Experimental Comparison

Initially, both avionic chassis are tested with a single circuit card mounted at the extremity of the base plate in the orientation of the cooling airflow. The small heat transfer area generated by a single card replicates a significant thermal hotspot. Figure 6-7 demonstrates the reduction in airflow temperature with increasing distance from the heat source for both aluminium and VCHS. The local temperature data is presented as a percentage of the maximum airflow temperature at various mass flow rates for a single heat source. The VCHS base plate clearly demonstrates a more uniform temperature distribution across the width of the avionic base plate. It is also seen that, by increasing the mass flow rate, the range of temperature distribution becomes greater.

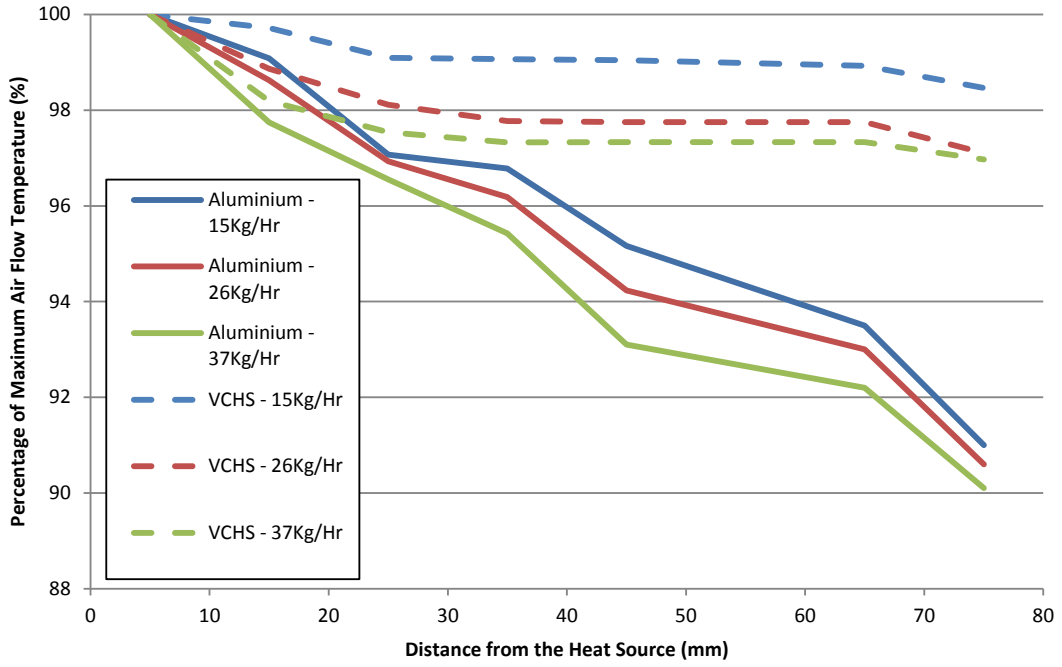

Figure 6-7: Localised temperatures presented as a percentage of the maximum recorded temperature for both materials.

The improved thermal conductivity of the VCHS base plate is directly responsible for the reduction in the component temperature across all comparative mass flow rates and thermal loads, as seen in Figure 6-8. It can be seen that the avionic exhaust temperature asymptotes to a constant value with increasing mass flow rate. As a result, a small temperature reduction equates to a large mass flow rate reduction at large mass flow rate settings. For example, when considering a fixed component temperature of 55ºC, a mass flow of 37.2kg/hr is required for an aluminium plate. To maintain the component temperature at 55ºC, a comparative lower 14.2kg/hr is required for the VCHS, equating to a mass flow rate reduction of over 65%. The reduction in mass flow rate for a fixed component temperature is as a result of a decrease in the conduction thermal resistance.

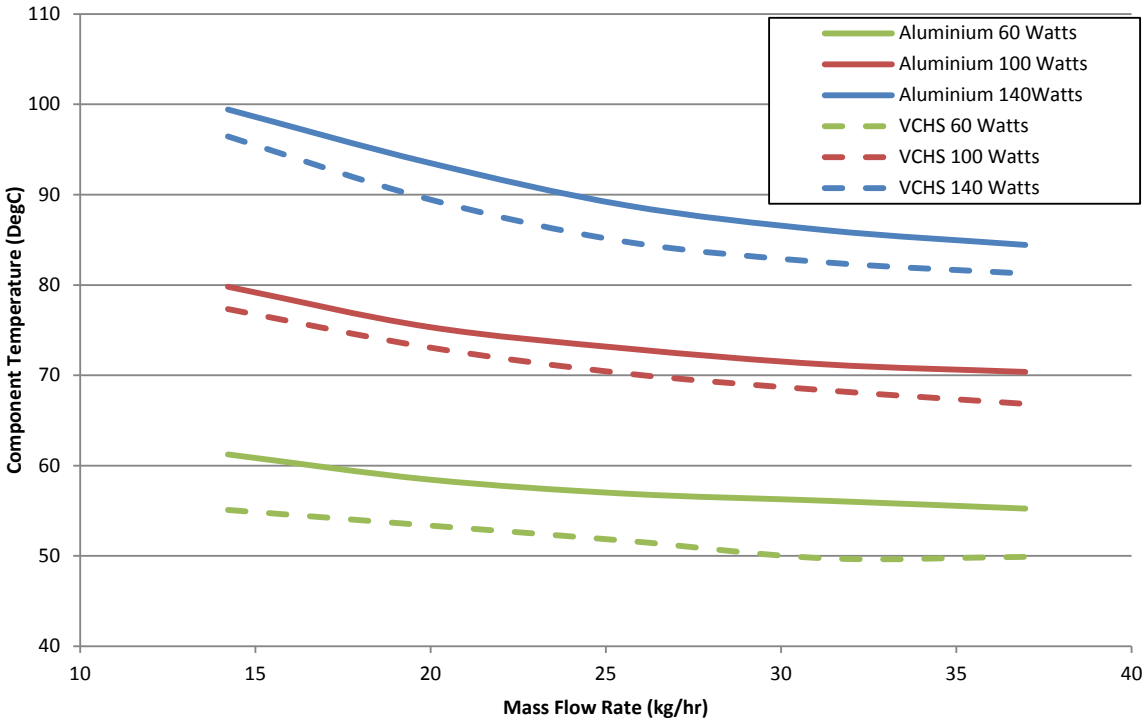

Figure 6-8: Component temperatures for both materials in relation to a mass flow rate sweep.

The increased mass flow rate for diminishing returns echoes previous findings. Figure 6-8 quantifies how attempting to thermally condition a single isolated hotspot with increased mass flow rate can be detrimental to TMS and aircraft fuel efficiency.

6.3.6. Thermal Network Validation

The thermal network and experimental data are compared in Figure 6-9. This figure displays temperature readings from four separate airflow locations with two different heat sources applied to both materials across a range of five mass flow rates to test the fidelity of the model. The correlation between the measured and modelled temperatures is within 8% across all conditions tested. The model validation provides an accurate measure of the Nusselt number correlation with experimental data across the upper transitional turbulent airflow conditions. As discussed, the limitation of the experimental testing is the ability to compare the two materials back-to-back in a geometrically correct environment. The experimental data is therefore only utilised for model calibration and validation and the remaining results are outputs of the thermal network model.

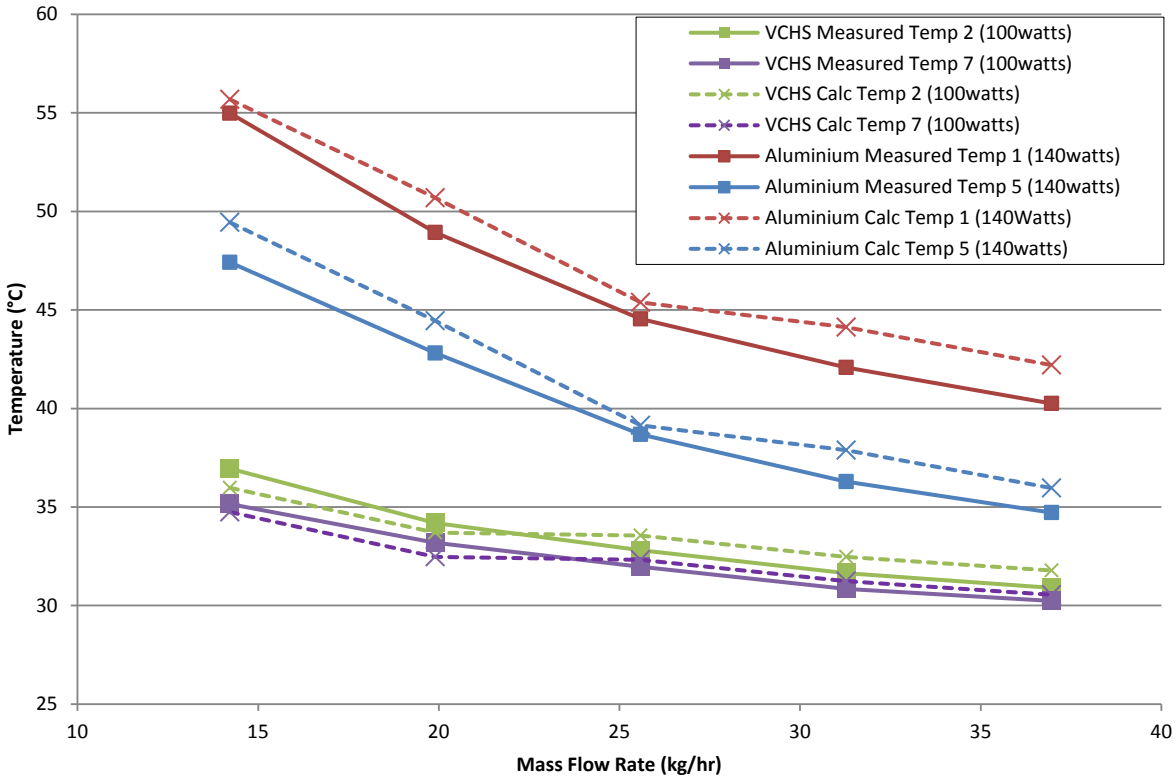

Figure 6-9: Experimental and simulated airflow temperatures for each material across a range of mass flow rates and power outputs.

6.3.7. Equal Heat Source Loading

Initially, three equal temperature heat sources located at an equal distance from each other are considered, as shown in Figure 6-10. When considering an analysis of the avionic module with multiple heat sources of equal temperature, the flow path of thermal transportation is short. As the heat transportation lengths are short, the aluminium chassis is able to effectively utilise the majority of the heat exchanger area and the benefit of a high thermal conductivity VCHS reduces. The majority of the conductive thermal resistance is generated through the avionic circuit card (aluminium) and by material contact resistances 'upstream' of the avionic chassis. As each heat source has the same temperature means that no thermal hotspot is simulated in this case. The result is a uniform distribution of a lower peak temperature, which reduces the temperature difference across the VCHS and therefore the VCHS plate equivalent thermal conductivity, according to Figure 6-5. The thermocouple number relates to the location of the thermocouples; T1 on the left hand side of the heat exchanger and equally spaced across the width to T7.

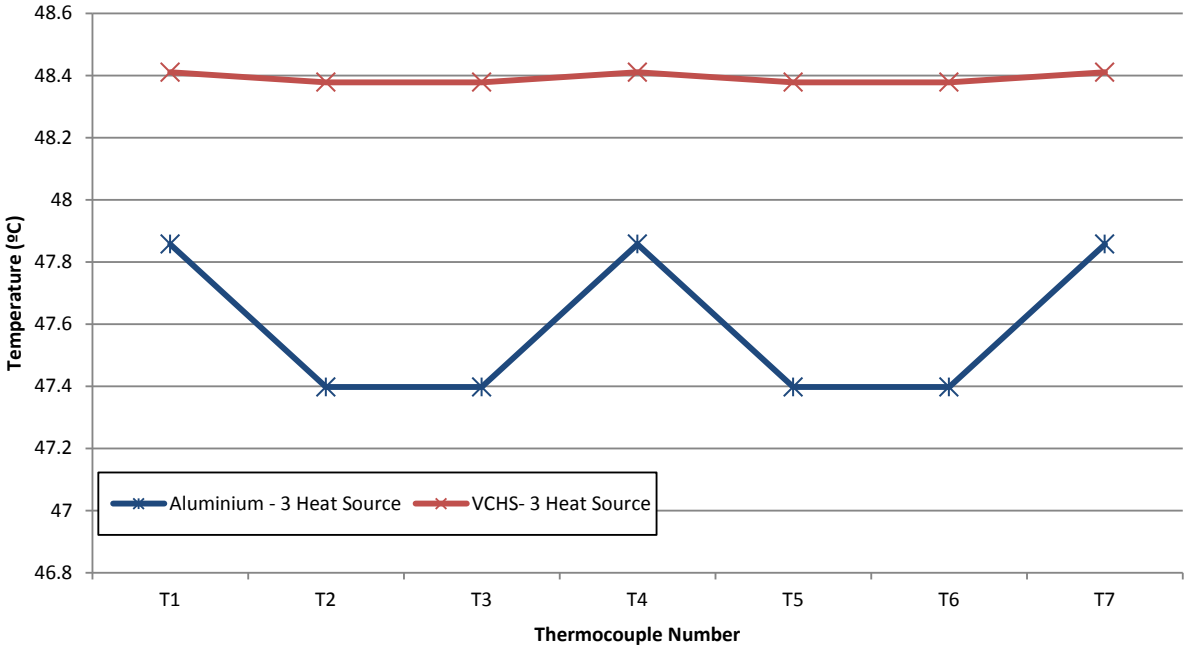

Figure 6-10: Equal thermal loading exhaust air temperature comparison.

It is seen in Figure 6-10 that the exhaust airflow temperatures are higher for the VCHS plate, albeit within 2%. The higher the surface temperature in this case shows a smaller temperature difference between the heat source and the coolant due to the reduction of the thermal resistance. When considering this thermal loading configuration, the performance benefit of VCHS is small, in agreement with experimental data presented previously (Jones & Chen 2015). As the total thermal resistance is very similar across both materials, the avionic growth capacity is small. When considering a total of 140W spread evenly across three circuit cards, an avionic growth capacity of 4% - 15% was found, depending on the air mass flow rate.

6.3.8. Unequal Heat Source Loading

The operational avionic module data presented in Figure 6-1 suggests that in fact the heat source thermal loading is not equal. The temperature difference from the average circuit card temperature to the hottest circuit card temperature was found to be as high as 13ºC. These thermal loading conditions have been replicated for a more representative comparison of the two materials and the results can be seen in Figure 6-11. The power output of circuit cards 2 and 3 are equal, with the power output of circuit card 1 set to achieve a component temperature 13ºC higher than the average of 2 and 3. The high temperature circuit card is located at one side of the avionic chassis as shown in Figure

6-11. It can be seen that the peak circuit card temperatures at the interface between each the heat exchanger chassis are at the location of the highest thermal loading for both materials. The circuit card temperatures of the VCHS present a much smaller thermal variation across the width of the module. The peak temperature is substantially reduced as the thermal energy is efficiently spread across the heat exchanger base plate, increasing the effective heat transfer area and improving the averaged heat rejection capability of each airflow channel.

The VCHS essentially acts as a thermal buffer between the circuit cards and the forced convection airflow. The function of a thermal buffer at the component thermal interface is highly desirable when considering its implementation within an airframe. The insensitivity of the VCHS to irregular thermal loading allows the equipment supplier to couple heat loads as required and the airframe integrator to operate on the basis of cooling an isothermal heat exchanger. IPR regarding the internal architecture of the module is not required for designing an effective avionic cooling air wall and the resulting avionic heat load can be more accurately integrated into the TMS.

It is considered that, as the intensity of the thermal loading at circuit card 1 is increased, the VCHS would be expected to continue to speculation to passively increase the thermal conductivity of the plate. The ability to better match heat rejection capability (through improved heat exchanger fin utilisation) and heat rejection demand is a highly desirable behaviour. This was previously defined as a requirement for improving the TMS efficiency and as a tool to accommodate future avionic growth demands (Jones et al. 2016).

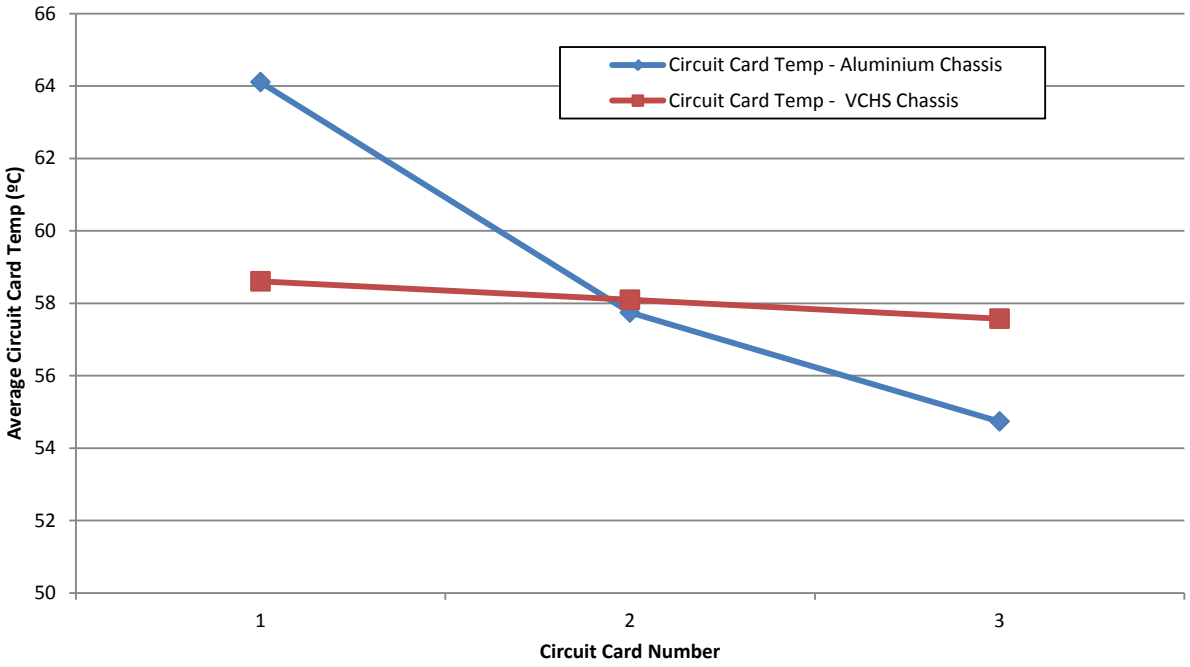

Figure 6-11: Component temperatures with thermal loading conditions to replicate real conditions.

When considering the avionic growth capacity, Figure 6-12 displays the avionic module exhaust temperatures for two thermal loading conditions.

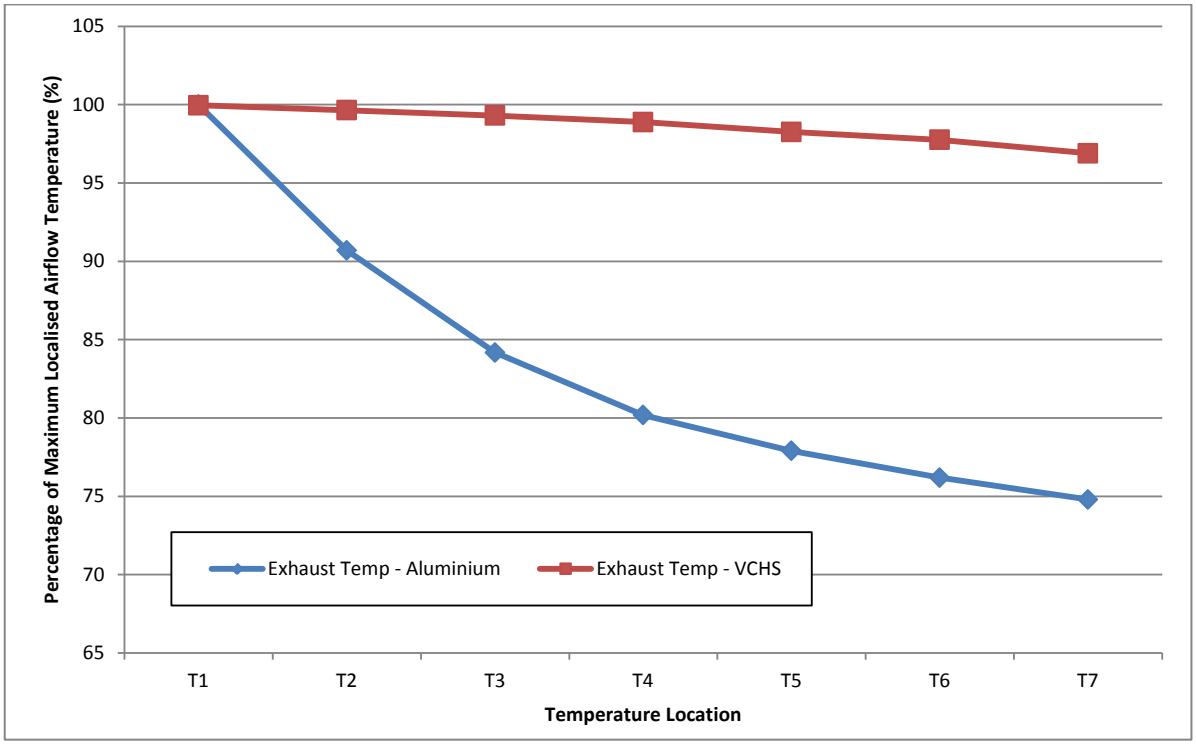

Figure 6-12: Module exhaust airflow as percentage of maximum localised temperature.

The results are presented as a percentage of the localised temperature against the maximum recorded exhaust temperature. The temperature distribution of the aluminium chassis is consistent with the results seen in Figure 6-11, while the VCHS chassis temperature distribution is more uniform, featuring higher exhaust temperatures that are almost equal to the temperature at the location of the hottest circuit and Temperature 1. The inlet mass flow rate and its temperature are kept constant. Also, circuit cards 2 and 3 are kept at a constant power output, with circuit card 1 replicating a hotspot. It was found that the VCHS module is able to accept 58% more thermal energy than the aluminium module in this test case. At this elevated thermal load, the airflow temperature variation with the VCHS module is 3% across the heat exchanger, compared to a 25% variation with the aluminium plate. The ability to provide an isothermal heat exchanger increases the effectiveness of forced convection cooling and fin utilisation, allowing the chassis to fully exploit the coolant heat removal capacity. The ability to efficiently spread thermal energy and vary the thermal conductivity of the plate based on the evaporator temperature allows the VCHS to be insensitive to thermal loading conditions and circuit card architecture within limits. The key advantage to this behaviour is the ability to better cope with uneven circuit card temperatures and to better specify coolant mass flow rate just based on the avionic (electric) power consumption. The reduction of thermal hotspots is a further factor allowing a better integration of avionic heat loads into the TMS, towards improving the system CoP and the component reliability.

6.3.9. Vapour Chamber Heat Spreader Conclusions

Considerable performance benefits are delivered from the implementation of VCHS in avionic module cooling. The improvement in heat exchanger isothermalisation increases the effective heat transfer area and therefore the heat rejection rate capability. The insensitivity of VCHS to heat source geometry, power output and mass flow rate allows it to act as an effective technology for thermal interface management between the heat source and air cooling cycle. The VCHS module allows the airframe manufacturer to better integrate the avionic subsystem, without requiring detailed IPR-protected knowledge of the avionic circuit card power distribution. It is considered that the improvement in

subsystem integration to the wider thermal management system and the combined reliability improvement would be the primary strength of this technology.

The improved isothermalisation of the VCHS chassis can reduce the range of the circuit card temperatures. The ability of all circuit cards to operate closer to an average temperature reduces the generation of isolated thermal hotspots and improves the plate-averaged heat rejection rate. Reliability improvements are not specifically quantified in this study but are assumed to be the result of adopting this technology. This is because the thermal failure of an avionic module through the total saturation of its heat removal capacity occurs at a much greater thermal loading than that required for the generation of a single hotspot. The improvement in the heat exchange thermal efficiency from the increased heat exchanger fin utilisation allows either a reduction in mass flow rate or an increase in the avionic heat removal rate, which provides avionic growth capability.

The final performance advantage of VCHS is the ability to passively control its thermal conductivity (and subsequently heat exchanger performance) with increasing thermal loading, within limits. This improves the ability to handle irregular and unknown circuit card power outputs; such as those found in genuine avionic modules.

6.4. Avionic Over-Cooling

The areas of avionic over-cooling are optimised by reducing the bleed air inlet power to provide the same TMS heat rejection rate by increasing avionic exhaust temperature. This is achieved through two main approaches to prevent avionic over-cooling; by the implementation of a VPRSOV to regulate the inlet energy based on the avionic airflow temperatures and by improvement of ECS bypass mass flow rate control.

6.5. Variable Pressure Relief and Shut off Valve (VPRSOV)

A Variable Pressure Relief Shut-Off Valve (VPRSOV) is used to regulate the TMS inlet power and its cooling capacity, based on a temperature feedback from the avionic module exhaust airflow. The TMS currently has a fixed Pressure Relief and Shut-Off Valve at the ECS inlet for downstream component protection, de-coupling of dynamic TMS flow conditions from the propulsion system and to shut down the ECS when required. The

VPRSOV will replace the fixed PRSOV (location seen in Figure 2-8) and regulate the TMS inlet pressure based on temperature feedback control from the avionic module exhaust temperature, with the target module exhaust temperature set at 65ºC.

For all of the ground cases in Table 4-2, the Auxiliary Power Unit (APU) provides the pneumatic power to drive the aircraft cooling cycle. The APU airflow pressure is below the operating range of the standard PRSOV and therefore no pressure reduction is applied. The VPRSOV would behave in the same manner and can be considered fully open at the ground cases of Table 4-2. The system inlet conditions are therefore a direct function of the APU performance and not actively controlled. The inducer flow rate is also taken from the APU and is tapped upstream of the VPRSOV. It is assumed that the inducer flow rate remains unchanged. The VPRSOV cannot generate an increased bleed air flow over the baseline system (to target existing areas of undercooling) and therefore it is complementary to the implementation of VCHS technology.

The optimisation is considered component-led, as the thermal conditions at the component level drive the total system inlet energy. The VPRSOV controls the avionic module exhaust temperature to 65ºC. The baseline bleed air flow rate is considered as the flow rate provided by the fixed PRSOV as presented in the characterisation study (Jones et al. 2016).

6.5.1. Single Flight Case Analysis

The system response to the VPRSOV and updated temperature schedule are presented separately for the same cruise flight condition on an ISA day. The inclusion of the VCHS technology and its application to the complete mission-level is detailed in Chapter 7.

The flight and atmospheric characteristics of the ‘Cruise 2’ flight case are detailed in Table 5-1. The aircraft operates at a cruise conditions (cruise 1 and cruise 2) for 55% of the total flight profile, providing a good basis for this analysis. Initially, the VPRSOV is considered and then the updated temperature schedule is detailed.

6.5.2. Variable Pressure Relief Shut off Valve

The airflow temperature distribution throughout the system as predicted are reported in Figure 6-13, together with the high and low temperature limits of the cabin and avionic environments. The heat addition and rejection rates of each component along the airflow path is reported in Figure 6-14. The combination of both figures is used to analyse system performance. These figures are detailed from system simulations.

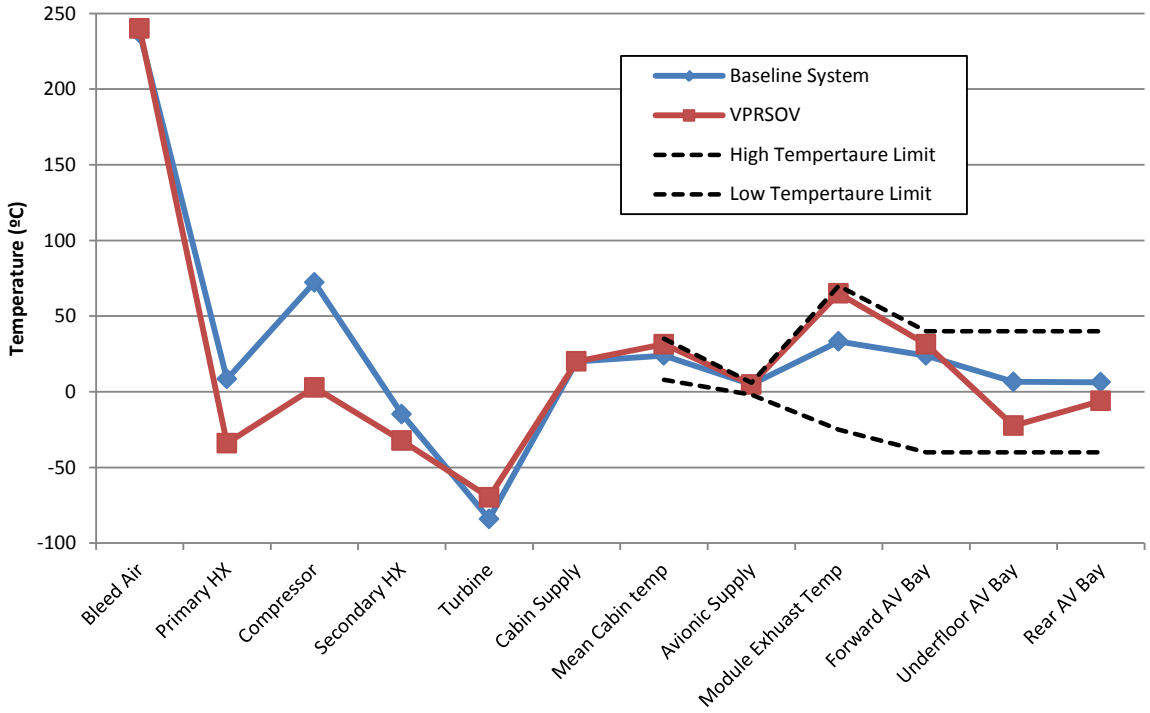

Figure 6-13: Airflow path temperatures for the baseline and VPRSOV systems at a cruise condition (International Standard Atmosphere conditions).

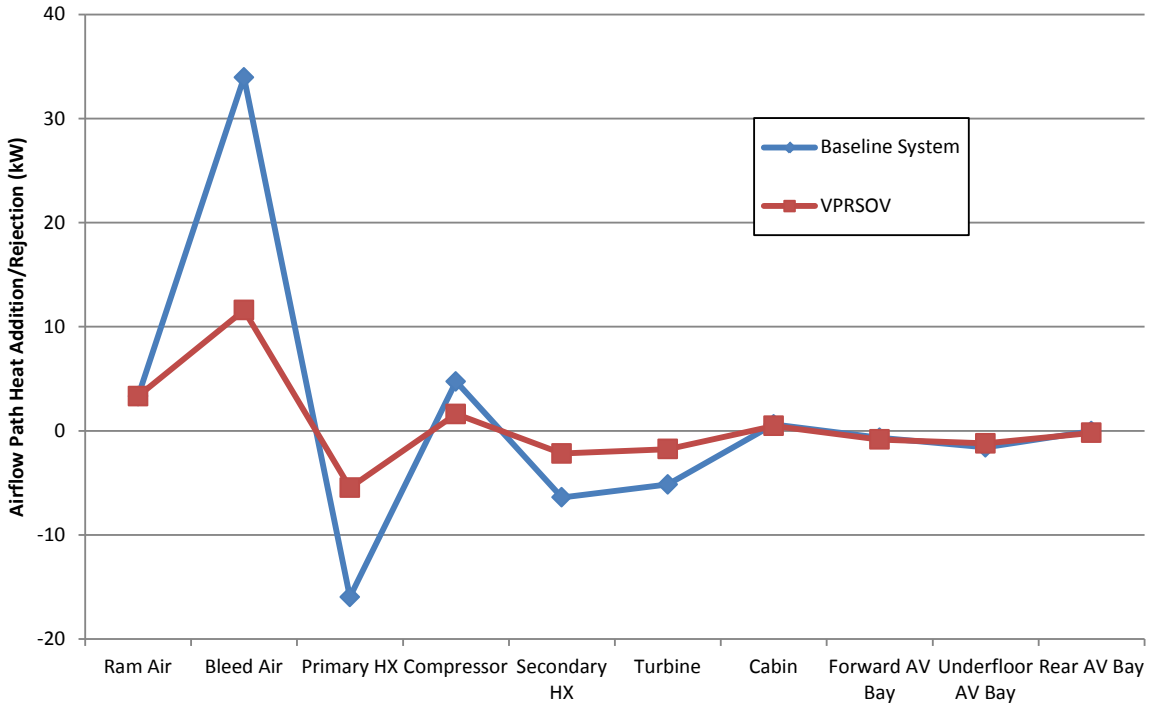

Figure 6-14: Airflow path heat addition/rejection rate for the baseline and optimised systems at a cruise condition (International Standard Atmosphere conditions).

The data of Figure 6-13 and Figure 6-14 clearly detail that the increased operating temperatures of the cabin and of the avionic subsystem reduce the magnitude of the heat addition rate and of the heat rejection rate across the complete airflow path. While a measure of irreversibility is not quantified in this section, the energy flow data of Figure 6-14 visibly details the more efficient thermodynamic process of the system fitted with the VPRSOV.

The low ambient temperatures of the cruise condition generate a negative kinetic thermal loading through the aircraft skin, reducing the reliance on the TMS to absorb thermal loads. For example, a recovery temperature of -35°C is seen for an ISA day at Mach 0.7 and 40 kft. As the required cooling capacity is balanced against the external heat rejection rate, at this flight condition, the TMS flow rate is reduced from 0.14 kg/s to 0.048 kg/s.

When considering the TMS CoP, the ECS system equipped with the VPRSOV is predicted to have a CoP of 0.805 in comparison to the baseline system of 0.392. This means that the system uses half of the air inlet power to provide the same heat rejection rate. The heat rejection rate of both systems remains relatively constant (all thermal conditions remain

within specification), however the air inlet power required to drive the system is reduced by half.

The following 7 sections detail the component and subsystem performance across the airflow path. It should be noted that all component efficiency maps discussed in the analysis (heat exchanger, compressor, turbine etc.) are provided by BAE Systems equipment suppliers from the experimental assessment of the specific components.

6.5.2.1. Ram Air

The consumption of aircraft fuel to overcome the aerodynamic drag of the ram air heat exchangers remains constant for both conditions, as this airflow path remains unmodified. At the high altitude (low ambient air density) and at low speed cruise condition, the ram air pressure drop is low and the ram air path energy consumption rate is small.

6.5.2.2. Bleed Air

The VPRSOV is located at the ECS inlet and regulates the system heat rejection by controlling the downstream pressure and by the mass flow rate. The temperature of the airflow remains the same, while the downstream pressure and therefore the mass flow rate is reduced. The input bleed air power calculation is based on the idealised isentropic compression process of ambient air to the downstream VPRSOV conditions. The ability to reduce the heat rejection rate demand on the ECS based on the fuselage negative kinetic heat load allows a reduction in the bleed air input power from 34 kW to 12 kW.

6.5.2.3. Primary Heat Exchanger

Both systems have the same temperature difference between the inlet coolant (ram air) and the inlet charge air (bleed air) streams. However, as the VPRSOV system regulates the flow to around one third of the flow rate with the PRSOV, the mean temperature difference across the heat exchanger is increased. Through consultation of the heat exchanger performance maps, the reduction of a charge flow rate at a fixed coolant flow rate increases the charge air temperature ratio of the heat exchanger core. The charge air temperatures ratio difference increases from 0.70 to 0.88 due to the increased heat exchanger contact time with the lower velocity airflow in the hot channel. At these

conditions the heat exchanger has a higher effectiveness. The operational performance of this component has been optimised without the requirement for any modification at this location which is a key output of the integrative approach.

6.5.2.4. Cold Air Unit

The calculation of the compressor pressure ratio and of the flow factor allows the use of empirical compressor maps to determine compressor efficiency. It is found that the VPRSOV reduces the compressor inlet temperature, the mass flow rate, the pressure ratio and the compression process isentropic efficiency. The result can be seen in Figure 6-13 and Figure 6-14 that report a reduced compressor heat addition rate and temperature difference between the compressor outlet and inlet. The reduced airflow temperature at secondary heat exchanger inlet reduces the charge and coolant temperature difference. While the temperature difference ratio of the secondary heat exchanger is improved with the installation of VPRSOV system due to the reduced charge air flow rate, the reduction in coolant/charge temperature difference is dominant. The result is a reduction in the secondary heat exchanger heat rejection rate. It has been reported in rate of the secondary heat exchanger (Jones et al. 2015). The compressor and turbine serve the secondary heat exchanger and the performance of this component is critical to CAU cycle efficiency.

The turbine is a work-producing device on a common shaft with the compressor. The lower compressor pressure ratio of the optimised system is due to an inability of the turbine to extract the same power from a lower flow rate of the working fluid. As a smaller amount of power can be extracted, the temperature difference across this component is reduced, reducing the total CAU heat rejection rate. The increased CAU heat rejection rate of the baseline system gives a turbine outlet temperature 12ºC lower than that with the VPRSOV system.

6.5.2.5. Temperature Control

As the turbine outlet temperature of the system with the VPRSOV is higher, less bypass airflow is required to achieve the demanded equipment and cabin supply temperatures. In addition, the lower flow rate through the system with the VPRSOV requires less bypass

mass flow to achieve a given temperature rise, further minimising the bypass air mass flow rate. Bypass airflow is thermodynamically wasteful to system performance, so the minimisation of this flow increases the thermodynamic efficiency of the system (Jones et al. 2015). It is found that the reduced heat rejection rate of the CAU for the optimised system actually improves the total system efficiency through the reduction of the bypass air mass flow rate. This is a further example of the integrative approach, in which a component level performance degradation actually improves the performance of a component in a separate subsystem. This highlights the requirement for the complete airflow path analysis as a single system in the design and analysis of TMS.

6.5.2.6. Cabin Environment

It can be seen from Figure 6-14 that the system fitted with VPRSOV operates much closer to the cabin thermal limit. It is interesting to note the proximity of the multiple subsystems (cabin and forward avionics bay) to the respective thermal design limits even though these subsystems are not the subject of VPRSOV control. The VPRSOV is purely regulating the system inlet air power input based on maintaining the avionic module exhaust temperature to 65ºC. The optimisation of the cabin and forward avionic bay subsystem thermal conditions is a beneficial secondary effect.

The baseline TMS was designed so that it could maintain the airflow distribution across the different units over a wide range of airflow pressures and mass flow rates. This was originally obtained through a complex and time-consuming process of balancing the pressure drops across the components and subsystems. The fixed mass flow rate distribution was configured for a single worst case scenario providing a very narrow band of its adjustment, resulting in a static solution to a dynamic problem. This finding suggests that the existing mass flow rate distribution can be maintained and the bleed air inlet pressure can be controlled to provide a better TMS efficiency to suit a given flight condition. This allows the optimisation of multiple subsystems as a passive by-product of the component temperature feedback, which represents the implementation of a dynamic solution to a dynamic problem.

6.5.2.7. Avionic Environment

The avionic module utilises the negative kinetic thermal loading at cruise flight conditions to reduce the system inlet air power input. As with the ECS heat exchangers, the avionic chassis heat exchanger effectiveness, is increased with a reducing mass flow rate, due to the increased air-fin contact time. The implementation of the VCHS generates an isothermal heat exchanger baseplate regardless of the internal avionic circuit card architecture, within limits. The resulting increase of heat exchanger fin utilisation coupled with the increased heat exchanger air flow contact time greatly improves the avionic thermal efficiency. The introduction of the VCHS in the system is purely a tool to allow the rest of the hardware to operate at a more optimal condition at the system level.

The underfloor and rear avionic bay temperatures show an operation within their temperature limits, using a mass flow rate of cooling air that is considerably lower than the baseline system. The baseline system oversupplies these bays with airflow, reducing the effect of kinetic thermal loading and the bay temperatures can be seen to remain at a lower temperature within the allowed temperature range. The optimised system allows these avionic bays to utilise the negative kinetic loading without exceeding the temperature limits.

6.5.3. Variable Pressure Relief Shut off Valve Conclusions

At the cruise 2 flight condition, it is found that regulating the TMS inlet based on component-level conditions allows the whole system to operate at thermodynamically enhanced conditions. The heat exchangers are more effective, the bypass airflow is reduced, component pressure drop reduces quadratically (reduction in pumping losses), the avionic heat exchanger effectiveness is increased and the cabin, forward and underfloor subsystem thermal safety factor is reduced. This is overall a positive result towards proving the methodology of a component-led integrative optimisation approach.

6.6. Optimised Temperature Schedule

As defined in Chapter 5, water separation of bleed air is a two-part process. The airflow pressure is dropped below its dew point by the turbine expansion process, before the

condensate is extracted through a coalescing sock. The temperature between the turbine and the water separation is critical, if it is too high the water will re-vaporise, and if it is too cold and the water will freeze. The water separator inlet airflow temperature is maintained between 0ºC to 4ºC. All types of open-loop ECS control the temperature of the airflow for the purpose of water separation, even if using a HPWS. The ECS has no ability to measure and account for humidity in the airflow; therefore the control system operates to fixed temperature limits across the complete flight envelope.

At high altitude, the water content in the air is very low and therefore water separation is no longer needed and the turbine exhaust temperature could be reduced. This was achieved with the F-15 and an additional 7kW of TMS heat rejection capability was found through the application of an avionic cooling schedule with colder avionic inlet air limit.

The rate of heat and work addition/rejection through the ECS for a cruise condition is detailed in Figure 6-15. It can be seen that a sizable rate of heat addition to the ECS is generates the heat addition rate from the bypass air flow. For the Cruise 2 case, the equipment temperature bypass mass flow rate accounts for around one third of total ECS flow. One third of the energy consumed in bleed air compression is not being converted into heat removal. The turbine outlet temperature is very low due to the low bleed air input power, a cold coolant stream (-56ºC) of the primary and secondary heat exchangers, therefore to, achieve an equipment temperature of 0ºC to 4ºC, the bypass air flow rate is large. The heat addition rate at the ETCV bypass is greater than the heat rejection rate from the secondary heat exchanger.

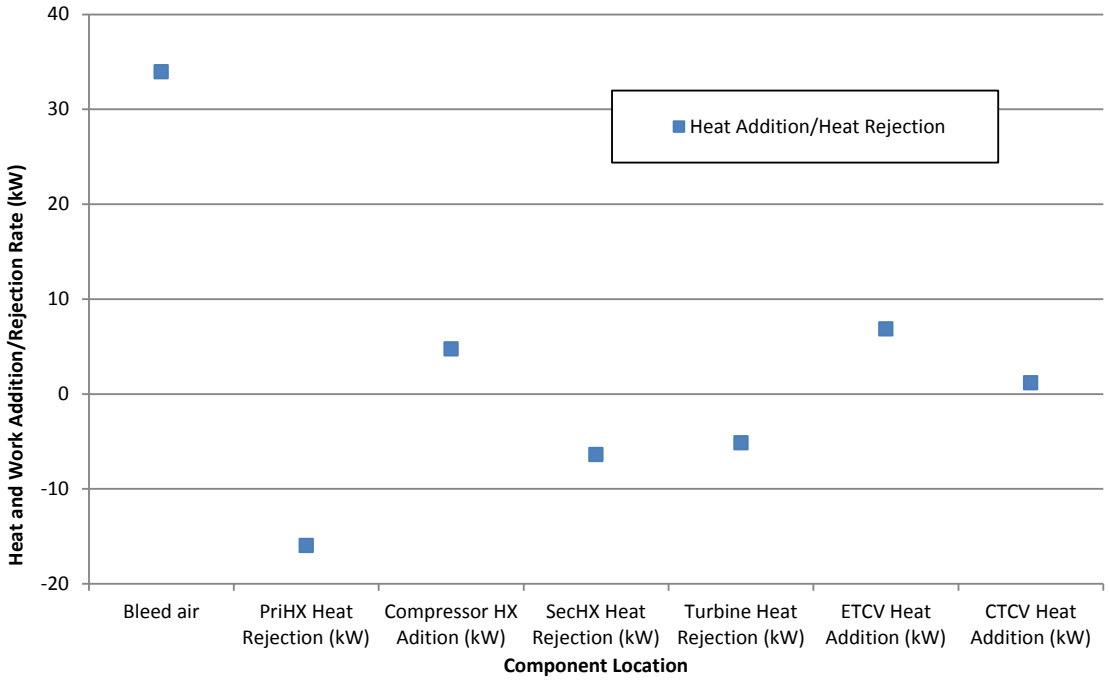

Figure 6-15: ECS energy flow for a cruise condition

The optimisation approach of revising the temperature schedule is based on an understanding developed through the investigation of the working fluid humidity. The temperature schedule remains the same for low altitude operations and, potentially for transient flight cases. The flight profile detailed in Chapter 4 is considered within the Ground Ops, Climb, Accelerate and Dive, Combat, Loiter and land are considered low altitude or transient cases. A new temperature schedule is considered for the remaining two high altitude cruise conditions. The two cruise conditions form the majority of the flight envelope by time.

6.6.1. Temperature Schedule

The turbine outlet temperature of the VPRSOV system is -70ºC, which is then heated through the addition of bypass air. The same system is simulated with no bypass air to achieve an avionic exhaust temperature of 65ºC. The temperature flow path can be seen in Figure 6-16. The reduction in the bypass mass flow rate allows a modest 8% reduction in the system mass flow rate. It can be seen that the reduction in the mass flow rate increases the temperature difference across the primary heat exchanger. As the complete airflow is passed through the cold air unit, the compressor pressure ratio is increased. The

result is a greater expansion across the turbine and a lower turbine outlet temperatures from a given bleed air to ram air temperature difference.

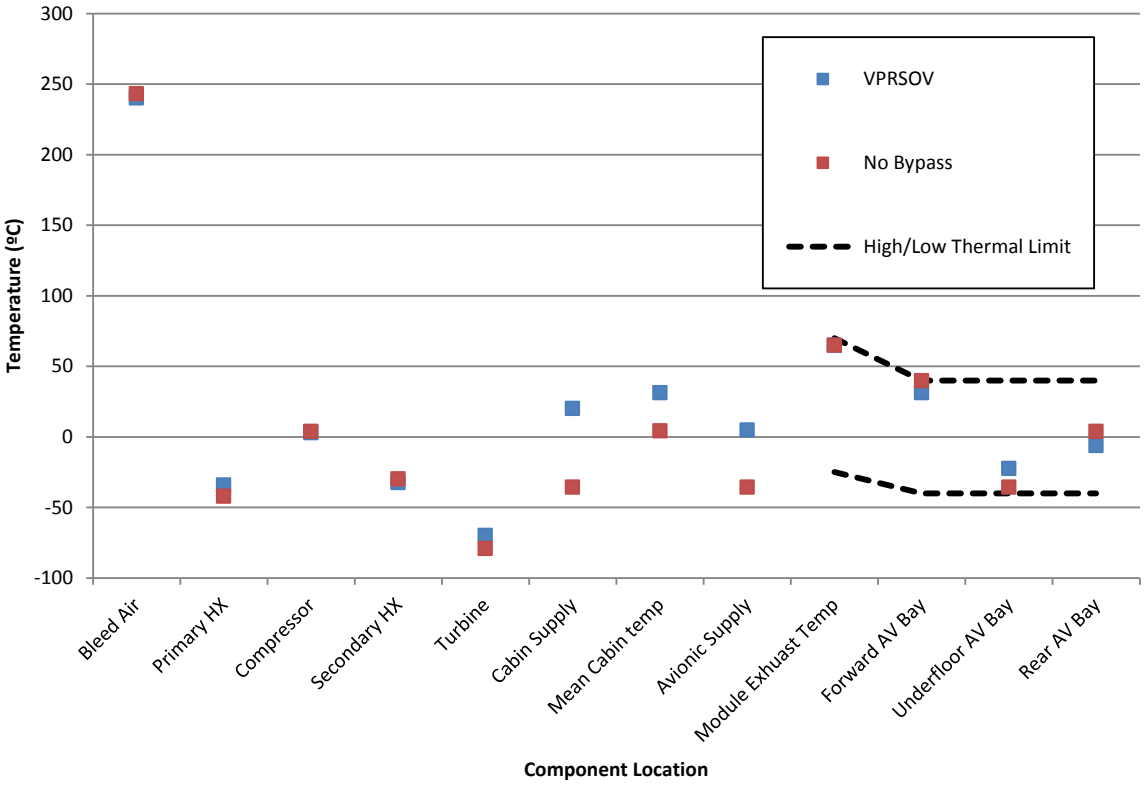

Figure 6-16: VPRSOV system and zero bypass air temperatures through the TMS

The airflow path with zero bypass air takes on heat from the surroundings, with the cabin and equipment feed temperature predicted at -35.6ºC. Obviously the airflow would require substantial mixing before providing to the pilot, however this represents to most thermodynamically efficient strategy of operation. The reduced airflow generates an increased temperature difference across the cabin and avionic modules. It was detailed in Chapter 4 that, at low avionic flow rates, the temperature difference reduces exponentially with a reducing mass flow rate. As the air flows through the remaining subsystems, the environmental loading becomes dominant and mean bay temperatures operate within the temperature limit. A system CoP improvement is predicted from 0.80 to 0.83.

6.7. Conclusions

Three key technologies have been identified for the optimisation of the avionic TMS. The technologies have been chosen based on the modelling and analysis of inflight conditions from Chapter 5 and in keeping with the optimisation methodology detailed in Chapter 2.

The implementation of the VCHS within the avionic chassis has been demonstrated and proven as useful technology for avionic cooling. The VCHS is not optimised for the application of bleed air minimisation and therefore its true strengths are slightly masked when considering the mission-level analysis of Chapter 7. The optimal application of the VCHS is as an integration tool for dynamic interface management. The VCHS makes the system insensitive to the variation in the input temperature distribution from individual circuit cards mounted on the same chassis and provides consistently an isothermal wall in all thermal loading and airflow conditions considered in this work. The prime application of this technology is to improve the certainty of the relationship between avionic module exhaust air temperature and internal component temperature. Using a VCHS would allow the airframe manufactures to fill a large part of the knowledge gap and make educated decisions on the mass flow rate supply of cooling air based on the exhaust air temperature. The reduction in isolated thermal hotspots should improve component reliability, however data is not available to quantify this potential reliability improvement.

The VPRSOV embodies the component-led integrative approach methodology. Through the optimisation of component-level temperature conditions, the complete TMS was optimised. The approach is particularly effective for the retrospective updates to existing 4^{th} generation aircraft as it works with the existing mass flow rate distribution and as regulated by the component pressure drops. The VPRSOV is particularly effective at cruise conditions, due to the high negative environmental kinetic thermal loading. This solution introduces a dynamic heat rejection capability to a dynamic thermal environment.

The current system measures avionic exhaust airflow temperatures, which are several heat transfer processes away from the electrical component temperature on the circuit cards.

This discrepancy in measurement location introduces a number of thermal behaviours which cannot be measured, resulting in a poor accuracy of extrapolation from the airflow temperature measurement to the actual circuit card temperature. The implementation of VCHS improves the accuracy of estimating the avionic component temperature from that of the exhaust airflow considerably, however assumptions are still required. The solution is to move the design specification of avionic cooling to the temperature control of the avionic cold wall. The cold wall is the closest instrumentable component to the avionic circuitry due to IPR. With the application of an isothermal VCHS plate, measuring the temperature at the cold wall would give a more accurate measure of the active electronic components, as the cold wall is thermally coupled to the active components. The control of cold wall temperature is a robust metric as the mass flow rate is an independent variable and temperature alone would provide a measure of the electronic module health. This concept is not pursued in this investigation as its retrospective application to 4^{th} generation aircraft would be too extensive. However, it is suggested that this concept warrants further investigation by BAE Systems and the technologies of VCHS and VPRSOV would be ideally suited for pursing this re-design of the avionic modules.

The updated temperature schedule as tested by simulation brought a modest reduction in mass flow rate. The concept is born from the findings of previous work and has potential for generating a substantial heat rejection rate capability across the flight envelope. The ability to combine this with the PRSOV allows the TMS to deliver a cooling demand based on heat rejection rate requirement. This is a similar approach to modern automotive engines, which deliver a torque demand based on driver input rather than an increase in airflow and fuel based on throttle position alone.

7. Component-Led Integrative System Operation

The aim of this chapter is to define the operation of a system which has been optimised following the component-led integrative optimisation methodology for avionic thermal management. The replication and analysis of a single system allows for an optimisation direction in keeping with a component-led approach. The optimisation technologies have been developed and this chapter aims to identify thermodynamic performance gains at mission-level.

7.1. Optimisation Technologies

7.1.1. Vapour Chamber Heat Spreaders

It is assumed that VCHS are structurally embedded within the avionic chassis to act as a heat exchanger baseplate. It has been shown that their variable thermal conductivity can be used to efficiently spread avionic circuit card heat loads for better heat exchanger fin utilisation [17]. The implementation of VCHS proved a very promising technology for avionic thermal management. Through proof-of-concept testing, the improvement in

effective heat transfer area generated an increase in heat transfer effectiveness. The VCHS technology can be used in two modes of operation:

- Reduce the component temperatures for a fixed cold wall mass flow rate (utilised for ground cases);
- Reduce the required mass flow rate for a fixed cold wall temperature (utilised for flight cases).

7.2. Variable Pressure Relief Shut off Valve

The TMS has a fixed Pressure Relief Shut-Off Valve at the ECS inlet for the protection of the downstream components of, de-coupling of dynamic TMS flow conditions from the propulsion system, and to shut down the ECS when required. It is proposed to replace the fixed PRSOV by a VPRSOV to regulate the TMS inlet conditions based on temperature feedback control from the avionic module exhaust temperature with target avionic module exhaust temperature of 65ºC.

7.2.1. Revised Temperature Control Schedule

The complete flight profile was assessed in Chapter 6. The control strategy was only changed for the two cruise conditions, which form the majority of the flight profile by time.

7.2.2. Component Led System Optimisation

Initially, results are presented with a VPRSOV temperature feedback from a single location which is avionic module exhaust air temperature. The requirement to minimise aircraft modification is paramount if considering the transferability of this work to retrospective aircraft updates. The system is assessed across the flight and atmospheric envelopes to analyse the thermodynamic robustness of the proposed optimisation. Results are then presented for VPRSOV taking a temperature feedback from every subsystem and regulating the air mass flow rate based on the subsystem closest to its thermal design limit. Finally, results of a comparative system efficiency study are presented.

7.3. Single Temperature Feedback VPRSOV and VCHS

The bleed air flow rate delivered to the ECS is a function of engine load and is variable across the flight envelope. The mass flow rate for the baseline configuration, VPRSOV,

VPRSOV with VCHS, and VPRSOV with VCHS and updated temperature schedule across the flight profile is detailed in Figure 7-1 for a simulated ISA day. A clear reduction in mass flow rate can be seen with the application of the VPRSOV. The VPRSOV is driven by a single temperature feedback; the forward avionic bay module exhaust temperatures are controlled to 65ºC. As mentioned previously, no flow rate saving is obtained at ground case as the pneumatic power is provided from the aircraft APU which is below the VPRSOV operating range. The requirement to reduce the avionic component temperature at ground case without APU modification is achieved with the VCHS implementation.

The VCHS are utilised to achieve a temperature reduction at the ground case and therefore no mass flow rate saving is achieved. Throughout the flight cases, the VCHS provide an additional modest mass flow rate saving. The updated temperature schedule is only implemented at the cruise conditions, where the high altitude and, low humidity negate the requirement for a bleed air water separation process. The reduction of bypass airflow provides an additional mass flow rate saving at these conditions.

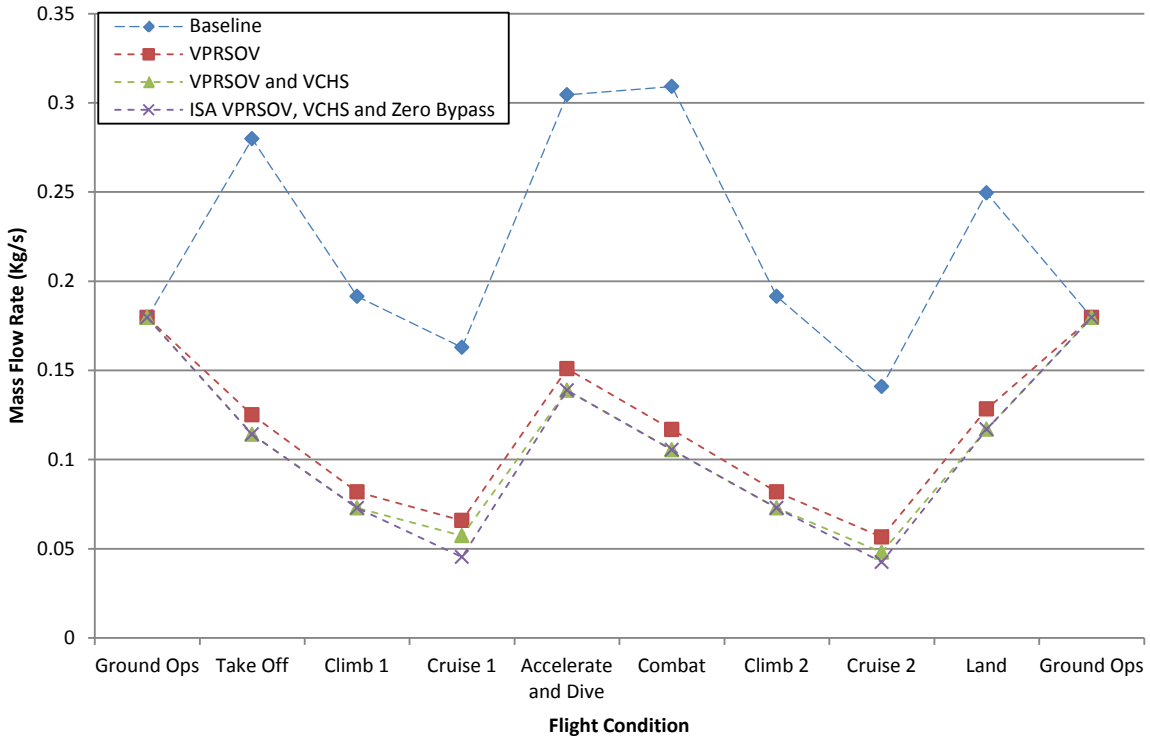

Figure 7-1: Bleed air mass flow rates across a flight profile for an ISA day. Dashed lines for indication only, data from steady state points at markers.

When considering the corresponding distribution of temperatures for the same flight profile and atmospheric conditions, the avionic module exhaust temperatures are controlled to 65ºC across all flight conditions. The implementation VCHS with the VPRSOV provides a 6% temperature reduction at ground operations. The remainder of the analysis will be shown for the three technologies as a single implementation, which is refused to as the optimised system.

The temperature of the forward and rear the avionic bays and their temperature limits across the flight envelope is shown in Figure 7-2 for the optimised system. It can be seen that the rear avionic bay temperature at the 'Accelerate and Dive' case is operating above the avionic temperature design limit. This is due to the low altitude and high speed nature of this flight phase generating an increase in the environmental thermal loading. The single feedback control of the VPRSOV in this condition, based on the avionic module exhaust temperature at a single measurement location is unable to account for this over-heating of the rear avionic bay. The temperature limits are provided from BAE Systems (Pearson & McCoy 2011).

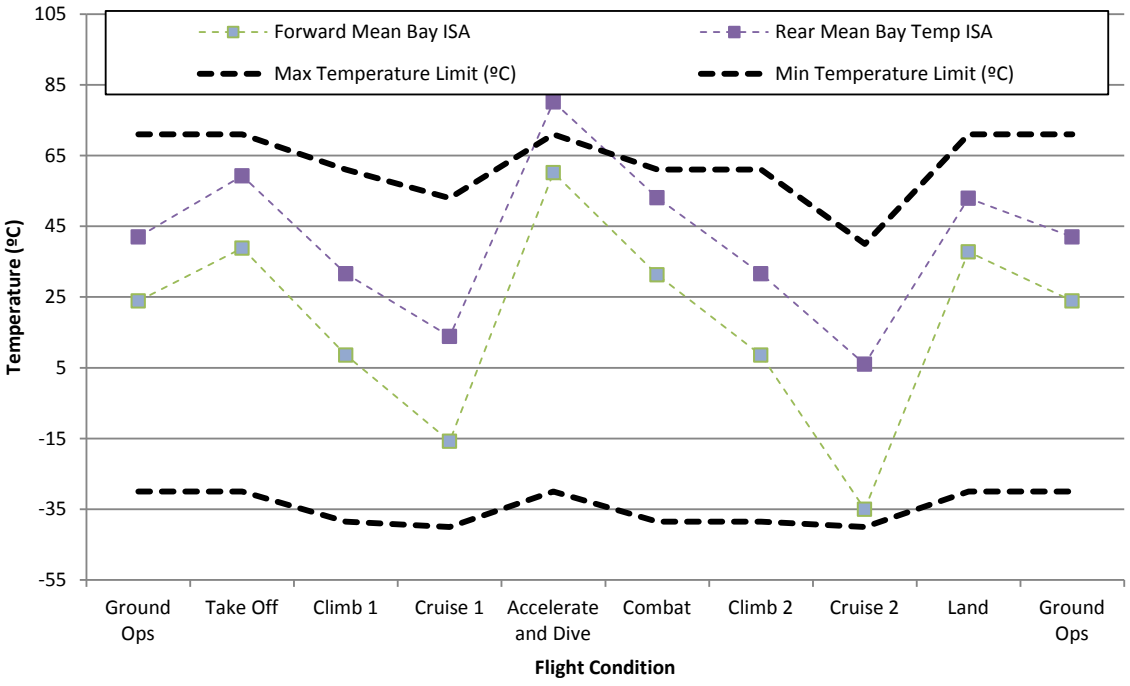

Figure 7-2: Bay temperatures across flight envelope with VPRSOV and VCHS active. Dashed lines for indication only, data from steady state points at markers.

The inability of the VPRSOV to maintain all bays within their temperature limits was not identified at a single flight condition, highlighting the requirement for mission-level analysis. It also shows that the use of a single temperature feedback location is not a robust optimisation approach. The over-temperature events of a single temperature feedback control system are increased when considering the complete atmospheric envelope. The avionic bay temperatures across every flight and atmospheric condition are displayed in Figure 7-3. It can be seen that the most thermally demanding area of the flight envelope is low altitude (flight or ground ops) and the most thermally demanding environment is the hot atmosphere.

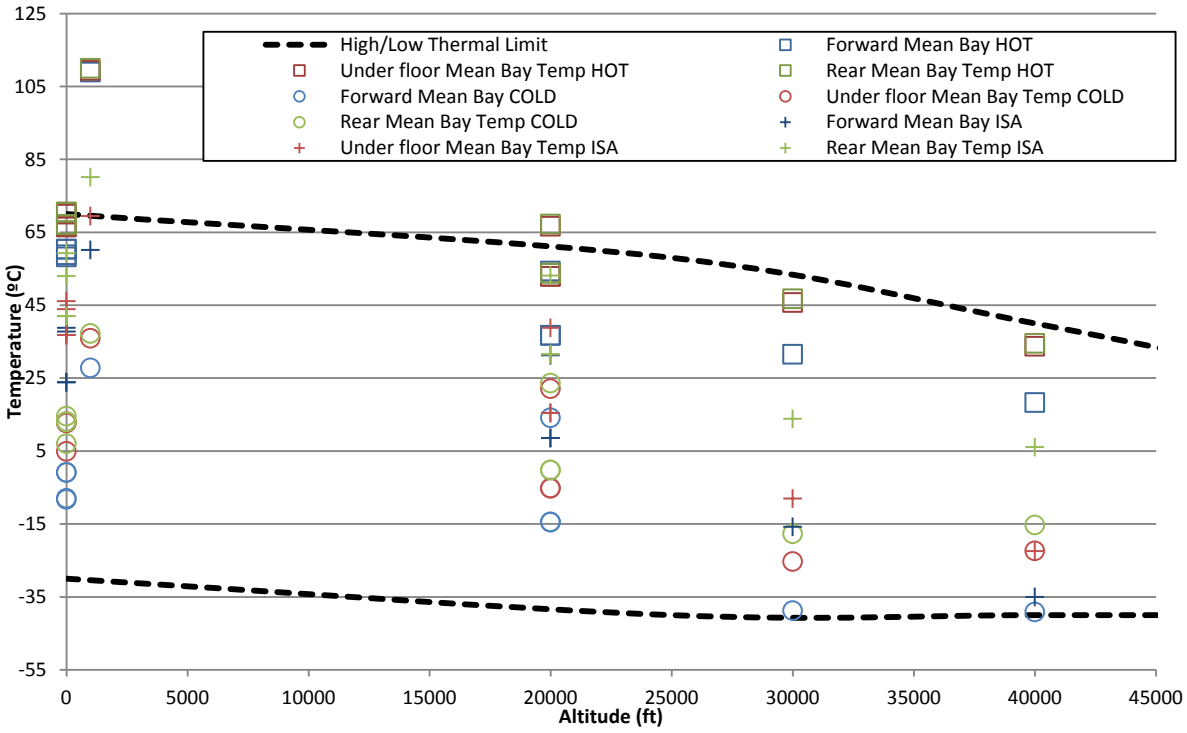

Figure 7-3: Avionic bay temperatures across the flight and atmospheric envelopes for a single feedback control system. Note; suffix in legend refers to atmospheric conditions.

The location, flight condition and severity of the over-temperature events are displayed in Table 7-1.

Flight Condition	Atmosphere	Failure Location	Percentage Over-temperature (%)
Climb 1	HOT	Cabin	10.2
Cruise 1	HOT	Cabin	8.2
Accelerate & Dive	HOT	Cabin	42.8
		All AV Bays	53.1 (ave.)
Accelerate & Dive	ISA	Rear AV Bay	12
Combat	HOT	Cabin	3.7
Cruise 2	HOT	Cabin	0.5
Land	HOT	Cabin	10.1

Table 7-1: Location, flight condition and severity of the over-temperature events.

A number of over-temperature events occur in the cabin environment during operations in a hot atmosphere. This is attributed to the single feedback temperature controller accounting for the aircraft skin kinetic thermal loading in the avionics bay, without accounting for the additional solar loading of the cabin transparencies. The combined solar and kinetic loading of the transparencies is particularly relevant in a hot environment, as the transparency is able to offer very little thermal insulation in comparison to a double or triple skinned avionic bay wall. It can be seen that the 'Accelerate and Dive' condition is also the most thermally demanding for the cabin environment. The cabin presents a higher thermal sensitivity to kinetic thermal loading in comparison to the other subsystems. Across the remainder of the flight envelope, the cabin over-temperature is no more than 10.2% (3.6ºC).

7.4. Multiple Temperature Feedback

The solution to the over-temperature events is to simulate four temperature feedback sensors, positioned in the cabin and in all three avionics bays. The VPRSOV will now regulate the bleed air inlet mass flow rate to the highest subsystem temperature. The cabin, avionic bay, and avionic module exhaust temperatures are displayed in Figure 7-4 and Figure 7-5. It can be seen that at least one subsystem is at its temperature limit throughout the flight profile.

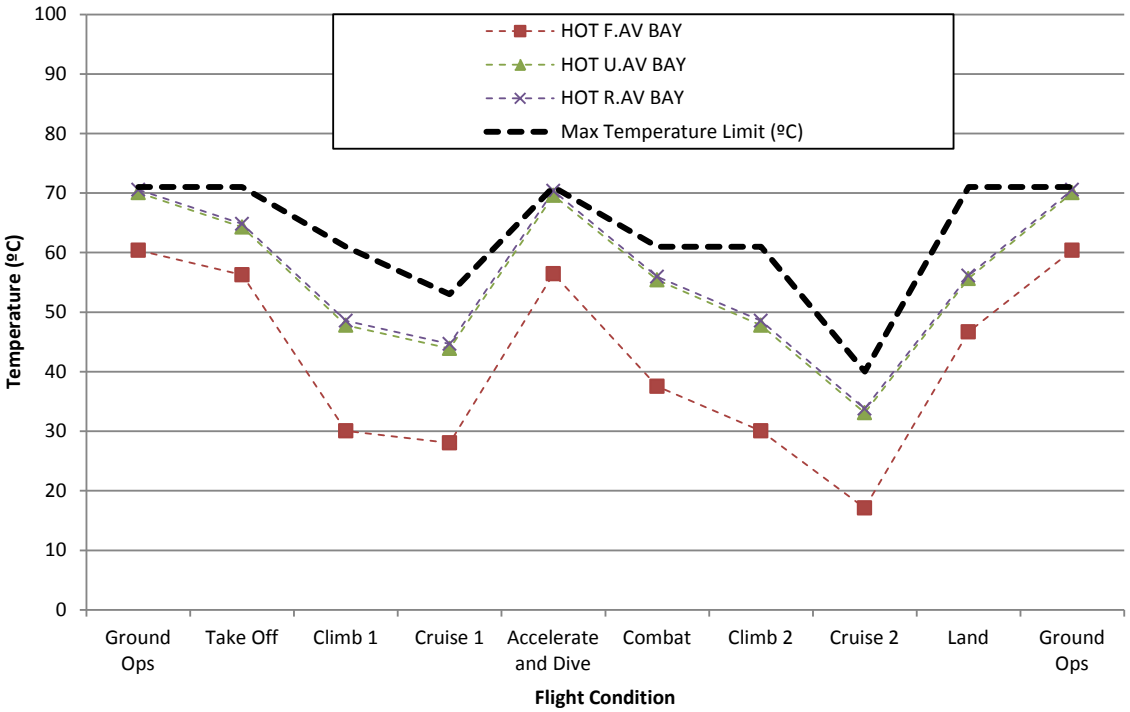

Figure 7-4: Avionic bay temperatures across the flight envelope. Hot environment with multiple temperature feedback. F.AV = Forward Avionics Bay, U = Underfloor, R = Rear. Dashed lines for indication only, data from steady state points at markers.

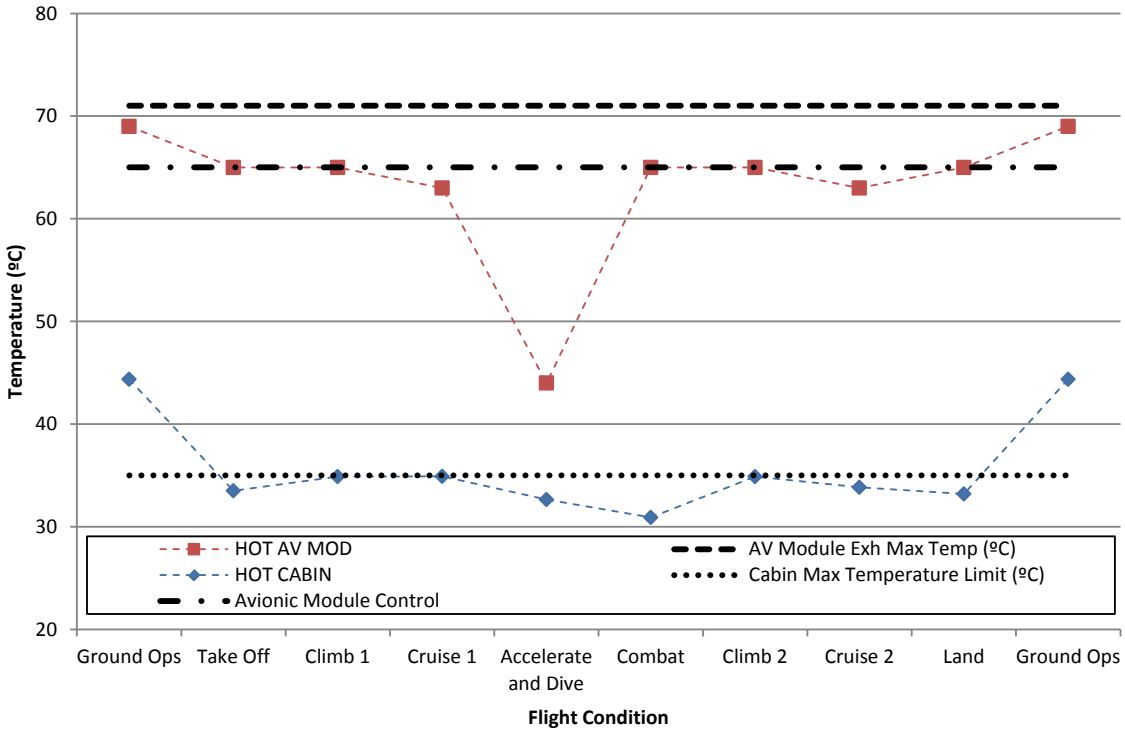

Figure 7-5: Cabin and avionic module exhaust temperatures across the flight envelope. Hot environment with multiple temperature feedback. Dashed lines for indication only, data from steady state points at markers.

Considering the thermally challenging 'Accelerate and Dive' case, it can be seen in Figure 7-4 that the underfloor and rear avionic bays operate at their temperature limit. The increased cooling mass flow rate provided by the multiple feedback control logic over the single feedback control at this flight condition reduces the cabin and avionic module temperature by 18ºC and 39ºC respectively. It is found that the mass flow rate saving over the baseline system is only 15%, with the majority of that saving found through the implementation of VCHS. The baseline TMS was initially configured for a single worst case scenario with an additional safety factor to cover any transient flight manoeuvres. It has been found that limited system optimisation is available at the most challenging flight condition, in the most challenging environmental condition. This suggests the sizing and TMS configuration is correct for the design specification. It is considered that it is the design specification that needs modification.

7.5. System Performance Study

The TMS CoP is shown in Figure 7-6 for the baseline system (ISA) and the optimised system (ISA, Cold and Hot). The ISA condition provides a direct comparison of the baseline and optimised system CoPs. When considering a fixed atmospheric condition, an averaged CoP gain across the flight envelope of 77.3% is achieved with the optimised system. The duration of each flight stage is detailed in Table 5-1.

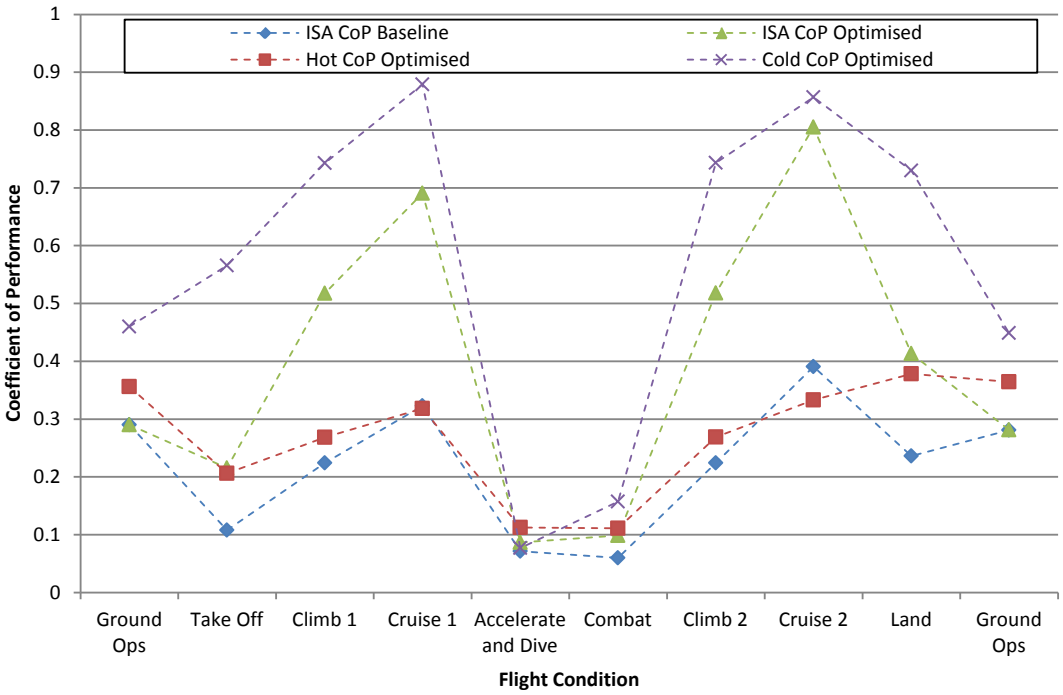

Figure 7-6: CoP for the baseline and optimised systems for three atmospheric conditions. Dashed lines for indication only, data from steady state points at markers.

The atmospheric condition associated to the highest CoP is the cold environment. The low atmospheric temperatures drive a negative kinetic thermal loading. The atmospheric conditions passively remove heat from the subsystems, reducing the heat rejection rate requirement of the TMS and inlet air input power requirement. The least efficient atmospheric condition is seen to be the hot atmosphere. The higher kinetic thermal loading due to the higher external air temperature across the flight profile requires more bleed air flow rate, than for the ISA and cold environments increasing system inlet power required by the TMS. The similarity in the CoP trends between the hot optimised system and the baseline system provides conformation that a narrow margin was available in the initial TMS configuration.

The highest TMS system CoP flight cases are the two cruise conditions. The cruise cases are high altitude (30,000ft and 40,000 respectively) and low speed flight conditions. The high altitude low provided atmospheric temperature and pressure conditions. As with the cold atmosphere, the system CoP is improved by a negative kinetic thermal loading that reduces the TMS inlet air power input requirement. In addition, Figure 7-7 shows that the combination of the low vehicle velocity and the low atmospheric pressure reduces the

calculated power consumption due to the lower aerodynamic drag of the ram air heat exchangers. While the TMS power consumption is substantially reduced at the cruise conditions, the heat removal rate performance by the TMS remains relatively constant across the flight envelope as all components operate within their temperature limits.

The least efficient flight case is the high load flight cases of 'Accelerate and Dive' and 'Combat'. These cases are high speed, and low altitude and have the highest kinetic thermal loading and the highest pressure drop across the ram air heat exchanger. The ram and bleed air input power consumptions are detailed in Figure 7-7. The ram air path remains constant for both system as the input power from the bleed air path reduces, the drag associated power of the ram air path becomes a bigger contributor to the TMS total power consumption. The power consumed by the ram air flow path is increased from under 20% to around 40% of the total TMS power consumed by the system across the flight profile.

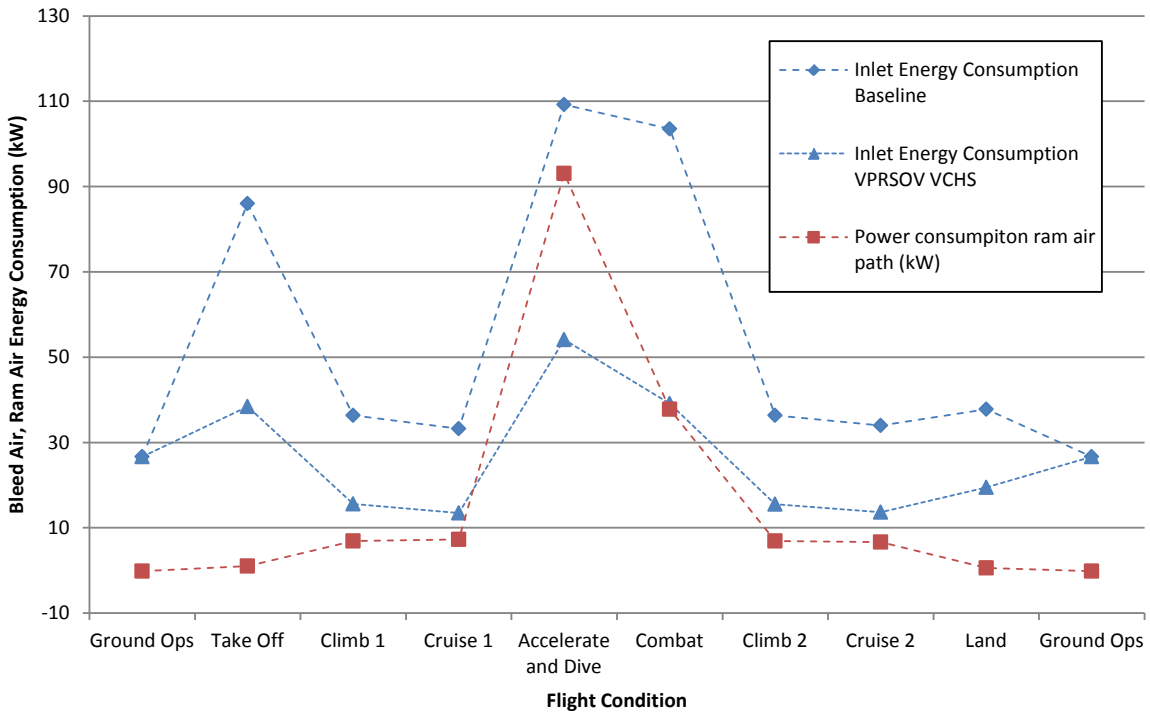

Figure 7-7: Ram and bleed air power consumption across the flight profile. Dashed lines for indication only, data from steady state points at markers.

The findings of Figure 7-7 suggest that a further improvement in the TMS efficiency may be realised by controlling both the coolant and the working fluid to adjust the heat exchanger

heat rejection rates. A variable ram air duct size may be a technology to consider in future work.

A comparison of the cumulative bleed air consumption between the baseline system and the optimised system is displayed in Figure 7-8. The cumulative bleed air consumption links the system CoP findings of Figure 7-6 to a real-world metric which can be used to identify specific fuel consumption savings. The optimised system is found to have the highest CoP at the two cruise conditions, which also are the longest (in time) flight cases. The cruise conditions constitute 55% of the total flight profile, yielding the highest bleed air consumption saving of any flight condition. In terms of the energy consumed from the 'Cruise 1' flight condition alone, the optimised system sees a reduction from 22.1kWh to 7.8kWh. A total bleed air consumption (in terms of air mass) saving of 32%, 58% and 66% is found for a Cold, ISA and Hot atmosphere respectively.

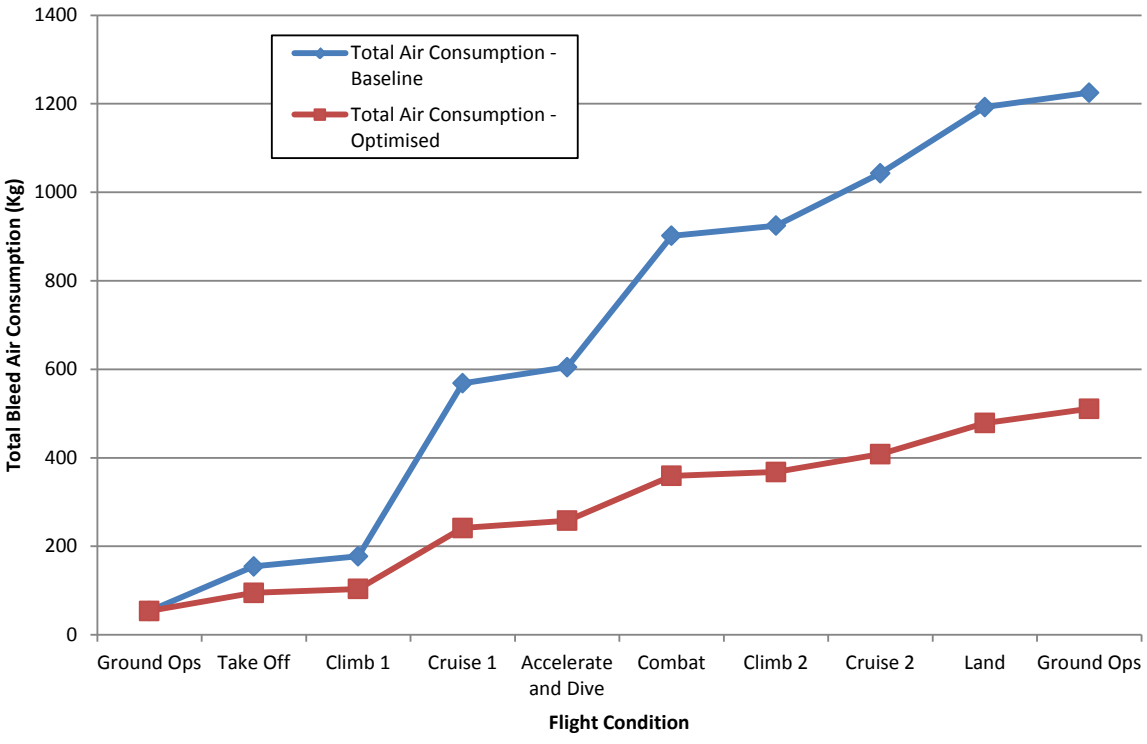

Figure 7-8: Cumulative bleed air consumption across the flight envelope.

The optimised TMS is capable of removing the same amount of heat (all subsystems operating within temperature design limits) with a lower total bleed air consumption through the maximisation of TMS CoP. The bleed air consumed is predicted to reduce from

1225kg to 510kg. Future work could consider what platform thermal loading growth capability could be realised if the full 1225kg were used by the optimised system in response to the ever increasing avionic cooling demands.

The energy required for the compression of bleed air is supplied from the aircraft fuel. A reduction of bleed air consumption at the same bleed air temperature and pressure outlet conditions produces a direct reduction in fuel consumption and therefore decreases the specific fuel consumption (SFC) of a given flight phases. The simulated engine in this analysis has a bleed airflow rate of between 0.3% and 2.3% of the total engine intake air, depending on the flight condition and assuming an ISA day. Assuming the relationship between bleed air consumption and SFC detailed by Evans (1991), the implementation of a VPRSOV and VCHS leads to a flight averaged SFC saving of 1%, with peak reductions at the cruise cases of 1.19% and 1.23%.

7.6. Chapter Conclusions

It has been demonstrated that substantial thermodynamic and system CoP gains can be realised on legacy airframes with a minimal architectural modification through a component-led system optimisation. The integrative approach considers the complete airflow path and a single system rather than a collection of subsystems and components operating simultaneously. It is seen that, through this approach, technologies at a component level can be matched with existing system behaviours to drive a global increase in CoP which can be measured at an aircraft level; by a reduction a SFC. The peak SFC savings are found at cruise conditions in a cold atmosphere, where saving of 1.19% and 1.23% are achieved while maintaining all equipment within the design temperature limits.

The largest system CoP gains are achieved at cruise conditions, with a CoP increase from 0.23 to 0.52 at ‘Cruise 1’ on an ISA day. The high altitude and low speed cruise condition has a high negative kinetic thermal loading that reduces the cooling requirement from the ECS. This flight condition also benefits from a low ram air heat exchanger pressure drop. Minimal system gains are predicted at high load conditions, where the drag associated power of the fixed geometry ram air pressure drop energy becomes the dominant

contribution to TMS power input during the 'accelerate and dive' and 'combat' phases. Reducing the flow rate or pressure drop across this component would further improve the system Cop and this requires additional investigation.

The highest system CoP is achieved in the cold atmosphere whereas with the smallest system CoP gain was found in the hot atmosphere. This acts to validate the baseline system design approach that was focused on a single worst case steady-state condition. At an 'Accelerate and Dive' condition, minimal system performance improvements can be achieved. However, this condition represents a minority of the total aircraft operation time across the flight profile.

The implementation of a VPRSOV and VCHS are two technologies that offer substantial benefits to legacy airframes. The key benefit is the ability to supplement existing system cooling distributions without the requirement for substantial architectural modification. The component-led integrative approach has been demonstrated with a legacy platform in this analysis, as system and operational information is abundant. However, the approach has equal merit in the design of a new airframe.

It is interesting to note a section of the original brief for this work. *"Once the 'hot spot' areas have been identified, it is then possible to begin the process of improving the thermal management inside the avionics bay. At this stage, some of the improvements maybe a redesign of how the conditioned air from the ECS enters and exits the bay, providing an improved airflow, or the design of the avionic boxes maybe updated in some way to improve the removal of heat from inside the boxes.*

A more innovative solution to the thermal management problem inside the avionics bay maybe to use new thermal materials either for the avionics bay construction or in the box design. These materials may aid in the transfer of heat away from the avionics bay resulting in a reduction, or removal, of the 'hot spot' areas identified during testing."

The application of a VPRSOV and new temperature control strategy could be defined as a redesign on how the conditioned air is used. The implementation of VCHS could be defined as a more innovative solution to thermal management by the removal of the “hot spot” areas. The aim of this chapter was to identify the applicability and effectiveness of this optimisation.

8. Conclusions

The conclusions of each chapter have been detailed throughout the thesis and this section aims to provide a synthesis of these conclusions. The conclusions are split into three main sections; those relating to the facility, the evaluation of the methodology, and, the evaluation results outcome.

Future work is then discussed to suggest the direction for the future project in this area. Since the onset of this project and the development of new GTF, further PhDs have been funded to continue the work. The future work section should act as a direction for the outputs of the facility over the following years.

8.1. Facility Development

1. An extensive new GTF has been developed from the ground up to act as a test bed for the application of a new methodology for avionic thermal management optimisation. The GTF has proven to be reliable through the careful installation and calibration of all data acquisition synthesis. The facility allows the experimental replication of the bleed air, ECS and avionic subsystem thermal conditions, within limits. The bleed air, ECS, avionic and cabin subsystems all have a corresponding 1D

thermodynamic model to expand the system test envelope beyond the infrastructural limitations of the experimental facility.

2. When considering validation of data generated at system level in this project, it performed well against the limited flight data provided from BAE Systems. It is considered that the relationships of aircraft performance which have been identified in this project are in agreement with anecdotal knowledge and experience from relevant BAE Systems staff when presented at quarterly industrial meetings.

3. The development of this facility was only achieved through the organisational structure of the project and the strong industrial links between Loughborough University and BAE Systems. Typically, industry has access to genuine equipment, but limited time for long research activities. Academia is free of industrial time constraints, but has limited access to genuine equipment and data. The ability to take advantage of both sectors was a key strength of this project.

8.2. Methodology Evaluation

1. The typical 4^{th} generation design process was proven to be ineffective when considering fuel cost of the thermal management system. The current (5^{th} generation) system design procedure, with its more extensive conceptual design phase, has to contend with high uncertainty and sometimes incomplete data sets, leading to the generation of unexpected system behaviours, as seen with the F-22 and the F-35 aircraft. This thesis has explored a new solution to poor performance design processes. The concept of this approach is to marry the contemporary design philosophies with existing high certainty genuine equipment in a single GTF. This enables to carry out a conceptual design approach using mature technology. The application of genuine equipment is a new approach to the development of a test bed. This developed new knowledge in two areas. Firstly, the results of this work can be used directly for retrospective aircraft thermal management technology upgrades. Secondly, the test bed can be used to identify future

methodologies and technologies that are not airframe specific. It has been seen that the studies into bleed air humidity and partial ECS failures have generated knowledge that is platform-transferrable.

2. The requirement to generate high fidelity data on the TMS led to completing a test campaign on the GTF. A number of key system findings have been developed as a result of this process. The key ECS findings are based around the system response to bleed air humidity and partial failures. The combination of this work has highlighted the limitations of traditional performance metrics, which are widely used in the design of aircraft TMS. The limitations of these metrics consists of unknown TMS behaviour occurring beyond the visibility of 1D modelling. The lack of visibility of the system dynamics highlighted in this work explains why many TMS exhibit unexpected system behaviour at the system level. This finding helps to identify the core reasons why the isolated design process of a 4^{th} generation aircraft leads to unexpected system behaviour when operating at aircraft level.

3. The reliance on metrics with limitations such as the ECS exhaust temperature without any complementary assessment of the air mass flow rate, can generate a situation where a partial ECS failure is only detected in downstream subsystems, such as in the avionics bay. A partial failure of the ECS can substantially reduce the cooling air mass flow rate while the exhaust temperature remains within the design limits, masking a reduction in the TMS cooling capacity. The avionic subsystem can measure a normal cooling air supply temperature while providing an insufficient avionic cooling capacity.

8.3. System Thermal Performance

1. Component reliability and aircraft effectiveness is always prioritised and it was concluded that the traditional TMS design approach yields a thermally reliable but not a thermodynamically efficient system. This concept has been confirmed by the finding that the avionic modules are overcooled for all flight conditions across the

atmospheric envelope, a finding confirmed by FCC validation data. It can be concluded that this approach was able to develop information on avionic thermal performance across the flight envelope, reducing unknown system thermal behaviour.

2. The baseline TMS approach can be defined as a static solution to a dynamic problem. The dynamic atmospheric conditions in flight provide a constantly moving target for the static TMS design. The static TMS configuration is designed to ensure reliability at the worst case scenario and had little scope for optimising the thermodynamic cycle at the remaining flight conditions. As a result, minimal optimisation opportunities were achievable at the high load cases (hot atmosphere, or accelerate and dive). Low load flight cases (such as cruise) presented the greatest opportunity for system optimisation through a component-led modification of the system and of its control logic.

3. The baseline system revealed a number of interesting thermodynamic trade-offs when considering the performance response to humidity and to partial failures. In the case of humidity, it was identified that the water extraction process requires a phase change at the turbine. However, it was also identified that phase change at the turbine generates poor thermodynamic efficiency. The temperature at the turbine exhaust is controlled to optimal conditions for generating free condensate within the airflow, however the aircraft spends most of its time in dry air. It is through the understanding of the system response to these variables gives scope for optimising the bleed air cycle.

4. The efficiency can be substantially degraded by the application of the system within the airframe. An example of this was seen as manual control of the TCVs could be used to make the ECS substantially more robust.

5. The origin of avionic thermal failures was assumed to be mainly a result of the generation of isolated hotspots and not due to the saturation of the TMS heat

removal capacity. While this assertion was plausible, it could not be confirmed until a relationship was made between flight and atmospheric conditions. The current approach to reducing the occurrences of avionic component failures is to increase the heat removal rate by increasing the cooling air mass flow rate. The growth capacity in the cooling air mass flow supply is a limited resource and it is quickly being exhausted on 4th generation jet TMSs. In addition, it was shown that an increase in mass flow rate increases the bleed air input power and is thermodynamically wasteful. This finding directed the analysis power of thermal failure investigation away from the TMS and towards the avionic module heat exchangers.

6. The optimisation in this work is approached as a study of bleed air minimisation, but the output is an improvement in the TMS CoP. In this case, the inlet air power supplied was minimised for a given heat rejection rate. The same approach could be used to provide an avionic growth capability, by increasing the heat rejection rate, for fixed amount of inlet air power supply.

7. The installation of a VPRSOV proved the component-led integrative approach methodology model predictions. Through the optimisation of component-level temperature conditions, the complete TMS was improved. For example, the optimisation of the avionic unit temperature conditions provided an improvement in ECS heat exchanger performance through a charge in the air coolant ratio. The assessment of the complete airflow path as a single system to improve the full system performance by implementing a component-level temperature management proved a successful methodology. The approach is particularly effective for the retrospective updates of existing 4th generation aircraft TMS, as it works with the existing mass flow rate distribution. The VPRSOV is predicted to be particularly effective at the cruise conditions, due to the negative environmental kinetic heating this flight phases provided. This solution provides a dynamic heat rejection rate in response to a dynamic thermal environment.

8. The updated temperature schedule brought a modest reduction in the bleed air mass flow rate. The concept has potential to generate a substantial inlet air power saving across the flight envelope; a concept proved by F15 and confirmed in this investigation. However, it only provides a partial solution as there is no spare heat rejection rate capacity at some hot and fast (low altitude) flight conditions. The generation of spare heat rejection rate capacity requires to move the water separator upstream to a HPWS system; as discussed in the humidity investigation.

9. The thermodynamic performance of the VCHS is better suited to increasing the avionic growth capability and the avionic component reliability than for bleed air minimisation. These are both goals that are not fully investigated in this work and could be studied by future work. The application of the VCHS was utilised for an additional mass flow rate reduction across the flight envelope and to reduce the avionic component temperature at the ground case. This application of the technology potentially masks its full performance benefit. The VCHS is seen as a very promising technology as it allows a thermal buffer at the interface location between equipment supplier IPR and airframe integration. The technology is passive, sealed, operates in negative G, within limits and has the capability to increase its thermal conductivity with increasing thermal loading, within limits. This is a key requirement for generating future avionic growth capability. If the TMS design specification were to be moved from specifying the avionic inlet mass flow rate and temperature supply to specifying an avionic cold wall temperature, the VCHS is a technology which would require serious consideration for its implementation in all fast-jet aircraft.

10. It was found that, as the bleed air path was optimised, the ram air path became the dominant source of aircraft drag power associated to the provision of an avionic cooling rate. This finding highlights the limitations of retrospective updates to a 4th generation platform and identifies the requirement for a more dynamic and variable approach to thermal management. The dynamic cooling demand should be

met by a dynamic supply of cooling capacity. The system should have the capability to vary its power input (from both air streams) to achieve this dynamic capacity.

8.4. Further Work

A number of key concepts have been developed in this work that warrant further investigation. Three prime examples are detailed below for the future design of a platform efficient TMS. The future work would look to build on the understanding and on the facilities developed in this work.

8.4.1. Cold Wall Temperature Driven Avionic Thermal Management

It is suggested that the avionic cooling design specifications should move to prescribing a cold wall temperature and not supplying an unknown mass flow rate at a given temperature. The cold wall is the closest instrumentable component to the avionic circuitry due to IPR. With the application of an isothermal VCHS plate, this would give a better measure of the avionic temperature conditions as the cold wall is directly thermally coupled to the active components. The control of the cold wall temperature is a robust metric as the mass flow rate is an independent variable and temperature alone would provide a measure of the module health. This concept is not pursued in this investigation as its retrospective application to 4th generation aircraft would be too expensive. However, this concept warrants further investigation by BAE Systems and the technologies of VCHS and VPRSOV would be ideally suited.

8.4.2. Robust ECS Efficiency Measure

It has been shown that the use of traditional performance metrics, such as temperature and CoP, are limited on their ability to represent the heat removal rate performance of the bleed air cycle ECS. There is a requirement for developing a more robust performance measure which can relate the ECS conditions to the aircraft cost, in terms of fuel consumption, subsystem reliability and cooling capacity. Initial work has begun on an entropy approach for the ECS performance evaluation. The analysis of the entire TMS identified the ECS as the primary entropy sink as well as the source of irreversibility

through the complete flow path. The calculation of entropy generation can be applied equally effectively at component- or system-level, providing a rigidly-defined metric which cannot be misinterpreted or miscalculated to the same degree as the CoP. The ability to remove the limits imposed by the sub-system boundaries ensures the flexibility of this methodology. By combining this information with the temperature distribution along the air cycle, this analysis is more reflective of the overall energy cost to the aircraft than traditional approaches.

It has been shown that the component location of the peak entropy generation within the ECS moves through the system with changes to either flight or atmospheric condition. Preliminary studies show that the bypass mixing is dominant at a cruise conditions, while the ram air heat exchangers are dominant at high load conditions; indicating a requirement for a variable strategy for system design, optimisation, and regulation. Consideration across the entire flight profile allows the design of future systems to be optimised for a broad window of operations, with subsequent implications to high-level aircraft architecture and sizing.

8.4.3. Variable Approach to Future System Design

The system is currently designed to a maximum inlet air power input that is assumed constant throughout the aircraft operation. For example, the propulsion supplier has designed the engine for a given bleed air mass flow rate and the airframe manufacture designs a system to this rate. To thermodynamically optimise the system, the airframe manufacturer should consider a dynamic approach to thermal management. A good example of this is an automotive powertrain. At part load, such as at motorway cruise conditions, the vehicle shuts its cabin air inlets to reduce aerodynamic drag, an active water pump can reduce the water coolant flow rate to minimise the engine shaft power used for water pumping, an active thermostat can control the heat exchanger heat rejection rate, the fuel rail pressure drops to reduce the power consumption through fuel compression, the fuel injection and spark ignition timing change to deliver only the torque that is required. This is a concept that should be considered for the aeronautical TMS. The requirement of the TMS system on fast jet aircraft in a cruise condition is very different to

that of an accelerate and dive condition. Initial entropy work has shown that the component of peak entropy generation moves from the TCUs to the heat exchanger depending on the flight condition. The TMS should have the capability to address this change. The new architecture could include a motor generator on the CAU shaft, the inclusion of a fuel loop with variable speed flow rate, active ram air inlets and a control system not constrained to temperature measurements only.

8.5. Publications

Published Articles

- Jones, A. B., and Chen, R., 2016. "Assessment of Vapour Chamber Heat Spreader Implementation for Avionic Module Thermal Management," International Journal of Thermal Technologies, 6(2), pp 103-111. Available at http://inpressco.com/wp-content/uploads/2016/05/Paper2103-111.pdf. Published June 2016.
- Jones, A. B., Childs, T., and Chen, R., "Development of a Full Scale Experimental and Simulation Tool for Environmental Control System Optimisation and Fault Detection," 53rd AIAA Aerospace Sciences Meeting, San Diego, CA: American Institute of Aeronautics and Astronautics, 2015, pp. 1–11.
- Jones, A. B., Childs, T., Chen, R., and Murray, A., "Evaluating Environmental Control System Thermal Response to Degraded Operating Conditions for Fault Detection and Isolation Purposes," San Diego, CA: AIAA, 2016, pp. 1–16.
- Jones, A. B., Childs, T., Chen, R., and Murray, A., "Thermal Sensitivity Analysis of Avionic and Environmental Control Subsystems to Variations in Flight Condition," San Diego, CA: American Institute of Aeronautics and Astronautics, 2016, pp. 1–15.
- Jones, A. B., Childs, T. G., Chen, R., and Murray, A., "A Study into Refrigeration Cycle Working Fluids using an Air Cycle Machine Environmental Control System," 54th

AIAA Aerospace Sciences Meeting, San Diego, CA: American Institute of Aeronautics and Astronautics, 2016, pp. 1–14.

- Jones, A. B., and Chen, R., "Experimental Assessment of Vapour Chamber Heater Spreader Implementation in Avionic Cooling," 53rd AIAA Aerospace Sciences Meeting, Kissimmee, FL: American Institute of Aeronautics and Astronautics, 2015, pp. 2–10.

Submitted for Review

- Jones, A. B., and Chen, R. Murray, A., "Component-led Integrative Approach to Retrospective Avionic Thermal Management," American Society of Mechanical Engineers, Journal of Heat Transfer. Submitted February 2016.

ix. Appendix

Appendix 1

Empirical convective heat transfer coefficient data

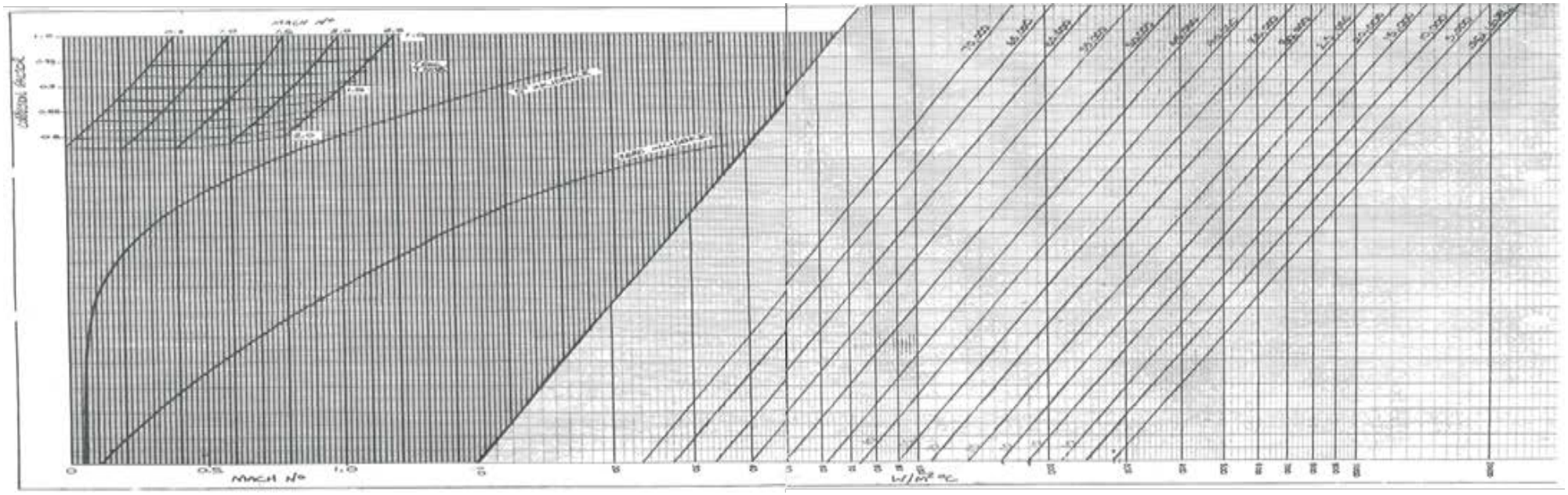

x. References

IISS. 2015. *The Military Balance 2015*, London: Routledge. http://www.iiss.org/en/publications/military-s-balance

Allison, D.L., Alyanak, E.J. & Shimmin, K., 2016. Aircraft System Affects Including Propulsion and Air Cycle Machine Coupled Interactions. In *57th AIAA/ASCE/AHS/ASC Structures, Structural Dynamics, and Materials Conference*. AIAA SciTech. San Diego, CA: American Institute of Aeronautics and Astronautics, pp. 1–16. Available at: http://dx.doi.org/10.2514/6.2016-0671.

Alyanak, E.J. & Allison, D.L., 2016. Fuel Thermal Management System Consideration in Conceptual Design Sizing. In *57th AIAA/ASCE/AHS/ASC Structures, Structural Dynamics, and Materials Conference*. AIAA SciTech. San Diego, CA: American Institute of Aeronautics and Astronautics, pp. 1–18. Available at: http://dx.doi.org/10.2514/6.2016-0670.

Andrade, R, A. & Zaparoli, E.L., 2004. A Thermodynamic Study of an Aircraft Air-Conditioning Air Cycle Machine. In *CONEM*. Belem PA: Brazilian Congress of Mechanical Engineering.

Arwidson, J. & Arwidson, J., 2013. *Thermal Fatigue Life Prediction of Solder Joints in Avionics by Surrogate Modeling – a Contribution to Physics of Failure in Reliability Prediction – a Contribution to Physics of Failure in Reliability Prediction*,

BAE Systems, 2007. *Hawk Mk. 132 Aircraft Maintenance Manual*, Brough, UK.

BAE Systems, 2015. Typhoon: King of Swing and a Whole Lot More. *BAE Systems*, p.1. Available at: http://www.baesystems.com/en/feature/typhoon-king-of-swing-and-a-whole-lot-more.

Baird, D. & Ferentinos, J., 1998. Application of MIL-C-87252 in F-22 Liquid Cooling System. Available at: http://dx.doi.org/10.4271/981543.

Bejan, A., 1997. *Advanced Engineering Thermodynamics (Second Ed.)* 2nd ed., New York: John Wiley & Sons.

Bodie, M. et al., 2010. Thermal Analysis of an Integrated Aircraft Model. In *48th AIAA Aerospace Sciences Meeting Including the New Horizons Forum and Aerospace Exposition*. Aerospace Sciences Meetings. Atlanta, GA: American Institute of Aeronautics and Astronautics, pp. 1–12. Available at: http://dx.doi.org/10.2514/6.2010-288.

Brown, K.D. et al., 2012. *Hawk Mk 132 ECS Rig Phase 1 & 2, Software and Top Tests in Lab*

B, Warton, UK.

Buckingham, R.D., 1984a. *Helicopter Cooling, Air Cycle/Vapor Cycle Trade-Offs*, SAE International.

Buckingham, R.D., 1984b. Helicopter Cooling, Air Cycle/Vapor Cycle Trade-Offs. Available at: http://dx.doi.org/10.4271/840942.

Campo, D., Weyant, J. & Muzyka, B., 2014. Enhancing thermal performance in embedded computing for ruggedized military and avionics applications. In *Fourteenth Intersociety Conference on Thermal and Thermomechanical Phenomena in Electronic Systems (ITherm)*. IEEE, pp. 840–845. Available at: http://ieeexplore.ieee.org/lpdocs/epic03/wrapper.htm?arnumber=6892368 [Accessed December 19, 2015].

Cavcar, M., 2000. The International Standard Atmosphere (ISA). *Anadolu University, Turkey*, pp.1–7. Available at: http://home.anadolu.edu.tr/~mcavcar/common/ISAweb.pdf.

Chakraborty, I. & Mavris, D.N., 2016. Integrated Assessment of Aircraft and Novel Subsystem Architectures in Early Design. In *54th AIAA Aerospace Sciences Meeting*. AIAA SciTech. sa: American Institute of Aeronautics and Astronautics, pp. 1–25. Available at: http://dx.doi.org/10.2514/6.2016-0215.

Chen, W.-H., 2007. *Avionic Systems*, Loughborough, UK.

Cirrito, V., 1982. Thermal Design of Integrated Avionic Racks for Aircraft. In *12th Intersociety Conference on Envrionmental Systems*. San Diego, CA: SAE International, pp. 1–9.

Clark, C., 2012. F-35 Total Costs Soar to $1.5 Trillion; Lockheed Defends Program. *Breaking Defense*, p.1. Available at: http://breakingdefense.com/2012/03/f-35-total-costs-soar-to-1-5-trillion-lockheed-defends-program/ [Accessed January 1, 2015].

Cole, H.H., 1974. Design, Integration, and Testing of the F-15. Available at: http://dx.doi.org/10.4271/740843.

Conceição, S.T., Zaparoli, E.L. & Turcio, W.H.L., 2007a. Thermodynamic Study of Aircraft Air Conditioning Air Cycle Machine: 3-wheel × 4-wheel. Available at: http://dx.doi.org/10.4271/2007-01-2579.

Conceição, S.T., Zaparoli, E.L. & Turcio, W.H.L., 2007b. Thermodynamic Study of Aircraft Air Conditioning Air Cycle Machine: 3-wheel × 4-wheel. Available at: http://papers.sae.org/2007-01-2579/ [Accessed November 24, 2015].

Cramer, O., 1993. The variation of the specific heat ratio and the speed of sound in air with

temperature, pressure, humidity, and CO2 concentration. *The Journal of the Acoustical Society of America*, 93(5).

Crickmore, P., Tooby, A. & Moreshead, H., 2014. *Lockheed F-117 Nighthawk Stealth Fighter*, New York: Bloomsbury Publishing.

Cronin, M.J., 2010. Design Aspects of Systems in All-Electric Aircraft.

Defence, D. of, 2011. F-35 Joint Strike Fighter (JSF). *http://www.dote.osd.mil/*, pp.25–38. Available at: http://www.dote.osd.mil/pub/reports/FY2011/pdf/dod/2011f35jsf.pdf.

Defence, D. of, 2008. *MIL-STD-810G - Environmental Engineeing Consderations and Laboratory Tests*,

DeFrancesco, G.L., 1989. Applications of the Reverse-Bootstrap Air Cycle Environmental Control System. Available at: http://dx.doi.org/10.4271/891437.

Defrancesco, G.L., 1993. Condensing Cycle Air Conditioning System. *SAE International1*, (1-8).

Dexter, P.F., Watts, R.J. & Haskin, W.L., 1990. Vapor Cycle Compressors for Aerospace Vehicle Thermal Management. Available at: http://dx.doi.org/10.4271/901960.

Dieckmann, R., Kosfeld, O. & Jenkins, L.C., 1986. Increased Avionics Cooling Capacity for F-15 Aircraft. In *Aerospace Environmental Systems - 16th Ices Conference*. SAE International, pp. 177–187. Available at: http://dx.doi.org/10.4271/860910.

Dieckmann, R.R., 1988. Improved Reliability and Maintainability for Fighter Aircraft Environmental Control Systems. Available at: http://dx.doi.org/10.4271/880999.

Diermen, W. van, 2015. F-22 Raptor History. *https://www.f-22raptor.com/index.php*. Available at: https://www.f-22raptor.com/index.php.

Dommelen, J. Van & Vos, R., 2012. A Conceptual Design and Analysis Tool for Blended Wing Body Aircraft. In *28th International Congress of the Aeronautical Sciences*. Brisbane, Australia: ICAS, pp. 1–13.

Donovan, A.B., Roberts, R.A. & Wolff, M., 2015. Fuel Pump Trade Study for a Conceptual Design of an Integrated Air Vehicle System. , (88), pp.1–9.

Evans, A.B., 1991. *The effects of compressor seventh-stage bleed air extraction on performance of the F100-PW-220 afterburning turbofan engine*, Available at: http://lb-primo.hosted.exlibrisgroup.com/primo_library/libweb/action/display.do?tabs=detailsTab&ct=display&fn=search&doc=TN_nasa119910010772&indx=1&recIds=TN_nasa119910010772&recIdxs=0&elementId=0&renderMode=poppedOut&displayMode=full&

frbrVersion=&dscnt=0 [Accessed October 28, 2015].

Fighter Aircraft Generations 2016. *www.globalsecurity.org*, p.1.

FLIR 2015. FLIR A320 (30Hz) Thermal Camera Specification Sheet. Available at: http://support.flir.com/DsDownload/Assets/48201-0201_en_51.pdf [Accessed January 17, 2016].

Ferran, L., 2012. Report: F-22 Raptor Loses $79 Billion Advantage in Dogfights - ABC News. *ABC News*, p.1. Available at: http://abcnews.go.com/blogs/headlines/2012/07/f-22-fighter-loses-79-billion-advantage-in-dogfights-report/ [Accessed December 1, 2015].

Fourquet, H. et al., 2000. Performance Validation of a New Water Separator Concept. Available at: http://papers.sae.org/2000-01-2269/ [Accessed November 24, 2015].

Franklin, J.L. & Charles, F., 1983. Thermal Characteristics of Standardized Air Force Avionic Enclosures. In *13th Intersociety Conference on Environmental Systems*. San Francisco, CA: SAE International, pp. 1–12.

Franklin, J.L. & Kramer, T.J., 1982. Thermal Design of Standard Avionic Enclosures. Available at: http://dx.doi.org/10.4271/820878.

Fraser-Mitchell, H., 2013. The HAWK Story - 2013/01. *Journal of Aeronautical History*, 01, pp.1–120. Available at: http://aerosociety.com/Assets/Docs/Publications/The Journal of Aeronautical History/2013-01_HawkStory-Fraser-Mitchell.pdf.

Gambill, J.M. et al., 1993. Integrated Aircraft Thermal Management and Power Generation. In Sa, ed. *23rd International Conference on Environmental Systems*. Colorado Springs, Colorado, pp. 1–12.

GE Measurement & Control, 2016. DPI 611 - Pressure Calibrator. *www.gemeasurement.com*. Available at: https://www.gemeasurement.com/test-calibration/calibrators/dpi-611-pressure-calibrator.

Giesing, J.P. & Barthelemy, J.-F.M., 1998. A Summary of Industry MDO Applications and Needs. In *7th AIAA/USAF/NASA/ISSMO Symposium on Multidisciplinary Analysis an Optimization*. St Louis, MO, USA: AIAA, pp. 1–12.

Gunston, B., 1980. *Modern Combat Aircraft 6 - Panavia Tornado* 1st Editio., Shepperton. Surrey: Ian Allen LTD.

Van Haver, S, F, G. & Vos, R., 2015. A Practical Method for Uncertainty Analysis in the Aircraft Conceptual Design Phase. In *53rd AIAA Aerospace Sciences Meeting*. Kissimmee, FL, pp. 1–14. Available at: http://arc.aiaa.org/doi/abs/10.2514/6.2015-1680 [Accessed January 28, 2016].

Hitzigrath, R.W., 1993a. Improving Aircraft Fuel-Thermal Management. Available at: http://dx.doi.org/10.4271/932086.

Hitzigrath, R.W., 1993b. Improving Aircraft Fuel-Thermal Management. , (412). Available at: http://dx.doi.org/10.4271/932086.

HM Government, 2015. *National Security Strategy and Strategic Defence and Security Review 2015*, Available at: https://www.gov.uk/government/uploads/system/uploads/attachment_data/file/478933/52309_Cm_9161_NSS_SD_Review_web_only.pdf.

Hoffman, G.L., 1985. Environmental Control System Simulation using EASY5, as Applied to the F-14. Available at: http://dx.doi.org/10.4271/851318.

Hunt, E.H. et al., 1995. Commercial Airliner Environmental Control System: Engineering Aspects of Cabin Air Quality. *Aerospace Medical Association annual meeting*, pp.1–8. Available at: https://web.archive.org/web/20120331055732/http://www.cabinfiles.com/?CFrequest=file;03032001100119.

Iden, S., 2012. *Integrated Vehicle Energy Technology (INVENT) Overview "Changing the Culture through Model Based Engineering,"* Cincinnati, Ohio. Available at: http://ieeeusa.org/calendar/conferences/annualmeeting/2012/program/files/Friday/Track3/INVENT-Overview-Iden.pdf [Accessed January 11, 2016].

Igarashi, T., Nakamura, H. & Fukuoka, T., 2004. Pressure drop and heat transfer of arrays of in-line circular blocks on the wall of parallel channel. *International Journal of Heat and Mass Transfer*, 47(21), pp.4547–4557. Available at: http://www.sciencedirect.com/science/article/pii/S0017931004001437 [Accessed February 4, 2016].

INCOSE, 2016. What is Systems Engineering. *www.incose.org*, p.1. Available at: http://www.incose.org/AboutSE/WhatIsSE [Accessed January 1, 2016].

Jaworski, M., 2012. Thermal performance of heat spreader for electronics cooling with incorporated phase change material. *Applied Thermal Engineering*, 35, pp.212–219. Available at: http://www.sciencedirect.com/science/article/pii/S1359431111005746 [Accessed November 6, 2015].

Johansson, J. & Leisner, P., 2012. Prognostics of thermal fatigue failure of solder joints in avionic equipment. *IEEE Aerospace and Electronic Systems Magazine*, 27(4), pp.16 – 24. Available at: http://ieeexplore.ieee.org/ielx5/62/6203706/06203714.pdf?tp=&arnumber=6203714&isnumber=6203706\nhttp://ieeexplore.ieee.org/xpl/articleDetails.jsp?tp=&arnumbe

r=6203714&contentType=Journals+&+Magazines&refinements=4291944246&matchBoolean=true&page.

Johnson, S.B. & Day, J.C., 2016. Theoretical Foundations for the Discipline of Systems Engineering. In *54th AIAA Aerospace Sciences Meeting*. AIAA SciTech. San Diego, CA: American Institute of Aeronautics and Astronautics, pp. 1–13. Available at: http://dx.doi.org/10.2514/6.2016-0212.

Jones, A.B. et al., 2016a. Evaluating Environmental Control System Thermal Response to Degraded Operating Conditions for Fault Detection and Isolation Purposes. In San Diego, CA: AIAA, pp. 1–16.

Jones, A.B. et al., 2016b. Thermal Sensitivity Analysis of Avionic and Environmental Control Subsystems to Variations in Flight Condition. In San Diego, CA: American Institute of Aeronautics and Astronautics, pp. 1–15.

Jones, A.B. & Chen, R., 2015. Experimental Assessment of Vapour Chamber Heater Spreader Implementation in Avionic Cooling. In *53rd AIAA Aerospace Sciences Meeting*. AIAA SciTech. Kissimmee, FL: American Institute of Aeronautics and Astronautics, pp. 2–10. Available at: http://dx.doi.org/10.2514/6.2015-0712.

Jones, A.B., Childs, T. & Chen, R., 2015. Development of a Full Scale Experimental and Simulation Tool for Environmental Control System Optimisation and Fault Detection. In *53rd AIAA Aerospace Sciences Meeting*. AIAA SciTech. San Diego, CA: American Institute of Aeronautics and Astronautics, pp. 1–11. Available at: http://dx.doi.org/10.2514/6.2015-1196.

Jones, F.E., 1995. *Techniques and Topics in Flow Measurement*, CRC Press.

Joslin, M., 2015. *Adour Mk871 Bleed Air Flow Rates*, Brough, UK.

Jubran, B.A., Swiety, S.A. & Hamdan, M.A., 1996. Convective heat transfer and pressure drop characteristics of various array configurations to simulate the cooling of electronic modules. *International Journal of Heat and Mass Transfer*, 39(16), pp.3519–3529. Available at: http://www.sciencedirect.com/science/article/pii/0017931096000142 [Accessed November 5, 2015].

Kelly, J., 2015. Why is the UK still so reliant on the Tornado. *BBC News*, p.1. Available at: http://www.bbc.co.uk/news/magazine-33772093.

Kestin, J. & Whitelaw, J.H., 1964. The viscosity of dry and humid air. *International Journal of Heat and Mass Transfer*, 7(11), pp.1245–1255. Available at: http://www.sciencedirect.com/science/article/pii/0017931064900663 [Accessed

December 18, 2015].

Laster, J.P., Maxwell, M.J. & Garner, J.E., 1990. Proven Dynamic Modeling Techniques for Concurrent Design and Analysis of ECS Controllers. Available at: http://dx.doi.org/10.4271/901234.

Lawrence, M.G., 2005. The Relationship between Relative Humidity and the Dewpoint Temperature in Moist Air: A Simple Conversion and Applications. *Bulletin of the American Meteorological Society*, 86(2), pp.225–233.

Lee, S. et al., 2013. EVALUATION OF HEAT TRANSFER COEFFICIENTS IN VARIOUS AIR-CONDITIONING MODES BY USING THERMAL MANIKIN. In *13th Conference of International Building Performance Simulation Association2*. Chambery, France: BS2013, pp. 1–10.

Letlow, J.T. & Jenkins, L.C., 1998. Development of an Integrated Environmental Control System. In *28th International Conference on Environmental Systems*. Danvers, Massachusetts: SAE International, pp. 1–7. Available at: http://dx.doi.org/10.4271/981544.

Limited, H.E., 1988. *An Atmosphere Model for Use in Aircraft Kinetic Heating Studies*, Bedford, England.

Lockheed_Martin, 2015. F-22 Raptor - 100 Years of Acclerating Tomorrow. *www.lockheedmartin.co.uk*. Available at: http://www.lockheedmartin.co.uk/us/100years/stories/f-22.html.

Lt Gen Hawk, C., 2012. *5th Generation Fighters*, Washington D.C.

Martell Calibrators, 2016. TC-100 Precision Thermocouple Calibrator. *http://www.martelcalibrators.com/*. Available at: http://www.martelcalibrators.com/product/tc-100-thermocouple-calibrator/.

Matulich, D.S., 2011. Aircraft Fog Control Systems. , pp.41–50.

Matullch, D., 1989. High-Temperature Bootstrap Compared with F15 Growth Air Cycle Air Conditioning System. Available at: http://papers.sae.org/891436/ [Accessed November 26, 2015].

Maxwell, D. et al., 2010. *Thermal Survey of the EFA FCC*, Rochester, UK.

McClain, C.H., 1947. *Fluid flow in pipes*, New York: The Industrial Press.

Messinger, B.L., 1946. *Refrigeration for Air Conditioning Pressurized Transport Aircraft*, Available at: http://papers.sae.org/460200/ [Accessed December 17, 2015].

MIL-E-85726, 1986. *ENCLOSURE AVIONICS FORCED AIR-COOLED*, Available at:

http://everyspec.com/MIL-SPECS/MIL-SPECS-MIL-E/MIL-E-85726_14256/ [Accessed October 28, 2015].

Mitani, H. & Saito, H., 2002. New Concept ECS for Civil Aircraft. Available at: http://dx.doi.org/10.4271/2002-01-2421.

Moir, I. & Seabridge, A., 2001. *Aircraft Systems: Mechanical, Electrical and Avionics Subsystems Integration* 3rd Editio., Available at: http://eu.wiley.com/WileyCDA/WileyTitle/productCd-1119965209.html [Accessed October 28, 2015].

Molyneaux, A, G., Hayles, A, J. & Greggs, M., 1997. *Modelling of the Hawk ECS System Using Easy5x - Hand Over Report*, Brough, UK.

Naphon, P. & Wiriyasart, S., 2012. Study on the vapor chamber with refrigerant R-141b as working fluid for HDD cooling. *International Communications in Heat and Mass Transfer*, 39(9), pp.1449–1452. Available at: http://www.sciencedirect.com/science/article/pii/S0735193312002096 [Accessed November 6, 2015].

Nuzum, S.R., Roberts, R.A. & Wolff, M., 2016. An Aerospace Vehicle Model Including a Cryogenic Thermal Subsystem. In *57th AIAA/ASCE/AHS/ASC Structures, Structural Dynamics, and Materials Conference*. AIAA SciTech. American Institute of Aeronautics and Astronautics, pp. 1–15. Available at: http://dx.doi.org/10.2514/6.2016-0673.

Nuzum, S.R., Roberts, R.A. & Wolff, M., 2015. Various Integrated Aerospace Systems utilizing a Cryogenic Fluid. In *Joint Propulsion Conference*.

Office of Mangament and Budget, 2013. *Historical Tables - Budget of the U.S Government*, Washington D.C.

Ordonez, J. & Bejan, A., 2003. Minimum power requirement for environmental control of aircraft. *Energy*, 28(12), pp.1183–1202. Available at: http://www.sciencedirect.com/science/article/pii/S0360544203001051 [Accessed February 9, 2016].

Oshman, C. et al., 2012. Thermal performance of a flat polymer heat pipe heat spreader under high acceleration. *Journal of Micromechanics and Microengineering*, 22(4), p.045018.

Osram Sylvania, 2012. Air Heaters. , 1, pp.149–157. Available at: https://assets.sylvania.com/assets/documents/Air Heater Catalog_2005.f827559b-7200-46b5-8669-3da80f422d47.pdf.

Pearson, J. & McCoy, S., 2011. *Thermal Management SEIC Report*, Loughborough, UK.

Pérez-Grande, I. & Leo, T.J., 2002. Optimization of a commercial aircraft environmental control system. *Applied Thermal Engineering*, 22(17), pp.1885–1904. Available at: http://www.sciencedirect.com/science/article/pii/S1359431102001308 [Accessed December 16, 2015].

Piccirillo, A.C., 1998. Origins of the F-22 Raptor. Available at: http://dx.doi.org/10.4271/985566.

Price, N.B. et al., 2016. Simulating Future Test and Redesign Considering Epistemic Model Uncertainty. In *18th AIAA Non-Deterministic Approaches Conference*. AIAA SciTech. American Institute of Aeronautics and Astronautics, pp. 1–16. Available at: http://dx.doi.org/10.2514/6.2016-0950.

RANNENBERG, G., 1969. Simple/bootstrap cooling system for a new transport airplane. In *Astrodynamics Conference*. Guidance, Navigation, and Control and Co-located Conferences. American Institute of Aeronautics and Astronautics. Available at: http://dx.doi.org/10.2514/6.1969-787.

Rebbechi, B., 1980. *A review of Aircraft Cabin Conditioning for Operations in Australia*, Melbourne, Victoria, Australia.

Reuter, R.A. et al., 2016. An Overview of the Optimized Integrated Multidisciplinary Systems Program. In *57th AIAA/ASCE/AHS/ASC Structures, Structural Dynamics, and Materials Conference*. AIAA SciTech. American Institute of Aeronautics and Astronautics. Available at: http://dx.doi.org/10.2514/6.2016-0674.

Reyes, M. et al., 2012. Experimental and theoretical study of a vapour chamber based heat spreader for avionics applications. *Applied Thermal Engineering*, 37, pp.51–59. Available at: http://www.sciencedirect.com/science/article/pii/S1359431111007472 [Accessed November 6, 2015].

Roberts, R.A. et al., 2016. Impact of High Energy Pulsed Systems on an Aircraft's Power and Thermal Management System. In *57th AIAA/ASCE/AHS/ASC Structures, Structural Dynamics, and Materials Conference*. AIAA SciTech. American Institute of Aeronautics and Astronautics, pp. 1–16. Available at: http://dx.doi.org/10.2514/6.2016-0672.

Roberts, R.A. & Eastbourn, S.M., 2014. Vehicle Level Tip-to-Tail Modeling of an Aircraft. *International Journal of Thermodynamics*, 17(2), pp.107–115. Available at: http://ijoticat.com/article/view/1034000523 [Accessed January 11, 2016].

Rogers, G.F.C. & Mayhew, Y.R., 1992. *Engineering Thermodynamics: Work and Heat Transfer : SI Units*, Longman Scientific & Technical.

Rosenbush, F.M., 1982. *ECS Schemes for All Electric Airliners*, SAE International.

Rossato, M. et al., 2014. Caloric Expenditure and Exercise Intensity on Fighter Pilots during Combat Flight. *Journal of Exercise Physiology Online*, 17(2), p.36. Available at: http://www.researchgate.net/publication/266476469_Caloric_Expenditure_and_Exercise_Intensity_on_Fighter_Pilots_during_Combat_Flight [Accessed October 16, 2015].

Ryan, S.K., 1990. F-15 Environment Control System Improvements. Available at: http://papers.sae.org/901235/ [Accessed November 26, 2015].

SAE, 2014. *Definition of Commonly Used Day Types - SAE ARP210*,

Safavi, E., 2012. *Collaboratiove Multidisciplinary Design Optimisation*. Linkoping University.

Sanitjai, S. & Goldstein, R.J., 2004. Forced convection heat transfer from a circular cylinder in crossflow to air and liquids. *International Journal of Heat and Mass Transfer*, 47(22), pp.4795–4805. Available at: http://www.sciencedirect.com/science/article/pii/S0017931004001917 [Accessed February 4, 2016].

Schaller, R.R., 1997. Moore's law: past, present and future. *Spectrum, IEEE*, 34(6), pp.52–59.

Söderholm, P., 2007. A system view of the No Fault Found (NFF) phenomenon. *Reliability Engineering & System Safety*, 92(1), pp.1–14. Available at: http://www.sciencedirect.com/science/article/pii/S0951832005002139 [Accessed November 5, 2015].

Sparrow, E.M., Niethammer, J.E. & Chaboki, A., 1982. Heat transfer and pressure drop characteristics of arrays of rectangular modules encountered in electronic equipment. *International Journal of Heat and Mass Transfer*, 25(7), pp.961–973. Available at: http://www.sciencedirect.com/science/article/pii/0017931082900710 [Accessed February 4, 2016].

Spencer-Gregory, H. & Rourke, F., 1957. *Hygrometry*, London: Crosby Lockwood & Son, Ltd.

Sprouse, J.G., 1996. F-22 Environmental Control / Thermal Management System Design Optimization for Reliability and Integrity - A Case Study. , (412).

Steadman, B. et al., 2002. Reducing No Fault Found using statistical processing and an expert system. In *IEEE AUTOTESTCON*. IEEE, pp. 872–878. Available at: http://ieeexplore.ieee.org/lpdocs/epic03/wrapper.htm?arnumber=1047966 [Accessed November 5, 2015].

Stow, A., Greggs, M. & Systems, B., 2006. *100 Series Hawk ECS Model Verification and Release Note*, Brough, UK.

Strattan, L.A., 1983. Capabilities and Limitations of Air Cooled Avionic Packages. In *13th*

Intersociety Conference on Environmental Systems. San Francisco, CA: SAE International, pp. 1–12. Available at: http://dx.doi.org/10.4271/831105.

Teertstra, P., Culham, J.R. & Yovanovich, M.M., 1997. Calculating Interface Resistance. *Electronics Cooling Magazine*, pp.1–9. Available at: http://www.mhtlab.uwaterloo.ca/pdf_papers/mhtl97-4.pdf.

Thornber, A., 2002. *The Munich Scene - Birth of Tornado*, Northmoor, UK.

Tsai, M.C., Kang, S.W. & Vieira De Paiva, K., 2013. Experimental studies of thermal resistance in a vapor chamber heat spreader. *Applied Thermal Engineering*, 56(1-2), pp.38–44. Available at: http://dx.doi.org/10.1016/j.applthermaleng.2013.02.034.

Vargas, J.V.C. & Bejan, A., 2001. Integrative thermodynamic optimization of the environmental control system of an aircraft. *International Journal of Heat and Mass Transfer*, 44(20), pp.3907–3917. Available at: http://www.sciencedirect.com/science/article/pii/S0017931001000333 [Accessed October 28, 2015].

Vargas, J.V.C., Bejan, A. & Siems, D.L., 2001. Integrative Thermodynamic Optimization of the Crossflow Heat Exchanger for an Aircraft Environmental Control System. *Journal of Heat Transfer*, 123(4), p.760. Available at: http://heattransfer.asmedigitalcollection.asme.org/article.aspx?articleid=1445092 [Accessed November 22, 2015].

Wang, L. et al., 2002. Collaborative conceptual design—state of the art and future trends. *Computer-Aided Design*, 34(13), pp.981–996. Available at: http://www.sciencedirect.com/science/article/pii/S0010448501001579 [Accessed May 18, 2015].

Williams, R. et al., 1998. An investigation of “cannot duplicate” failures. *Quality and Reliability Engineering International*, 14(5), pp.331–337. Available at: http://dx.doi.org/10.1002/(SICI)1099-1638(199809/10)14:5<331::AID-QRE183>3.0.CO.

Woodfield, A, A. & Haynes, P, J., 1965. *Measurement of Air Temperature on an Aircraft Travelling at High Subsonic and Supersonic Speeds*, Cranfield, UK.

Zentner, R.C. & Kramer, T.J., 2010. Development and Testing of Forced = Air Cooled Enclosures for High Density Electronic Equipment.

Zhao, H. et al., 2009. Experimental study on the performance of an aircraft environmental control system. *Applied Thermal Engineering*, 29(16), pp.3284–3288. Available at: http://www.sciencedirect.com/science/article/pii/S1359431109001458 [Accessed

November 26, 2015].